Development and validation of an *in vitro* human model of drug-induced vascular injury

Dora Lopresto

Corpus Christi College

This dissertation is submitted for the degree of Doctor of Philosophy

July 2019

Department of Pharmacology

University of Cambridge

Preface

This dissertation is the result of my own work and includes nothing which is the outcome of work done in collaboration except as declared in the Preface and specified in the text.
This thesis is not substantially the same as any that I have submitted, or, is being concurrently submitted for a degree or diploma or other qualification at the University of Cambridge or any other University or similar institution except as declared in the Preface and specified in the text. I further state that no substantial part of my dissertation has already been submitted, or, is being concurrently submitted for any such degree, diploma or other qualification at the University of Cambridge or any other University or similar institution except as declared in the Preface and specified in the text.
It does not exceed the prescribed word limit for the relevant Degree Committee.

Acknowledgments

I would firstly like to thank my Supervisor Dr. Matthew Harper for giving me the opportunity to work on this exciting PhD project and for always supporting me along the way. I have always valued your advice and your enthusiasm for research. I would also like to thank my co-Supervisor Dr. Kelly Gray for all the guidance and precious advice that you have been so kind to give me. Also thank you for giving me the opportunity to work at AstraZeneca, which has been a very useful and pleasant experience. I am also grateful to Dr. Amy Pointon for her support and advice.
I extend my sincerest gratitude to AstraZeneca for providing the generous funding throughout my PhD.

I am deeply grateful to Dr. Jessica Davies. Thank you for your endless help during the past years. Without your constant advice and supervision, I do not think my PhD would have reached completion. My thanks also go to my lab members past and present, Sarah, Jess, Bonita, Hao, Ivelin, Nima, Rebecca, Roxana, who have contributed to make long days in the lab more enjoyable. And thank you to Dandan and Rosie for being great office mates.
I express my gratitude to Dr. Ewan Smith, for being a great mentor and giving me advice especially at the beginning of my PhD, when it was much needed. I thank Dr. Jon Holdich for all the help with troubleshooting.

Thank you to all the friends I met during my time in Cambridge that made these years unforgettable: Juliana, Jakob, Faryal, Giulia and especially my best friend Shruti.

Thank you to my amazing parents and especially to my mum, who inspired me to do a PhD and I will always be grateful to you for this. Thank you to my wonderful sister and brother for always being there. Finally, I would like to thank my boyfriend Leonard for his infinite patience and support throughout this entire time. Certainly, this journey would have not been the same without you and I feel incredibly lucky for having shared every single moment, from start to finish, with you.

Abstract

Drug safety is a major cause of attrition in contemporary drug development. Many promising candidate drugs are terminated in the developmental process or withdrawn in the post-approval stage because of adverse drug reactions (ADRs). Among these, cardiovascular (CV) ADRs occur with a high incidence. Affecting the heart, blood vessels and blood components, CV ADRs can lead to hypertension, heart failure, cardiac arrhythmias and thrombosis. The prompt identification of CV toxicity would reduce both the delay and cost of drug development and increase patient safety.

Drug-induced vascular injury (DIVI) in pre-clinical toxicology studies involves damage to endothelial (EC) and smooth muscle cells (SMC) in small and medium sized vessels, but little is known about the mechanisms of DIVI. Damage includes microhaemorrhage, endothelial junction disruption, SMC necrosis and inflammation. DIVI is often observed preclinically, driving a need to study this in human tissue.

The aim of this thesis was to develop and characterise an *in vitro* human model that would allow the study of DIVI in human tissue during drug development.

The first stage was to effectively reproduce DIVI in an animal model. To reduce the utilisation of live animals, a vessel explant was used. To determine whether DIVI was recapitulated *ex vivo* von Willebrand factor (VWF) release, one of the hallmarks of DIVI, was analysed using four drugs reported in the literature to produce DIVI. The same four drugs were then tested in human EC and SMC for the following features of DIVI: (1) VWF release; (2) EC monolayer disruption; (3) inflammation; (4) EC and SMC death. Both *ex vivo* in rats and *in vitro* in humans, the drugs did not exhibit common characteristics and each expressed DIVI features in different ways.

The human *in vitro* model was also assessed in a co-culture of EC and SMC, and in the presence of a flow-mimetic that reproduces *in vivo*-derived hemodynamics. It was concluded that DIVI cannot be fully recapitulated *in vitro* in such a reductionist cellular model, suggesting that exposure to the complex microenvironment of the vasculature may be required for the lesions to develop, or that DIVI may, in fact, not be relevant to humans at all.

Table of Contents

Preface ii

Acknowledgments iii

Abstract iv

List of figures ix

List of tables xiii

Abbreviations xiv

1. Introduction 1

1.1 Timeline of drug production 2

1.2 Cardiovascular adverse drug reactions 5

1.2.1 Cardiac ADRs 5

1.2.2 Vascular ADRs 7

1.2.3 Translational problems between pre-clinical to clinical trials for cardiovascular drugs 7

1.3 Drug-induced Vascular Injury 9

1.3.1 Histopathological signs of DIVI 9

1.3.2 Physiological signs of DIVI 17

1.4 Drugs that cause DIVI 18

1.4.1 Approved or approvable drugs responsible for vascular injury in animals 18

1.4.2 Selected DIVI drugs 23

1.5 Mechanisms of DIVI 29

1.5.1 Mechanism 1. Hemodynamic alterations 29

1.5.2 Mechanism 2. Direct pharmacological or chemical toxicity on vascular and circulating blood cells 30

1.5.3 Mechanism 3. Vascular injury secondary to inflammation 33

1.6 Vascular and circulating blood cells that may be affected in DIVI 33

1.6.1 Endothelial cell barrier 33

1.6.2 Endothelial activation 39

1.6.3 Smooth muscle cells 56

1.6.4 Endothelial-smooth muscle cell interactions 61

1.6.5 Circulating blood cells 63

1.6.6 Cross-talk of cells during inflammation, a typical feature of DIVI 72

1.7 The importance of flow in blood vessel function 74

1.7.1 Piezo-1 channel controls blood flow on EC 74
1.7.2 Yoda-1 activates EC Piezo-1 channels mimicking shear stress 75
1.8 An *in vitro* model of DIVI 76
1.8.1 Existent *in vitro* models to study DIVI 76
1.9 Aims and objectives 79
2. Materials and Methods 80
2.1 Materials 81
2.2 Methods 87
2.2.1 *Ex vivo* studies 87
2.2.2 Cell culture 88
2.2.3 Whole blood experimentation 92
2.2.4 Flow cytometry 93
2.2.5 Confocal microscopy 95
2.2.6 Investigating cell death using an ATP viability assay 96
2.2.7 Protein biochemistry 98
2.3 Statistical analysis 99
3. Developing an *ex vivo* model of DIVI 100
3.1 Introduction 101
3.2 Methods 102
3.3 Results 105
3.3.1 Thrombin promotes VWF release from EC *ex vivo* 112
3.3.2 DIVI-related drugs induce VWF release from EC 114
3.4 Discussion 117
4. Investigating DIVI *in vitro* 122
4.1 Introduction 123
4.2 Results 123
4.2.1 VWF release with DIVI-related drugs in HUVEC 126
4.2.2 Assessment of disruption to EC monolayer 133
4.2.3 Investigating cell death with an ATP viability assay 137
4.2.4 Exploring inflammation in DIVI 142
4.3 Discussion 155
5. Exploring the effects of DIVI-related drugs in whole blood 164
5.1 Introduction 165

5.2 Methods 165
5.3 Results 166
5.3.1 TRAP-6 amide activates platelets, as shown by $\alpha_{IIb}\beta_3$ activation and increased P-selectin surface expression 166
5.3.2 fMLP activates leukocytes, as indicated by CD11b activation 168
5.3.3 DIVI drugs do not activate platelets, as shown by P-selectin expression and $\alpha_{IIb}\beta_3$ activation 170
5.3.4 Minoxidil and bosentan activate leukocytes, as indicated by CD11b activation 173
5.4 Discussion 178
6. Investigating DIVI in a co-culture system 183
6.1 Introduction 184
6.2 Methods 185
6.2.1 Optimisation of co-culture cell density 185
6.3 Results 188
6.3.1 Characterisation of EC and SMC in co-culture 188
6.3.2 VWF release with DIVI-related drugs in co-culture 190
6.3.3 Investigating cell death by flow cytometry 199
6.4 Discussion 204
7. The role of flow in DIVI 213
7.1 Introduction 214
7.2 Methods 216
7.3 Results 216
7.3.1 Establishing a working concentration of Yoda-1 216
7.3.2 Yoda-1 mimics the effect of flow in static EC 219
7.3.3 DIVI-related drugs in the presence of Yoda-1 do not induce VWF release 222
7.3.4 The particle size of VWF does not differ across treatments 227
7.3.5 The drugs do not affect EC junctional integrity 229
7.3.6 Bosentan and fenoldopam in the presence of Yoda-1 cause EC but not SMC death 233
7.4 Discussion 236
8. General Discussion 242
8.1 VWF release with DIVI-related drugs *ex vivo* and *in vitro* 243
8.2 Investigation of other markers of DIVI *in vitro* 249
8.2.1 EC junctional breakage 250

8.2.2 EC inflammation 253
8.2.3 EC death 255
8.2.4 SMC death 258
8.2.5 Platelet and leukocyte activation 260
8.3 Exploring other potential markers of DIVI *in vitro* 262
8.4 The optimum device to study DIVI 264
8.5 Concluding remarks 265
References 268

List of figures

Figure 1.1 Drug development process. 3

Figure 1.2 Structure of the arterial wall. 10

Figure 1.3 Haematoxylin and eosin staining of rat and dog arteries. 12

Figure 1.4 Scanning electron microscope images of a control dog and a dog treated with SK&F 95654. 14

Figure 1.5 Timeline of the development of the lesions in DIVI in rats, dogs and monkeys. 16

Figure 1.6 Mechanism of action of bosentan. 24

Figure 1.7 Mechanism of action of fenoldopam. 25

Figure 1.8 Mechanism of action of minoxidil. 26

Figure 1.9 Mechanism of action of rolipram. 27

Figure 1.10 Simplified schematic of the formation of free radicals from nitric oxide. 31

Figure 1.11 Schematic of VE-cadherin function at the endothelial junctions. 35

Figure 1.12 Endothelial Type I activation. 40

Figure 1.13 Endothelial Type II activation. 43

Figure 1.14 VWF synthesis, storage and release. 49

Figure 1.15 Schematic of VWF domains. 50

Figure 1.16 Function of VWF. 53

Figure 1.17 The leukocyte adhesion cascade. 65

Figure 1.18 Proposed schematic model showing the cross-talk between the cell types involved in DIVI. 72

Figure 2.1 Typical cell passaging timescale from P1 to P4. 89

Figure 2.2 ATP luminescence assay. 95

Figure 3.1 Extraction of the rat gut and localisation of the superior mesenteric artery (SMA). 101

Figure 3.2 Flow diagram of the experimental procedure. 102

Figure 3.3 Cross section (10 µM thickness) of the SMA in a control rat. 104

Figure 3.4 Assessment of the level of non-specific staining. 105

Figure 3.5 Quantification of VWF. 106

Figure 3.6 Plot profile with three fluorescence intensities representing CD31 (red), DAPI (blue) and VWF (green). 107

Figure 3.7 VWF, CD31 and α-SMA staining in a rat vessel explant. 109

Figure 3.8 VWF expression in a thrombin-stimulated and in a control vessel. 111

Figure 3.9 VWF and CD31 staining in rat mesenteric explants. 113

Figure 3.10 Quantification of VWF release in EC and SMC in the vessel. 114

Figure 4.1 Bright field images of EC and SMC. 120

Figure 4.2 Representative confocal images of specific HUVEC and HCASMC markers. 122

Figure 4.3 Representative confocal pictures of VWF release in HUVEC at 1 hour. 124

Figure 4.4 Representative confocal pictures of VWF release in HUVEC at 24 hours. 125

Figure 4.5 VWF release after 1 and 24 hours in HUVEC. 127

Figure 4.6 Average particle size of WPB at 1 and 24 hours. 129

Figure 4.7 Assessment of EC junctional integrity with DIVI-related drugs at 1 hour. 131

Figure 4.8 Assessment of EC junctional integrity with DIVI-related drugs at 24 hours 132

Figure 4.9 Quantification of EC junctional disruption. 133

Figure 4.10 Investigating cell death with the ATP viability assay. 135

Figure 4.11 ATP viability assay in HUVEC. 137

Figure 4.12 ATP viability assay in HCASMC. 138

Figure 4.13 ICAM-1 and VCAM-1 expression in HUVEC. 140

Figure 4.14 ICAM-1 and VCAM-1 expression in HUVEC after treatment with increasing concentrations of TNF-α. 142

Figure 4.15 Quantification of ICAM-1 and VCAM-1 expression in HUVEC. 144

Figure 4.16 ICAM-1 and VCAM-1 expression mimicking underlying inflammatory conditions 145

Figure 4.17 Increasing concentrations of TNF-α incubated with bosentan 100 μM on ICAM-1 and VCAM-1 expression in HUVEC. 147

Figure 4.18 Increasing concentrations of bosentan on VCAM-1 and ICAM-1 expression. 149

Figure 4.19 ET receptor antagonism effect on ICAM-1 and VCAM-1 expression. 151

Figure 5.1 Acquisition of platelets with flow cytometer. 163

Figure 5.2 Acquisition and analysis of leukocytes with flow cytometer. 165

Figure 5.3 Effects of the drugs on platelet integrin $\alpha_{IIb}\beta_3$ activation.....167
Figure 5.4 Effects of the drugs on platelet P-selectin expression. 168
Figure 5.5 Effects of the drugs on leukocyte activation. 170
Figure 5.6 Effects of bosentan and minoxidil on neutrophils.....172
Figure 5.7 Effects of bosentan and minoxidil on monocytes. 173
Figure 6.1 Optimisation of co-culture seeding density.....183
Figure 6.2 Bright field image of monocultured EC and SMC and cells in co-culture.....184
Figure 6.3 Shape descriptors in a co-culture of EC and SMC.....185
Figure 6.4 Assessment of VWF expression in SMC.....188
Figure 6.5 Representative confocal images of VWF release in EC and SMC co-culture at 1 hour.....190
Figure 6.6 Representative confocal pictures of VWF release in EC and SMC co-culture at 24 hours. 191
Figure 6.7 VWF release from SMC and EC in co-culture after 1 and 24 hours treatment with DIVI drugs.....192
Figure 6.8 Average particle size of WPB at 1 and 24 hours.....194
Figure 6.9 Gating of EC and SMC to assess cell death. 196
Figure 6.10 Propidium iodide (PI) is used to assess cell death.....198
Figure 6.11 Cell death induced by DIVI-related drugs and analysed by flow cytometry using PI. 199
Figure 6.12 Phenotype switching in SMC. 205
Figure 7.1 Assessment of cytotoxicity using an ATP viability assay. 213
Figure 7.2 Assessment of cytotoxicity using immunofluorescence.....214
Figure 7.3 ICAM-1 and VCAM-1 expression in HUVEC under flow or using the flow-mimetic Yoda-1. 216
Figure 7.4 Representative blots and quantification by densitometric analysis of phospho-eNOS and phospho-Akt.....217
Figure 7.5 Representative confocal pictures of VWF release in HUVEC pre-treated with Yoda-1 1 μM at 1 hour. 220
Figure 7.6 Representative confocal pictures of VWF release in HUVEC pre-treated with Yoda-1 at 24 hours. 221

Figure 7.7 VWF release after 1 (A) and 24 (B) hours in HUVEC pre-treated with Yoda-1 1 µM. 222

Figure 7.8 Average particle size of VWF at 1 (A) and 24 hours (B). 224

Figure 7.9 Representative confocal pictures of assessment of EC junctional integrity with DIVI-related drugs in the presence of Yoda-1 (1 µM) at 1 hour. 226

Figure 7.10 Representative confocal pictures of assessment of EC junctional integrity with DIVI-related drugs in the presence of Yoda-1 1 µM at 24 hours. 227

Figure 7.11 Assessment of junctional disruption at 1 hour (A) or 24 hours (B) in HUVEC. 228

Figure 7.12 Assessment of cell death using an ATP assay in HUVEC pre-treated with Yoda-1 1 µM. 230

Figure 7.13 Assessment of cell death using an ATP assay in HCASMC pre-treated with Yoda-1 1 µM. 231

List of tables

Table 1.1 Approved or approvable drugs that cause arterial toxicity in animals. 20

Table 1.2 Drugs responsible for causing DIVI in animals. 22

Table 1.3 EC biomarkers reported in DIVI. 46

Table 1.4 SMC biomarkers reported in DIVI. 59

Table 1.5 Biomarkers of circulating blood cells investigated in DIVI. 70

Table 2.1 List of reagents and chemicals used in alphabetical order. 82

Table 2.2 List of cells, media and reagents used in cell culture. 83

Table 2.3 List of primary and secondary antibodies and isotype controls used within this thesis. 84

Table 2.4 List of reagents used for protein biochemistry. 85

Table 4.1 Summary of the effects of DIVI-related drugs *in vitro*. 159

Table 5.1 Summary of the effects of DIVI-related drugs *in vitro* on blood cells 178

Table 6.1 Summary of the effects of DIVI-related drugs in co-culture. 208

Table 7.1 Summary of the effects of DIVI-related drugs in the presence of the flow-mimetic Yoda-1. 237

Table 8.1 Comparative effects of VWF release seen *in vivo* in previous studies with *ex vivo* and *in vitro* investigation conducted within this thesis. 243

Table 8.2 Comparative effects of EC junctional breakage seen *in vitro*/*vivo* in previous studies with *in vitro* investigation conducted within this thesis. 247

Table 8.3 Comparative effects of EC inflammation seen *in vitro*/*vivo* in previous studies with *in vitro* investigation conducted within this thesis. 250

Table 8.4 Comparative effects of EC death seen *in vitro*/*vivo* in previous studies with *in vitro* investigation conducted within this thesis. 253

Table 8.5 Comparative effects of SMC death seen *in vitro*/*vivo* in previous studies with *in vitro* investigation conducted within this thesis. 255

Table 8.6 Comparative effects of inflammation seen *in vitro*/*vivo* in previous studies with *in vitro* investigation conducted within this thesis. 257

Abbreviations

A	Adenosine
Abl	Abelson
ADP	Adenosine diphosphate
ADRs	Adverse drug reactions
Akt	Protein kinase b
ANOV	Analysis of variance
Ang-1	Angiopoietin-1
AP-1	Activating protein-1
APC	Allophycocyanin
ATP	Adenosine triphosphate
bFGF	Basic fibroblast growth factor
BSA	Bovine serum albumin
Ca^{2+}	Calcium
CAM	Cell adhesion molecule
cAMP	Cyclic adenosine monophosphate
CCL5	Chemokine ligand 5 (C-C motif)
CD	Cluster of differentiation
CO_2	Carbon dioxide
COX-1	Cyclooxygenase-1
COX-2	Cyclooxygenase-2
CXCL4	Chemokine ligand 4 (C-X-C motif)
CXCL5	Chemokine ligand 5 (C-X-C motif)
CV	Cardiovascular
DA	Dopamine
DAPI	4', 6-Diamidino-2-Phenylindole
dH_2O	Distilled water
DIVI	Drug-induced vascular injury
DMSO	Dimethyl sulfoxide
DNA	Deoxyribonucleic acid
DTT	1,4-Dithiothreitol
Dyn	Dyne, 1 dyn= 10^{-5} newtons, 1 newton=1 $kg \cdot m \cdot s^{-2}$
EC	Endothelial cells
ECM	Extracellular matrix
EDTA	Ethylenediaminetetraacetic acid
eNOS	Endothelial cell-specific nitric oxide synthase
Erk	Extracellular signal-regulated kinase
ESL-1	E-selectin ligand 1
ET	Endothelin
FACS	Fluorescence activated cell sorting
FBS	Fetal bovine serum
FC	Flow cytometry
FITC	Fluorescein isothiocyanate
fMLP	N-Formylmethionine-leucyl-phenylalanine
GP	Glycoprotein
GPCR	G-protein-coupled receptor

HCASMC	Human coronary artery smooth muscle cells
HDAC6	Histone deacetylase 6
HUAEC	Human umbilical arterial endothelial cells
HUVEC	Human umbilical vein endothelial cells
hERG	Human Ether-à-go-go- related gene
H&E	Hematoxylin and eosin stain
ICAM-1	Intercellular adhesion molecule-1
ICAM-2	Intercellular adhesion molecule-2
ICH	Immunocytochemistry
IF	Immunofluorescence
IgG	Immunoglobulin G
IFN-γ	Interferon-gamma
IL-1	Interleukin-1
IL-1α	Interleukin-1-alpha
IL-1β	Interleukin-1-beta
IL-8	Interleukin-8
IL-1R1	IL-1 receptor1
iNOS	Inducible NOS
JAM-A	Junctional adhesion molecule-A
JAM-B	Junctional adhesion molecule-B
JAM-C	Junctional adhesion molecule-C
K^+	Potassium
kDa	Kilodaltons
kg	Kilogram
KLF-2	Kruppel-like factor-2
L-Arg	L-Arginine
LFA-1	Lymphocytes function-associated antigen-1
L-NMMA	N-monomethyl-k-arginine
LPS	Lipopolysaccharide
LTB_4	Leukotriene B_4
m^2	Square meter
µg	Microgram
µm	Micrometer
µM	Micromolar
mm	Millimetre
MAC-1	Macrophage-1 antigen
MAPK	Mitogen activated protein kinase
MCP-1	Monocyte chemoattractant protein
MFI	Median fluorescence intensity
Mg^{2+}	Magnesium
MIG	Monokine induced by γ interferon
Min	Minute
MIP-3β	Macrophage inflammatory protein-3-beta
MLC	Myosin light chain
MLCK	Myosin light chain kinase
mRNA	Messenger ribonucleic acid
nm	Nanometre

NC3Rs	National Centre for the Replacement Refinement and Reduction of Animals in Research
NF-κβ	Nuclear factor-κ-beta
NO	Nitric oxide
nNOS	Neuronal NOS nitric oxide synthase
NOS	Nitric oxide synthase
NOS3	Nitric oxide synthase 3
O.C.T.	Optimal cutting temperature
O_2	Molecular oxygen
oxLDL	Oxidised low-density lipoprotein
PAK	p21 activated kinase
PAF	Platelet-activating factor
PAR-1	Protease-activated receptor-1
PBS	Phosphate buffered saline
PDE IV	Phosphodiesterase IV
PDE III	Phosphodiesterase III
PDGF	Platelet-derived growth factor
PDMS	Polydimethylsiloxane
PE	Phycoerythrin
PECAM-1	Platelet endothelial cell adhesion molecule-1
PE-Cy7	Phycoerythrin Cyanine 7
PFA	Paraformaldehyde
PGE2	Prostaglandin E2
PGI_2	Prostaglandin I_2
Phospho-	Phosphorylated
PI	Propidium iodide
PKC	Protein kinase C
PKC-α	Protein kinase C-alpha
PLA_2	Phospholipase A_2
Plako	Plakoglobin
pM	Picomolar
PPACK	D-Phenylalanyl-L-prolyl-L-arginine chloromethyl ketone
PSGL-1	P-selectin glycoprotein ligand-1
qPCR	Quantitative polymerase chain reaction
3Rs	Replacement, Reduction and Refinement
Rac	Ras-related C3 botulinium toxin substrate
RBC	Red blood cells
R&D	Research and Development
Rho	Ras homologue
RIPA	Radioimmunoprecipitation assay buffer
RNA	Ribonucleic acid
RNS	Reactive nitrogen species
ROS	Reactive oxygen species
RPM	Revolutions per minute
RPMI	Roswell Park Memorial Institute
SDF-1	Stromal cell-derived factor-1
SDS-PAGE	Sodium dodecyl sulfate polyacrylamide gel electrophoresis

SEM	Standard error of the mean
SOD	Superoxide dismutase
SMA	Superior mesenteric artery
α-SMA	Alpha-smooth muscle actin
SMMHC	Smooth muscle myosin heavy chain
S1P	Sphingosine-1-phosphate
SMC	Smooth muscle cells
TdP	Torsades de Pointes
TEM	Transmission electron microscopy
TGF-β	Transforming growth factor-beta
TIMP-1	Tissue inhibitor of metalloproteinase-1
TNF-α	Tumor necrosis factor-alpha
TNFR-1	TNF-α receptor-1
TRAP-6 amide	Thrombin Receptor Activator Peptide-6 amide
TxB2	Thromboxane B2
VCAM-1	Vascular cell adhesion molecule-1
VE-cadherin	Vascular endothelial-cadherin
VEGF	Vascular endothelial growth factor
VEGFR2	Vascular endothelial growth factor receptor 2
VLA-4	Very late antigen-4
VWF	Von Willebrand factor
VWFpp	VWF pro-peptide
WPB	Weibel-Palade bodies
ZO-1	Zonula occludens-1
α	Alpha
β	Beta
α-cat	Alpha-Catenin
β-cat	Beta-Catenin
γ	Gamma
λ	Lambda
μ	Mu
π	Pi

1. Introduction

1.1 Timeline of drug production

The research and development (R&D) process of a new drug takes on average 15 years, costs over 1 billion dollars and only 0.01 % of compounds are successful in making it to market[1]. In spite of years of effort to improve R&D efficiency and performance, bringing a new drug to market still remains a very expensive and time-consuming process[1,2].

The drug development pipeline can be divided into different stages (**Figure 1.1**)[3]. The first stage is the discovery phase, which is aimed at finding a promising drug candidate, which means that numerous compounds will be synthesised and screened before a lead series emerges. This is proceeded by the preclinical phase, which usually takes 3-6 years to complete and is conducted through *in vitro* studies and animal work, usually using rodents and dogs. If successful, the compound proceeds to clinical phases I, II and III, which usually require 1, 2, and 3 years, respectively, for completion, though this depends on the disease indication[3]. The clinical phase I trial examines the pharmacokinetics and safe dosage range. The drug is administered at low doses to a small group of closely monitored healthy volunteers (20 to 100). On average, about two thirds of phase I compounds will progress to the next phase. Phase II is conducted on a larger cohort, perhaps 100 to 300 volunteers, who suffer with the condition for which the new drug has been developed. In these studies, the drug efficacy, method of delivery and the dosing intervals are assessed. Simultaneous animal and human studies continue to evaluate further its safety. At phase II, compounds can be discontinued due to adverse clinical side effects, or lack of efficacy. Phase III trials include a greater number of volunteer patients (usually thousands) with the aim to assess the drug therapeutic effect in a disease population and determine low-incidence adverse reactions[3]. If the drug successfully completes all clinical phases it is then submitted for regulatory approval and marketed. Phase IV runs alongside commercialisation of the drug, enabling monitoring on a larger scale for potential serious but rare side effects over the longer term. (**Figure 1.1**).

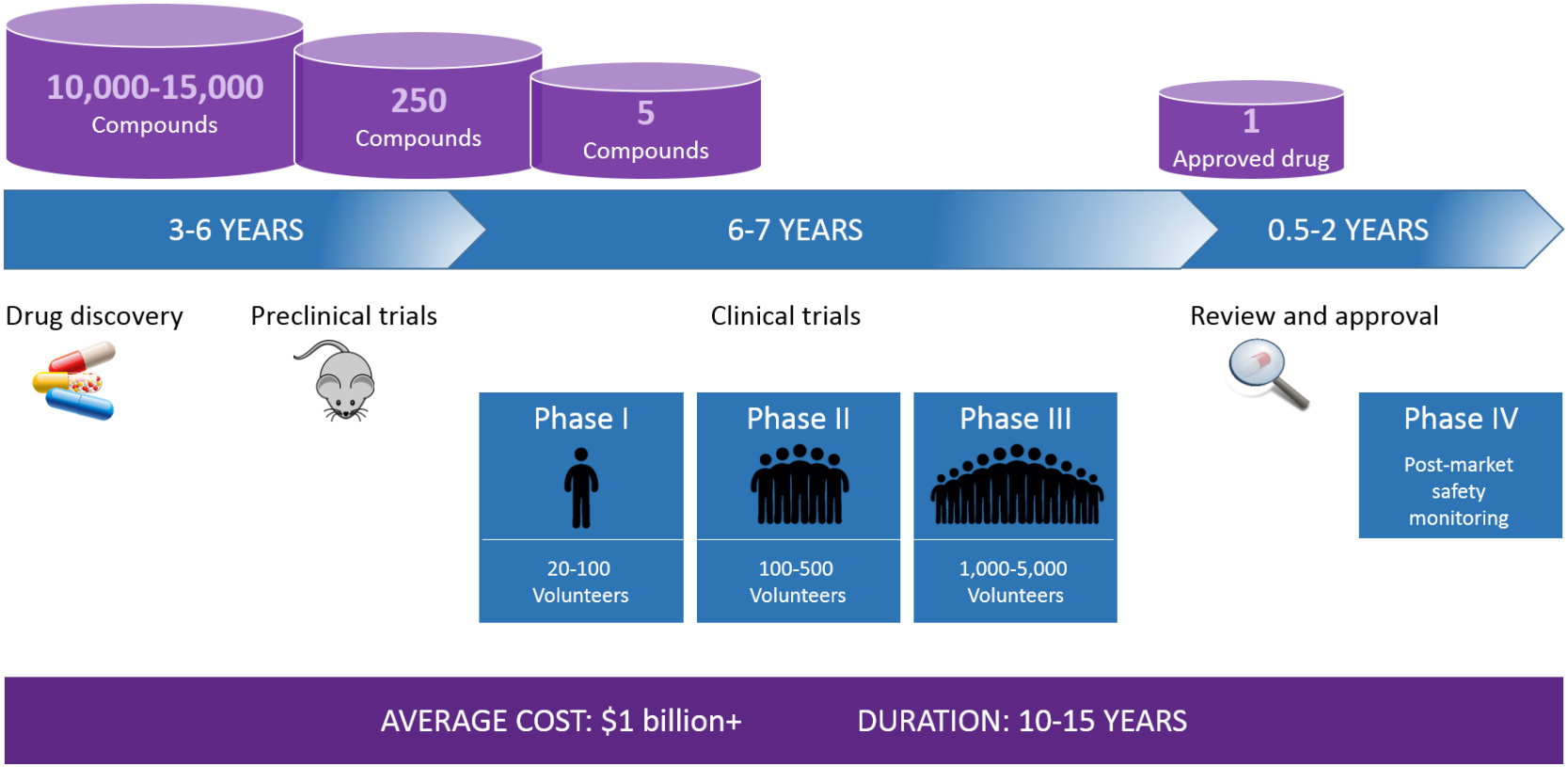

Figure 1.1 Drug development process. It includes preclinical and clinical research, after which a drug is marketed. The process can take up to 15 years on average to complete and can cost over 1 billion dollars. Author's own drawing.

In the past, the drug development process was not as stringent as it is today. During the 1950s and 1960s, the widely used hypnotic drug, thalidomide, was introduced to the market and administered to thousands of pregnant women to treat morning sickness, and was thought to be safe when it was marketed in 1957. Over 10,000 children were born with severe limb deformities[4]. In response to this and other accidents, stricter regulations were introduced making the drug development process more stringent to increase patient safety.

Drug development is associated with a high level of attrition, especially in early discovery and also in its II and III phases, which are also the most costly[5,6]. The success rates of developing a drug vary considerably depending on the different therapeutic areas: for example, cardiovascular (CV) has a ~20 % rate of success, compared with oncology and central nervous system disorders have ~5 % and ~8 % success, respectively[7].

Drug attrition can happen for several reasons: for example, in 1991, pharmacokinetics, and particularly bioavailability, were the most significant cause of attrition, accounting for ~40 % of all attrition. By 2000, these factors had dramatically reduced to less than 10 %, as efforts had been made to improve the prediction of pharmacokinetics and bioavailability[7].In 2000, the major cause~~s~~ of attrition were lack of efficacy, accounting for around 30 % of failures, with safety accounting for a further 30 %[8–11]. Presently, failures due to efficacy and safety issues remain high[7,10,11]. This demonstrates the need to develop more predictive animal models and experimental medicine paradigms that are prognostic of the outcomes.

At present, promising candidate drugs are often terminated in the developmental process or withdrawn in post-approval stage because of adverse drug reactions (ADRs)[12,13]. ADRs are defined as “a response to a drug which is noxious and unintended, and which occurs at doses normally used in man for the prophylaxis, diagnosis, or therapy of disease, or for the modifications of physiological functions”[14]. ADRs are one of the leading causes of morbidity and mortality in healthcare. Previous studies show that ADRs happen in 6.5 % - 20 % of hospitalised patients[15], and that ADRs are themselves one of the more frequent causes of hospitalisation[16].

1.2 Cardiovascular adverse drug reactions

CV ADRs occur with a high incidence, accounting for 45 % of all ADRs[17]. Phase I clinical trials are very safe from a CV point of view, which may reflect that the preclinical studies were effective[17]. However, when drugs are administered for longer periods of time and to larger patient groups, high-risk ADRs such as arrhythmias, coronary artery disorders, embolism and thrombosis are detected, suggesting that subtle events are either not identified in earlier clinical trials or not believed to be biologically significant. It is important however to consider the complexity of the patient condition, as later stage trials involve disease subjects, who may have a weakened immune system and lower CV output and thus it is challenging to predict the effect of the drugs in these patients from healthy volunteers.

Therefore, prompt identification of CV toxicity is of fundamental importance to i) reduce delays and costs of drug development, ii) increase the number of new drugs registered, iii) reduce the number of withdrawals, and above all iv) improve patient safety.

1.2.1 Cardiac ADRs

Cardiac arrhythmias are the most commonly reported CV ADRs. Between 1990 and 2006, one-third of all drug withdrawals occurred because of drug-induced Torsades de Pointes (TdP), a potentially fatal arrhythmia[18]. Over the last decade, progress has been made into understanding the molecular mechanisms of TdP with a physical read-out and biomarker of drug-induced TdP, i.e. the prolongation of the QT interval on the electrocardiogram and addressed by assessing the blockade of the human Ether-à-go-go- related gene (hERG) potassium (K^+) channel (Kv11.1)[19]. The availability of the biomarker, coupled with an understanding of the major molecular mechanism that underlies this ADR, has minimised the TdP risk through *in vitro* and *in silico* screening during early discovery.

In contrast, myocardial ischaemia, myocardial necrosis, heart failure and coronary artery disorders are not always identified during early drug development, and are reported at the post-approval stage[17], suggesting that current preclinical and clinical testing is failing to detect these liabilities. High-profile examples are the withdrawal of rofecoxib (Merck & Co., Inc.) in

2004 and valdecoxib (Pfizer, Inc.) in 2005, drugs that were associated with an increased risk of potentially fatal CV events[20,21].

Cardiac valve dysfunction, epicardial and endocardial disorders, and disorders affecting blood components are also not often reported during drug development and are more likely reported post-approval. This might be since these CV events are difficult to assess in preclinical models or are not deemed to be biologically significant at early stages, as the aetiology of drug-induced cardiac dysfunction is poorly understood, but then ADRs emerge when drugs are administered for longer periods of time to larger patient populations with a wide variety of co-morbidities. In principle, the risk of heart failure, cardiomyopathy and coronary artery disorders can be assessed by monitoring left ventricular function and coronary blood flow. There are sensitive and predictive imaging technologies such as ultrasound and magnetic resonance imaging to measure changes in cardiac function that might precede myocardial damage. However, these technologies are not routinely performed in preclinical studies unless triggered by other signals[22]. In addition, we are still unable to predict other serious ADRs, such as pericardial and endocardial disorders for which only histopathological examination is currently available.

1.2.2 Vascular ADRs

Drug-induced vasculitis is an inflammation of blood vessels that causes thickening, weakening, narrowing and scarring[23]. It is caused by a number of drugs, including antibiotics, psychoactive agents and anti-tumor necrosis factor-α (TNF-α) agents[23]. The pathogenesis of drug-induced vasculitis is unclear and there is no standard treatment. In addition, the only approach to stop the ADRs is treatment cessation.

Other vascular adverse events have been described as a serious consequence of some of the newer tyrosine kinase inhibitors (such as imatinib mesylate, which targets the abnormal gene BCR-ABL, used in the treatment of chronic myeloid leukaemia)[24]. These issues were initially unnoticed, but as clinical experience with these drugs evolved, vascular toxicity had become clearer with ADRs including pulmonary hypertension, acute and chronic arterial and venous occlusion, vasospastic phenomena and platelet dysfunction observed.

1.2.3 Translational problems between pre-clinical to clinical trials for cardiovascular drugs

One of the difficulties with preclinical evaluation of compounds is the limited translatability cross-species. There are numerous differences between animal species used in preclinical studies and humans and this is the reason why mice, rats, dogs, monkeys, guinea pigs, and zebrafish are used in preclinical studies. Despite over 95 % genome homology between mice and humans, there is great disparity between gene redundancies and regulation of gene expression levels.

There are also intraspecies differences. For example, laboratory mice have been developed as inbred strains and therefore will have a highly homogeneous genetic composition. A study reported that some mouse strains are fully resistant to Ebola virus, whereas other mice die without reporting specific symptoms[25]. This points to the complexity of *in vivo* models.

There have also been examples whereby mouse models have not accurately represented the human condition. For example, genetically engineered mouse models of cystic fibrosis

develop intestinal diseases similarly to humans but do not show the pulmonary complications that are a major part of the morbidity of human cystic fibrosis[26]. Therefore, preclinical *in vivo* studies need to be conducted in more than one species to give more confidence.

A comparative study of the vasculature of a range of mammals revealed that the peripheral vasculature of the human resembled that of the monkey closely, was similar to that of the dog, and was dissimilar to that of the pig, rat, guinea pig and rabbit[27]. Moreover, it is known that vessel distribution between species greatly differ. Coronary collateral flow in certain species is the most important factor involved in the rate and extent of cell death within an ischaemic area in myocardial infarction[28,29]. In species such as the pig, where there is no coronary collateral circulation, coronary occlusion will result in a region of severe ischaemia causing irreversible injury and cell death in the absence of reperfusion. In contrast, the dog has extensive collateral connections, which will reduce ischaemia, slow down cellular injury and may deliver sufficient blood to allow survival of the original ischaemic area. Although the rat is widely used in drug experimentation, its collateral flow status in myocardial ischaemia has not been extensively studied, however one study has shown that the rat is unique among species in that it has both extracardiac and intracardiac coronary collateral vessels[30]. Another study measured collateral flow during myocardial ischaemia in eight species and found it to be in this order: high (guinea pig); significant (dog and cat); minimal (rat); and zero (ferret, baboon, rabbit and pig)[31]. It has been speculated that the level of collateral flow in ischemia in humans depends on the age and pathology of each individual but is generally low[31]. These examples highlight the differences between species and the difficulty in finding a representative model of the human physiology.

Species differences in CV pathophysiology have been observed also with compounds that are toxic in animals and not in humans, such as caffeine that causes arteritis in rats[32]. Furthermore, there are differences in the human and laboratory animal immune system[33]. For example, interleukin-8 (IL-8), a chemokine responsible for the migration of neutrophils to the site of inflammation, is absent in the mouse, but present in humans. In most cases, there are limitations to the preclinical models used in drug development and this is the reason why numerous approaches are employed throughout the process.

1.3 Drug-induced Vascular Injury

Drug-Induced Vascular Injury (DIVI) is often reported with candidate drugs that reach the preclinical *in vivo* stage of development[34,35] and can cause considerable delays in the drug developmental process because compounds that cause DIVI in preclinical studies are often stopped from further development or the entire process delayed[35,36]. DIVI is also reported with drugs that are routinely used and the vascular complications will depend on the specific drug mechanism, e.g. anti-VEGF therapeutics that block endothelial growth in the treatment of certain types of cancers have an impact on vascular injury.

DIVI is difficult to detect due to the absence of specific and sensitive biomarkers cross-species, and the lack of *in vitro* models that are currently available to screen candidate drugs for DIVI risk during development. As such, DIVI is crudely defined through nonspecific cell death, vasoactive and inflammatory markers (**section 1.3.1**). So far DIVI has been documented in pathology (through histochemistry) and *in vivo* through changes in physiological cues. Furthermore, there remains speculation as to whether DIVI exists in humans, since no clinical observations have been reported as several drugs known to cause DIVI preclinically have caused no CV ADRs representative of DIVI. These will be discussed in more detail below. Besides histological methods, the non-invasive detection of DIVI in animals or humans is currently not possible due to the absence of biomarkers. The need to confirm that a candidate drug is safe for administration to humans, when toxicity is observed preclinically, remains.

1.3.1 Histopathological signs of DIVI

DIVI is characterised by arterial lesions. The anatomy of the large vessels consists of three tunicae: (1) intima, composed of endothelial cells (EC); (2) media, composed of smooth muscle cells (SMC) and bounded by a porous internal and external elastic lamina; and (3) adventitia, composed mainly of fibroblasts that in large vessels are surrounded by vasa vasorum (small blood vessels), and adipose tissue, macrophages, mast cells, and nerve terminations (**Figure 1.2**).

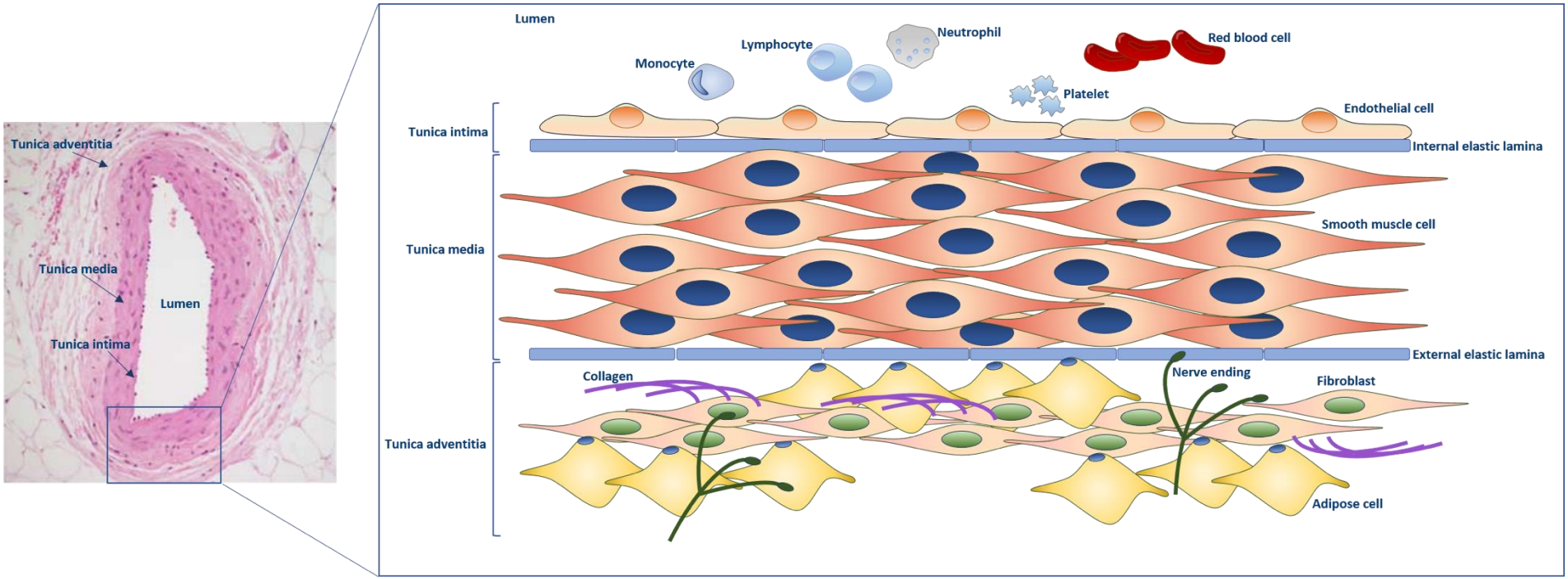

Figure 1.2 Structure of the arterial wall. The arterial wall is composed of three layers: tunica intima (endothelial cells and internal elastic lamina), tunica media (smooth muscle cells and external elastic lamina), and tunica adventitia (perivascular adipose tissue cells, fibroblast cells, collagen fibers and nerve endings). Image on the left is taken from[203], image on the right is the author's own drawing.

DIVI was first identified using histology in the late 1970s[37], characterised by arterial lesions in selected vascular beds that are induced within hours of drugs administration in rats, mice, dogs, pigs, and monkeys. A lesion is defined as a histopathologic change, characterised by haemorrhage, inflammation, endothelial activation (the endothelium remains intact but gaps are formed between EC) and SMC necrosis to the vessel structure (**Figure 1.2**). This can range from barely noticeable (in mild lesions) to severe, resulting in significant tissue or organ dysfunction or failure[38].

Common histopathological signs of DIVI in rats and dogs are shown in **Figure 1.3.** In the rat, DIVI mostly affects mesentery arteries and generally only large calibre arteries with an external diameter of 100-800 μm[38–46]. In these studies following 24 hours of drug treatment, lesions are characterised by mild to moderate perivascular accumulation of mononuclear inflammatory cells, with necrosis and haemorrhage within the tunica media. Although the endothelium was generally intact, there was significant loss of SMC, and the red blood cells (RBC) were observed in the cavities vacated by dead SMC[39]. The lesions typically diminished over 3-14 days as leukocytes (mainly macrophages, T-cells and B-cells) adhered to the endothelium and fibroplasia (the process of forming fibrous tissue) occurred. This process has been shown in arterial lesions where damage evoked by dopaminergic agonists such as dopamine and fenoldopam undergo regeneration or repair[39]. In this study, lesions induced by dopamine were repaired in all rats as observed morphologically by 14 days after exposure to dopamine[39]. Lesions induced by fenoldopam also had undergone significant repair by 28 days, however these arteries had a thickened media surrounded by adventitial fibrosis. The presence of scar tissue could lead to narrowing of blood vessels, reduced physiological blood flow or reduced ability of the vessel to dilate causing secondary problems. However, it has been noted that vessel repair tended to depend on the specific experimental design and the literature is conflicting on this point[34].

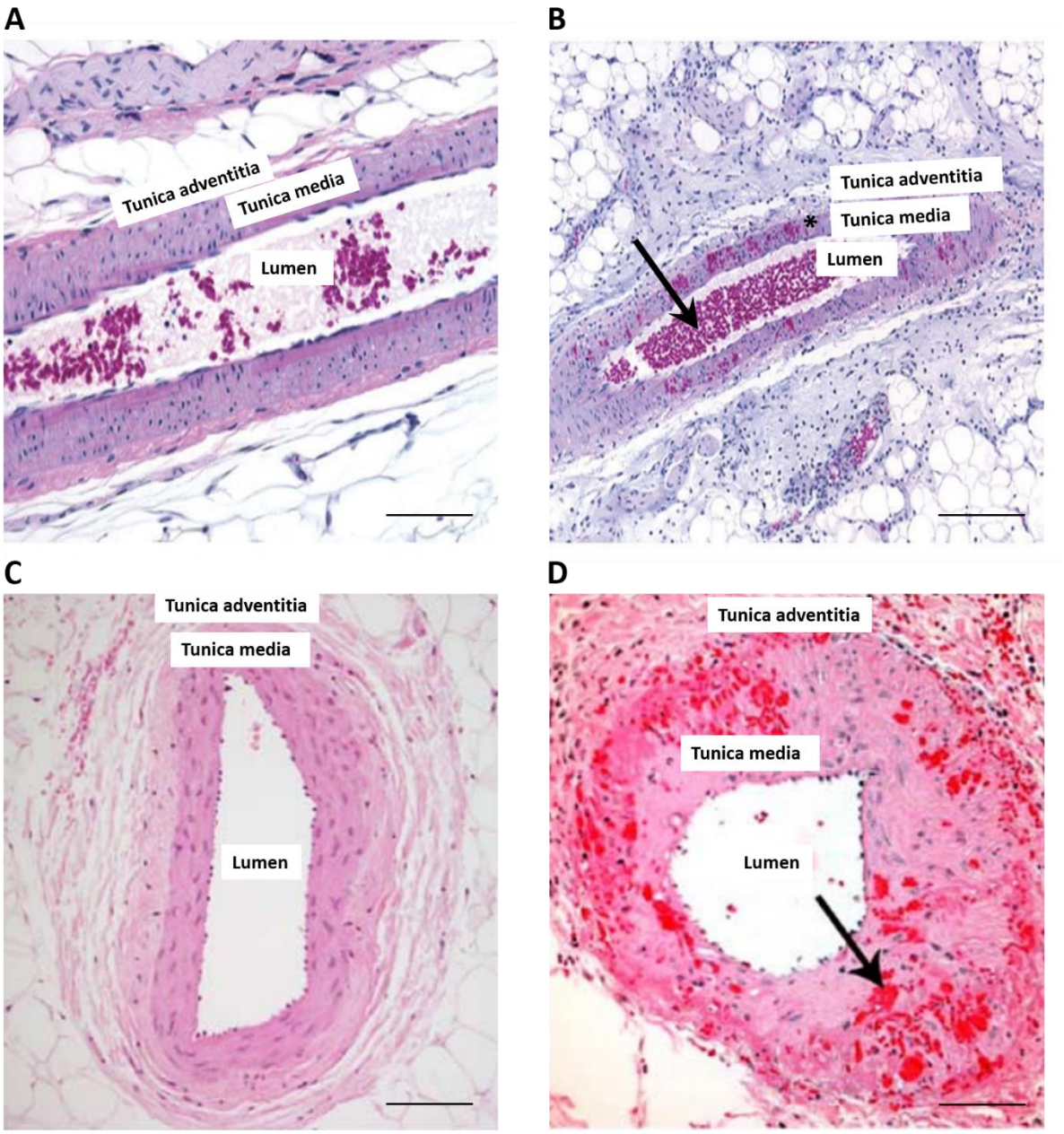

Figure 1.3 Haematoxylin and eosin staining of rat and dog arteries. (A) Mesentery artery of a control rat with no vascular injury present; (B) Mesentery artery of a rat 24 hours after treatment with fenoldopam showing perivascular accumulations of mononuclear cells (arrow) along with haemorrhages in the media (*)[38]; (C) Coronary artery of a control dog; (D) Coronary artery of a dog treated with a K^+ channel opener showing RBC infiltrate into the vessel wall (arrow)[203]. Scale bars represent 200 µm. Taken from[38,203].

In studies conducted in the dog, in all vessels investigated, DIVI primarily affected 200-500 µm epicardial segments of the left and right coronary arteries[47,48,57–63,49–56]. The histology and time frame were similar to that seen in the rat, consisting of necrosis of the tunica media with accumulation of RBC. In advanced lesions, all vascular tunicae shown in **Figure 1.2** were involved and in addition haemorrhage and accumulation of mononuclear and polymorphonuclear leukocytes, and proliferation of fibroblasts occurred in the tunica adventitia. Studies in dogs reported petechial and ecchymotic haemorrhages predominantly on the epicardium of the right atrium and coronary arteries of the atrioventricular groove[35]. Microscopically, arterial lesions were characterised by distensive haemorrhagic necrosis with inter-endothelial separation and adhesion of leukocytes and platelets. Images taken with scanning electron microscopy (SEM) showed severe EC and SMC damage, with RBC occupying cavitations in the SMC and leukocytes adhering to the lumen in the inter-endothelial gaps (**Figure 1.4**). Similarly to the rat model, it was shown that lesions in dogs resolved with time. For example, dogs treated with the opener of K_{IR} (inward rectifier) 6.X ATP sensitive K^+ channels minoxidil the lesions were evaluated at 1,3,10 and 34 day post-dosing and it was observed that substantial repair of the arterial lesions occurred such that by day 34, all sections of extramural coronary artery were apparently normal[61].

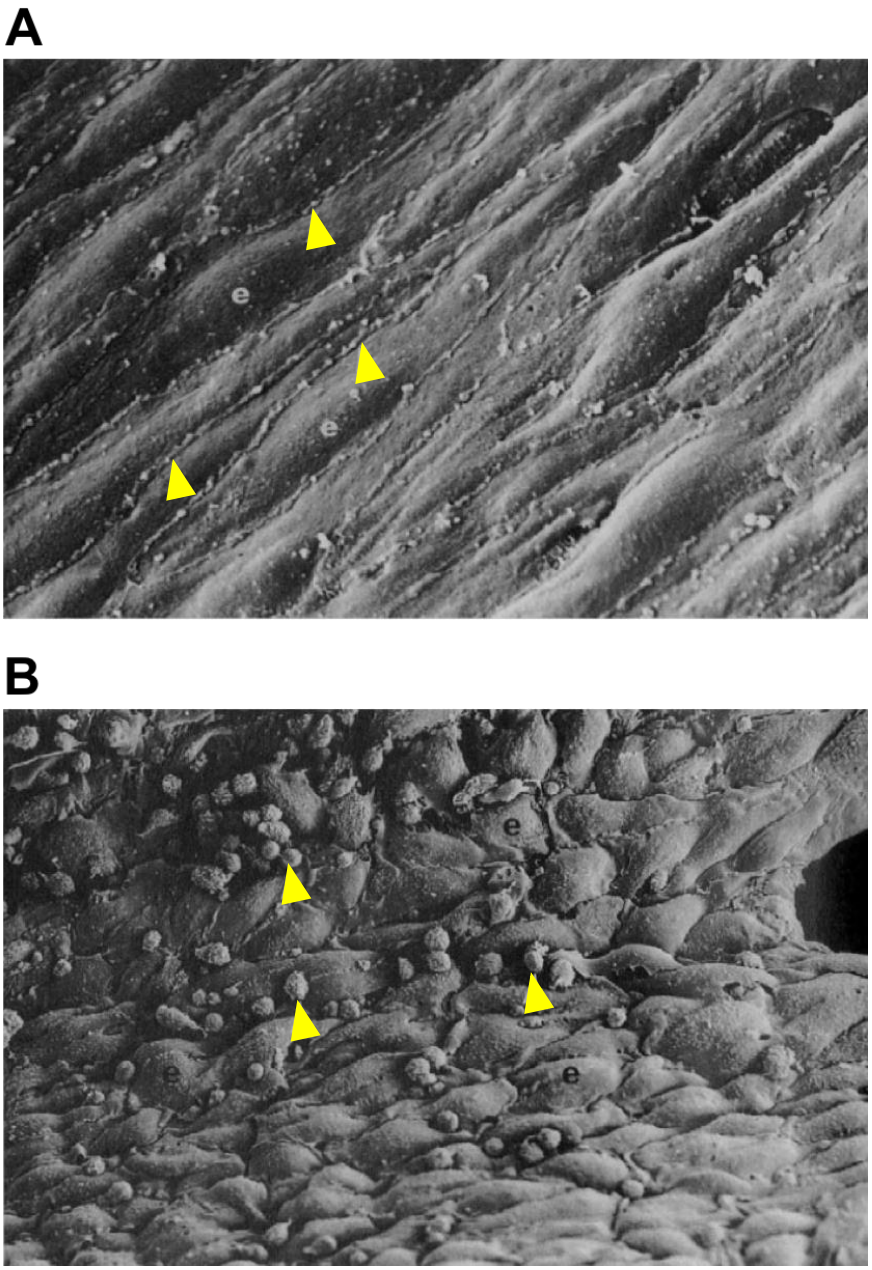

Figure 1.4 Scanning electron microscope images of a control dog and a dog treated with SK&F 95654. A represents a dog control coronary artery, where EC (e) are flattened and demarcated by closely apposed, raised, irregular plasmalemmal ridges (arrowheads). 3200x. B represents a dog treated with SK&F 95654 for 24 hours, where EC (e) appear more rounded with gaps present at the intercellular boundaries. Numerous inflammatory cells (arrowheads) adhere to the surface, often lying at the intercellular boundaries. 800x. Taken from[61].

In larger mammals (e.g. pigs and monkeys), studies have shown that DIVI lesions are similar to those described in the dog and consist of medial necrosis with cellular debris and inflammation in the intima, media and adventitia[64,65]. Interestingly, arterial lesions have been also described in the small and large intestines and testis. In some affected vessels, inflammatory cell infiltrates were accompanied by intimal proliferation in more severe lesions, marked fibrinoid necrosis was present in the tunica media, with loss of the internal elastic lamina. Necrotic vessels had edema and numerous inflammatory cells in the tunica adventitia and surrounding tissues. In severely affected vessels, the lumen was often occluded by intimal proliferation, inflammatory cells, necrotic debris, and thrombus formation. Veins, venules, arterioles, and capillaries were usually unaffected.

A timeline of the lesion development in the different species described is depicted in **Figure 1.5**.

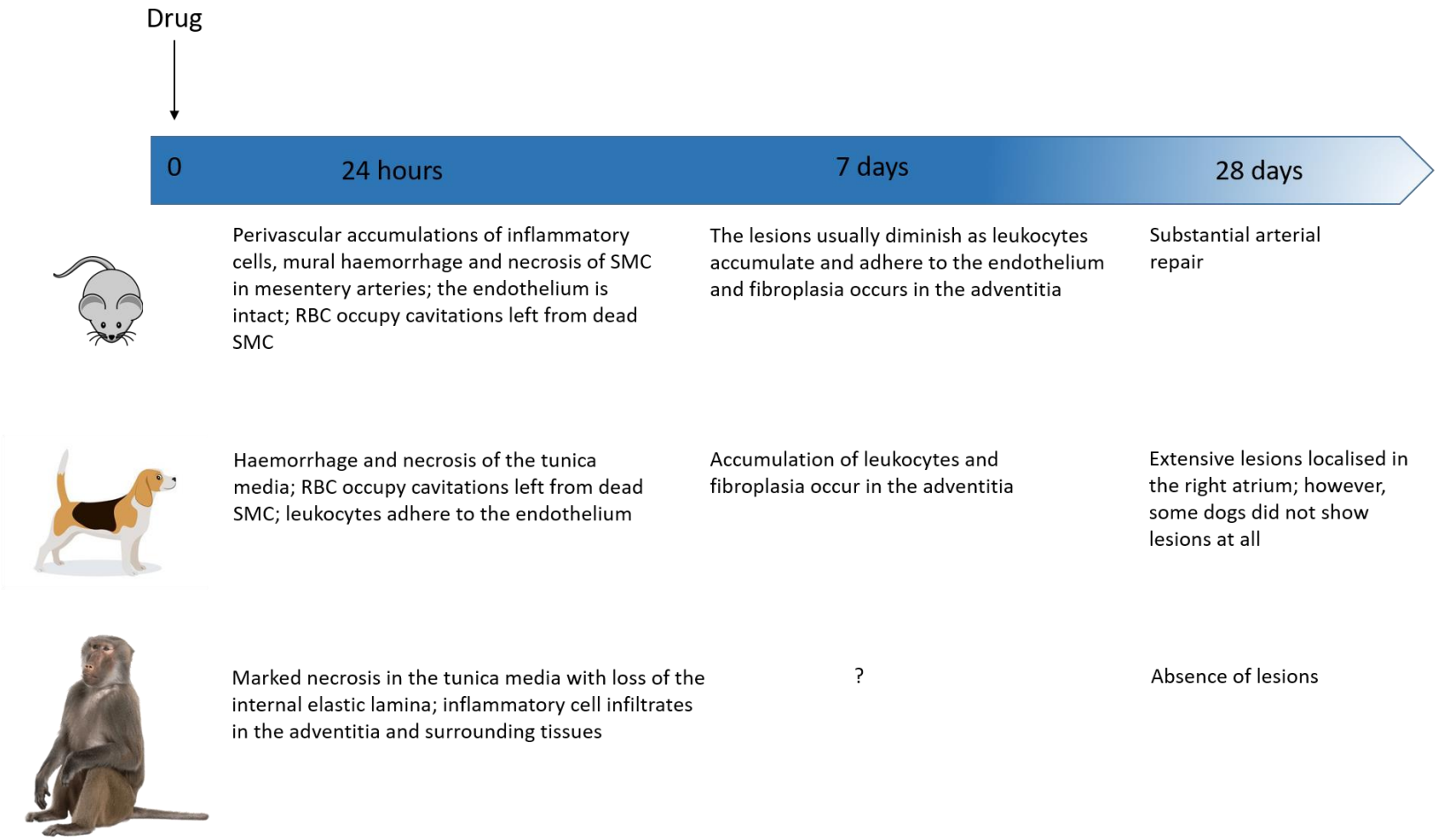

Figure 1.5 Timeline of the development of the lesions in DIVI in rats, dogs and monkeys.

Spontaneous or background lesions such as arteritis in control animals have been reported in almost a quarter of studies performed during drug development in rats and dogs and confound the identification of DIVI[47,49,66]. These spontaneous lesions usually develop with age in hypertensive rats, and have also been reported in dogs[57].

One method to differentiate spontaneous lesions from DIVI may be to assess the nature and distribution of the lesions. Spontaneous arteritis usually occurs in medium to small arteries in many organs, in addition to the mesentery and coronary arteries; haemorrhage in the tunicae media and adventitia is absent in spontaneous arteritis whereas is always present in DIVI[47].

In addition, polyarteritis nodosa, an idiopathic vasculitis, affects small to medium-sized arteries in several vascular beds in humans[67,68]. Rash is a common manifestation of human drug-induced vasculitis, where eosinophils are prominent in biopsies[69,70]. Neither rash nor eosinophils are common in DIVI.

The tissue specificity of DIVI can be linked to differences in flow in different vascular beds (refer to **Introduction 1.7**) and depends on the mechanism of the specific drug.
Currently, there are multiple biomarkers available for DIVI (summary tables of these biomarkers are provided later in this chapter), however there is not a robust marker that translates across species and is observed in all vascular beds. Moreover, the current available biomarkers are assessed post-mortem using histopathology, providing limited utility as a clinical diagnostic. The ideal marker would ideally have the following characteristics: (1) it should be specific and sensitive, and correlate with the severity of damage; (2) it should detectable very early, before any histopathological damage; (3) it should return to baseline values when there is no further cell and/or tissue damage; (4) it should be accessible in the circulation for easy monitoring without requiring an intrusive biopsy; and finally (5) it should be translational, i.e. it should bridge across species.

1.3.2 Physiological signs of DIVI

Many of the potent vasodilators, such as the opener of K_{IR} (inward rectifier) 6.X ATP sensitive K^+ channels minoxidil, phosphodiesterase (PDE) III inhibitors, and hydralazine are associated with significant haemodynamic changes, sufficient to induce marked reflex tachycardia, and CV lesions[51,52,61,71,72]. These drugs progress to clinical studies where patients are monitored for changes in blood pressure and heart rate, and doses that cause marked decreases in systemic vascular resistance, hypotension, and reflex tachycardia are avoided. However, other drugs do not induce significant systemic changes, but rather cause local increases in blood flow in selected vascular beds[62,73,74]. This will be explored more in detail in the mechanisms of DIVI (section **1.5.1**).

1.4 Drugs that cause DIVI

1.4.1 Approved or approvable drugs responsible for vascular injury in animals

Many drugs associated with DIVI in preclinical animals are known vasodilators. In the past, it was generally accepted that as long as therapeutic doses of candidate drugs in humans did not cause marked hypotension and reflex tachycardia, these drugs progressed to clinical studies[34,51,61,75]. Therefore, some drugs reported to produce DIVI in animal models have been developed and are currently on the market, as no adverse events in humans were observed[76]. However, recent studies have suggested that vascular injury is not always associated with profound systemic hemodynamic changes in blood pressure and heart rate, meaning that these parameters are of little clinical value to monitor vascular injury in humans[56,74]. Therefore, there is a need to identify whether DIVI occurs in humans, and if so, work toward generating tools to assess this adverse event both preclinically and clinically.

DIVI incidence has been reported with at least six different pharmacological classes of drugs in preclinical species. Examples of approved or approvable drugs that cause arterial toxicity in animals but not in humans are summarised in **Table 1.1** and include: PDE III and IV inhibitors, DA_1 and A_1 agonists, K^+ channel openers, and ET receptor antagonists. This is not an exhaustive list and other compounds have also been shown to induce DIVI. **Table 1.1** also illustrates the drugs that have been selected for the experiments within this PhD thesis (inside

the red box). Four drugs with different mechanisms of action have been selected: bosentan, an ET receptor antagonist, fenoldopam mesylate, a DA_1 agonist, minoxidil sulfate, an opener of K_{IR} (inward rectifier) 6.X ATP sensitive K^+ channels and rolipram, a PDE IV inhibitor. The drugs in **Table 1.1** are considered safe in humans, as no evidence of clinical risk has been reported. The reason for selecting drugs from four different pharmacological classes was to understand whether a common underlying mechanism of DIVI exists among them. A summary of the commercial uses, dosage and half-life of these drugs in humans is also presented in **Table 1.1**, and experiments conducted in animals with these and other drugs reported to cause DIVI in animals are listed in **Table 1.2**.

Drug	Pharmacological class	Commercial use	Dosage in humans	Half life	Reference
Bosentan	ET receptor antagonist	Treatment of pulmonary artery hypertension	62.5 mg/125 mg (tablets)	5 hours	35,62,77,78
Fenoldopam mesylate	DA_1 agonist	Treatment of hypertension	10 mg/ml (intravenous)	5 minutes	76,79,80
Minoxidil sulfate	K^+ channel opener	Treatment of resistant hypertension and alopecia	2.5 mg/10 mg (tablets) for hypertension; 2-5 % solution (topical) for alopecia	3-4 hours	50,57,81,82
Rolipram	PDE IV inhibitor	Antidepressant (only used in preclinical and clinical research)	n/a	3 hours	83
Cilomilast	PDE IV inhibitor	Under development to treat respiratory disorders	n/a	7 hours	34
Hydralazine	?	Treatment of hypertension	25 mg/50 mg (tablets) 200 µg/min (intravenous)	7 hours	34
Adenosine	A_1 receptor agonist	Treatment of tachycardia	6 mg/second (intravenous)	10 seconds	34
Nicorandil	K^+ channel opener	Treatment of angina	5-10 mg (tablets)	1 hour	34

Table 1.1 Approved or approvable drugs that cause arterial toxicity in animals. The drugs used in this thesis are highlighted in the box.

Drug	Pharmacological class	Physiological signs	Histopathological signs	Species	Administration route	Dosage	Time course	Reference
Bosentan	ET receptor antagonist	No significant change in blood pressure nor heart rate	n/a	n/a	n/a	n/a	n/a	[35,62,77]
SB209670	ET receptor antagonist	No significant change in blood pressure nor heart rate	Medial haemorrhage and necrosis of extramural coronary arteries	Dog	Continuous infusion	50 µg/kg/min	5 days	[62,77]
Dopamine	DA_1 agonist	Increase in blood pressure (mediated by D_2, D_3, D_4 receptors)	Lesions of small calibre mesentery arteries, medial necrosis but little hemorrhage	Rat	Continuous infusion	5 µg/kg/min	24 hours	[39]
Fenoldopam mesylate	DA_1 agonist	Decrease in blood pressure	Perivascular accumulations of neutrophils in adventitia, haemorrhage and necrosis in media	Rat	Continuous infusion	1-100 µg/kg/min	4,8,24 hours	[38,39,76,84,85]
Minoxidil sulfate	K_{IR} 6.X (K^+ channel) opener	Decrease in blood pressure, reflex tachycardia	Coronary/mesentery arterial injury, necrosis, hemorrhages	Rat, dog, monkey	Oral gavage	10-100 mg/kg	Up to 1 year	[37,50,57,81]
CI-1044	PDE IV inhibitor	Decrease in blood pressure	Hemorrhage and necrosis in the mesentery with periarterial inflammation	Rat	Oral gavage	10-60 mg/kg	Up to 3 days	[86]

Rolipram	PDE IV inhibitor	No significant change in blood pressure nor heart rate	Necrosis in coronary and mesentery arteries, and inflammation	Rat	Oral gavage	10-100 mg/kg/day	Up to 2 weeks	[83]
SCH 351591 and SCH 534385	PDE IV inhibitor	No significant change in blood pressure nor heart rate	Hemorrhage and necrosis in the mesentery but also pancreas, kidney, liver and stomach. Lesions characterised by fibrin deposition and perivascular inflammation	Rat, monkey	Oral gavage	3-80 mg/kg/day	Up to 3 months	[87,88]
SK&F 95654	PDE III inhibitor	Decrease in blood pressure	Perivascular accumulations of neutrophils in adventitia, haemorrhage and necrosis in media	Rat, dog	Oral gavage	200 mg/kg	4,8,24 hours	[38]

Table 1.2 Drugs responsible for causing DIVI in animals.

1.4.2 Selected DIVI drugs

This section provides more background information on the four drugs studied within this thesis.

Bosentan, is currently used to treat pulmonary artery hypertension, and is an oral dual endothelin receptor antagonist given at a dose of 1.2 mg/kg in humans and reaching a plasma concentration of 3366 ng/ml, acting on both ET_A (Ki=6.5 nM) and ET_B (Ki=343 nM) receptor subtypes but with a greater effect on ET_A[78] (**Figure 1.6**). Metabolic products of bosentan have not yet been investigated. Although histopathological signs of DIVI have not been described with bosentan in preclinical models, the drug has been chosen as it has been suggested as potential DIVI-related drug by several reviews[36,77]. Endothelin is a peptide predominantly produced by the endothelium and to a lesser extent by SMC and fibroblasts[78]. There are three endothelin isoforms, ET-1, ET-2, and ET-3, encoded by three distinct genes[89]. ET-1 is the most abundant isoform in the human CV system. ET-1 and ET-2 activate two receptors, ET_A and ET_B with equal affinity (Ki value ET-1 and ET-2 on ET_A = 0.4±0.2 nM; on ET_B = 0.2±0.0 nM), whereas ET-3 has a lower affinity for the ET_A subtype[90] (Ki value on ET_A = 820±260 nM; on ET_B = 0.4±0.2 nM). ET_A and ET_B are ubiquitously distributed on various cell types and are part of the G-protein-coupled receptor (GPCR) family. Only the ET_B subtype is expressed on EC, whereas SMC express both subtypes[91]. The two receptor subtypes exhibit contrasting CV actions under normal physiologic conditions. After release from EC, endothelin causes vasoconstriction, mainly via ET_A receptors on SMC that are the main subtype in the vascular tunica media in large arteries and veins[90]. Binding of ET-1 to ET_B receptors on EC stimulates the production of nitric oxide (NO) from L-Arginine, resulting in relaxation of SMC. This receptor distribution offers an explanation as to the phenomenon that ET-1 causes transient vasodilation (initial EC ET_B activation), followed by prolonged vasoconstriction through ET_A on SMC.

In dogs, continuous administration of SB209670, a dual endothelin antagonist, for five days at 50 µg/kg/min was associated with minor but sustained increases in heart rate, slight decreases in arterial pressure, and signs of DIVI as shown by medial haemorrhage and necrosis of extramural coronary arteries in the right atria[77] (**Table 1.2**). The lesions in the right atrium were associated with the highest density of endothelin receptors[62].

Radio ligand protein binding was used to quantify both endothelin subtype receptors in untreated healthy dog heart. The results showed a two-fold higher density of endothelin receptors in atrial regions versus ventricular regions and a 6-fold higher density of endothelin receptors in coronary arteries compared to that in atria or ventricles. Endothelinreceptor subtype characterization showed that ET_B receptors were three times more prevalent in right compared to left coronary arteries and *in situ* hybridization confirmed the abundance of ET_B in SMC in right coronary arteries, whereas ET_A receptor density was comparable in right and left coronary arteries in SMC. It was concluded in this study that the disproportionate distribution of ET_B receptors within right coronary artery predispose dogs to exaggerated pharmacological responses and subsequent damage to right coronary arteries by endothelin and/or endothelin receptor antagonists. *In vitro* studies in dog[92] and pig coronary arteries[93], in rabbit veins[94] and in rat systemic circulation[95] indicated that the physiological effect of ET_B receptor signalling (vasoconstriction/vasodilation) can differ between species and vascular bed, and this occurs because GPCRs are known to have multiple functional roles[96,97], which could explain differences in DIVI in terms of site and resolution of the lesions among different species.

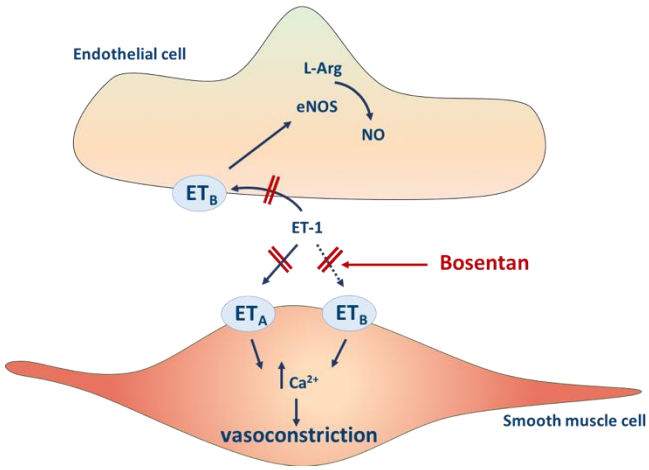

Figure 1.6 Mechanism of action of bosentan. ET-1 released from EC causes prolonged vasoconstriction of SMC via ET_A (mainly) and ET_B receptors on SMC by increasing intracellular. ET_B receptors on EC mediate transient vasodilation of SMC via production of NO in EC. Bosentan is a dual antagonist on ET_A and ET_B receptors that causes vasodilation.

Fenoldopam is a selective DA_1 agonist (Ka of 0.018±0.008 µM and efficacy of 0.46±0.11 as opposed to DA Ka of 0.58±0.17µM and efficacy of 1.0), that has been shown to increase

vascular levels of cyclic adenosine monophosphate (cAMP) in the rabbit mesentery artery[80] (**Figure 1.7**). Fenoldopam produces significant falls in systolic and diastolic blood pressures and is currently used as an antihypertensive agent in humans. A study has also revealed that, in addition to being a DA_1 agonist, fenoldopam is also an antagonist at α_2-adrenoceptors[98]. Fenoldopam was evaluated for its ability to inhibit both α_1- and α_2-adrenoceptors in rabbit, dog and guinea pig vessel explants enriched with those receptor subtypes[98]. In rabbit isolated aortic rings, fenoldopam was a weak antagonist of α_1-mediated contraction induced by noradrenaline. In contrast, in isolated dog saphenous venous rings where α_2-adrenoceptors mediate vascular contraction, fenoldopam was found to be a potent antagonist. Fenoldopam has no significant affinity for DA_2, 5_{HT1} and muscarinic receptors. It was found to have a moderate affinity for 5_{HT2} receptors (pK_A of 5.84±0.04 and efficacy of 0.57±0.04 as opposed to pK_A of 6.65±0.12 and efficacy of 2.66±0.41 of 5_{HT}[80].

Fenoldopam induces mesentery arterial lesions in rats but not dogs nor monkeys[85]. In a study in rats, fenoldopam did not induce arterial lesions in rats infused intravenously with the drug for 1 or 4 hours at 50 µg/kg/min, however at 5 and 100 µg/kg/min for 24 hours, fenoldopam caused medial necrosis and haemorrhage[85]. The endothelium of affected arteries was intact, except in areas of severe medial damage. The internal elastic lamina and connective tissue within the arterial wall were also unaffected. Haemorrhagic areas showed aggregates of RBC occupying the space of necrotic SMC. Several other studies observed similar effects[38,99,100]. Importantly, studies in conscious spontaneously hypertensive rats found that fenoldopam produced a dose-dependent reduction in arterial blood pressure and increases in renal and mesenteric blood flow, providing evidence for the role of local flow changes in the pathogenesis of DIVI[101]. In the clinic, fenoldopam reaches a plasma concentration of 30 ng/ml when administered at 0.8 µg/kg/min as a continuous IV infusion.

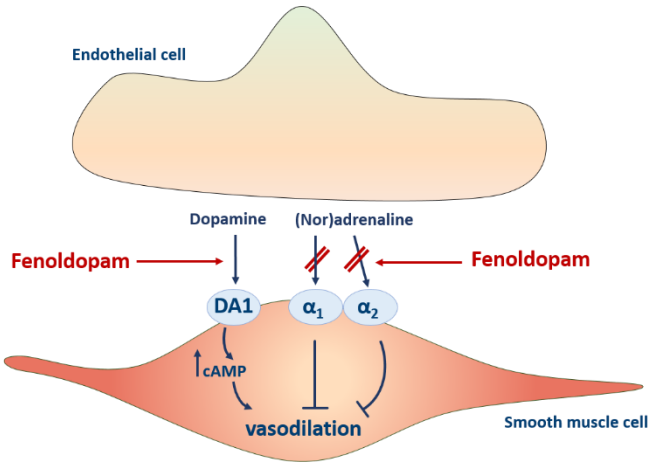

Figure 1.7 Mechanism of action of fenoldopam. Physiologically, adrenaline and noradrenaline activate both α_1 and α_2 receptors, causing vasoconstriction of SMC. Dopamine activates DA_1 receptors, causing an increase in cAMP and subsequent vasodilation. Fenoldopam acts as an agonist of DA_1 receptors and as a weak antagonist of α_1 and a potent antagonist to α_2 receptors, inducing vasodilation.

Minoxidil is an agent used to treat resistant hypertension for patients who have not responded to conventional multidrug antihypertensive regimens, and is also used to treat alopecia as it increases local blood flow[82]. It is administered at a maximum dose of 100 mg/day in adults, at which the plasma concentration observed is 2441 ng/ml. The antihypertensive activity of minoxidil is due to its sulphate metabolite, minoxidil sulfate. It is thus administered as a prodrug. Minoxidil acts by opening adenosine triphosphate (ATP)-sensitive K^+ channels in vascular SMC (**Figure 1.8**), and specifically it is an opener of K_{IR} (inward rectifier) 6.X ATP sensitive K^+ channelsThe predominant site of minoxidil is arterial, and venodilation does not occur with minoxidil treatment (likely due to a higher density of channels in arteries as opposed to veins)[82]. The mechanism by which minoxidil induces hair growth has also been related to the action on K^+ channels[82]. In animals, minoxidil has been studied in mice, rats, dogs, pigs and monkeys and its effects have been investigated for up to one year[37,52]. Minoxidil was found to cause hypotension, tachycardia, and increased blood flow to several tissues, especially to the heart, together with coronary arterial injury, right atrial haemorrhagic lesions and subendocardial necrosis in dogs[52]. The specific lesions observed in the right atrium in dogs were absent in the other species[37]. In the same study, when the

treatment continued for up to one year, some dogs did not show prolonged lesions, suggesting a potential resolution of the injury.

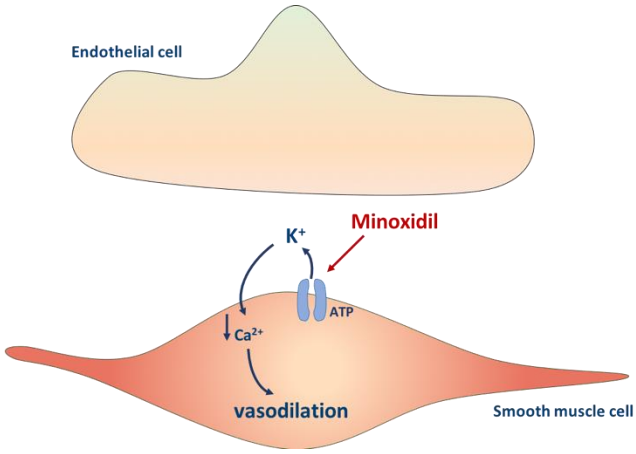

Figure 1.8 Mechanism of action of minoxidil. Minoxidil acts by opening the ATP-sensitive K^+ channels on SMC, increasing the efflux of K^+, which causes membrane hyperpolarisation, a reduction in Ca^{2+} entry and intracellular Ca^{2+}, resulting in relaxation of SMC and vasodilation.

Rolipram is a phosphodiesterase (PDE) IV inhibitor (Ki of 0.6 µM), one of the 30 PDE forms responsible for hydrolysing cAMP, and therefore causes an increase in calcium (Ca^{2+}) and consequent vasodilation[102] (**Figure 1.9**). Although rolipram is highly specific for the PDE IV enzymes, it is non-selective within the PDE IV multigene family. Therefore, at therapeutic doses, it inhibits all PDE IV isoenzymes to an equal degree[103]. Originally designed to treat depression, rolipram has also been used to treat asthma, arthritis, multiple sclerosis and Alzheimer's Disease[104–107]. It is used in clinical trials at an oral dose of 1 mg, at which the peak plasma concentration reached is 16 ng/ml. SCH 351591 and SCH 534385 are two PDE IV inhibitors that induced vascular injury primarily in rats in the mesentery arteries but also in the pancreas, kidney, liver and stomach[87]. Vascular lesions occurred as early as one hour but were not detected after nine days. The pathology of the lesions consisted of haemorrhage and necrosis, fibrin deposition, and perivascular inflammation of various blood vessels. Activation of mast cells, EC and macrophages was also common. SCH 351591 showed toxicity also in monkeys, where perivascular haemorrhage of the stomach and heart were common features[88]. In addition, inflammation of small to medium-sized arteries in various organs

including the heart, stomach, pancreas and kidneys was observed in this study. SCH compounds have not been used in this thesis but they are worth investigation in the future.

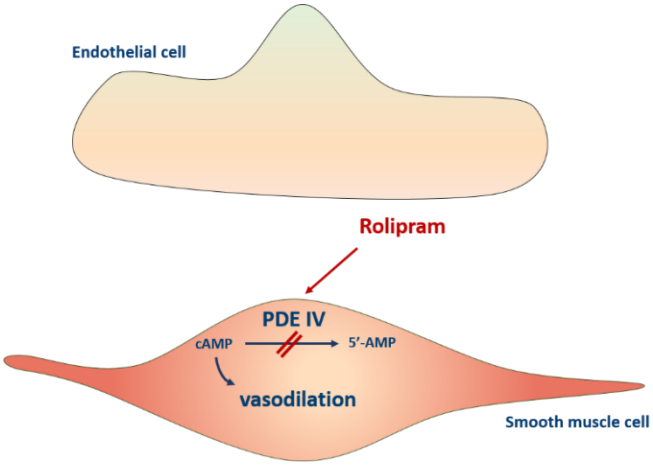

Figure 1.9 Mechanism of action of rolipram. Rolipram acts by inhibiting PDE IV, the enzyme responsible for the hydrolysis of cAMP. This results in an increase of cAMP and consequent vasodilation.

Other PDE IV inhibitors that induced arterial lesions in rats are CI-1044[38,108], and SCH 351591 and SCH 534385[87], and are summarised in **Table 1.2**. The effects of SK&F 95654[38], a PDE III inhibitor, are also listed in **Table 1.2**.

1.5 Mechanisms of DIVI

The mechanisms that underlie DIVI remain to be established, although three hypotheses have been proposed: (1) drugs alter hemodynamics which then has a detrimental effect on the endothelium; (2) direct drug toxicity on vascular cells (EC, SMC) or circulating blood cells; (3) inflammation. Most likely, it is a combination of these mechanisms inducing DIVI.

1.5.1 Mechanism 1. Hemodynamic alterations

The vasoactive pharmacology of compounds reported to cause DIVI has been suggested to be the reason of their arterial toxicity. PDE III inhibitors, minoxidil, dopamine and DA_1 agonists, potent vasodilators that induce systemic changes in mean arterial blood pressure (see **Table 1.2**), have been all shown to produce arterial lesions[56,76,109]. Among the DA_1 agonists, fenoldopam has been associated with marked vasodilation and arterial lesions in the rat, dog, and monkeys[40,43,110]. Fenoldopam is also responsible for acute lesions in large calibre (100-800 µm) splanchnic and renal arteries of rats[76]. However, when administered with DA_1 receptor antagonists, or with the potent vasoconstrictor methoxamine, the lesions were prevented[40,71]. In a similar way, arginine vasopressin, a vasoconstrictor, prevented the vasodilator PDE III inhibitor SK&F 95654 from inducing mesenteric lesions[76]. This indicates that vasodilation may be a causal factor in the development of DIVI.

Nonetheless, recent work with ET receptor antagonists, which did not induce these systemic changes and still caused DIVI, suggests that reduced mean arterial pressure and increased heart rate are not prerequisites for development of coronary artery injury in dogs[62,73,74]. For example, SB 209670, an ET receptor antagonist, caused a 6-fold increase in coronary blood flow and arterial lesions in dogs, but did not significantly increase the heart rate or decrease the mean arterial pressure[62]. It was thus suggested that DIVI may be induced by a local increase in blood flow in specific tissues rather than a systemic change in blood pressure. Furthermore, minoxidil not only caused systemic hemodynamic changes but also induced a 6-10 fold increase in regional cardiac blood flow and coronary arterial lesions in dogs[52,111], also suggesting that it may be local haemodynamic change that is important, not systemic

change. Minoxidil, SK&F 95654 and fenoldopam have been reported to increase mesenteric blood flow in rats[76] and an increase in coronary blood flow and coronary lesions in dogs have been observed with compounds from different classes[60,62,112].

These data indicate that arterial lesions develop in coronary arteries in dogs and mesentery arteries in rats potentially due to sustained vasodilation in particular vascular beds (the most responsive to the pharmacological action of the drug) and the consequent increase in blood flow.

Altered shear stress (the frictional force generated by blood flow on EC) in regions such as branching points where shear stress is very high[113], can result in leukocyte adhesion, inter-endothelial breaks, gradual breakdown of vessel wall integrity, breaks in the internal elastic lamina, and haemorrhage[43,76]. Moreover, it has been hypothesised that vasodilation induced by certain drugs causes normal laminar flow to change into turbulent flow that mimics shear stress alterations thereby producing a cascade of events that eventually culminates in haemorrhage and necrosis[100]. Monitoring regional blood flow, even though it is correlated with vascular injury in dogs and rats, is not practical during clinical trials, as the procedure is tedious, low throughput and requires specialised equipment and skilled technicians. Furthermore, it is not clear which vascular beds should be monitored in terms of DIVI assessment.

However, an *in vitro* study with the PDE IV inhibitor CI-1044 found that one of the features of DIVI, extravasation of RBC, occurred without changes in blood flow, which implies that for some drugs it may not be a local increase in blood flow that causes DIVI but rather a direct mechanism on vascular and circulating blood cells[114], described in the sections below.

1.5.2 Mechanism 2. Direct pharmacological or chemical toxicity on vascular and circulating blood cells

Vascular toxicity results from the pharmacological interaction with a target that initiates a cascade of events leading to vascular damage. Drugs involved in inducing direct toxicity are classes of cancer drugs and some immunomodulators[115–118]. Damage to EC by cancer drugs is

related to their pharmacological activity, but hemodynamic factors may also be involved[119,120]. It is also possible that they release secondary signals such as NO. It is impossible to differentiate between direct cell toxicity and flow being the major cause of DIVI, certainly these drugs may act as modulators of both mechanisms *in vivo*.

1.5.2.1 NO as a cytotoxic secondary signal

Nitric oxide (NO) is a short-lived second messenger responsible for maintaining vascular tone by inducing relaxation of SMC[121]. However, significantly elevated levels of NO can induce increase levels of reactive oxygen/nitrogen species (ROS/RNS) (**Figure 1.10**). ROS induces oxygenation of lipids, proteins and DNA, which cause cell damage, necrosis and apoptosis[122] and RNS induce nitrosylation reactions that alters the structure and function of proteins. These effects result in EC apoptosis, SMC proliferation and fibrosis. Serum nitrite is a stable breakdown product of NO and it has been reported to be elevated in DIVI, indicating a potential correlation between NO and DIVI development[108,123,124]. Indeed, a NO donor increased the induction of DIVI, whilst a nitric oxide synthase (NOS) inhibitor reduced DIVI. Fenoldopam, a dopaminergic-1 agonist, caused NO-mediated mesentery artery injuries in rats[100]. It has been suggested that DIVI-related drugs act through this common mechanism involving RNS[125].

NO is made by 3 isoforms of NOS: inducible NOS (iNOS), endothelial cell-specific NOS (eNOS), and neuronal NOS (nNOS)[126]. eNOS is constitutively expressed, and for this reason the regulation of its activity is essential for normal function. Alteration in eNOS signalling has also received attention as a pathogenic factor of DIVI. Studies showing increased expression of nitrotyrosine, an indirect indicator of NO *in vivo*, and iNOS (source of NO) on EC and SMC suggest that NO produced by activated SMC and EC play an important role in injuries induced by vasodilatory compounds[124,127,128]. There is also some evidence of altered eNOS signalling with vasoconstrictors[125]. Furthermore, macrophages produce reactive oxygen intermediates, which combined with nitrogen intermediates, can cause protein nitration of EC, i.e. the introduction of a nitro group ($-NO_2$) into proteins, which can induce post-translational modifications and affect their function[129].

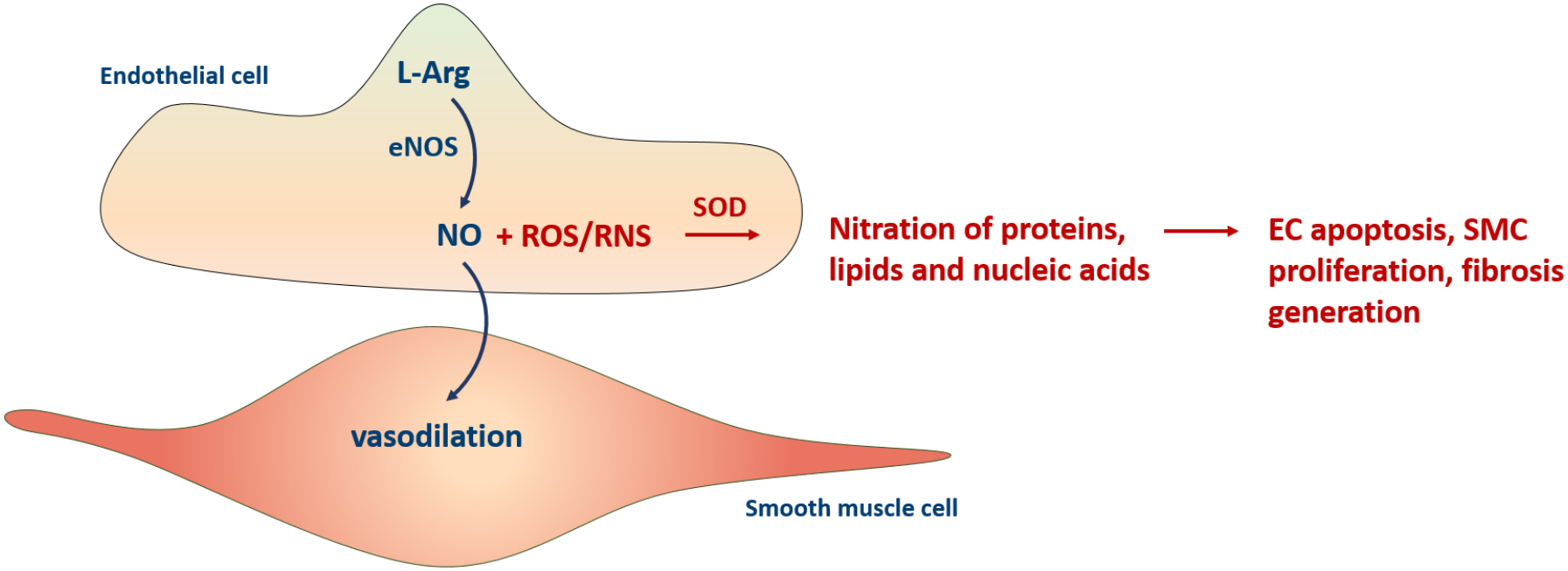

Figure 1.10 Simplified schematic of the formation of free radicals from nitric oxide (NO). Physiologically, NO is produced by eNOS from L-Arginine (L-Arg) and contributes to relaxation of SMC (blue pathway). When there is an excess of NO in pathological conditions, NO can react with ROS and RNS through superoxide dismutase (SOD) causing nitration of proteins, lipids and nucleic acids which compromises cell function (red pathway).

1.5.3 Mechanism 3. Vascular injury secondary to inflammation

DIVI has been proposed to occur as the result of inflammation and immune complexes deposition[130,131]. In this mechanism, some components of the innate immune system, such as granulocytes, mast cells, and/or monocytes, are activated by the drug and the damage is due to the release of mediators by these cells. The activation of T cells has been shown to result in expression of Fas ligand, which in turns causes EC apoptosis[129,132]. Furthermore, macrophages produce reactive oxygen intermediates, which combined with nitrogen intermediates, cause protein nitration in EC[129]. This hypothesis is supported by the observation that pre-treatment with the immunosuppressive drug dexamethasone blocks the development of lesions seen after treatment with CI-1018, a PDE IV inhibitor[127].

In the proceeding paragraphs the key cellular subtypes implicated in mediating the mechanisms of DIVI (EC, SMC, and blood cells) are explored, together with biomarkers that have been investigated with DIVI-related drugs in each of those cell types.

1.6 Vascular and circulating blood cells that may be affected in DIVI

1.6.1 Endothelial cell barrier

At the interface between blood and tissues, the endothelium forms a selective barrier that allows selective exchange of molecules[133]. The total area of this surface has been estimated to be around 350 m^2 in humans[134]. EC are linked to each other by different types of adhesive structures or cell-to-cell junctions, complex structures constituted by transmembrane adhesive molecules linked to a network of cytoplasmic/cytoskeletal proteins. On the basis of morphological and functional characterisation, three types of junctions have been defined: tight, adherens and gap junctions[135,136].

Tight junctions seal the endothelium and are formed by closely opposed neighbouring plasma membranes, which appear to be partially fused. The principal transmembrane constituents of tight junctions are proteins named occludins, which are associated to several cytosolic

proteins, even though the detailed structure of this complex is still unclear[137,138]. Junctional adhesion molecules are also part of tight junctions[139]. Adherens junctions are formed by cadherins, and vascular endothelial-cadherin (VE-cadherin) is localised at the endothelial cell surface. Cadherins are cell adhesion molecules, which are anchored with their cytoplasmic tail to several intracellular cytoplasmic proteins, named catenins, that are connected to the actin-based microfilament system[140].

Furthermore, adhesive proteins such as platelet endothelial cell adhesion molecule (PECAM-1), intercellular adhesion molecule 2 (ICAM-2), CD34, are involved in the control of vascular permeability. PECAM-1 is described in **1.6.1.2**. Endothelial permeability changes are associated with redistribution of surface cadherins and occludins, stabilisation of focal adhesion bonds and progressive activation of matrix metalloproteinases[141]. Stimuli such as histamine and thrombin promote a rapid and short-lived increase in vascular permeability, and other cytokines and vascular endothelial growth factor (VEGF) induce a sustained response. Most of these agonists are released in acute or chronic inflammatory situations.

1.6.1.1 VE-cadherin in controlling endothelial permeability

VE-cadherin is specific to EC[139] and is linked through its cytoplasmic tail to the adherens junction proteins p120, β-catenin and plakoglobin[142]. β-catenin and plakoglobin bind to α-catenin, which interacts with several actin-binding proteins, such as α-actinin and zonula occludens-1 (ZO-1)[143], to support the interaction of the VE-cadherin-catenin complex with the actin cytoskeleton, controlling junctional permeability and junction stabilisation[142,143] (**Figure 1.11**). The importance of VE-cadherin in maintaining vascular integrity is reflected in that in the adult mouse, administration of anti-VE-cadherin antibodies resulted in a dramatic increase in permeability, vascular fragility and haemorrhages[144]. This effect lasted for several hours as the antibodies remained bound to VE-cadherin subsequently blocking junction reorganisation. Other stimuli including histamine or low concentrations of VEGF, are naturally occurring molecules which also produced breakage of VE-cadherin homotypic interactions leading to loss of vascular integrity.

VE-cadherin activity is regulated by phosphatases and kinases, which modify protein function, signalling, and junctional permeability[145,146]. The most prominent tyrosine kinase is Src, which phosphorylates VE-cadherin at tyrosine 658 in response to histamine, TNF-α, platelet-activating factor (PAF), VEGF and shear stress[147–150], leading to VE-cadherin internalisation and impaired barrier function[145,151,152] (**Figure 1.11**). VEGF-induced phosphorylation of VE-cadherin is inhibited in Src-deficient mice or in wild-type mice treated with Src inhibitors[153]. Conversely, dephosphorylation of VE-cadherin by protein-tyrosine-phosphatases increases junctional strength[145,146].

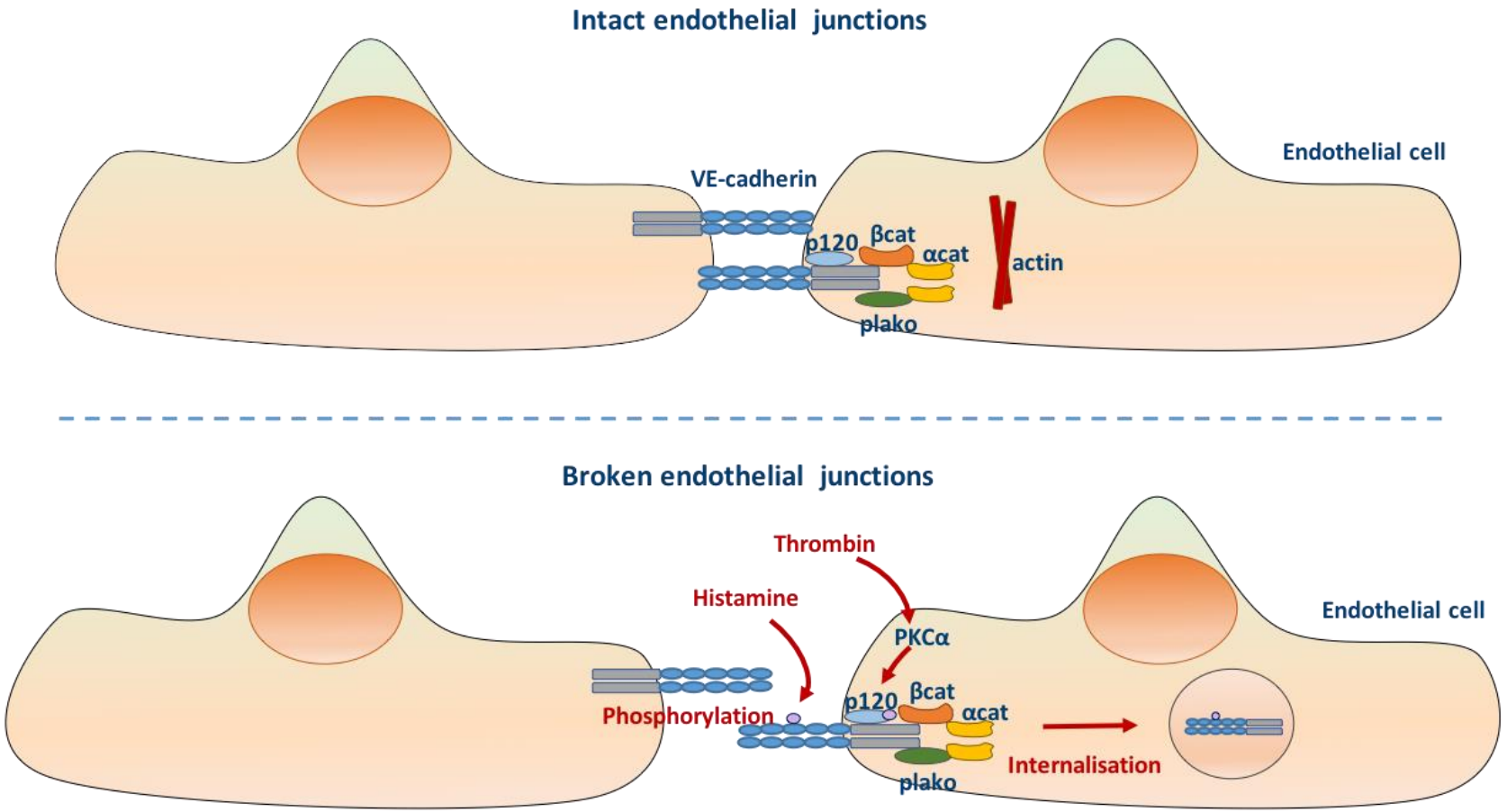

Figure 1.11 Schematic of VE-cadherin function at the endothelial junctions. VE-cadherin is a dimeric protein. Proteins that are well known to interact with VE-cadherin include the catenin proteins p120, β-catenin (βcat) and plakoglobin (plako). β-catenin and plakoglobin associate directly with VE-cadherin and α-catenin (αcat) and contribute to the interaction of VE-cadherin with the actin cytoskeleton[142]. In response to stimuli such as histamine or thrombin, VE-cadherin is phosphorylated and internalised inducing permeability.

Thrombin activates its receptor, protease-activated receptor-1 (PAR-1), through cleavage of the N-terminal domain to reveal a tethered ligand in the new N-terminus[154]. This initiates activation of heterotrimeric G-proteins, which induce a decrease in cAMP levels in the cell, an increase in intracellular Ca^{2+} and diacylglycerol (DAG) concentration, and activation of the small G-protein Ras homologue (RhoA)[154]. This triggers activation of myosin light chain kinase (MLCK) and subsequent phosphorylation of myosin light chains (MLC), which causes actomyosin contraction and rearrangement of the cytoskeleton regulated by Ca^{2+}/calmodulin-dependent protein kinase, tyrosine protein kinases and protein kinase C (PKC).

There are three proposed mechanisms for increased EC permeability: (1) Activation of the serine/threonine kinase PKC-α induces VE-cadherin complex disassembly by phosphorylation of p120 and the subsequent internalisation of VE-cadherin. In studies in mouse lung vessels, expression of the p120-deficient mutant prevented the increase in vascular permeability induced by thrombin[155]. Blocking of PKC-α-mediated p120 phosphorylation has been suggested as a novel anti-inflammatory strategy to prevent disruption of vascular endothelial barrier function. (2) In VEGF-stimulated EC, Src mediates Rac1 activation, leading to VE-cadherin phosphorylation via the serine/threonine kinase p21 activated kinase (PAK), increasing endothelial permeability[156]. (3) VE-cadherin is finally sensitive to enzymatic lysis, which causes permeability. It has been reported that exposure to metalloproteases, elastase, cathepsin G or trypsin can induce the digestion of VE-cadherin extracellular domain in cultured cells, disrupting intercellular junctions[157].

Several studies have reported the effects of molecules that increase vascular permeability[136,150,153,158,159]. Some agents such as histamine and thrombin act very rapidly and the effect is reversible once they are removed. Other agents such as inflammatory cytokines require several hours to increase permeability, but the effect is sustained for much longer, up to 48 hours. These observations suggest that the mechanisms regulating vascular permeability differ greatly. However, the common mechanism is that which affects the organisation of adherens junctions that can be accompanied by EC retraction and by opening of intercellular gaps.

When the endothelial monolayer is compromised, following vascular damage, the EC retract and the subsequent increase in permeability can be accompanied by disruption of the vessel, together with haemorrhage, adhesion of leukocytes and the formation of thrombi. This effect has been shown to be irreversible.

1.6.1.2 PECAM-1 as a regulator of intercellular adhesion

EC express other adhesive proteins, which are not confined to the adherens or tight junctions. Among these, PECAM-1, also known as CD31, is a transmembrane immunoglobulin present on EC but that is also expressed in leukocytes and platelets[139]. Homophilic PECAM-1/PECAM-1 interactions are responsible for helping to maintain the integrity of the EC barrier, whereas heterophilic interactions allow PECAM-1 to interact with glycosaminoglycans (components of the extracellular matrix involved in a variety of biological functions), lymphocytes and neutrophils[160]. PECAM-1 has been shown to be involved in the restoration of the EC barrier following barrier disruption with histamine[161], and also during lipopolysaccharides (LPS)-induced endotoxemia, a condition where blood vessels of PECAM-1-deficient mice show increased permeability[162].

Recent mechanistic studies employing Electric Cell-substrate Impedance Sensing technology found that, compared with PECAM-1-deficient EC, PECAM-1-expressing EC show increased barrier function at rest, as well as more rapid restoration of barrier integrity following thrombin-induced perturbation of the EC monolayer integrity[163]. This effect was found to be dependent on the homophilic PECAM-1 interaction, as a homophilic mutant form of PECAM-1 that could not localize to cell-cell borders was unable to support efficient barrier function. PECAM-1 has been demonstrated to be also a mechano-responsive molecule that enables EC to respond to shear stress, which modulates inflammatory signalling pathways, cytoskeletal structure, and cell-matrix interactions[164]. PECAM-1 is also involved in the trans-endothelial migration of leukocytes during their extravasation to sites of inflammation (refer to **section 1.6.5.3.1**). Studies blocking PECAM-1 have shown that PECAM-1 plays a key role in transmigration of leukocytes *in vitro*[165,166] and in animal models of inflammation[167–169].

1.6.2 Endothelial activation

It has been demonstrated that activation of EC is an early critical event in DIVI[170]. Subsequent events include apoptosis, dysfunction, and necrosis of EC, as well as reversible or irreversible injury to other vascular smooth muscle cells[171].

EC undergo changes that allow them to participate in the inflammatory response; this is knows as EC activation. EC activation may be divided into two phases, referred to either as an early event called 'EC stimulation' and a later event named 'EC activation', or referred to as 'Type I EC activation' and 'Type II EC activation', respectively[172–174]. Both types of activation are characterised by four components: (1) an increase in local blood flow; (2) a localised leakage of plasma-protein-rich fluid (exudate) into the tissue; (3) localised recruitment of circulating leukocytes; and (4) a change in EC phenotype from antithrombotic to prothrombotic.

1.6.2.1 Type I activation

Type I EC activation happens immediately following stimulation with agents such as thrombin, TNF-α, interleukin-1 (IL-1), histamine, LPS and drugs (bleomycin, cisplatin, PDE inhibitors) and does not involve *de novo* protein synthesis or gene transcription[171]. In general, Type I activation is mediated by ligands that bind to the extracellular domains of GPCRs, such as histamine H1 receptors[173].

Binding of these ligands to EC triggers a transient intracellular elevation of Ca^{2+} from endoplasmic reticulum stores (**Figure 1.12**). The rise in cytosolic Ca^{2+} activates phospholipase A_2 (PLA_2) to liberate arachidonic acid, which is converted by cyclooxygenase-1 (COX-1) and prostacyclin synthase into prostaglandin I_2 (PGI_2), a potent vasodilator that relaxes SMC. Elevated levels of free Ca^{2+} also binds to calmodulin and the Ca^{2+}-calmodulin complex activates nitric oxide synthase 3 (NOS3), producing NO from L-Arginine, which synergises with PGI_2 to relax SMC[175]. Production of these vasodilators by EC increases blood flow and leukocyte delivery to the tissues. At the same time, the Ca^{2+}-calmodulin complex also

activates the enzyme MLCK, which in turns phosphorylates MLC[176]. Phosphorylated MLC contracts actin filaments, which attach to the proteins forming the tight junction and adherens junction complexes, resulting in opening of the junctions. Loss of EC contact leads to haemorrhage, edema, and increased vascular permeability[172]. Phosphorylated MLC also initiates the exocytosis of secretory vesicles Weibel-Palade Bodies (WPB), bringing P-selectin (normally contained in the WPB) to the cell surface[177,178]. The display of P-selectin on EC surface provides a signal that causes the tethering of circulating neutrophils, which initiates neutrophil extravasation[179] (refer to **section 1.6.5.3.1**).

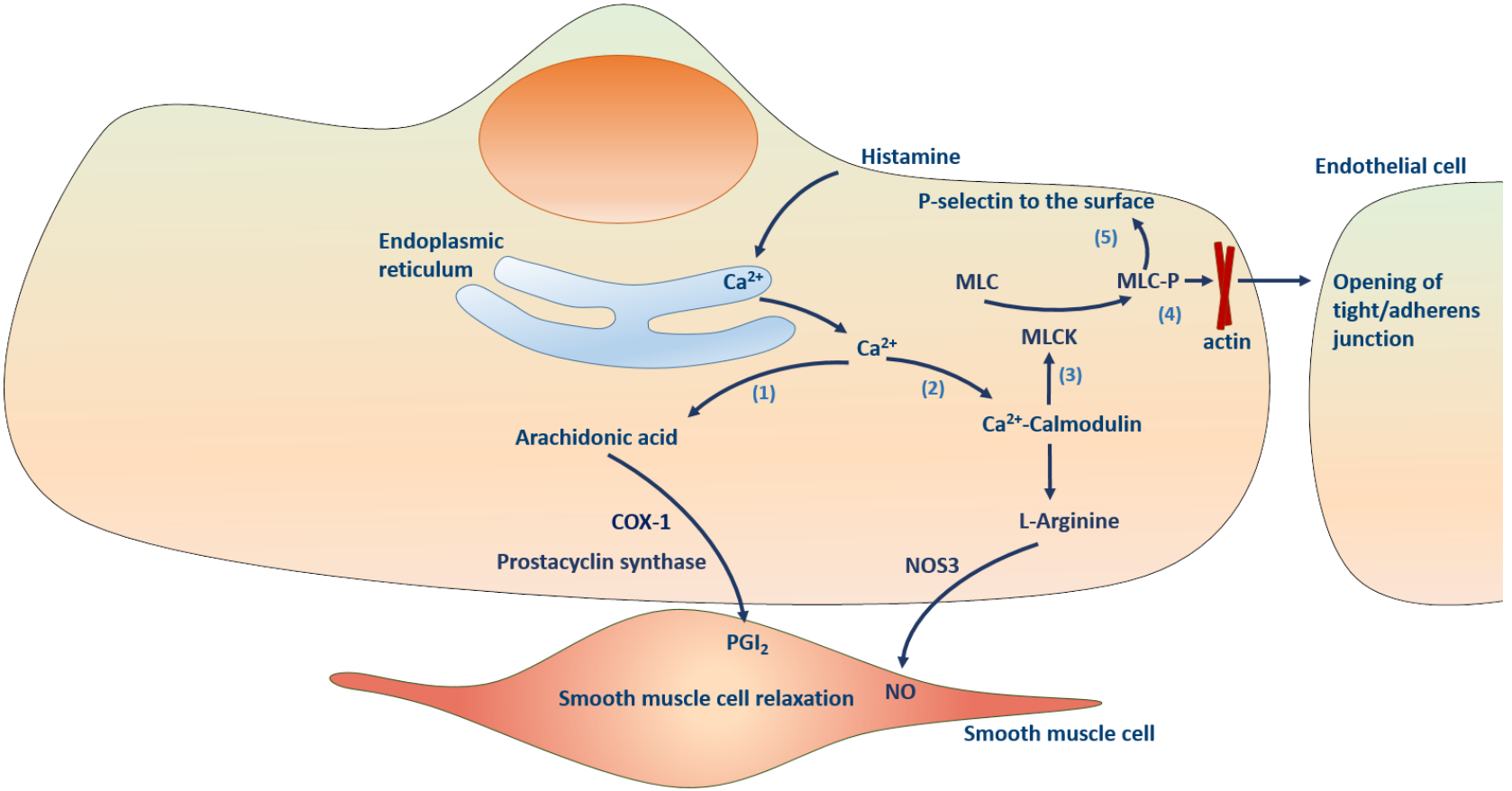

Figure 1.12 Endothelial Type I activation. Binding of stimulators such as histamine to EC triggers a transient intracellular elevation of Ca^{2+} from endoplasmic reticulum stores, which (1) activates the conversion of arachidonic acid to PGI_2; (2) forms a complex with calmodulin, which stimulates the production of NO; (3) calmodulin also causes the phosphorylation of MLC resulting in contraction of the actin filaments and EC permeability (4); (5) phosphorylation of MLC also leads to exocytosis of WPB bringing P-selectin to the surface, a signal for neutrophil extravasation.

Release of von Willebrand factor (VWF) also occurs in Type I activation and its release from EC will be described in detail in **section 1.6.2.4**. In addition, EC show prothrombotic effects, which include loss of the surface anticoagulant molecules thrombomodulin and heparan sulphate; reduced fibrinolytic potential due to enhanced plasminogen activator inhibitor type 1 (PAI-1) release; production of platelet activating factor; and expression of tissue factor[180].

1.6.2.2 Type II activation

Signals by heterotrimeric G protein-coupled receptors (GPCRs) last for between 10-20 minutes and the receptor is desensitised preventing restimulation[181]. This limits the degree of neutrophil extravasation caused by Type I activation alone. A more sustained EC activation is provided by Type II activation, a delayed response that requires time for the stimulating agent to cause the activation of gene transcription and the de novo synthesis of proteins[173,174]. The genes involved encode adhesion molecules, chemokines, cytokines, and procoagulant factors[172,182].

The principal mediators of this response are TNF-α and IL-1 derived from activated leukocytes and stromal cells[183]. TNF-α and IL-1 bind to TNF-α receptor 1 (TNFR1) and type 1 IL-1 receptor (IL-1R1) respectively, and this binding promotes the formation of signalling complexes within the cell[180] (**Figure 1.13**). These complexes initiate various kinase cascades that lead to activation of the transcription factor nuclear factor-κβ (NF-κβ) and activating protein 1 (AP1)[184]. Pro-inflammatory responses arise from new gene transcription mediated by NF-κβ and AP1. Since these responses require gene transcription and translation of new proteins, the responses of Type II activation require hours to be initiated compared to minutes in Type I activation. However, similarly to Type I activation, in Type II there is increased blood flow due to vasodilation, increased vascular leakage of plasma proteins and increased leukocyte recruitment. Furthermore, the rise in cytosolic Ca^{2+} (as in Type I) leads to activation of PLA_2 which liberates arachidonic acid, a substrate for constitutively activate COX-2. COX-2 produces PGI_2 to relax SMC but at a much higher rate compared to COX-1. Vascular leakage is triggered by reorganisation of the actin cytoskeleton in EC, which leads to opening of gaps between adjacent cells[185,186].

In type II activation, leukocyte recruitment is much more effective compared to Type I. Neutrophils are recruited by the synthesis and display of chemokines, such as IL-8 and leukocyte adhesion molecules like E-selectin[187]. Other proteins expressed on activated EC include intercellular adhesion molecule 1 (ICAM-1) and vascular cell-adhesion molecule 1 (VCAM-1), which allow leukocytes to adhere to the endothelium and then move into the tissues[188]. The endothelium also secretes NO and VWF[182], the latter explained in detail in section **1.6.2.4**.

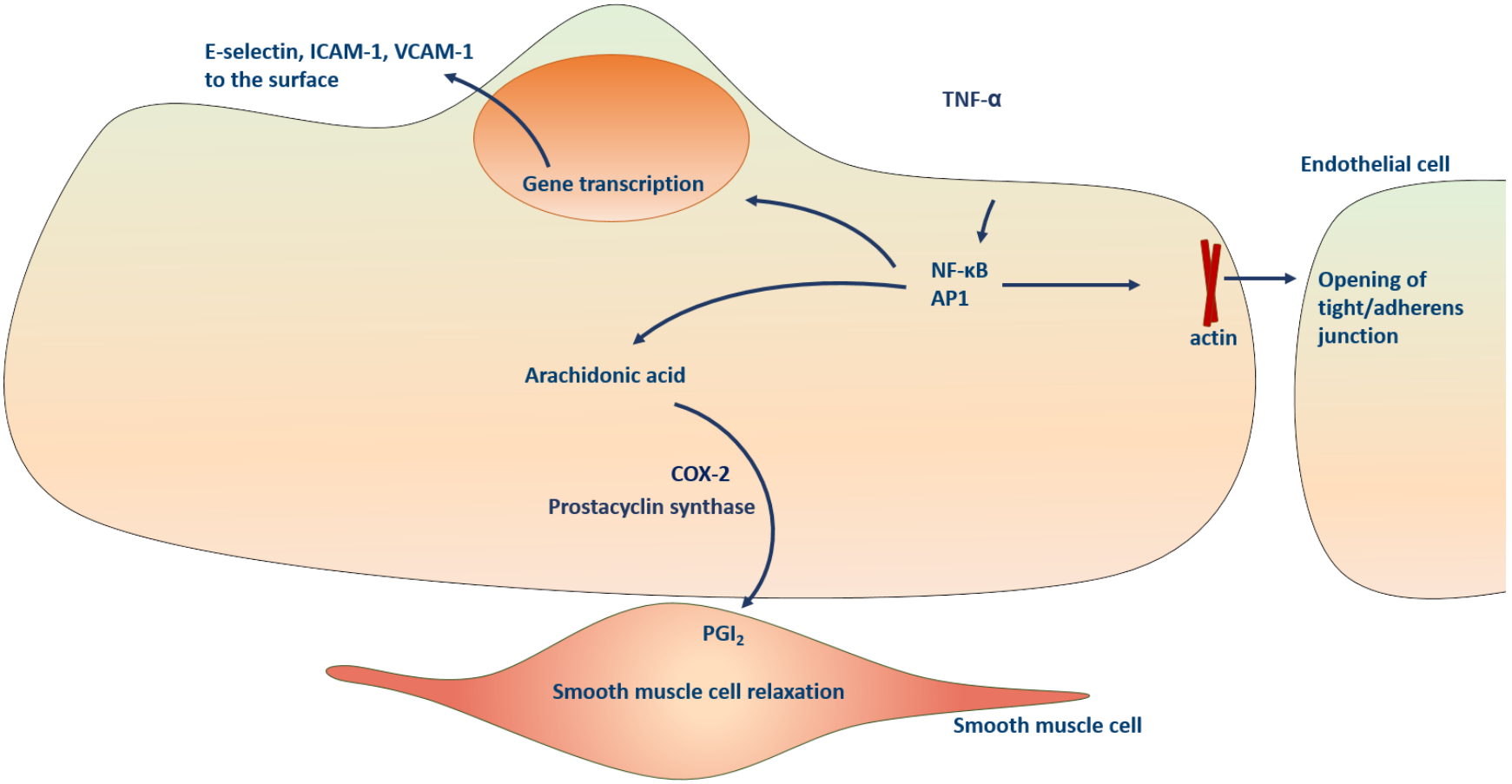

Figure 1.13 Endothelial Type II activation. Inflammatory cytokines such as TNF-α and IL-1 bind to TNF-α receptor 1 (TNFR1) and type 1 IL-1 receptor (IL-1R1) respectively, and this binding promotes the activation of NF-κB and AP1. This initiates the transcription of genes in the nucleus leading to expression of pro-inflammatory proteins, such as E-selectin, ICAM1, VCAM1, COX2 and chemokines.

Endothelial cell activation may precede DIVI *in vivo*[171]. Endothelial cell activation is a reversible alteration resulting in morphological rearrangement and induction of new functions, but without loss of monolayer integrity[171].The phenotype of activated EC may return to the quiescent, non-activated phenotype[189] however, the EC activation process, if uncontrolled, can progress to EC apoptosis, which represents irreversible endothelial injury, endothelial fragmentation, and EC separation from the intima[190].

1.6.2.3 Endothelial cell death

The main examples of cell death are apoptosis, autophagy and necrosis. Apoptosis is defined by characteristic morphologic features including condensation of the cytoplasm and nucleus with cell shrinkage[191], and the re-organisation of cellular material into plasma membrane derived blebs. During apoptosis the cell membrane remains intact, preventing the release of cellular contents, however there is exposure of several surface molecules that signal to neighbouring or phagocytic cells for initiation of engulfment[192]. Therefore, during apoptosis there is limited inflammation, in contract to necrosis in which the cell swells and the membrane is disrupted leading to release of constituents, triggering an inflammatory response.

Adherens junction proteins are degraded with disruption of barrier function *in vitro*[193]. *In vivo*, this could trigger vascular leak and inflammation in adjacent tissue by extravasated plasma constituents such as complement and coagulation components. Since EC are exposed to flowing blood and shear stress, apoptotic EC could detach prior to engulfment. Loss of even a small number of EC by this process could induce vascular leak and expose a thrombogenic subendothelial matrix. Apoptotic EC display an 'eat me' signal with phosphatidylserine (PS) exposure, they become pro-adhesive for platelets and leukocytes and procoagulant, and promote coagulation in situ before engulfment or detachment, or in the circulation once detached[194–196]. Some proapoptotic stimuli are: TNF-α, Fas/FasL, LPS and oxidants such as oxidised low-density lipoprotein (oxLDL)[197].

Biomarkers of EC activation and EC death have been explored in DIVI and are summarised in **Table 1.3**. Among these, VWF is a biomarker that has been extensively investigated in DIVI and will be described in detail in **section 1.6.2.4**.

Biomarker	Function	Response in DIVI	Drug reported with	Species	Administration route	Reference
VWF	Platelet adhesion and aggregation in hemostasis and carrier of FVIII	Increase in plasma levels at 2 and 6 hours post dose and return to baseline after 24 hours	Fenoldopam, minoxidil	Rat	Subcutaneous injection	36,198–200
VWFpp	Formed in the Trans-Golgi after cleavage of pre-pro VWF, regulates the hemostatic potential of VWF	Increase in plasma levels at 3 hours post dose and sustained for 24 hours only with endotoxin	Endotoxin, arginine vasopressine	Human, dog	Intravenous injection	201
Connexin 43	Maintains integrity of gap junctions	Decrease in immunoreactivity	Fenoldopam	Rat	Continuous infusion	100
Claudin	Maintains integrity of tight junctions	Decrease in immunoreactivity	Fenoldopam	Rat	Continuous infusion	100
ZO-1	Maintains integrity of tight junctions	Decrease in immunoreactivity	Fenoldopam	Rat	Continuous infusion	100
Caveolin-1	Major structural protein of caveolae; modulates the function of signal transduction in EC and SMC	Decrease (in mild lesions) or loss (severe lesions)	ET receptor antagonist, minoxidil, fenoldopam	Dog, rat	Intravenous injection	100
E-selectin	Cell adhesion molecule expressed on EC	Marked decrease in serum at 24 hours	CI-1044	Rat	Oral gavage	202
NO_{2^-}	Inflammation	Marked increase in serum at 24 hours	CI-1044, SCH 351591 and SCH 534385	Rat	Oral gavage	202

Table 1.3 EC biomarkers reported in DIVI.

1.6.2.4 VWF: a potential DIVI biomarker

Although the pathogenesis of DIVI remains unclear, it has been predicted that an early event that causes the disruption of the integrity of the blood vessel structure is likely to occur[34]. EC activation is an early step in the development of DIVI, and, as discussed, EC when activated release a range of molecules, among which there is VWF. VWF and VWF pro-peptide (VWFpp) have been suggested as the most promising potential biomarker for DIVI[198,201]. It has been extensively shown that plasma VWF is increased significantly over time during DIVI[201]. For example, dogs treated with a K^+ channel opener VWF plasma levels were observed to increase for 3 hours post-dosing[203], primarily from EC, and thus elevation in plasma is suggestive of EC compromise.

VWF secretion has been documented in dogs and rats with various drugs responsible for DIVI, such as fenoldopam, dopamine, vasopressin, the K^+ channel opener ZD6169, and endotoxin[198,201,204,205]. Moreover, it has also been suggested as a useful diagnostic indicator of plasma penetration into damaged arteries caused by the K^+ channel opener, ZD6169 and the ET receptor antagonist ZD1611[199].

VWF is a multimeric glycoprotein present in blood plasma, the subendothelial matrix, storage granules in EC (WPB) and α-granules in platelets[206]. It has been reported that EC injury leads to increased secretion of VWF, rendering soluble VWF a marker for EC activation and/or damage. For example, elevated plasma levels of VWF have been reported in patients with systemic inflammation[207] and also in patients with type 2 diabetes and dyslipidemia[208], suggestive of EC injury.

The role of VWF is dual: (1) contributing to the haemostatic process by mediating platelet adhesion and aggregation at sites of vascular injury and (2) carrying coagulation factor VIII (FVIII) in the circulation in a tight complex[206]. FVIII acts as a co-factor to accelerate the activation of factor X in the coagulation cascade, which results in the formation of a fibrin clot[209]. Individuals lacking VWF show a severe haemorrhagic phenotype, originating from defective formation of platelet-rich thrombi and a secondary deficiency of FVIII impairing the generation of a fibrin network.

1.6.2.4.1 Synthesis and storage

VWF is synthesised by EC and megakaryocytes as a single pre-pro-polypeptide (a protein precursor that will undergo post-translational modifications in order to become active) of 2813 amino acids, and is stored in the cytoplasmic WPB of EC together with P-selectin, and in α-granules in platelets[189]. The pre-pro VWF undergoes intracellular modifications including signal peptide cleavage, C-terminal dimerization, glycosylation, sulfation, and aminoterminal multimerisation. Proteolysis occurs in the trans-Golgi where the VWFpp is cleaved but remains stored together with mature VWF in α-granules in megakaryocytes and WPB in EC. After secretion into plasma, VWFpp dissociates from VWF (**Figure 1.14**).

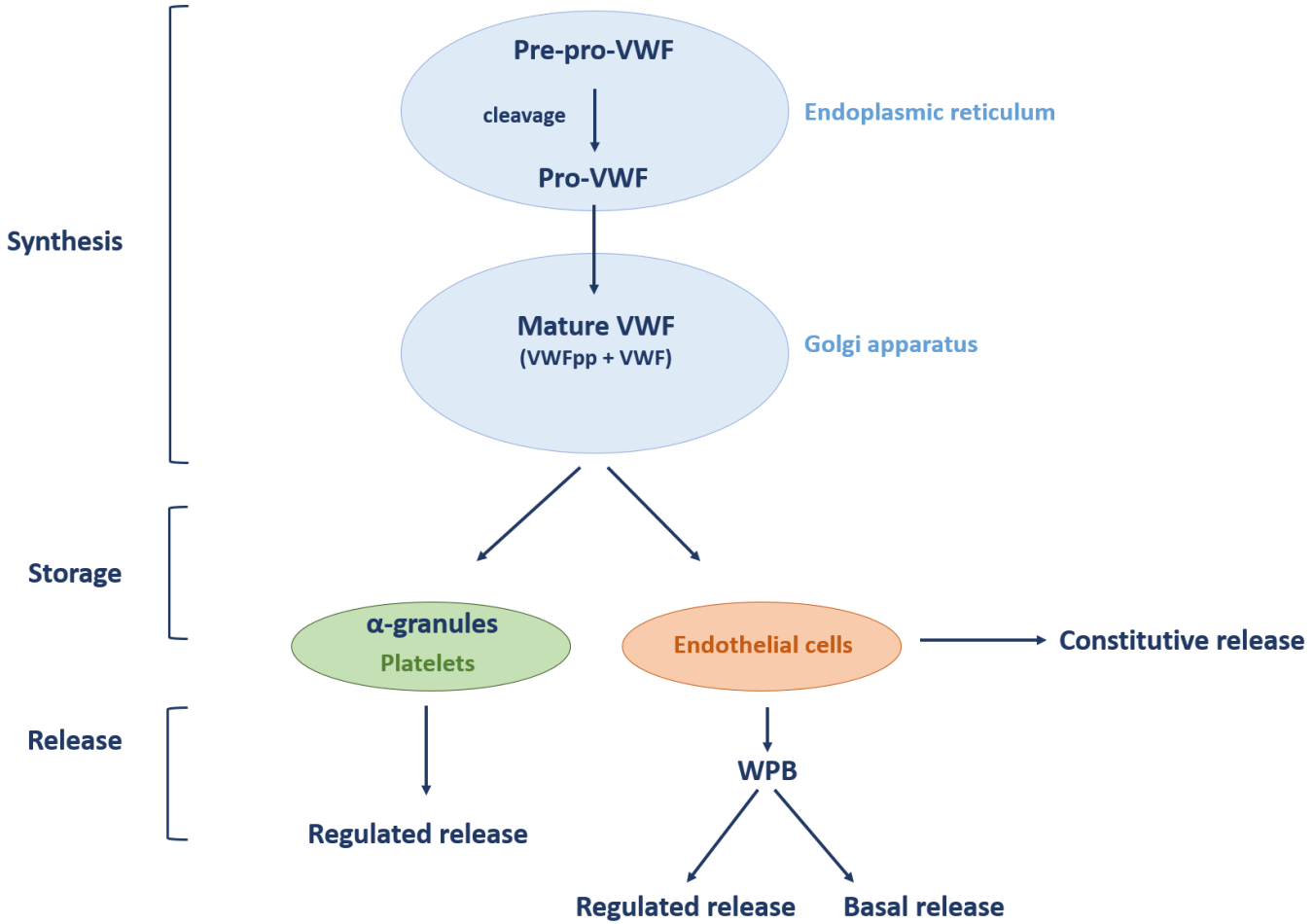

Figure 1.14 VWF synthesis, storage and release. VWF is synthesised as pre-pro-VWF and directed into the endoplasmic reticulum where the pro-VWF is formed by cleavage. Other modifications occur in the Golgi apparatus. The mature VWF multimers, which include VWF and VWFpp, are trafficked to EC, from where VWF is directly released or packaged into WPB, and α-granules in platelets from where release occurs.

Post synthesis, VWF is transported to storage organelles in α-granules in megakaryocytes/platelets and in the WPB of EC. It is unknown whether the process of WPB formation begins in the Golgi apparatus or the Trans-Golgi network. Organelle formation requires VWF multimers to be packaged into a helicoidal structure, where VWF is compacted by 100-fold. The tubular structure of WPB reflects how VWF is folded in these organelles. The VWF cargo originating from different ministacks is copackaged together into organelles that produce WPB of sizes varying from 0.5 to 5 µm. The VWF tubules induce membrane protrusions from the Trans-Golgi network, leading to vesicles budding off and formation of immature WPB. At the molecular level, a clathrin coat appears necessary for VWF packaging into nascent organelles, probably to provide a scaffold and form the typical rod-shaped structure of the WPB[206].

The mature VWF released into circulation has all the adhesive sites required for its haemostatic function. These are: D'-D3 domain that binds factor VIII, A1 domain that binds platelet glycoprotein (GP)Ib receptor, A2 domain that serves a site for ADAMTS-13-mediated cleavage of VWF, A3 domain that binds exposed collagen, and C1 domain that binds platelet GPIIb/IIIa[210–213] (**Figure 1.15**).

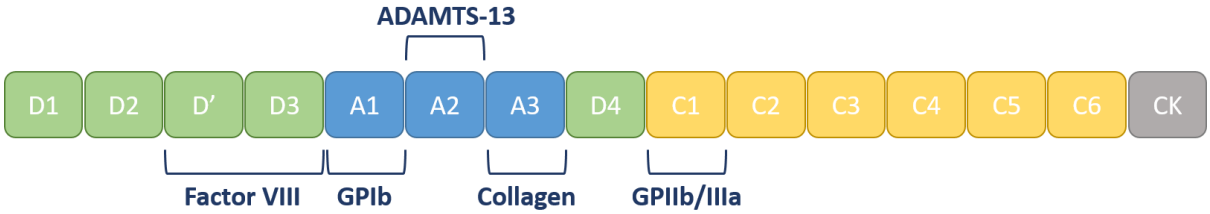

Figure 1.15 Schematic of VWF domains. D' and D3 are implicated in the binding of coagulation factor VIII, A1 and C1 of platelets through GPIb and GPIIb/IIIa, respectively, and A3 of exposed collagen. In addition, A2 domain is the site for cleavage of VWF by ADAMST-13.

1.6.2.4.2 Release

Whereas α-granules release VWF predominantly upon platelet activation, release of VWF from EC occurs through one of the following mechanism: (1) regulated secretion from WPB,

in response to a specific agonist upon vascular injury; (2) basal secretion from WPB, independent from an agonist; (3) constitutive, independent from an agonist from non-WPB compartments. When present in the endothelial cell cytoplasm, WPB move around eventually locating single WPB to the cellular periphery, allowing them to fuse with the plasma membrane and release their contents into the extracellular space (blood or subendothelium)[214]. Exocytosis of VWF results in a rapid unfolding of VWF tubules into ultralong strings (up to 100 µm) docking on the EC, allowing platelets to adhere[215].

Following secretion, VWFpp dissociates from VWF multimers and circulates independently as a non-covalent homodimer with a short half-life of around 2 hours. By contrast, VWF multimers are cleared more slowly (see below), with a half-life of around 12 hours. It has been reported that VWFpp regulates the hemostatic potential of VWF by reducing binding of VWF to platelets[216].

Regulated VWF release from EC by thrombin

Following EC injury, EC and recruited platelets release the stored VWF[217]. The exact mechanism by which thrombin-induced VWF is released is not clear, although it appears to depend on the proteolytic activity of thrombin[218]. In mice with EC specific knockout of G protein subunits ($G_{\alpha12}$ and $G_{\alpha11}$), thrombin-induced release of VWF was reduced whereas basal secretion of VWF was decreased in $G_{\alpha12}$ knockout mice, suggesting that VWF secretion is G protein-dependent[219]. An *in vitro* study showed the difference in the structure of VWF released after stimulation with thrombin compared to VWF secreted constitutively, which contained predominantly dimers with a significant proportion of precursor subunits[220].

1.6.2.4.3 Interaction of VWF with other cells

Released VWF binds to exposed collagen through its A1 and A3 domains, resulting in VWF immobilisation at the injury site. At this stage, VWF is subjected to shear stress in the circulation and undergoes conformational change exposing GPIb-binding site within its A1 domain resulting in platelet adhesion via their GPIb site[221,222].

Adhered and activated platelets roll on the endothelium causing a GPIIb/IIIa conformational change and binding of platelet GPIIb/IIIa to VWF via its C1 domain, a process that is irreversible and culminates in the formation of a platelet plug[223,224]. VWF also binds and stabilises FVIII through D'-D3 domains[212], activated FVIII subsequently activates factor X through formation of a complex with FIX and calcium[225,226]. The activation of the coagulation cascade leads to the formation of a fibrin clot (**Figure 1.16**).

In summary, VWF is important in platelet adhesion (through GPIb binding), platelet aggregation (through GPIIb/IIIa binding) and in coagulation by prolonging the half-life of FVIII. Since VWF is also stored in EC, its increase in plasma levels is indicative of EC compromise and thus can be used as a useful biomarker in DIVI.

Although micro-thrombi or thrombi have not been observed as a phenotype in DIVI, this is likely due to post mortem analysis where these thrombi will be removed prior to analysis. However, the result of increased VWF release coupled with EC damage would be very likely to result in platelet activation and micro-thrombosis[171].

VWF has been also found in SMC in disease states. For example, VWF has been reported to breach the endothelium in cerebral small vessel disease[227]. In a co-culture study using Notch ligand expressing rat SMC to stimulate Notch in astrocytes (A7R5), it was found that VWF strongly inhibits Notch signalling and the activation of mature smooth muscle gene promoters. Similar effects were seen in primary human cerebral vascular SMC. Moreover, expression of the intracellular domain of Notch3 allowed cells to bypass the inhibitory effect of VWF. It has also been observed that VWF forms molecular complexes with all four mammalian Notch ectodomains, indicating a new function of VWF as an extracellular inhibitor of Notch signalling. These experiments demonstrate a novel role of VWF in the promotion of vascular disease through a non-haemostatic mechanism.

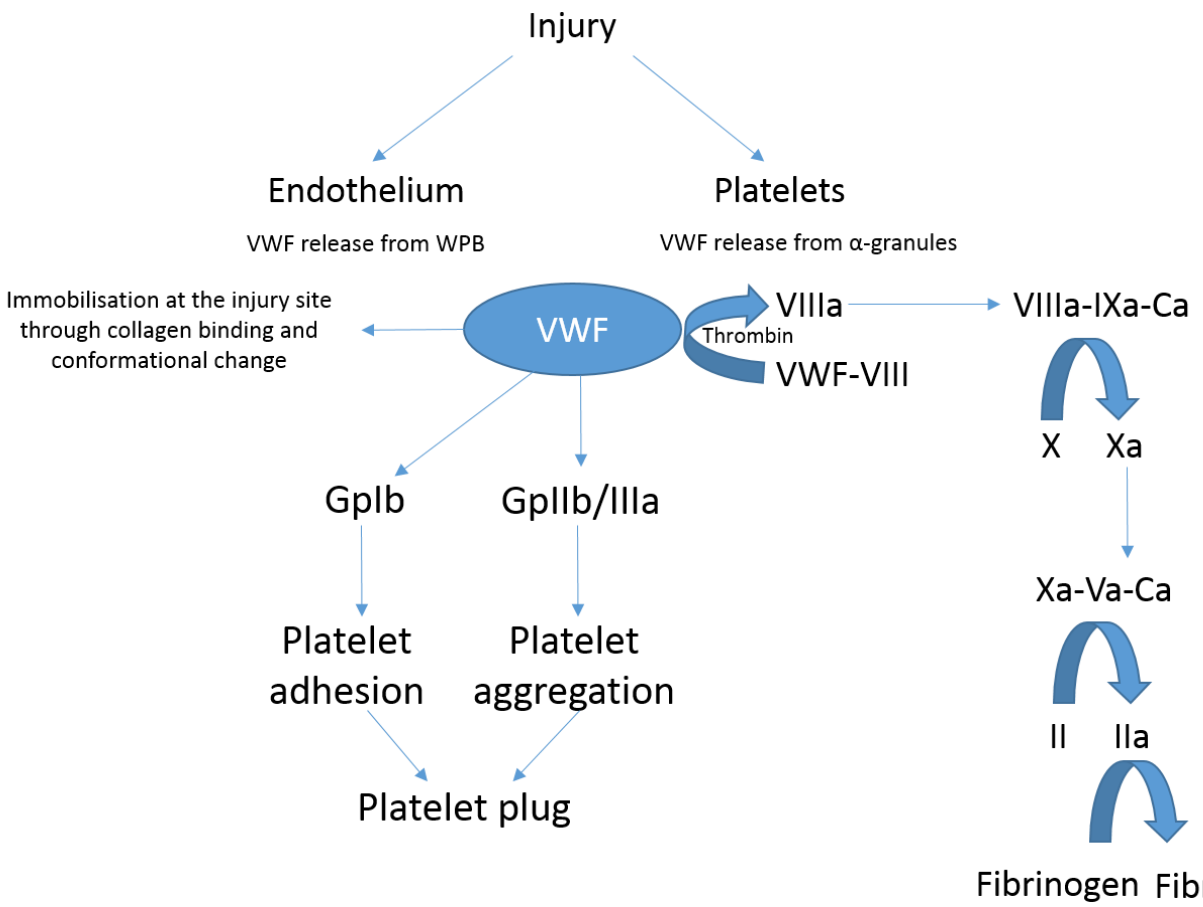

Figure 1.16 Function of VWF. At the injury site, activated EC and recruited platelets release stored VWF which bind to collagen through A3 domain and gets immobilised. Subjected to shear stress, VWF undergoes a conformational change exposing GPIb binding site within A1 domain. Circulating platelets bind to exposed GPIb binding site on immobilised VWF, leading to platelet adhesion. Adhered platelets then roll on EC until GPIIb/IIIa-mediated binding occurs resulting in platelet aggregation and the formation of a platelet plug. VWF also binds and stabilises FVIII. Once FVIII is activated, it activates FX by forming a complex with FIX and calcium. Activation of the coagulation cascade results in the formation of a fibrin clot.

1.6.2.4.4 Clearance

Following release in the circulation and the interaction with platelets, VWF is cleared by ADAMST-13, a metalloprotease that cleaves VWF decreasing its activity[228]. VWF circulatory lifespan is limited and varies between 4 to 26 hours a variation that is most likely due to different glycosylation patterns. The majority of VWF is targeted to the liver, indicating that VWF is cleared via an active regulatory mechanism rather than through passive elimination. Immunohistochemical analyses of liver and spleen showed that VWF principally colocalises with macrophages[229]. This was confirmed in other studies whereby the chemical depletion of macrophages led to an increase in VWF survival. In addition, experiments with human macrophages confirmed that VWF is bound and endocytosed by macrophages. However, this does not exclude the participation of other non-macrophage cells in this process. By clearing cell debris, resolving inflammation and promoting fibrosis, macrophages have a central role in the response to injury[230]. However, they have also been linked to chronic inflammation in situations of continuous injury or failed resolution, in which their activity became detrimental.

1.6.3 Smooth muscle cells

SMC provide the main support for the structure of the vessel wall and they regulate vascular tone through contraction[231]. Compared to other cell types, SMC retain significantly more plasticity to regulate functions such as contraction, proliferation and extracellular matrix synthesis[232]. SMC plasticity depends on variations in environmental cues and extracellular signals sensed by the cell. SMC can switch between two phenotypes: (1) quiescent SMC are differentiated, and express a range of upregulated markers such as α-smooth muscle actin (α-SMA), smooth muscle myosin heavy chain, and calponin, and (2) a synthetic or proliferating phenotype, characterised by decreased contractile marker expression, and increased proliferation, migration and extracellular matrix synthesis[233–235]. Mature SMC are defined as differentiated or contractile under normal physiological conditions. SMC switch to a proliferative state under pathological conditions, such as atherosclerosis[236] in response to environmental stimuli, such as growth factors, mitogens, inflammatory mediators, where SMC lose the ability to contract, but migrate, proliferate and accumulate in the intima[237].

The mechanisms involved in SMC differentiation are still not entirely known. SMC can arise from multipotent progenitors and can further mature into different SMC subtypes[238]. This process depends on several stimuli, including cytokines or growth factors, the extracellular matrix, microRNAs, chromosome structural modifiers and mechanical forces[239].

The main signals involved in SMC differentiation are (1) transforming growth factor (TGF)-β, (2) Notch signalling, and (3) platelet-derived growth factor (PDGF). TGF-β signalling plays a pivotal role in SMC differentiation during vascular development as well as phenotypic switching in disease states[240]. TGF-β has been shown to be involved in the development of many CV diseases including atherosclerosis, congenital heart diseases, aortic aneurysm, hypertension and hereditary haemorrhagic telangiectasia[241–243]. Overexpression of TGF-β increases the neointimal formation and SMC proliferation and differentiation in a model where rabbits were induced arterial injury with a balloon catheter[244,245]. Its role in DIVI has never been fully explored, but it is likely that TGF-β is involved in the progression of the lesions. Given the plasticity of SMC and their ability to switch between phenotypes, it would be interesting to understand if this mechanism is also implicated in the resolution of the

lesions in DIVI. In atherosclerosis, SMC play a maladaptive role in lesion development and the progression of the disease; in apolipoprotein E (a protein involved in the metabolism of fats) deficient mice, it was found that high expression of TGF-β contributes to the stability of the lesion[246,247].

Similarly to TGF-β, Notch signalling induces SMC differentiation[248]. Several studies have shown that Notch induces SMC specific marker expression including α-SMA, SM22α, calponin and smooth muscle myosin heavy chain (SMMHC) in a number of cell lines[248–250]. Although there are four types of Notch receptor, only Notch1 and Notch3 are expressed in SMC and Notch3 in particular is involved in SMC differentiation. It has been described that the expression of late stage SMC marker smoothelin B is significantly inhibited in Notch 3 mutant arteries, suggesting a pivotal role in the maturation of SMC[251] .

PDGF has the ability to induce phenotypic switching from contractile to proliferative state in SMC[252]. Using human aortic SMC, it has been demonstrated that prolonged PDGF treatment leads to sustained increases in the phosphorylation of protein kinases such as Akt, p70S6kinase, and ERK1/2, which mediate SMC proliferation[253]. An increase in the expression of PDGF and its receptor has been shown in a model of angioplasty using human coronary arteries, which could suggest that PDGF released from SMC is involved in repair processes after injury[254].

Finally, shear stress has also been found to affect SMC differentiation. *In vitro* studies of the effects of shear stress on vascular cells have focused primarily on EC because under normal physiological conditions they are directly exposed to blood flow[255–257]. However, it is becoming increasingly clear that shear stress and NO also affect SMC function. SMC produce both NO[258] and iNOS[259] in response to elevated shear stress levels, and it has been reported that shear stress inhibits SMC migration via NO-mediated downregulation of matrix metalloproteinase-2 (MMP-2) activity. This was demonstrated in a study with rat aortic SMC that were seeded onto Matrigel-coated cell culture inserts, and their migratory activity quantified when exposed to shear stress in a rotating disk apparatus[260].

1.6.3.1 SMC activation

SMC activation upon injury produces cytokines, including PDGF, TGF-β, macrophage inhibitory factor, interferon (IFN)-γ, and monocyte chemoattractant protein (MCP-1), that attract and activate leukocytes, induce proliferation of SMC, promote EC dysfunction, and stimulate production of extracellular matrix components[261]. Most importantly, SMC undergo phenotypic changes in diseases states that will be described in detail in **chapter 6**.

1.6.3.2 SMC death

1.6.3.2.1 Apoptosis

SMC apoptosis is induced by pro-inflammatory cytokines, oxidised low-density lipoprotein (oxLDL), high levels of NO and mechanical injury. Pro-inflammatory cytokines such as TNF-α and IFN-γ produced by macrophages and T-cells, respectively, sensitise SMC to death receptor Fas (CD95) mediated apoptosis by causing Fas trafficking to the cell surface[262,263].

1.6.3.2.2 Necrosis

As with EC, necrosis is characterised by an increase in cell volume and swelling of organelles followed by breakage of the plasma membrane and release of intracellular contents which initiates inflammation. Although originally necrosis was considered a non-programmed form of death, there is new evidence suggesting that necrosis is regulated via different pathways that result in the formation of a necrosome, a complex consisting of Fas-associated protein among others that stimulates an inflammatory response[263].

Markers of SMC function and death have been explored in DIVI and are summarised in **Table 1.4**. As already mentioned, α-SMA and calponin are specific markers of mature and differentiated SMC and they have been shown to be reduced in DIVI[203].

In addition, caveolin-1 has been found to decrease or be lost in SMC (and in EC, refer to **Table 1.4**). In addition to the ones listed, TGF-β, Notch3, PDGF and NO are also markers that may be interesting in identifying biomarker for DIVI.

Biomarker	Function	Response in DIVI	Drug reported with	Species	Administration route	Reference
Activated caspase-3	Involved in the execution phase of apoptosis	Increased activation	Fenoldopam	Rat	Continuous infusion	127
α-SMA	Involved in cell motility, structure and integrity	Decreased immunoreactivity	Fenoldopam	Rat	Continuous infusion	202
Caveolin-1	Major structural protein of caveolae; modulates the function of signal transduction in EC and SMC	Decrease (in mild lesions) or loss (in severe lesions)	ET receptor antagonist, minoxidil, fenoldopam	Dog, rat	Continuous infusion	35,100,203
Calponin	Regulates the actin/myosin interaction	Mild increase at 8 hours post dose followed by robust decrease at 24 hours	CI-1044	Rat	Oral gavage	2

Table 1.4 SMC biomarkers reported in DIVI.

1.6.4 Endothelial-smooth muscle cell interactions

As previously mentioned, blood vessels are characterised by three layers: (1) the intima, a single concentric layer of EC that forms the inner tube of the vessel; (2) the media, surrounding the intima, composed of SMC (or SMC-related pericytes); (3) the adventitia, a mixture of extracellular matrix (ECM), fibroblasts, and nerve cells[264] (**Figure 1.2**).
Despite vascular bed-specific differences, EC and SMC share similar functions in all blood vessels. The largest arteries, such as the aorta, consist of multiple layers of SMC intertwined with a matrix made of elastin and collagen to sustain systemic pressure under pulsatile flow. In contrast, veins operate under low pressure and facilitate the return of blood from the organs to be reoxygenated. Veins are characterised by fewer layers of smooth muscle and a less complex ECM component. The smallest vessels, the capillaries, have limited smooth muscle (or pericyte) coverage to allow for maximum diffusion, with EC that are highly permeable to permit gas exchange and nutrient delivery to cells via tiny pores or fenestrations[264].

Communication between EC and SMC begins early on in embryogenesis when the blood vessels begin to form[265,266]. Mechanistically, the signalling strategies can occur through a soluble or secreted molecule, or they can require direct physical contact between the EC and SMC.

1.6.4.1 Diffusible signalling

The ratio between PDGF and VEGF plays a pivotal role in the fine balance required for blood vessel growth and maturation[267,268]. It has been shown that inhibition of VEGF signalling in the endothelium and PDGF signalling in mural cells using different kinase inhibitors increased the antitumor effects of pericytes that are potential antiangiogenic targets in tumour therapy, as compared to VEGF inhibition alone[269].

Another important signalling pathway involved in EC-SMC communication is the Angiopoietin-1-Tie-2 pathway[270]. Angiopoietin-1 (Ang-1) is a growth factor largely secreted by

SMC and ligand for endothelium-specific receptor tyrosine kinase Tie-2. It has also been suggested that Ang-1/Tie-2 is critical for maintaining the physical interaction of EC and SMC and in preventing cell death[271–273]. It was demonstrated using endothelial Abelson (Abl) kinase knockout mice that loss of Abl kinase (involved in different cellular processes including proliferation, survival, adhesion and migration) leads to a decreased Tie-2 expression, diminished Tie2 receptor signalling and loss of Ang-1-mediated survival. Loss of Abl resulted in lethality at late embryonic and perinatal stages of development, with focal regions of vascular loss and tissue necrosis/apoptosis[271]. It was also found that Abl kinases are activated by Ang-1/Tie-2 signalling.

Another receptor-ligand combination implicated in EC-SMC communication is the sphingosine-1-phosphate (S1P) pathway[274,275]. S1P is a sphingolipid metabolite that signals through a family of G-protein-coupled receptors. It has been shown that deletion of the $S1P_1$ receptor on EC results in significant defects in smooth muscle coverage, suggesting the importance in smooth muscle recruitment by EC. The role of NO in EC-SMC signalling is also important in promoting SMC relaxation, as well as the previously mentioned PGI_2, a potent vasodilator produced by EC that relaxes SMC.

1.6.4.2 Contact-dependent signalling

Physical communication relies on membrane-bound proteins 'hooking up' on adjacent cells. Studies revealed that EC-SMC interactions in adult vessels are controlled by Notch signalling, as Notch3 was found to regulate vascular tone in small arteries. In addition, deletion of Notch ligand Jagged 1 in EC leads to vascular defects associated with SMC differentiation, whereas EC appeared normal. Some studies showed that EC-expressed Jagged 1 can induce the expression of Notch3 in co-cultured SMC, and this induction is critical for smooth muscle differentiation[276].

In mature blood vessels, the basement membrane and the internal elastic lamina are considered significant barriers to physical interactions of EC-SMC. Despite this, myoendothelial communication exists via myoendothelial junctions that link the plasma

membranes of juxtaposed EC and SMC[277,278]. In 1973, it was demonstrated for the first time that cellular extensions from two different cells could form heterocellular gap junctions, as revealed by freeze-fracture transmission electron microscopy (TEM) images[279]. In 2000, three-dimensional reconstructions of the myoendothelial junctions from sequential TEM sections confirmed that very small gap junctions could exist between EC and SMC[280]. These and other EC-SMC interactions are dysregulated during vascular injury and thus are likely to be disrupted in DIVI. It has been suggested that alterations in direct EC-SMC cross-talk (involving physical contact through cell surface proteins such as connexins, Eph/ephrins, and Jagged/Notch3) and indirect cross-talk (involving cell-secreted factors and the extracellular matrix) promotes atherogenesis[281].

1.6.5 Circulating blood cells

Haemorrhage including extravasation of RBC into the tunica media of blood vessels is a feature of DIVI, where RBC are lost through inter-endothelial gaps[76]. The crosstalk of RBC with leukocytes may be an important player in the pathogenesis of DIVI. There is evidence that oxidised RBC contribute to the perpetuation of inflammation in the pathogenesis of CV disorders[282,283].

1.6.5.1 RBC activation

Under physiological conditions, RBC act as circulating scavengers of ROS and RNS generated in the vasculature through their antioxidant machinery such as reduced glutathione, thioredoxin, ascorbic acid, and vitamin E[284]. When RBC cross a tissue characterised by an intense production of pro-oxidant reactive species, the RBC are unable to counteract the new pro-oxidant status of the microenvironment and become themselves a source of ROS. Oxidative stress can cause several RBC changes, such as cytoskeleton rearrangement and oxidation. These RBC become more rigid and therefore undergo lysis more easily releasing cytotoxic species in the vasculature. Oxidized RBC release Hb, heme-Fe, and iron[285], which are powerful oxidants able to activate an inflammatory response[286–288].

RBC extravasation has been investigated in DIVI in a microfluidic system with the PDE IV inhibitor CI-1044, a drug known to cause DIVI in rats and it was shown that the drug caused extravasation of RBC in the smooth muscle layer after 8 hours infusion[114]. However, the extravasation phenomenon in DIVI has only been evaluated qualitatively as present or absent in the device and further assessment of the underlying mechanisms remain to be conducted. It is possible that RBC contribute to the progression of the lesions through free radical formation.

1.6.5.2 Platelet activation

Platelets play a key role in haemostasis. In **section 1.6.2.4** the interaction of VWF with platelets has been described. Platelet activation is stimulated by bound platelet secretion products and local pro-thrombotic factors such as tissue factor[289].

Platelet activation requires activation of the GPIIb/IIIa receptor (also known as integrin $\alpha_{IIb}\beta_3$), which results in the cross-linking of fibrinogen or VWF between receptors, leading to platelet aggregation[290,291]. This induces the recruitment of additional platelets to the site of injury, allowing the thrombus formation. The function of the integrin $\alpha_{IIb}\beta_3$ depends on its capacity to transit from a low to a high affinity state for its ligands, fibrinogen and VWF, resulting in aggregation and thrombus stabilisation.

When activated, platelets also express large amounts of P-selectin, which is mobilised from α-granules to the surface[292–294]. P-selectin interacts with its ligand P-selectin glycoprotein ligand-1 (PSGL-1) on leukocytes, resulting in the formation of platelet-leukocyte aggregates.

Moreover, ADP released from damaged EC and activated platelets stimulates platelet $P2Y_1$ and $P2Y_{12}$ GPCRs, which causes further platelet activation and release of ADP. Thromboxane A_2 produced and released by stimulated platelets also activates further platelets, promoting plug formation.

1.6.5.3 Leukocyte activation

Activation of leukocytes and their migration towards an extravascular site of damage involves a series of highly organised events collectively termed the 'multi-step leukocyte adhesion cascade'[295] and is depicted in **Figure 1.17**.

1.6.5.3.1 The leukocyte adhesion cascade

The first stage in the leukocyte cascade is the contact between the endothelium and leukocytes, termed tethering or capture, where upon tissue damage the selectin molecules, L-selectin (expressed by most leukocytes), P-selectin and E-selectin (expressed by inflamed EC, P-selectin also by activated platelets), mediate tethering of the leukocytes[296]. PSGL-1, expressed on almost all leukocytes and by certain EC[297], has a dominant role as a ligand for all selectins[298] and it is functional only when glycosylated correctly[299].

Besides PSGL-1, E-selectin also binds to glycosylated CD44 and E-selectin ligand 1 (ESL-1)[300]. The binding of PSGL-1 to L-selectin allows leukocyte–leukocyte interactions, by which adherent leukocytes and leukocyte-derived fragments facilitate secondary leukocyte capture[301,302].

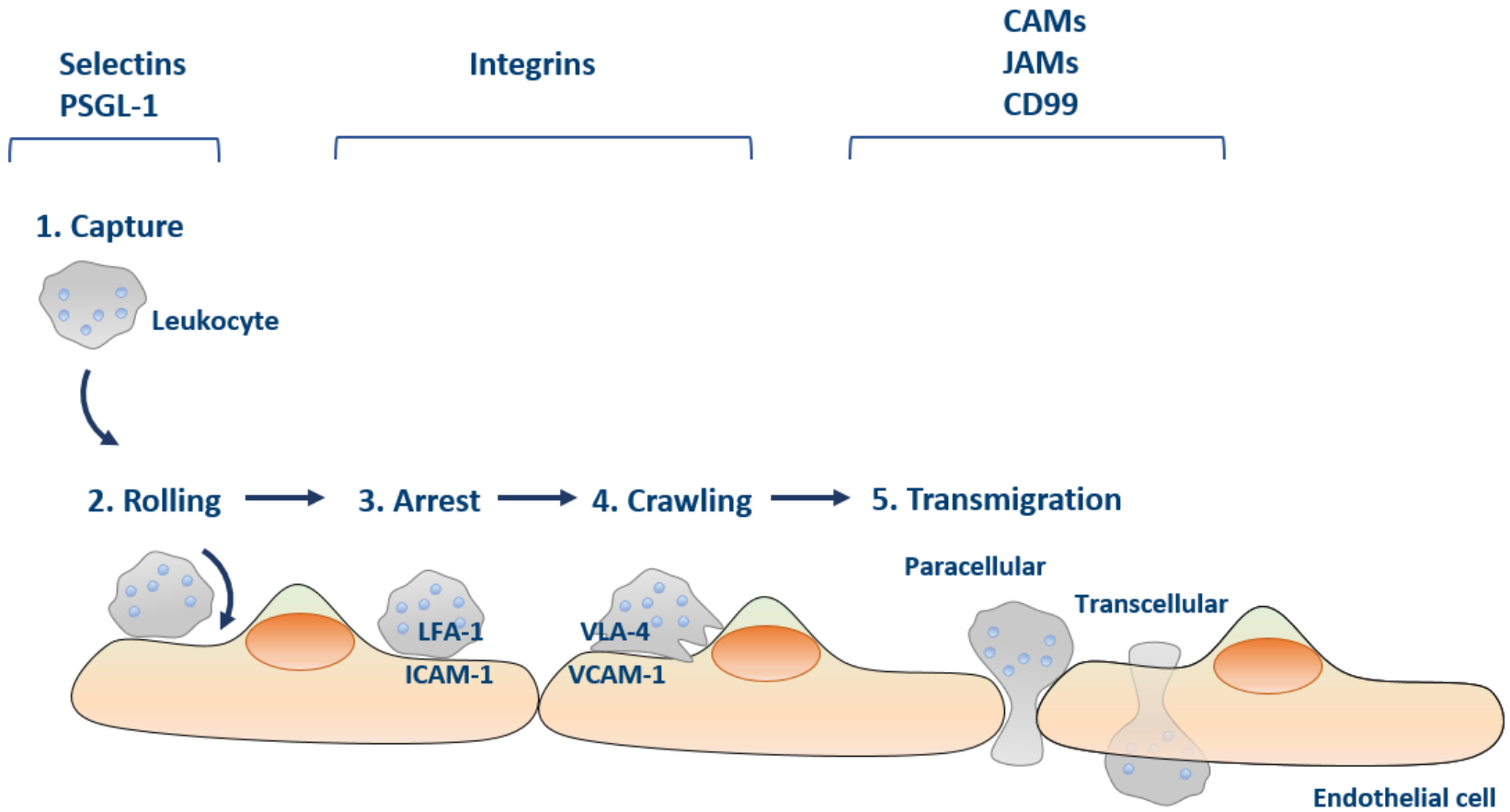

Figure 1.17 The leukocyte adhesion cascade. The recruitment of leukocytes to sites of inflammation requires interaction between EC and the leukocytes. Leukocytes are captured from blood flow and interact with EC through interaction of selectins (on EC) and PSGL-1 (on leukocytes). Leukocyte rolling also entails interaction with selectins. Activation of integrins result in the arrest of the leukocytes and subsequent transmigration that can occur through a paracellular (between EC junctions) or transcellular route (through the EC body). The pivotal role of VCAM-1 and ICAM-1 expression on EC is also highlighted.

Leukocyte rolling provides sustained contact between the leukocytes and the endothelium. Rolling is mediated by L-selectin, P-selectin and E-selectin, and their interaction with PSGL-1. The pivotal role of these selectins in rolling has been demonstrated using a triple L-,E-,P-selectin knock-out mouse that exhibited a dramatic decrease in rolling[303,304]. Integrins, heterodimers composed of an α and β subunit, which are both type I transmembrane proteins, mediate leukocyte arrest and firm adhesion to the endothelium[305]. Integrins are 'activatable' receptors, because intracellular signalling through cell-surface molecules, such as GPCRs is required to increase their ligand-binding capability. The most important integrins for leukocyte adhesion to the endothelium are: (1) lymphocytes function-associated antigen-1 (LFA-1), also known as $\alpha_L\beta_2$-integrin and expressed on all leukocytes; (2) very late antigen-4 (VLA-4), known as $\alpha_4\beta_1$-integrin and expressed on monocytes, eosinophils and neutrophils in certain situations; and (3) macrophage-1 antigen (MAC-1), also known as $\alpha_M\beta_2$-integrin or CD11b-CD18 and expressed on neutrophils and monocytes[306,307].

One of the key events in the cascade is expression of immunoglobulin superfamily members vascular cell adhesion molecule-1 (VCAM-1) and intracellular cell adhesion molecule-1 (ICAM-1) on EC. In the active conformation, integrins bind with high affinity to VCAM-1 and ICAM-1, allowing the leukocytes to firmly adhere to the endothelium. LFA-1 binds to ICAM-1, whereas VLA-4 binds to VCAM-1. Measuring VCAM-1 and ICAM-1 expression on EC allows assessment of leukocyte interaction with the endothelium and their transmigration (see below) during inflammation.

Leukocytes also bind to E-selectin, P-selectin or L-selectin activates integrins[308]. In addition, *in vitro* and *in vivo* studies have demonstrated that leukocyte arrest during rolling is triggered by chemokines or other chemoattractants[309,310]. During inflammation, EC are activated by inflammatory cytokines to express adhesion molecules and produce chemokines and lipid chemoattractants presented on their surface. Other chemoattractants, such as chemokine ligand 5 (C-C motif) (CCL5), chemokine ligand 4 (C-X-C motif) (CXCL4) and chemokine ligand 5 (C-X-C motif) (CXCL5) can be generated by proteolytic cleavage in activated mast cells and platelets and delivered to EC through circulating microparticles or exocytosis of intracellular granules. These molecules also trigger the arrest of rolling leukocytes[311,312].

Following firm adhesion to the endothelium, leukocytes can move away from their initial site of arrest, and extend membrane protrusions into the EC body or at the junctions between EC[313]. This phenomenon promotes myosin contractility within EC and induces the formation of gaps between EC. It has been shown that binding of MAC-1 to ICAM-1 is critical in this process, as neutrophils lacking MAC-1 emigrated without crawling in a murine study[314]. At a molecular level, binding of ICAM-1 is associated with increased intracellular Ca^{2+} and activation of p38 MAPK and Rho GTPase[295].

Transmigration of leukocytes through the endothelium can occur in two different ways: (1) paracellular, between adjacent EC; and (2) transcellular, through the body of a single EC. Some endothelial junctional molecules, such as immunoglobulin superfamily members PECAM-1, ICAM-1, ICAM-2, junctional adhesion molecules JAM-A, JAM-B, JAM-C, as well as the non-immunoglobulin molecule CD99, actively mediate leukocyte transendothelial migration[315,316]. Whereas ICAM-1 and ICAM-2 interact with LFA-1 integrin, PECAM-1 and CD99 exert homophilic interactions, and the JAMs support both homophilic and integrin interactions. Different molecules mediate transmigration in either a stimulus-specific or leukocyte-specific manner. For example, PECAM-1, ICAM-2 and JAM-A mediate leukocyte transmigration in response to interleukin-1β (IL-1β) but not TNF-α[317]. Leukocyte transmigration can be modulated by translocation of PECAM-1 to EC junctions from a cell-surface-connected vesicular compartment and the loosening of adhesive contacts between VE-cadherin on neighbouring cells[318]. Leukocyte migration through the transcellular route occurs in the blood brain barrier and in various inflammatory scenarios[319,320] and *in vitro* models[321,322]. The same molecules that mediate migration through endothelial-cell junctions may also be involved in transcellular migration[320]. ICAM-1 binding results in the translocation of ICAM-1 to F-actin- and caveolae-rich regions[321,323]. ICAM-1-containing caveolae link together forming vesiculo-vacuolar organelles that produce an intracellular channel through which a leukocyte can migrate. Following penetration of the EC barrier, leukocytes then need to migrate through the endothelial basement membrane and the pericyte sheath, which occurs through gaps between adjacent pericytes and regions of low protein deposition within the extracellular matrix. This response can be facilitated by $\alpha_6\beta_1$-integrin and proteases, such as matrix metalloproteinases and neutrophil elastase[324].

Biomarkers of circulating blood cells described in the above sections have been investigated in DIVI and are summarised in **Table 1.5**.

Biomarker	Function	Response in DIVI	Drug reported with	Species	Administration route	Reference
Chemokine ligand-1	Recruitment of neutrophils	Serum levels markedly increased at 4 hours	CI-1044, SCH 351591 and SCH 534385	Rat	Oral gavage	202
Lipocalin-2	Produced by activated neutrophils	Serum levels markedly increased at 8 hours	CI-1044	Rat	Oral gavage	202
TIMP-1	Modulator of lipocalin-2 and matrix metalloprotease	Serum levels markedly increased at 8 hours	CI-1044, SCH 351591 and SCH 534385	Rat	Oral gavage	123,325
Interleukin-1β	Mediator of the inflammatory response		CI-1044	Rat	Oral gavage	202,325
Interleukin-6	Mediator of the inflammatory response	Serum levels markedly increased at 24 hours	CI-1044, SCH 351591 and SCH 534385	Rat	Oral gavage	123,202,325
Macrophage inflammatory protein 3a	Chemotactic for lymphocytes and weak attractant for neutrophils	Serum levels markedly increased at 24 hours	CI-1044	Rat	Oral gavage	202

TNF-α	Mediator of the inflammatory response	No change	SCH 351591 and SCH 534385	Rat	Oral gavage	202
α1-acid glycoprotein	Mediator of the inflammatory response	Serum levels markedly increased at 8 hours	SCH 351591 and SCH 534385	Rat	Oral gavage	123,202
Thrombomodulin	Stimulator of blood vessel formation	Serum levels decreased	CI-1044, SCH 351591 and SCH 534385	Rat	Oral gavage	123
VEGF	Binds free plasma hemoglobin	Serum levels markedly increased at 8 hours	SCH 351591 and SCH 534385	Rat	Oral gavage	123,202
Haptoglobin	Levels rise in response to inflammation	Serum levels markedly increased at 8 hours	SCH 351591 and SCH 534385	Rat	Oral gavage	123,325
C-reactive protein	Levels rise in response to inflammation	Serum levels markedly increased at 8 hours	SCH 351591 and SCH 534385	Rat	Oral gavage	123,325

Table 1.5 Biomarkers of circulating blood cells investigated in DIVI.

1.6.6 Cross-talk of cells during inflammation, a typical feature of DIVI

Figure 1.18 summarises the cross-talk between vascular and circulating blood cells. These phenomena collectively occur in DIVI and the related biomarkers investigated have been listed in **Tables 1.3, 1.4 and 1.5**.

An element that should have more attention in DIVI is the role of extracellular vesicles. For example, it has been demonstrated that extracellular vesicles are elevated in pigs after a single administration of roflumilast, a PDE IV inhibitor. This could provide to be a novel marker that can be easily detected in peripheral blood.

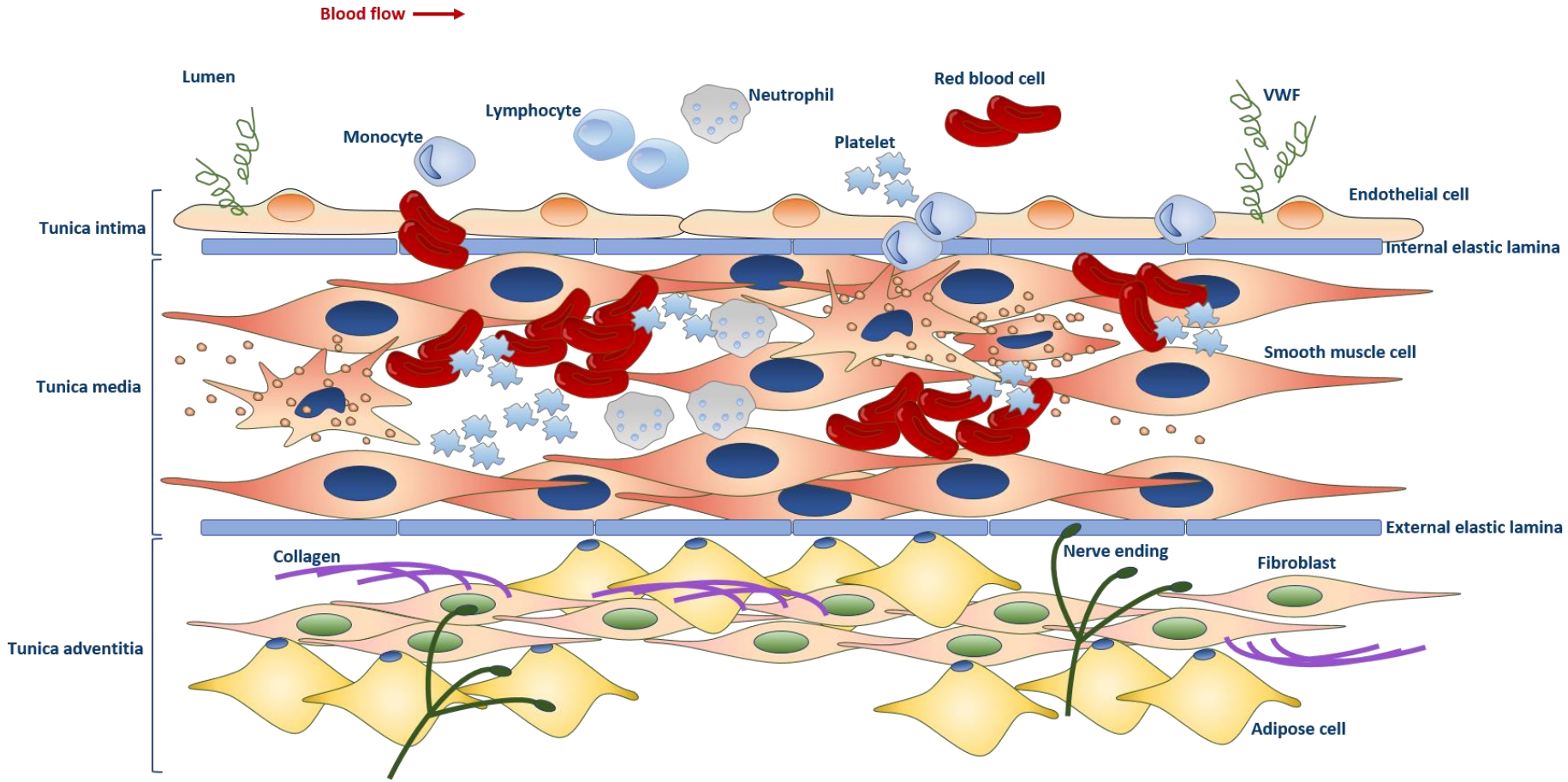

Figure 1.18 Proposed schematic model showing the cross-talk between the cell types involved in DIVI. At the site of the injury, leukocytes adhere to the inter-endothelial gaps, RBC extravasate into the tunica media and occupy cavitations left from necrotic SMC. Cell debris from dead SMC promotes inflammation with recruitment of leukocytes. RBC may acquire an oxidised phenotype sustaining the inflammatory process. Activated platelets congregate at the lesion, contributing to thrombus formation together with VWF released from activated EC. Platelets also form aggregates with leukocytes, upregulating release of pro-inflammatory cytokines. Author's own drawing.

1.7 The importance of flow in blood vessel function

EC in the normal circulation are exposed to two types of forces induced by blood flow: (1) shear stress, the frictional force per unit area parallel to the wall deriving from flowing blood, and (2) circumferential or hoop stress, deriving from blood pressure that drives blood flow, which acts on both EC and SMC[326]. The ability of EC and SMC to respond to shear stress exerted by blood flow is fundamental for the development and function of the vascular system. EC in arteries respond to increased blood flow by causing relaxation of the surrounding SMC and they do so by producing vasodilator substances such as NO, and prostacyclin[326]. By contrast, decreased flow causes vessel narrowing that is also mediated by signals from EC[327]. Under pathological conditions, low flow can lead to apoptosis of EC[328]. VEGF inhibition in mouse tracheas was shown to induce apoptosis of EC marked by activated caspase-3 in capillaries without blood flow.

The changes in EC functions were demonstrated using a model of local stenosis obtained by narrowing large arteries such as abdominal aorta or carotid artery in rats, dogs, and rabbits. It was observed that expression of endothelial genes (see below) greatly differed in areas with laminar as opposed to disturbed flow. In areas of laminar flow, expression of transcription factor Kruppel-like factor-2 (KLF-2), which is responsible for maintaining EC survival, was increased. VE-cadherin expression, which promotes the integrity of the EC junctions, was also upregulated. By contrast, in the post-stenotic region, expression of KLF-2 and VE-cadherin was reduced, and SMAD1/5, a marker of proliferation, was increased[329,330]. These changes in EC functions demonstrate the importance of shear stress in the study of DIVI.

1.7.1 Piezo-1 channel controls blood flow on EC

EC express specific mechanotransducers that convert physical stresses into biochemical signals. Several mechanotransducers have been proposed to function in sensing flow, including ion channels, integrins, receptor tyrosine kinases, the apical glycocalyx, primary cilia, heterotrimeric G proteins, PECAM-1 and VE-cadherin[331,332].

Piezo-1 and Piezo-2 are mechanically activated cation channels that form homomultimeric complexes that mediate mechanically induced currents[333,334]. Piezo-2 is the main sensor of mechanical stimuli in mammalian Merkel cells (located in the basal epidermal layer of the skin)[335], whereas Piezo-1 has been shown to mediate mechanically activated cation currents in various other cell types, including EC[336,337]. It has been demonstrated that deficiency of Piezo-1 leads to disruption of vascular development in the mouse embryo and yolk sac demonstrated with hematoxylin and eosin (H&E) staining and PECAM-1 immunostaining to observe vessel morphology. These vascular defects resulted in embryonic lethality. In the same study, it was also demonstrated that Piezo-1 can be activated by shear stress and that loss of Piezo-1 affects the ability of HUVEC to alter their alignment when subjected to shear stress[336].

Furthermore, it has been shown using Piezo-1 deficient mice, that Piezo-1 mediates flow-induced ATP release and subsequent activation of G_q /G_{11}–coupled purinergic $P2Y_2$ receptors that are involved in NO formation and thus regulation of vascular tone and blood pressure[338]. Activation of G_q /G_{11}–coupled purinergic $P2Y_2$ receptors promotes the phosphorylation and activation of Akt, which in turns phosphorylates and activates eNOS, responsible for the production of NO from L-Arginine[339]. Piezo-1 deficient mice lost the ability to induce NO formation and vasodilation in response to flow and developed hypertension.

1.7.2 Yoda-1 activates EC Piezo-1 channels mimicking shear stress

In addition to flow, Piezo-1 channels can also be activated by the synthetic small molecule Yoda-1. Yoda-1 stabilizes the open conformation of the Piezo-1 channel, reducing the mechanical threshold for activation in the absence of flow. Interestingly, Yoda-1 does not activate Piezo-2, despite the high sequence similarity between these two homologs.

In vitro, administration of Yoda-1 mimicked the effect of shear stress and induced activation of eNOS and vasodilation of isolated arteries[338]. Moreover, Yoda-1 in static HUVEC cultures mimicked the effect of laminar shear stress by promoting phosphorylation of Akt and eNOS, the well-established effects of shear stress on expression of ICAM-1 and VCAM-1[340]. It was

also shown that Yoda-1 inhibited the ability of TNF-α to increase ICAM-1 and VCAM-1 expression in HUVEC.

Given the similarities between the effects of flow and Yoda-1 on Piezo-1 channels, Yoda-1 may represent a useful tool in constructing an *in vitro* human model without the use of complicated systems involving flow.

1.8 An *in vitro* model of DIVI

An *in vitro* model would be a very useful tool for the study of DIVI among other vascular disorders. Specifically, a model that allows study of EC and SMC injury and subsequent inflammation would help understand the human relevance of DIVI that is currently unclear. As mentioned earlier, drugs that cause DIVI in preclinical species are often stopped from further development or the drug development is delayed to allow further safety evaluation. An *in vitro* model to understand the mechanisms of DIVI would be the first step to allow screening of compounds for DIVI risk in drug development making the entire process more time- and cost-efficient.

Currently, there is a lack of *in vitro* human systems to study DIVI and only two models of DIVI are available. The limitations with these models are that they are quite complicated to build and to standardise across different laboratories. An overview of these systems is given in the below sections.

1.8.1 Existent *in vitro* models to study DIVI

Efforts have been made to identify biomarkers of DIVI and in developing *in vitro* models. The most successful models focus on the study of EC-SMC interaction and flow in order to recapitulate the *in vivo* physiology of blood vessels.

An *in vitro* model of DIVI has been developed by the American company HemoShear, whereby a co-culture platform of rat primary EC and SMC separated by a synthetic internal elastic lamina allowed exposure of the endothelium to *in vivo*-derived hemodynamics[79]. In this

system it was observed that fenoldopam enhanced permeability and expression of inflammatory, cell death and oxidative stress genes.

A second model for the study of DIVI is a microfluidic vascular device, whereby primary rat aortic EC and SMC are co-cultured across a porous membrane that mimics the internal elastic lamina, and the cells are exposed to arterial flow rates within the endothelial chamber[114]. This model also allows for study of extravasation of RBC into the smooth muscle layer, a phenomenon common in DIVI. A previously identified compound that causes DIVI, the PDE IV inhibitor CI-1044 (**Table 1.5**), has been tested in this device and it has been found to induce significant extravasation of RBC (which has been qualitatively assessed in this study, as present or absent in the device). Extravasation may have been due to the deleterious effects of the drug on the EC junctions, or perhaps via vascular oxidant stress and inflammation[114]. Importantly, blood flow does not change in this model, suggesting that DIVI phenotype can occur without a local increase in blood flow. Therefore, complex co-culture models can give insights into mechanisms that cannot be seen *in vivo*. However, although this model allows recapitulation of many of the mechanisms implicated in DIVI, it has some limitations. For example, flow in the device is laminar and non-pulsatile as it is *in vivo*. In addition, the SMC in the device do not undergo mechanical stresses as they do in resistance vessels and likely do not have a contractile phenotype. This phenotype could be induced *in vitro* by reducing the growth factors and serum in the cell medium, which causes the cells to differentiate.

Currently, there is nothing available beyond these *in vitro* models. Furthermore, these systems are complex and neither time- nor cost-efficient. In order to have utility as an *in vitro* screening test of candidate drugs with DIVI risk, the model should be easy to build, reproducible, high-throughput and predictive. However, it may be unrealistic to expect that one model may be able to capture the mechanism by which all the drugs contribute to DIVI. The aim of this PhD is to rather study a toxicological event in human cells, and specifically define a toxicological limit around which the therapeutic index (IT) of a drug can be set, so that in the future the number of DIVIs seen in the clinic would be reduced. Although the on-target effect of each drug has been presented in this Introduction, it is more likely that an off-target action is implicated in DIVI. No studies so far have been directed at understanding the off-target effect of DIVI-related drugs.

In summary, the mechanisms driving DIVI are poorly understood. Vasodilatation and changes in blood flow are critical events in the pathogenesis of injuries, but a clear understanding of the onset and progression of the lesions is lacking. Finally, the clinical relevance of DIVI remains uncertain, as there are no reports of DIVI in humans treated with the same drugs that caused DIVI in preclinical species. However, in the absence of methodologies to effectively assess the drug-induced vascular lesions in humans, the occurrence of DIVI during preclinical assays can hinder the development of potentially novel medicines. Therefore, a model to accurately translate from preclinical observation to clinical setting is needed. This would be beneficial to cut time and costs of drug development and to reduce morbidity and mortality associated with ADRs.

1.9 Aims and objectives

Reports suggest that the research and development (R&D) process of a new drug takes on average 15 years and costs over 1 billion dollars, with only 0.01 % of compounds making it to market[1,2]. This is, in part, due to toxicity, which accounts for 22 % of drugs that enter the clinical phase, with an even larger proportion of drugs being halted during preclinical development. Despite years of effort to improve R&D efficiency and performance, bringing a new drug to market still remains a very expensive and time-consuming process. A major issue is the ability to predict and translate drug toxicity from the pre-clinical animal studies to clinical trials.

The aim of this thesis was to help define a toxicological limit around which the therapeutic index (TI) of a drug can be set, in order to reduce in the future the number of DIVIs seen in the clinic. Throughout this PhD this is achieved by determining the dose window for DIVI.

The drugs chosen in this thesis (refer to **Introduction**, section **1.4.1**, for selection criteria) have all been shown to produce DIVI at the non-clinical stage.

This thesis, in collaboration with the Cardiovascular Safety Group, Drug Safety and Metabolism at AstraZeneca, had two specific objectives:

1) Reproduce DIVI in an *ex vivo* model using the selected drugs in relevant animal tissue (refer to **Introduction**, section **1.4.1**).

2) Identify whether the selected drugs could induce vascular injury either directly on human vascular cells or indirectly through interaction with human blood cell, using conditions that would mimic the *in vivo* physiology.

2. Materials and Methods

2.1 Materials

A list of reagents and chemicals used within this thesis is presented in **Table 2.1**. **Table 2.2** illustrates cells, media and reagents used in cell culture, and **Table 2.3** shows a list of primary, secondary antibodies and isotype controls. Finally, in **Table 2.4** a list of reagents used for protein biochemistry is presented.

Reagent	Manufacturer	Catalog number	Composition/ Working concentration	Application
Bosentan	Cayman Chemicals	11731	1, 10, 100 µM	FC, ICH, IF, Luminescence
BQ 123	Sigma Aldrich	B150	1 µM	FC
BQ 788	Sigma Aldrich	B157	1 µM	FC
BSA	Sigma Aldrich	A7906	2 % or 10 % w/v	ICH, IF
CellTiter-Glo	Promega	G7572	n/a	Luminescence
Cell tracker™ green	Life Technologies	C7025	10 µM	IF
Cell tracker™ deep red	Life Technologies	C34565	0.5 µM	IF
DAPI	Thermo Fisher	D1306	300 nM	ICH, IF
DMSO	Sigma Aldrich	276855	Neat	FC, ICH, IF, Luminescence
Fenoldopam mesylate	Cayman Chemicals	17629	1, 10, 100 µM	FC, ICH, IF, Luminescence
Fix/lyse solution	eBioscience	00-5333-54	1x	FC
fMLP	Sigma Aldrich	F3506	10 µM	FC
Goat serum	Sigma Aldrich	S-26M	5 % v/v	ICH
ibidi mounting medium	ibidi	50001	Neat	IF
Krebs buffer	Made in house	n/a	10x stock (used at 1x): 1.26 M NaCl, 25 mM KCl, 250 mM $NaHCO_3$, 12 mM NaH_2PO_4, 12 mM $MgCl_2$, 25 mM $CaCl_2$	ICH
Minoxidil sulfate salt	Sigma Aldrich	M7920	1, 10, 100 µM	FC, ICH, IF, Luminescence
O.C.T.	Thermo Fisher	23-730-571	Neat	ICH
PBS	Sigma Aldrich	P4417	1x	FC, ICH, IF
PFA	Alfa Aesar	J61899	4 % v/v	FC, ICH, IF
PPACK	Cayman Chemicals	15160	75 µM	FC
ProLong Gold antifade mounting medium	Life Technologies	P36930	Neat	ICH
PI	Sigma Aldrich	P4170	10 µg/ml	FC
Rolipram	Sigma Aldrich	R6520	1, 10, 100 µM	FC, ICH, IF, Luminescence
Saponin	Sigma Aldrich	47036	0.15 % v/v	Luminescence

Shandon embedding matrix	Thermo Fisher	1310	Neat	ICH
Sylgard 184	Dowsil	101697	n/a	ICH
Thrombin from bovine plasma	Sigma Aldrich	T4648-1KU	1 U/ml	ICH, IF
TRAP-6 amide	Bachem	H-2936	100 µM	FC
Triton X-100	Sigma Aldrich	T9284	0.1 % v/v	IF
TNF-α	R&D systems	210-TA-010	1 - 100 U/ml	FC
Tween 20	Santa Cruz	SC-29113	0.1 % v/v	ICH
Yoda-1	Sigma Aldrich	SML 1558	0.05 - 100 µM	IF, Luminescence

Table 2.1 List of reagents and chemicals used in alphabetical order. Abbreviations: FC = Flow cytometry, ICH = Immunocytochemistry, IF = Immunofluorescence.

Product	Manufacturer	Catalog number	Composition/ Working concentration	Application
HCASMC	Promocell	C-12511	500,000 cryopreserved cells	Cell culture
HCASMC media	Promocell	C-22062	n/a	Cell culture
Supplements HCASMC media	Promocell	C-39267	Fetal calf serum (0.05 ml/ml), epidermal growth factor (recombinant human, 0.5 ng/ml), basic fibroblast growth factor (recombinant human, 2 ng/ml), insulin (recombinant human, 5 µg/ml)	Cell culture
HUVEC	Promocell	C-12203	500,000 cryopreserved cells	Cell culture
HUVEC media	Promocell	C-22010	n/a	Cell culture
Supplements HUVEC media	Promocell	C-39215	Fetal calf serum (0.02 ml/ml), endothelial cell growth supplement (0.004 ml/ml), epidermal growth factor (recombinant human, 0.1 ng/ml), basic fibroblast growth factor (recombinant human, 1 ng/ml), heparin (90 µg/ml), hydrocortisone (1 µg/ml)	Cell culture
Cryo-SFM	Promocell	C-29912	n/a	Cell culture
FBS	Gibco	26140079	1x	Cell culture
Gentamycin	Sigma Aldrich	G1272	35 µg/mg	Cell culture
Medium M199	Sigma Aldrich	M2520	1x	Cell culture
Trypsin-EDTA 0.25 % v/v	Gibco	25200-056	1x	Cell culture

Table 2.2 List of cells, media and reagents used in cell culture.

Antibody	Host	Manufacturer	Catalog number	Dilution	Application
Primary antibodies					
CD31	Mouse	Abcam	Ab119339	ICH 1 : 100 IF 1 : 500	ICH, IF
Human CD11b (APC)	Mouse	eBioscience	340937	1 : 100	FC
Human CD14 (PE)	Mouse	eBioscience	12014942	1 : 100	FC
Human CD15 (FITC)	Mouse	eBioscience	562370	1 : 100	FC
Human CD31 (APC)	Mouse	eBioscience	17031942	1 : 100	FC
Human CD41 (PE-Cy7)	Mouse	eBioscience	303718	1 : 50	FC
Human ICAM-1 (FITC)	Mouse	eBioscience	BMS108FI	1 : 100	FC
Human PAC-1 (FITC)	Mouse	eBioscience	340507	1 : 20	FC
Human P-selectin (PE)	Mouse	eBioscience	304905	1 : 20	FC
Human VCAM-1 (PE-Cy7)	Mouse	eBioscience	25106942	1 : 100	FC
Phospho-Akt	Rabbit	Cell Signaling	9272	1 : 1000	WB
Phospho-eNOS	Rabbit	Cell Signaling	9572	1 : 1000	WB
β-tubulin	Rabbit	Cell Signaling	2146	1 : 1000	WB
VWF	Rabbit	Abcam	Ab6994	ICH 1 : 200 IF 1 : 1000	ICH, IF
Secondary antibodies					
F(ab')2 Goat Anti-Rabbit IgG (FITC)	Goat	Invitrogen	11483981	ICH 1 : 500 IF 1 : 1000	ICH, IF
Goat Anti-Mouse IgG (Alexa Fluor 647)	Goat	Thermo Fisher	A21235	ICH 1 : 500 IF 1 : 1000	ICH, IF
Isotype controls					
Mouse IgG1 κ (APC)	Mouse	eBioscience	17471482	1 : 100	FC
Mouse IgG1 κ (FITC)	Mouse	eBioscience	11471442	1 : 100	FC
Mouse IgG1 κ (PECy7)	Mouse	eBioscience	25471442	1 : 100	FC

Table 2.3 List of primary and secondary antibodies and isotype controls used within this thesis. Abbreviations: FC = Flow cytometry, ICH = Immunocytochemistry, IF = Immunofluorescence, WB = Western blot.

Product	Manufacturer	Catalog number	Composition/ Working concentration	Application
Chemiluminescent substrate	Thermo Fisher	34577	n/a	WB
DTT	Sigma Aldrich	10197777001	10 mM	WB
PBS-T	Made in house	n/a	1x PBS 0.1 % w/v Tween 20	WB
Protease inhibitor cocktail	Sigma Aldrich	P8340	1 : 100	WB
RIPA lysis buffer	Made in house	n/a	100 mM tris pH 8; 2 % v/v Triton X-100; 0.2 % w/v SDS; 1 % w/v sodium deoxycholate; 300 mM sodium chloride	WB
Running buffer	Made in house	n/a	10x stock (used at 1x): 0.1 % sodium dodecyl sulfate; 190 mM glycin; 25 mM tris-base	WB
Transfer buffer	Made in house	n/a	10x stock (used at 1x): 190 mM glycin; 25 mM tris-base	WB

Table 2.4 List of reagents used for protein biochemistry. Abbreviation: WB = Western blot.

2.2 Methods

2.2.1 *Ex vivo* studies

Animal handling and experiments conformed to the UK Animal Scientific Procedures Act – specifically schedule 1 procedures that cover methods of euthanasia appropriate for different species, weights and stage of development, and were planned in order to minimise the usage of animals. Animal handling and sacrifice was carried out by AstraZeneca scientists. Han Wistar male and female rats 8 weeks old were euthanised using carbon dioxide (CO_2) before confirmation of death. A total of 4 rats was used for an experimental set. This is a limited number for *in vivo* studies and more animals should have been included in the study. However, previous studies in the field describe similar experiments using a comparable number of animals. In addition, considerations related to the Replacement, Refinement and Reduction of Animals in Research (3Rs) have been made and the number of rats used kept to the minimum.

2.2.1.1 Isolation of the rat superior mesenteric artery, treatment and fixation

Fresh gut tissue from rats was transported to the department of Pharmacology on ice in carbogenated Krebs buffer (see **Table 2.1** for recipe) and processed immediately. Krebs buffer pH was adjusted to 7.2 and the solution autoclaved and stored for a maximum of 24 hours. The rat gut was carefully dissected to isolate the superior mesenteric artery (SMA) (see **chapter 3** for location of the artery). Care was taken to minimise trauma to the artery. The dissection was conducted using a dissection microscope with high quality sharp forceps and micro scissors. A petri dish coated with Sylgard 184 was used to pin down the tissue to facilitate the isolation of the artery. The Krebs solution in the petri dish was replenished when needed, to ensure that the tissue remained hydrated and alive. An oxygen cylinder was used to oxygenate the Krebs buffer throughout the dissection and also later for the entire treatment duration.

Following isolation, the SMA was cut into six equal length segments (approximately 2 mm in length). Each segment was incubated separately with a drug (refer to I**ntroduction**, **Table 1.1**)

or the appropriate control and kept at 37 °C for 24 hours. Following treatment, segments were washed twice in Krebs buffer and fixed overnight using 4 % v/v PFA.

2.2.1.2 Tissue freezing and cryostat sectioning

Aortic tissue segments were frozen promptly as described below to avoid large ice crystal formation that can cause morphological distortions that can damage the tissue. Vessel segments were adjusted in labelled cryomolds with Shandon embedding matrix to cover the tissue ensuring optimal conditions for freezing, by avoiding the formation of crystals in those specimens containing high water content. The orientation of the vessel segment was labelled on the cryomold to make sure its horizontal or vertical direction during cryo-sectioning was known. The cryomolds holding each vessel segment were then immersed in liquid nitrogen until completely frozen and then stored at - 80 °C until further use.

Before sectioning with the cryostat (Leica CM1900, Leica Biosystems), the frozen blocks were allowed to equilibrate in the cryostat chamber (-24 °C) for approximately 30 minutes. Optimum cutting temperature formulation was used to make the frozen block adhere to the sample support and left to freeze. Sections were cut to 10 µM thickness and collected on Superfrost Plus glass slides. The anti-roll plate, made of coated glass, was used to prevent frozen sections from curling upwards, after sectioning.

2.2.2 Cell culture

All primary cells were cultured at 37 °C, 5 % CO_2, under humidifying conditions. Appropriate sterile tissue culture treated plasticware was used.

Human umbilical vein endothelial cells (HUVEC) and human coronary artery smooth muscle cells (HCASMC) were purchased from PromoCell as cryovials containing 500,000 cells and seeded at the recommended density of 10,000 cells/cm^2 into a T25 flask. HUVEC were from pooled donors, and HCASMC were isolated from tissue from a single donor (**Table 2.2**). It would have been ideal to use for the studies endothelial and smooth muscle cell lines

originating from arteries usually affected by DIVI. HUVEC are derived from veins from immune-naïve foetal tissue and show differences from adult vascular endothelium.
However, HUVEC were selected as the source of EC since they have been extensively characterised in the literature[341] and HCASMC were used as the source of arterial vascular SMC as they have also been widely described[342]. Limitations related to the sensitivity to drugs and shear stress should be taken into considerations and will be described more in detail in the specific chapters sections.

2.2.2.1 Cell passaging, storage and thawing

All cells were cultured in medium supplemented with growth factors and 35 µg/ml antibiotic (gentamycin) to prevent infections (**Table 2.2**). Medium was changed 24 hours after plating and subsequently every 2 days, until cell confluency was reached. Cells were passaged when they reached 70 - 90 % confluency until passage 6. A schematic of a typical passaging timescale is shown in **Figure 2.1**.

Firstly, the cells were washed with ethylenediaminetetraacetic acid solution (EDTA), a chelator used to remove calcium from the media. Cadherin and integrin protein which hold cells to each other and their underlying substrate rely on calcium ion binding to maintain their globular structure. Cells are detached with addition of pre-warmed trypsin. The cells detach once pre-warmed trypsin is added. Trypsin is a serine protease which hydrolyses adhesion proteins. Complete cell detachment was verified by light microscopy. Trypsin was neutralised with an excess of pre-warmed M199 media containing 20 % filtered fetal bovine serum (FBS) and the cells were centrifuged at 1,500 RPM for 4 minutes. After centrifugation, the pellet was resuspended in fresh EC or SMC medium (as described above) and the cells were reseeded. Upon reaching passage 6, cells were harvested, pelleted and resuspended in 1 ml cryopreserving medium aliquots (Cryo-SFM). Cryo-SFM is a protein-free medium containing methylcellulose and DMSO to provide preservation of cells. Cells were stored for at least 4 hours at - 80 °C, before being transferred to liquid nitrogen for long-term storage.

For thawing, the cryovial was removed from the liquid nitrogen container and immediately placed on dry ice for transportation to the correct location. The vial was then immersed into a water bath (37 °C) for approximately 2 minutes until only a small cell ice pellet could be observed; the cells were transferred to a T25 flask containing pre-warmed medium. The medium was replaced after 24 hours and the cells grown for 48 hours post thawing before conducting an experiment. HUVEC were not used experimentally after passage 8 as it has been shown that HUVEC lose their characteristic phenotype and become more fibroblast-like in nature[343].

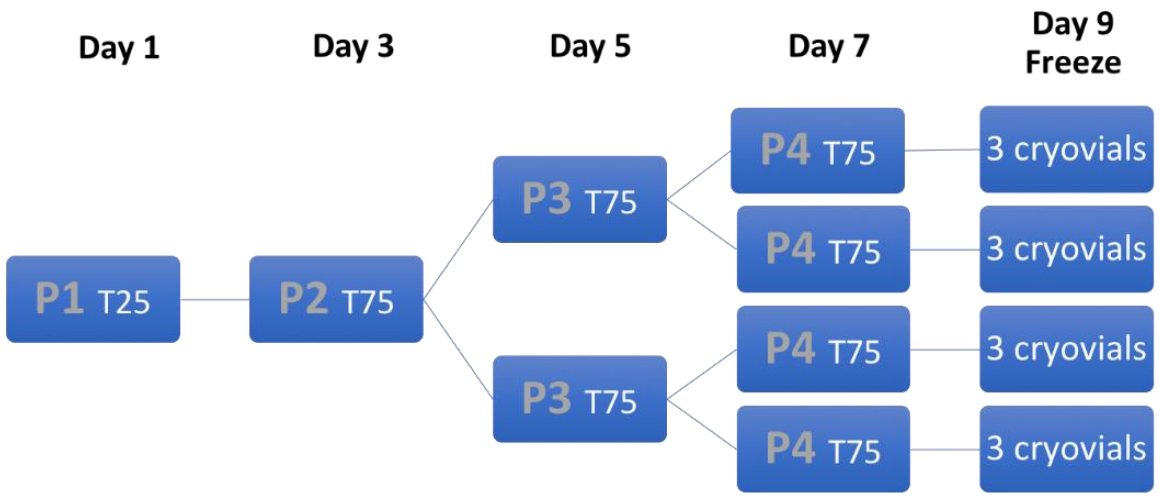

Figure 2.1 Typical cell passaging timescale from P1 to P4.

2.2.2.2 Co-culture of HUVEC and HCASMC

HUVEC and HCASMC at passage 6 were grown in T25 flasks separately until confluent. Cell trackers were used to visualise the two cell types. SMC were labelled with Cell Tracker Deep Red (0.5 µM), while EC were labelled with Cell Tracker Green (10 µM) (**Table 2.1**). The working concentration was selected (according to manufacturer's guidance) such that normal cellular physiology would be maintained whilst producing a signal sufficient enough to observe without providing artefacts. Since the red dye produces a higher fluorescent signal compared to the green, the selected concentration was lower in these experiments. Cells were washed with RPMI and incubated for 20 minutes with the trackers at 37 °C. Trackers were washed off

to remove excess dye and the stained cells resuspended together at the correct density. Cells were seeded into ibidi slides and incubated for 24 hours before fixation in 4 % v/v PFA and microscopy imaging.

2.2.2.3 HUVEC culture under shear stress

HUVEC were seeded into a µ-slide $VI^{0.4}$ (ibidi) at 6 x 10^4 cells/channel and left to adhere for 2 hours prior to the addition of flow through the connection of a perfusion pump set (ibidi, 10902). The perfusion system is a computer-operated positive air pressure pump (ibidi). HUVEC were exposed to a continuous shear rate of 5 dyn/cm^2, according to the manufacturer's instructions. HUVEC were maintained at 5 % CO_2 and 37 ^oC while under shear stress.

2.2.3 Whole blood experimentation

2.2.3.1 Whole blood collection and treatment

Blood was taken from healthy volunteers who gave full informed consent. Care was taken to select donors that were not on medication or pain relief that may interfere with blood cell activation. Blood was taken through venipuncture by trained phlebotomists in the Harper lab. Blood was collected in Vacuettes containing 75 µM D-Phenylalanyl-propyl-arginyl Chloromethyl Ketone (PPACK). PPACK is a synthetic peptide derivative that acts as an anticoagulant, irreversibly and specifically inhibiting thrombin-mediated platelet activation by binding with high affinity to an allosteric site of thrombin. Unlike more commonly used anticoagulants, such as sodium citrate or EDTA, the divalent cation concentration in plasma is maintained at normal levels.

Never longer than 5 minutes after being taken, blood was aliquoted into 1.5 ml centrifuge tubes and treated with either bosentan, fenoldopam mesylate, minoxidil sulfate salt, and rolipram (**Table 2.1**) at 1 µM, 10 µM, and 100 µM concentrations. 100 µM thrombin receptor-activating peptide (TRAP)-6 amide and 10 µM N-formyl-Methionyl-Leucyl-Phenylalanine (fMLP) were used as a positive control for platelet activation and leukocyte activation, respectively.

After a 20, or 60 minute stimulation, conducted at room temperature, 50 µl of blood per condition was aliquoted into fresh 1.5 ml centrifuge tubes and stained with the appropriate

antibodies for 5 minutes in the dark. Antibodies used in this study were CD41 PE-Cy7, P-selectin PE, and PAC-1 FITC for platelets; CD14 PE, CD15 FITC, and CD11b APC for leukocytes. Isotype controls were used for each antibody. See **Table 2.3** for corresponding catalogue numbers and dilutions.

Following antibody staining, 350 µl fix-lyse solution diluted to 1x in dH_2O was added to cells and incubated for 15 minutes at room temperature. Fix-lyse solution contains ammonium chloride which lyses red blood cells (RBC) with minimal effect on leukocytes. This lysis of only RBC allowed clear visualisation of the other fixed blood components after staining with antibodies. Samples were read using a flow cytometer (BD Accuri C6, BD Biosciences).

2.2.4 Flow cytometry

2.2.4.1 Instrument parameters

FITC signal was excited at 488 nm and detected at 530 nm; APC signal was excited at 633 nm and detected at 660 nm; PE was excited at 488 and detected at 575 nm; Pe-Cy7 was excited at 488 nm and detected at 774 nm. Data were acquired and analysed with the software BD Accuri C6. Gating strategies are explained in detail in appropriate results chapters.

2.2.4.2 Investigating inflammation by measuring VCAM-1 and ICAM-1 expression

HUVEC were grown for 24 hours in a 24-well plate. Cells were treated separately with drugs or 100 U/ml TNF-α, a known inflammatory stimulus that served as a positive control for 24 hours. Cells were detached from the wells using accutase, a less stringent protease than trypsin that would leave the surface adhesion molecules intact or uncleaved. Cells were pelleted using the protocol in section **2.2.2.1**. The supernatant was removed, and the cell pellets were resuspended in 100 µl of filtered PBS. For each treatment, cells were stained with the following antibody cocktails for 5 minutes in the dark: i) ICAM-1 FITC, VCAM-1 PECy7; ii) IgG FITC, IgG PECy7; iii) CD31 APC; iv) IgG APC (refer to **Table 2.3**). Unbound antibody was washed off by centrifugation, and the samples read with the flow cytometer BD Accuri C6. A

total of five N was conducted. Analysis was conducted using the BD Accuri C6 software (see section **2.2.4.5** below).

2.2.4.3 Investigating cell death with propidium iodide in co-culture

HCASMC were tracked with Cell Tracker Deep Red (0.5 µM) as described in section **2.2.2.2**, then HUVEC and HCASMC were seeded in a 2:1 mixture in 24 well plates, left to grow for 24 hours and then treated with the drugs at 100 µM for 24 hours or with cisplatin 50 µM used as positive control. Single HUVEC and single HCASMC were also seeded in parallel. Following treatment, cells were washed with EDTA and incubated with accutase for cell detachment. Accutase was neutralised with M199 containing 20 % v/v FBS, cells were harvested, spinned down, HUVEC were stained with CD31, and propidium iodide (PI) 10 µg/ml was added to all cells. Finally, cells were analysed by flow cytometry.

2.2.4.4 Acquisition of events with flow cytometer

Initially, live cell populations were gated using the forward and side scatter profiles (representing the size and granularity of cells, respectively) to exclude dead cells and cellular debris. These populations were then further gated using a cell type specific antibody. For each experiment, at least 20,000 events were collected in the platelet gate, and 1,000 events were collected in the neutrophil- and monocyte-gate. For EC or SMC, at least 10,000 events were acquired. For compensation beads, a gate was drawn around the beads and 5,000 events were acquired.

2.2.4.5 Analysis from data acquired by flow cytometry

Prior to the analysis each channel was compensated to account for fluorescence bleed-through. OneComp eBeads (eBioscience) were used for compensation according to the manufacturer's instructions. Compensation analysis and analysis of the compensated data were carried out using the BD Accuri C6 software, using the median fluorescent intensity (MFI) to reflect the abundance of a specific surface protein.

2.2.5 Confocal microscopy

2.2.5.1 Equipment and imaging parameters

Images were acquired using the Leica TCS SP5 confocal microscope (Leica Microsystems). DAPI (4', 6-diamidino-2-phenylindole) was excited at ʎ=405 using a UV laser line; AlexaFluor® 488 nm was excited with an Argon laser at ʎ=488, AlexaFluor® 633 was excited with a helium-neon laser at ʎ=633. Images were acquired using LAS AF software (Leica Microsystems) with a 20x (for the mesenteric artery experiment) or 63x (for cell culture) oil immersion objective at 1024 x 1024 pixels with a 16-bit resolution at a frequency of 100 Hz and 3-line average.

2.2.5.2 Vessel fixation and staining procedures

Cryo-sections were outlined with a hydrophobic wax pen to minimize antibody usage. Cryo-sections were permeabilised with 0.1 % v/v Tween 20, and then incubated for 1 hour in block solution (10 % w/v BSA, 5 % v/v goat serum, and 0.1 % v/v Tween 20, in PBS). The sections were then incubated with a combination of one of the primary antibodies (**Table 2.3**) overnight at 4 °C in block solution (without 0.1 % v/v Tween 20). Sections were washed twice in PBS and incubated in blocking solution with fluorescently conjugated secondary antibodies and DAPI (**Table 2.3**) for 1 hour at room temperature. Following two washes, sections were mounted using ProLong Gold antifade mounting medium that preserves the fluorescent signal and reduces the degree of photo bleaching when imaging. Slides were stored at 4 °C prior to imaging to ensure the stability of the samples. One picture of a complete vessel cross section was analysed for every condition per N, for a total of 4 N performed with different animals on separate days.

2.2.5.3 Cell fixation and immunostaining

Cells were seeded at 100,000 cells/well in ibidi slides and left to grow for 24 hours. After treatment, cells were washed with PBS and fixed with 4 % v/v PFA for 10 minutes at room temperature, permeabilised with 0.1 % v/v Triton X-100 for 5 minutes and then blocked with 2 % w/v BSA in PBS prior to immunostaining. The antibodies used for staining are shown in

Table 2.3. The cells were mounted using ibidi mounting media. Six images were collected per treatment per N, for a total of four N. Analysis was conducted in ImageJ. Images in the green channel (VWF) were thresholded to remove background noiseand the VWF-positive cells were counted. Analysis of VWF and endothelial junctional breakage is described in detail in **chapter 4**.

2.2.6 Investigating cell death using an ATP viability assay

The luminescent cell viability assay was used to determine the number of viable cells in culture based on the quantification of the nucleotide adenosine triphosphate (ATP). The reaction is catalysed by the enzyme luciferase obtained from the firefly (Photuris pennsylvanica). In the presence of ATP, luciferin gets catalysed by the enzyme luciferase to the light-emitting product, oxyluciferin (**Figure 2.2**). Cell injury or cell death results in loss of plasma membrane integrity leading to a decrease in cytoplasmic ATP, therefore in this assay the luminescence signal is proportional to the number of viable cells present.

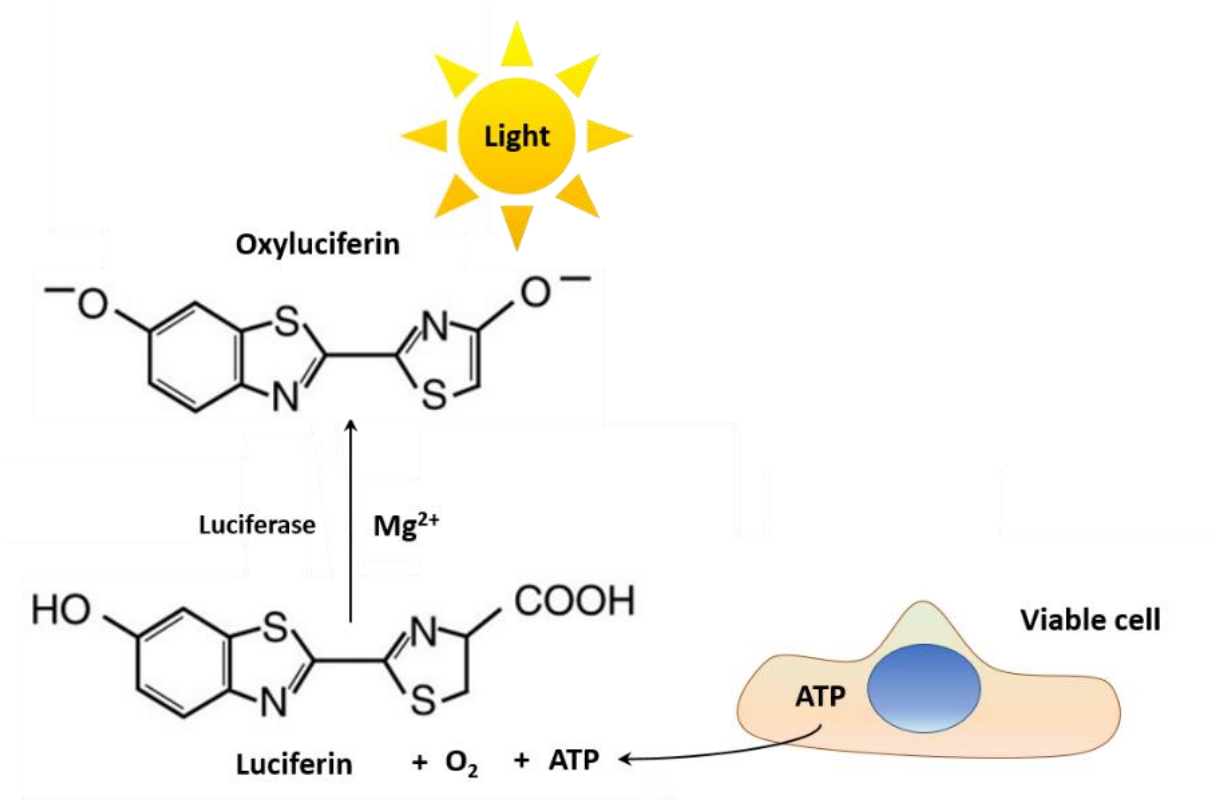

Figure 2.2 ATP luminescence assay. Mono-oxygenation of luciferin is catalysed by luciferase, contained in the reagent, in the presence of Mg^{2+}, O_2, and ATP.

HUVEC and HCASMC were seeded in an opaque-walled (to prevent luminescence bleed-through) 96-well plate at a density of 10,000 cells/well and grown for 24 hours. Cells were treated with the drugs (refer to **Introduction**, **Table 1.1**) or DMSO (to serve as a control) for 1, 4 and 24 hours at 37 °C. 0.15 % w/v of the detergent saponin was used as positive control for cell death. The detergent (also present in the assay reagent) induces cell lysis, enabling the released ATP to react with the luciferin and emit light. 30 minutes before each time point, the plate was left to equilibrate at room temperature, after which CellTiter-Glo® reagent was added to the cells to induce cell lysis at a volume equal to the cell culture medium present in each well. The content was mixed for 2 minutes on an orbital shaker and the plate was then incubated at room temperature for 30 minutes in the dark. During this time, unstable ATP is catalysed to ADP. For the Yoda-1 experiment, experimental conditions remained the same except that cells were pre-treated with Yoda-1 for 24 hours before drug treatment.

The luminescence was measured and recorded with a microplate reader (CLARIOstar *Plus*, BMG Labtech). Data were expressed as % survival compared to a vehicle treated cells on the

same plate. In addition, wells containing medium without cells were used to obtain a value for background luminescence. A standard curve with 4 concentrations of ATP (1 nM, 10 nM, 100 nM, 1 μM) was also obtained in order to understand the working range of the assay prior to the biological experiments. The curve was generated by preparing serial tenfold dilutions of ATP in culture medium and following the same protocol explained previously. Experiments were conducted in triplicates for each drug condition and a total of 5 experiments was performed.

2.2.7 Protein biochemistry

2.2.7.1 Gel electrophoresis

HUVEC lysates were made by scraping cells off their support using a cell scraper. This was carried out in ice cold RIPA lysis buffer. Protease inhibitor cocktail mix was added to prevent protein degradation (refer to **Table 2.4** for recipe and concentrations). To decrease the viscosity of the sample and ensure accurate gel loading, the preparation was sonicated for a few pulses to shear the DNA. Samples were subsequently placed in a heat block at 95 °C for 5 minutes to complete protein denaturation. Prior to gel loading, lysate concentrations were established via Bradford assay. BSA standards from 0 to 1000 μg/ml (the range over which the assay is linear) were prepared. Samples were incubated at different concentrations with Bradford reagent for 5 minutes at room temperature. Absorbance was measured at 595 nm using a microplate reader (CLARIOstar *Plus*, BMG Labtech).

Once the protein concentration had been established, 4x sample buffer containing 20 μg protein was separated by SDS-PAGE on 12 % polyacrylamide gels under reducing conditions (10 mM DTT). Electrophoresis was performed at a voltage between 100 - 180 volts and was stopped when the dye front reached the base of the gel casing. Pre-stained protein standard molecular weight markers (Life Technologies) were used on all gels.

2.2.7.2 Western blotting

Proteins were transferred to a PVDF membrane that was previously activated with methanol. Membranes were pre-wet in transfer buffer. Wet transfer was carried out in a Biorad transfer blot module at 100 volts for 1 hour. Membranes were blocked for 1 hour at room temperature with 5 % w/v BSA in PBS-T (Tris-buffered saline containing 0.1 % v/v Tween-20, and subsequently incubated with eNOS and Akt antibodies in blocking solution (**Table 2.3**) at 4 ^{o}C for overnight incubation. After washing with PBS-T 3 times, membranes were blocked for 1 hour in 5 % w/v milk block, followed by incubation for 2 hours at room temperature with anti-rabbit HRP 1 : 5,000 or anti-mouse HRP 1 : 10,000. β-tubulin was used as loading control. Membranes were washed as described above before imaging. Images were collected through high resolution chemiluminescent substrate chemistry and documented on X-ray film.

2.2.7.3 Densitometry analysis

Bands were analysed and quantified using ImageJ. Protein levels were determined based on their band intensities and normalised to the respective loading control intensities.

2.3 Statistical analysis

All quantified data was evaluated using the statistical software package GraphPad Prism®. Statistical test information can be found within figure legends. Data was deemed significant when $p < 0.05$. The number of experiments conducted is defined in each section.

3. Developing an *ex vivo* model of DIVI

3.1 Introduction

DIVI has been shown to occur in rats, mice and dogs treated with compounds from various pharmacological classes[39,53,76]. The primary aim of this chapter was to develop an *ex vivo* model that could replicate the features of DIVI. The work was carried out on rat vessel explants, where multiple drug treatments or conditions could be undertaken from the same animal. In this way, the number of animals required could be reduced. Studies have reported that the rat superior mesenteric artery (SMA), which arises from the anterior surface of the abdominal aorta and supplies arterial blood to the organs of the midgut, is particularly affected by DIVI, and therefore was selected for these experiments[76,203].

Activation of EC stimulates the release of several proteins, including VWF. VWF has been used as a clinical biomarker for non-drug related endothelial dysfunction diseases, as increased circulating levels are associated to EC damage in patients with arteritis, diabetes, sepsis, or atherosclerosis[344,345]. An increase in plasma levels of VWF has also been observed in rats and dogs following administration of fenoldopam and a K^+ channel opener, demonstrating the cross-species translation of VWF as a biomarker for EC dysfunction[198,200].

Assessment of VWF release from the endothelium of the rat mesenteric explants was conducted following 24 hours of treatment because this is usually the timeline for DIVI[198,203]. Four drugs with different mechanisms of action were selected (**Table 1.1**, **Introduction**): (1) bosentan, an endothelin (ET) receptor antagonist, (2) fenoldopam mesylate, a dopamine DA_1 receptor agonist, (3) minoxidil, an opener of K_{IR} (inward rectifier) 6.X ATP sensitive K^+ channels, which increases the permeability of K^+ ions into the cell, and (4) rolipram, a phosphodiesterase (PDE) IV inhibitor.

3.2 Methods

Animal handling and experiments conformed to the UK Animal Scientific Procedures Act – specifically schedule 1 procedures that cover methods of euthanasia appropriate for different species, weights and stage of development. A total of 4 rats (3 males and 1 female) were employed in this experiment. Gender has been closely associated with vascular disease and injury, e.g. female rodents demonstrate reduced vascular injury through reduced intimal and medial thickening. It would have been ideal to perform the study with a statistically powered number of animals (both females and males) to assess these gender differences but this could not be addressed in this thesis for limitations in the rats availability as well as time constraints. The superior mesenteric artery (SMA) was isolated and dissected away from the protective adipose tissue (**Figure 3.1**). In order to minimise variability across arteries, for each rat only the first part (branching from the aorta) of the SMA was used and no first or second order branches were taken. Vessel size ranged between 300 μm and 500 μm in inner diameter. **Figure 3.2** schematically depicts the work-flow for this procedure. A detailed description of the protocol is given in **Methods**, section **2.2.1**.

Each SMA was cut into 6 segments, each 1 mm long, for separate drug treatments. For each experiment a segment was treated with 0.1 % v/v dimethyl sulfoxide (DMSO) (vehicle) to serve as a control. Segments were treated for 24 hours in a water bath at 37 °C in Krebs solution and bubbled with oxygen, and subsequently fixed overnight in 4 % v/v PFA. Vessels were then cut to 10 μM thickness sections with a cryostat followed by permeabilisation with 0.1 % v/v Triton X-100 for 5 minutes. Sections were stained (see below) and images were taken by laser scanning confocal microscopy at a 20x magnification. Images were processed and analysed using the imaging software Fiji (Image J). In these experiments 20x did not allow a complete cross section of the vessel. As such, several images were taken and stitched using the pairwise stitching Fiji plugin. One picture of a complete vessel cross section was analysed for every condition per experiment, for a total of 4 experiments conducted with different animals on separate days.

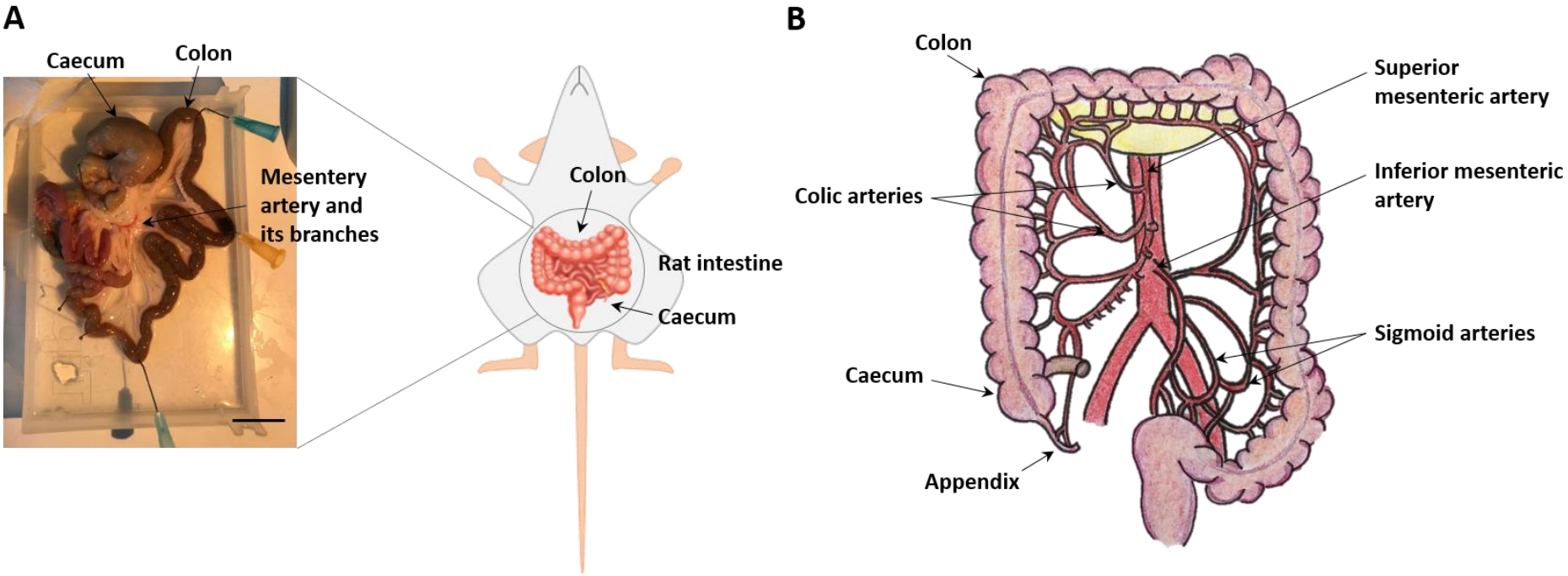

Figure 3.1 Extraction of the rat gut and localisation of the superior mesenteric artery (SMA). Scale bar in A represents 2 cm.

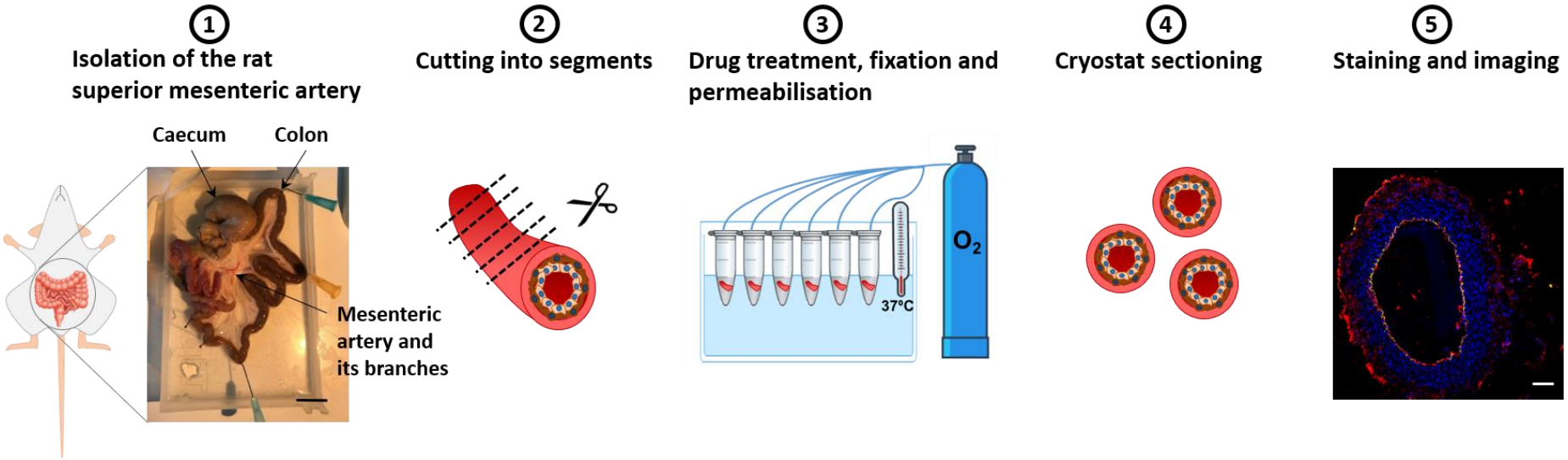

Figure 3.2 Flow diagram of the experimental procedure. (1) The rat gut was collected and the superior branch of the mesenteric artery carefully isolated. (2) The vessel was cut in six segments and (3) each segment treated with a drug (**Table 1.1**, **Introduction**) at 37 °C for 24 hours under oxygenated conditions. Subsequently, segments were fixed in PFA overnight and then promptly frozen in liquid nitrogen. (4) Each segment was then cut into 10 µM slices using a cryostat, and then (5) stained for VWF and CD31. Images were acquired on a Leica confocal microscope. Analysis was performed using ImageJ Fiji software.

3.3 Results

Figure 3.3 shows a representative picture of a rat control vessel explant stained for VWF and the platelet endothelial cell adhesion molecule 1 (PECAM-1)/CD31, to mark the endothelium. CD31 is highly expressed at endothelial cell-cell junctions, where it functions as an adhesive protein to maintain cell junctional integrity (refer to **Introduction**, section **1.6.1.2**). DAPI was used to stain DNA and thus locate the nuclei. As expected, CD31 stained the endothelium uniformly. VWF was also found in the endothelium and co-localised with CD31.

To measure the degree of non-specific binding, both the secondary antibodies used (anti-rabbit IgG for VWF and anti-mouse IgG for CD31) were incubated alone, as a control, to assess the background fluorescence levels (**Figure 3.4**). For each experiment the intensity of the background fluorescence was subtracted from the fluorescent intensity values of the experimental data.

The CD31 signal that is prominent around the outside of the vessel in **Figure 3.3** is not a consequence of non-specific binding of the secondary antibody. Its pattern of staining suggests that the primary antibody sticks to the fatty layer in the vessel.

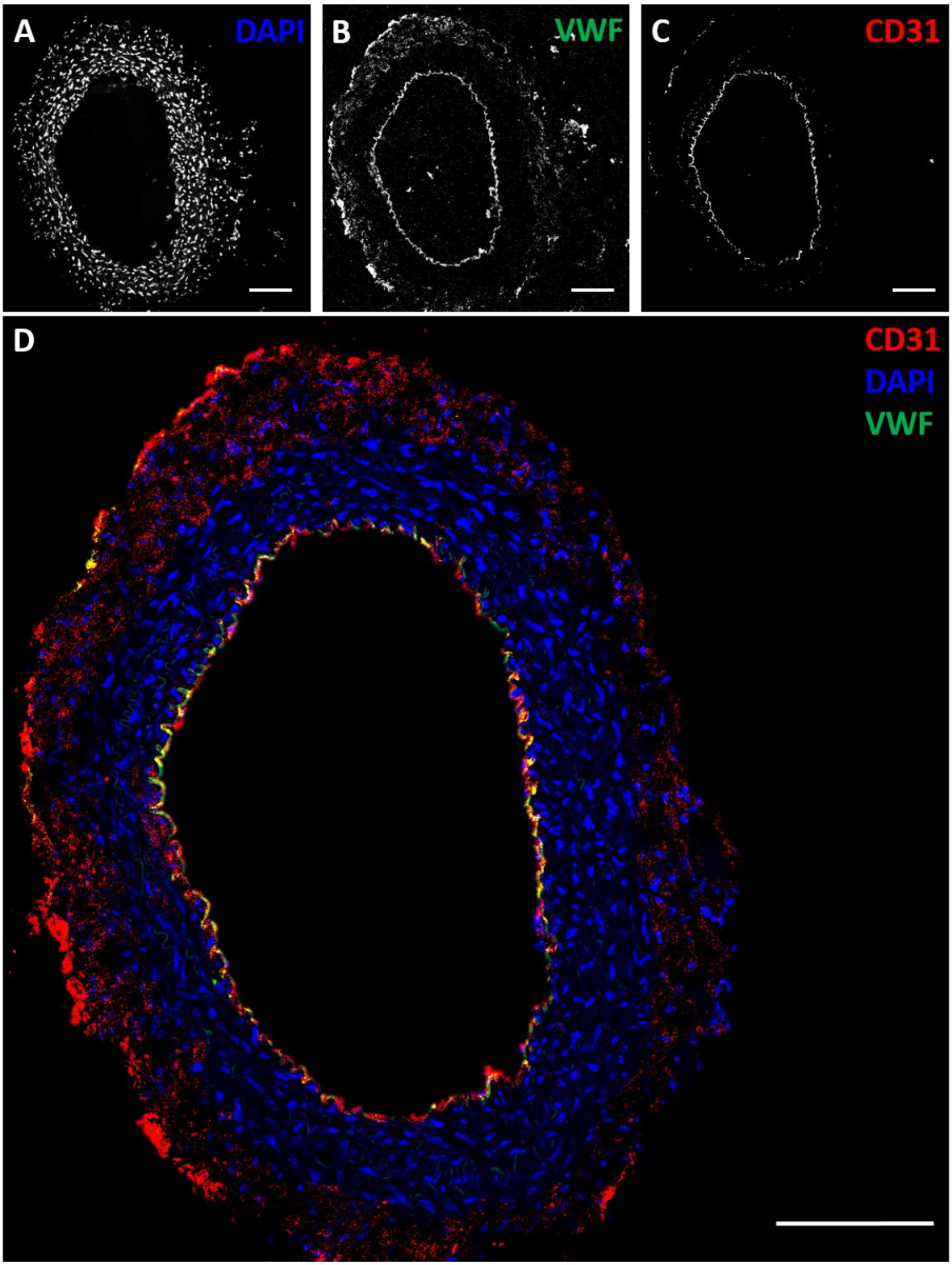

Figure 3.3 Cross section (10 µM thickness) of the SMA in a control rat. Cell nuclei were stained with DAPI (A). VWF and CD31 (endothelial marker) are shown in B and C, respectively. D is a merged picture of DAPI (blue), CD31 (red) and VWF (green). Images were taken with a confocal microscope, using a 20x oil immersion objective and stitched together using the pairwise stitching Fiji plugin. Scale bars represent 100 µm.

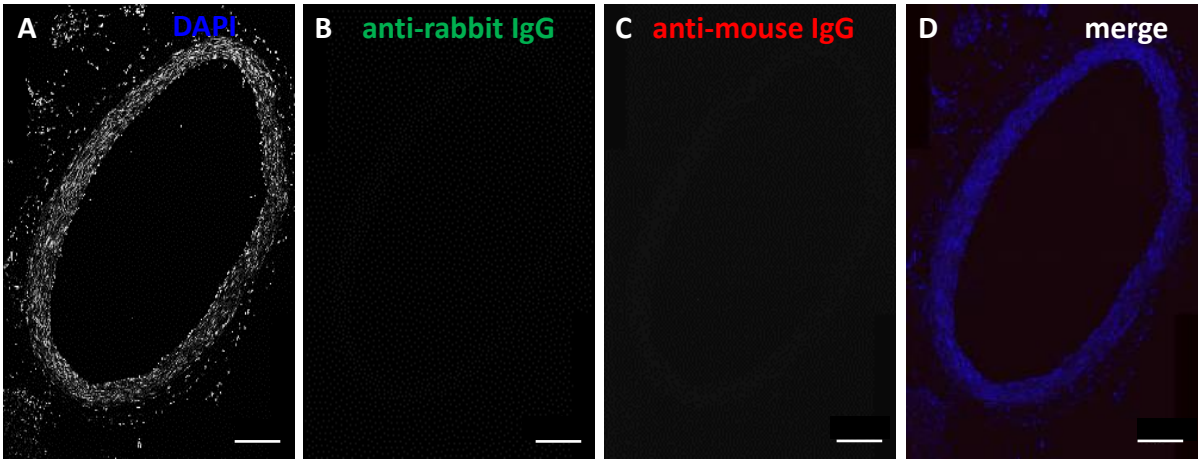

Figure 3.4 Assessment of the level of non-specific staining. Rat segments were stained with secondary antibodies alone. Images were taken with a confocal microscope, using a 20x oil immersion objective. Scale bars represent 100 µm.

To quantify the fluorescent signal corresponding to VWF, the images were analysed with the image analysis software Fiji (ImageJ). The image was split into the different colour channels (DAPI-blue, VWF-green, CD31-red) and a grid was used to aid in visually identifying the centre of the vessel. To remove bias, four lines were drawn starting from the centre towards each corner of the picture, obtaining a top right, bottom right, top left and bottom left lines (**Figure 3.5**). The line thickness was 20 pixels and was chosen because this width generated the peak with the least noise. The CD31 signal was used as a guide for two reasons; firstly to ensure that the endothelium was intact following the treatment, and secondly to accurately locate VWF. DAPI was used to mark the lumen and the outer edge of the vessel.

Thus, a plot with three fluorescence intensities along the line corresponding to the blue (DAPI), green (VWF) and red (CD31) channels was generated for each of the four lines (**Figure 3.6**). Fluorescence intensities from the VWF, CD31 and DAPI signals were converted to greyscale values between 0=black and 255=white. The range between black and white is a continuous spectrum of grey shades. The greater the greyscale value the greater the fluorescence signal intensity. To directly compare greyscale values between vessels, imaging parameters and microscope settings remained constant.

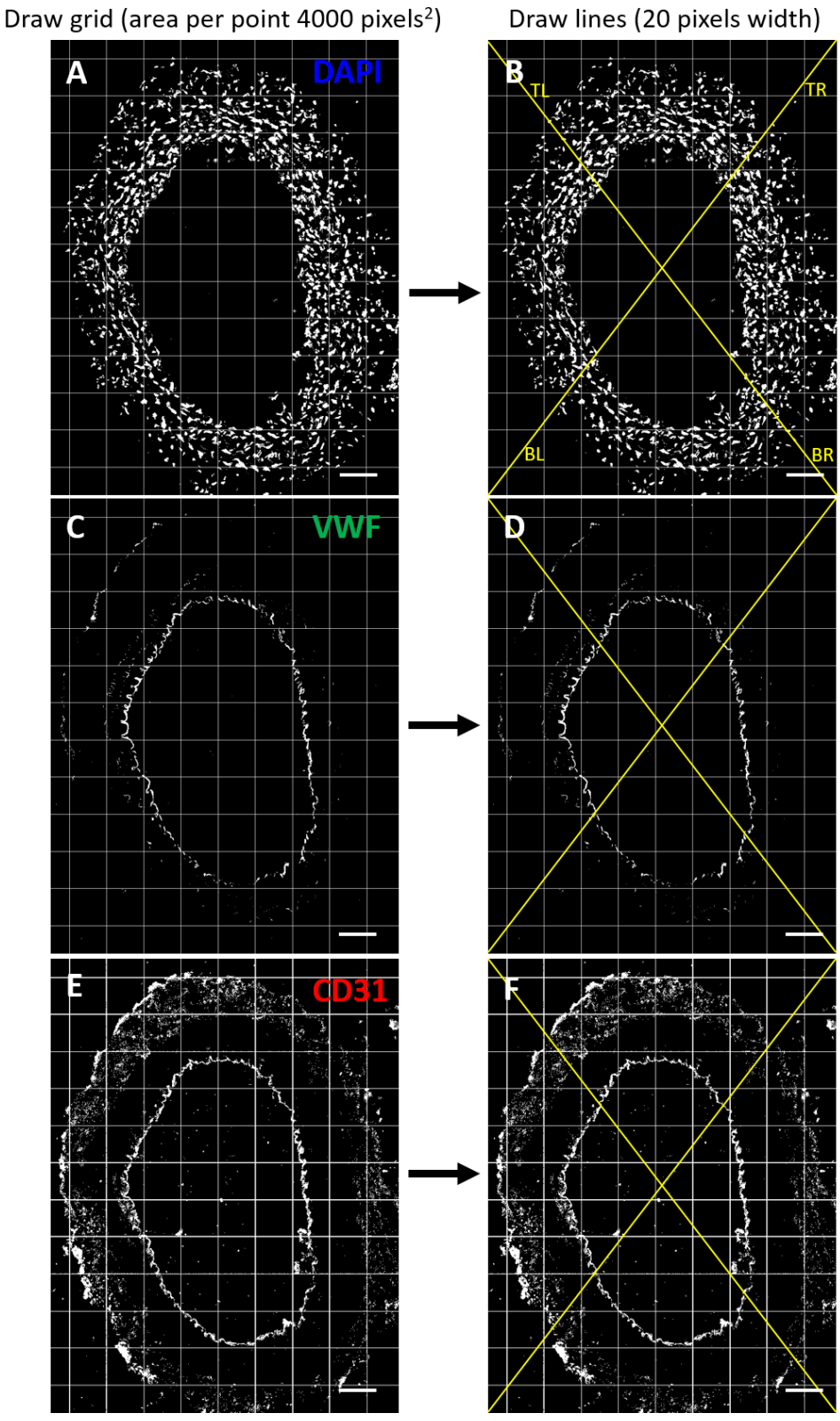

Figure 3.5 Quantification of VWF. Each image was split into the different colour channels (DAPI-blue, VWF-green, CD31-red) (A, C, E). A grid tool was used to locate the centre of the vessel. From the centre, four lines 20 pixels width were drawn towards each corner of the image obtaining a top right, bottom right, top left and bottom left lines (B, D, F). Images were taken with a confocal microscope, using a 20x oil immersion objective. Scale bars represent 100 µm. TL= top left, TR= top right, BL= bottom left, BR= bottom right.

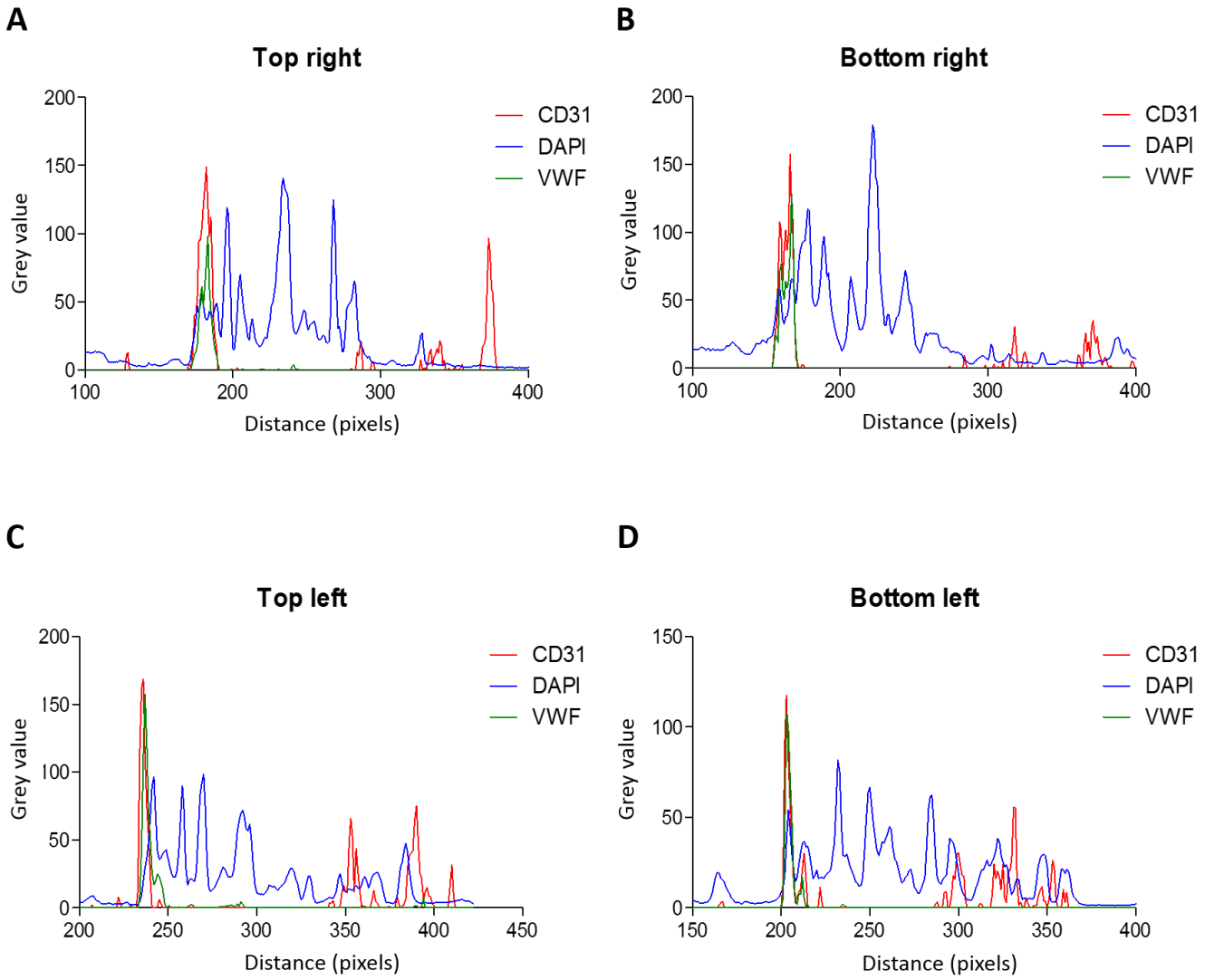

Figure 3.6 Plot profile with three fluorescence intensities representing CD31 (red), DAPI (blue) and VWF (green). Fluorescence intensity is presented as grey values.

CD31 was used to accurately locate the endothelium. From the direction of the lumen outwards, the first peak corresponded to the endothelium. An interval of 20 pixels before and after the highest value was taken in the CD31 plot profile to define the thickness of the endothelium. The intensity of VWF staining in this region was quantified as the average of VWF greyscale values and was expressed as a percentage of the control vessel. CD31 expression was used to quantify VWF and to qualitatively ensure that the endothelium remained intact after treatment but was not quantified. The smooth muscle region was identified using α-smooth muscle actin (α-SMA) staining and was detected directly beneath the endothelium (**Figure 3.7**).

It was not possible to co-stain α-SMA, CD31 and VWF due to antibody cross reactivity. The smooth muscle layer was determined as the area 20 pixels past the highest CD31 value moving further into the vessel and away from the lumen. To quantify VWF in the smooth muscle region, the interval of intensity values between the last value of CD31 and the last value of DAPI was taken and averaged and expressed as percentage of the control vessel. An example of this approach is shown in **Figure 3.7**.

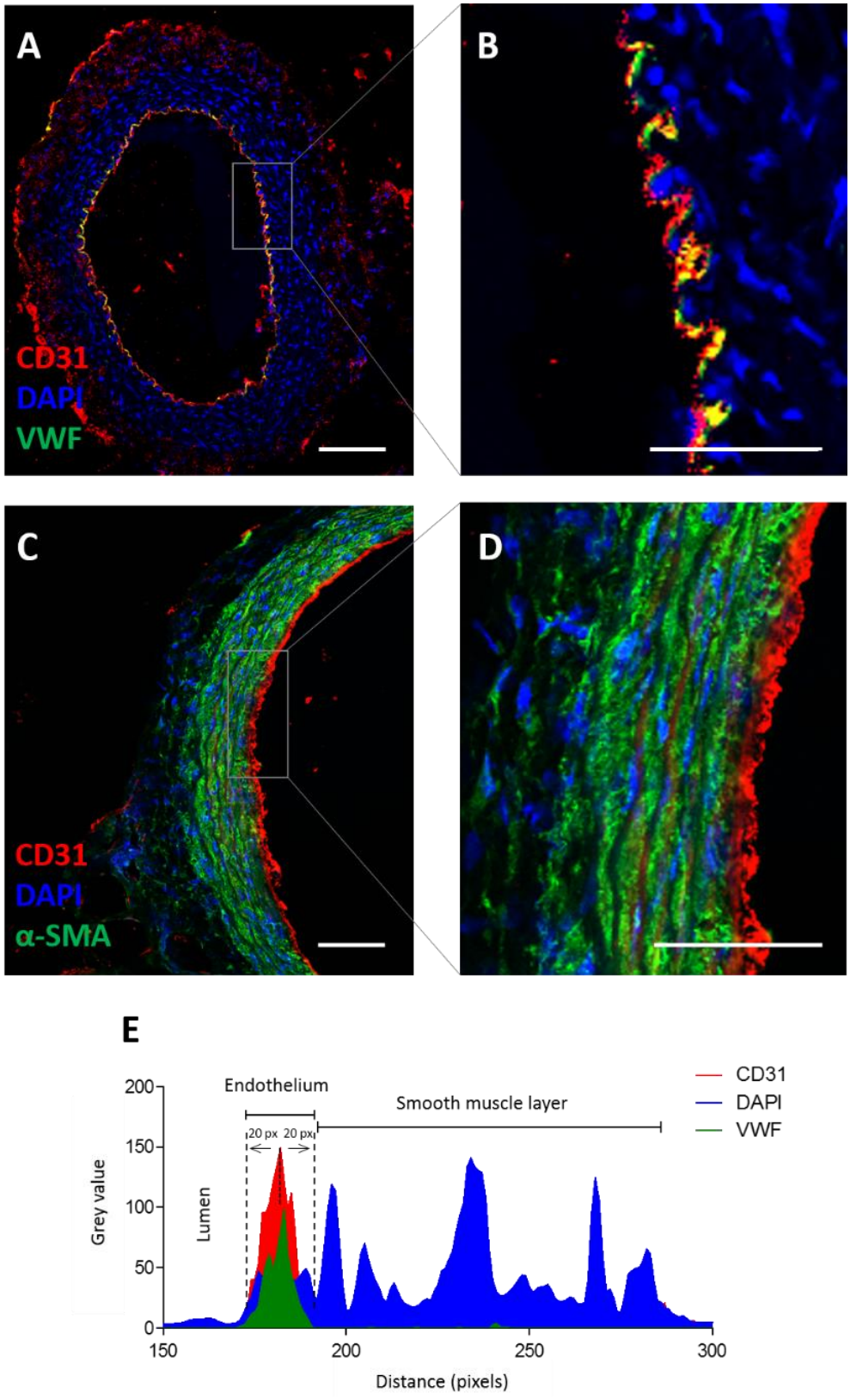

Figure 3.7 VWF, CD31 and α-SMA staining in a rat vessel explant. A represents a control vessel and B a zoomed-in region showing VWF (green), CD31 (red) and DAPI (blue).C and D (zoomed-in) represent α-SMA staining in a different control vessel. Quantification of VWF in the endothelium and smooth muscle region is shown in E. Scale bars represent 100 µm.

3.3.1 Thrombin promotes VWF release from EC *ex vivo*

VWF is stored in Weibel-Palade bodies (WPB) in EC[346]. The release of VWF from EC is mediated by both basal and stimulus-induced signalling pathways[219] (refer to **Introduction**, section **1.6.2.4.2**). Regulated release occurs in response to several agonists including histamine and thrombin. Thrombin has been used *in vitro* and *in vivo* to stimulate VWF release[218]. For the purposes of this study, these findings were recapitulated so that VWF levels could be assessed in the vessel explants. Moreover, measuring this would allow to demonstrate that these vessel explants are functionally active and able to respond to stimulation.

Vessels were stimulated with thrombin 10 U/ml for 24 hours. Thrombin induced significant VWF release from the endothelium, as shown qualitatively by the loss of VWF signal compared to the matched control (**Figure 3.8,** B and F). To ensure that the loss was not associated with loss of integrity, the endothelium was stained with CD31 and maintained its integrity after 24 hours, as shown by the CD31 signal that is no different from the control vessel (**Figure 3.8,** A and E).

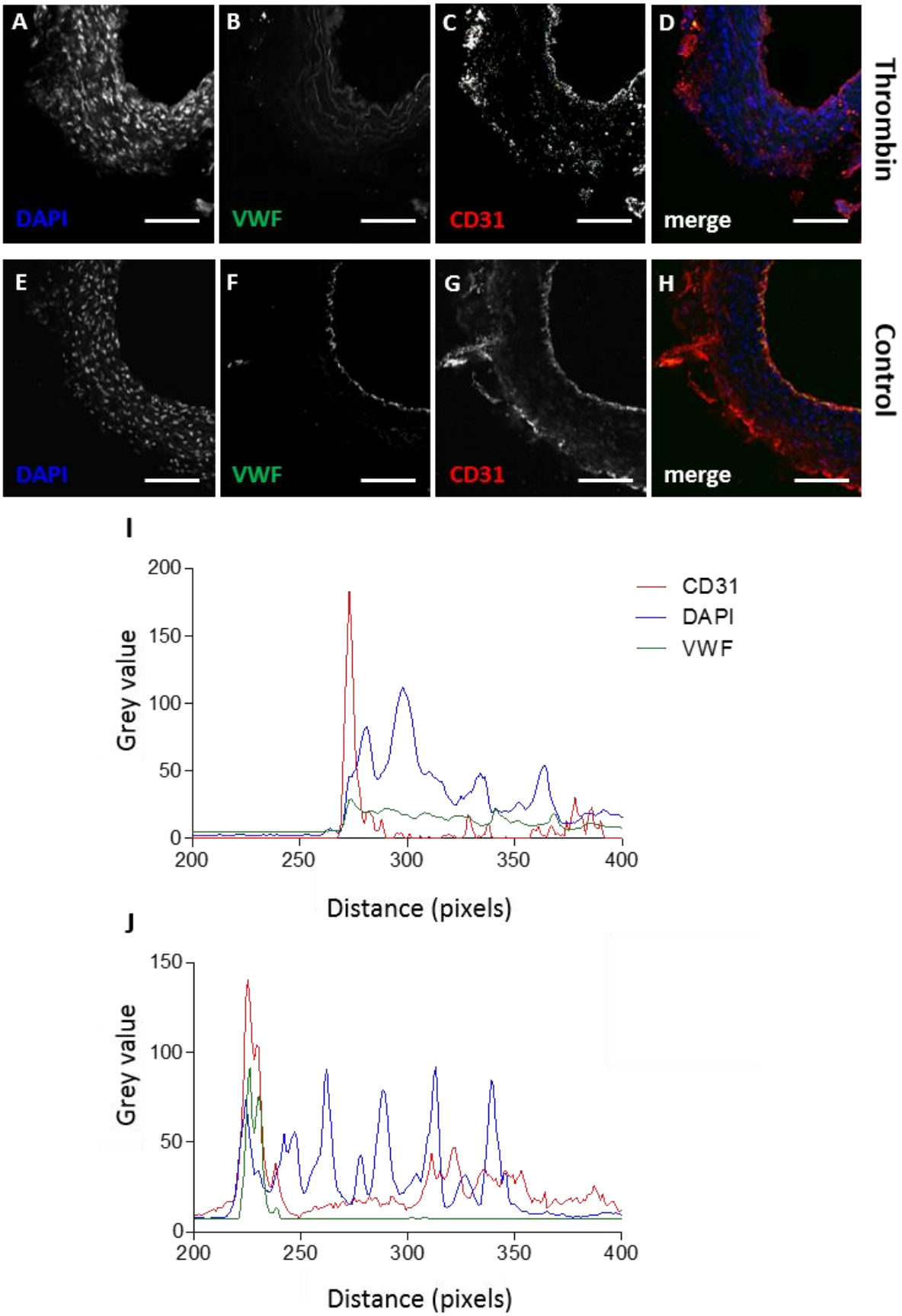

Figure 3.8 VWF expression in a thrombin-stimulated and in a control vessel. I and J show a thrombin and a control plot, respectively. Scale bars represent 100 µm.

When data was quantified and expressed as normalised percentage compared to the matched control vessel, thrombin stimulation reduced endothelial VWF intensity to 39.32 ± 8.52 % of control (N=4, $p < 0.01$) (**Figure 3.9** and **3.10**). This data confirms that thrombin is a robust positive control for endothelial cell VWF release.

3.3.2 DIVI-related drugs induce VWF release from EC

Vessel segments were treated with four drugs, all reported to actively induce DIVI in animal models, at 100 µM for 24 hours under oxygenated conditions. A total of 4 rats were used in these experiments. Bosentan, fenoldopam and minoxidil induced a significant VWF release from EC compared to the matched vehicle control, as shown by over 50 % reduction (bosentan stimulation reduced endothelial VWF intensity to 39.12 ± 3.46 % of control (N=4, $p < 0.01$), fenoldopam to 43.99 ± 6.44 % of control (N=4, $p < 0.01$), minoxidil to 46.78 ± 5.92 % of control (N=4, $p < 0.05$)) (**Figure 3.9** and **3.10**). Conversely, rolipram induced a lower, insignificant level of VWF compared to the matched control (reduction in VWF intensity to 89.0 ± 23.20 (N=4, $p > 0.05$). No difference was observed between the drugs and the thrombin positive control; thrombin, bosentan, fenoldopam and minoxidil all induced a comparable amount of VWF release from the endothelium. The VWF staining detected in the SMC layer of the vessels was not altered by treatment with any of the DIVI drugs (**Figure 3.10**, B).

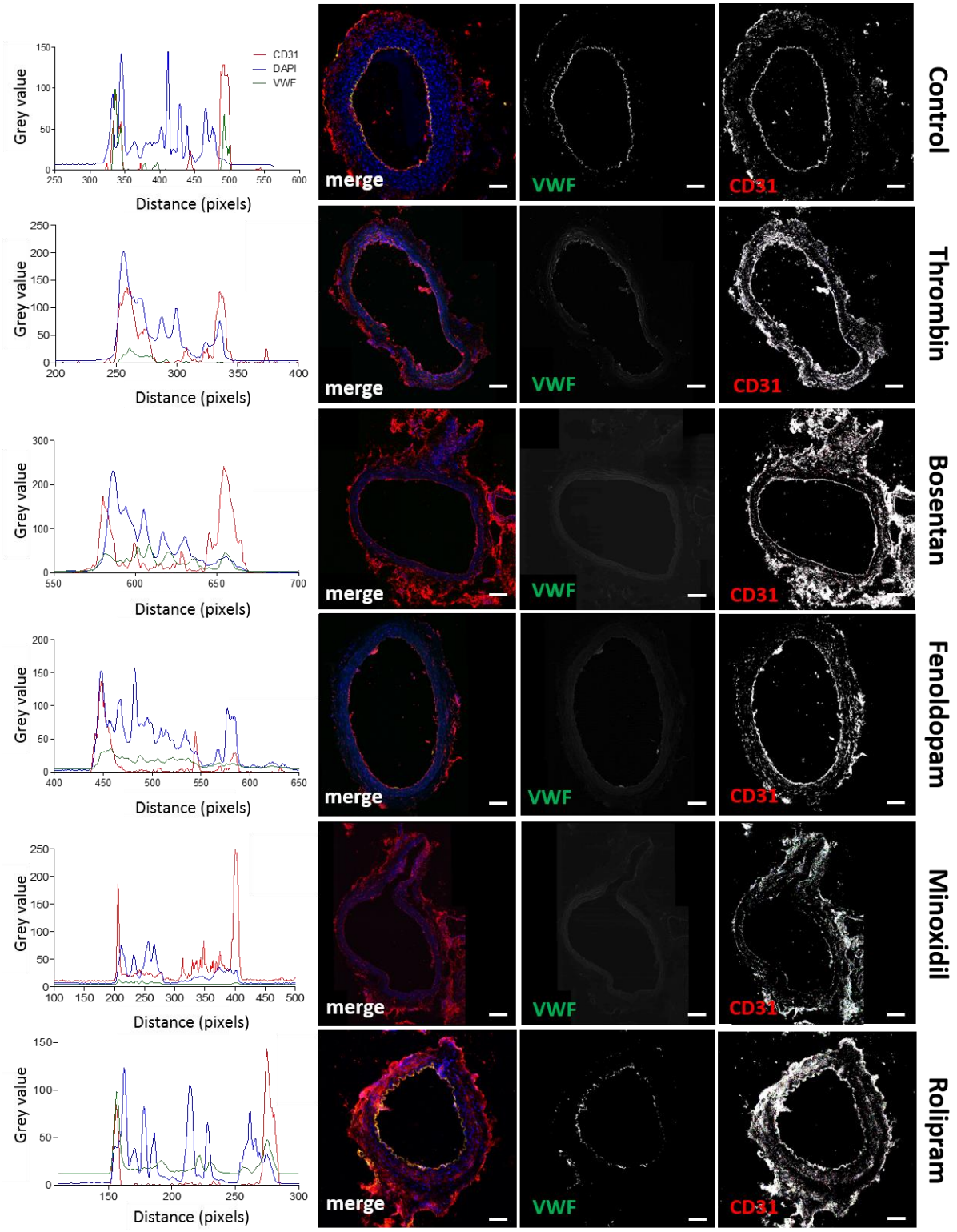

Figure 3.9 VWF and CD31 staining in rat mesenteric explants. The endothelium in control vessels stains uniformly for VWF and remains intact after treatment, as shown by CD31+ stain. Images were taken with a confocal microscope, using a 20x oil immersion objective. Scale bars represent 100 µm.

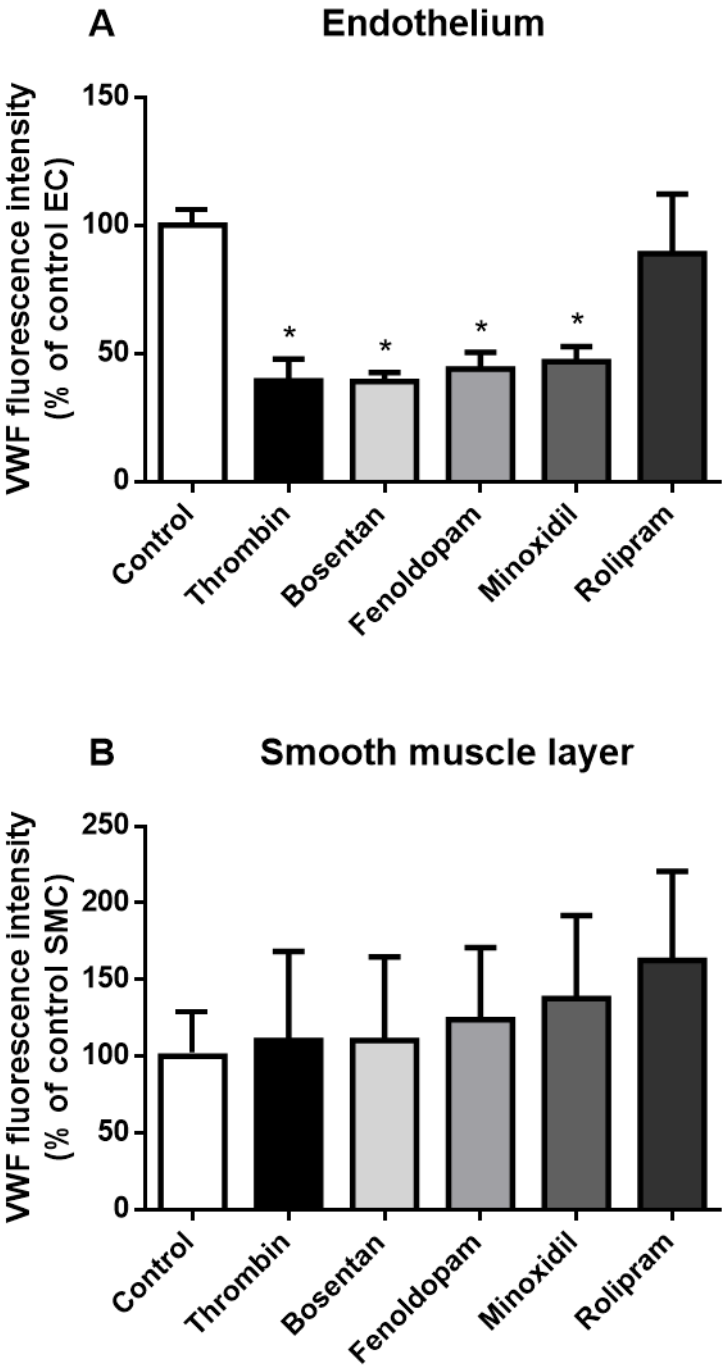

Figure 3.10 Quantification of VWF release in EC and SMC in the vessel. Data are expressed as percentage reduction of VWF intensity relative to matched untreated control (white bars) and represent mean ± SEM of 4 independent experiments, analysed by one-way ANOVA followed by Dunnett's post test. *$p < 0.05$. Note that control VWF levels in SMC were very low.

3.4 Discussion

The aim of this first set of experiments was to determine whether a DIVI-like phenotype could be recapitulated using a novel vessel explant approach. These data showed that DIVI can been recapitulated *in vitro* and demonstrated the utility of this approach in enabling parallel drug treatments to be carried out on the same vessel. Minimising the variation caused by animal heterogeneity increases experimental reproducibility and could contribute to the reduction of the number of animals required for preclinical evaluation studies.

VWF was selected as a marker in this model because of a known association with DIVI. Several studies in rats and dogs employed VWF as a biomarker of vascular injury[198–200,203]. However, most DIVI studies have used conventional histopathological examination, such as H&E staining. In this study this was replaced with immunofluorescence imaging, which generated a greater dynamic signal range. Immunofluorescence has other important advantages, such as a higher sensitivity and accuracy.

The endothelium in control vessels stained uniformly for VWF. Although the vessels are circular, they are not uniformly-shaped, which made it difficult to accurately quantify VWF in the endothelium. Here, an analysis method that enabled quantification of the VWF in the endothelium in an unbiased manner was developed, using nuclei to define the vessel and CD31 staining to define the endothelium. Defining the region of the endothelium was important since it was possible that some VWF may be released into the SMC layer (see below). This method is robust, however there is a limitation as this approach would not be suitable for vessels in which treatments cause endothelial loss (although this will be seen in the CD31 staining). However, this was not observed for the drug treatments or our positive control in this study.

Thrombin was used a positive control as it is an effective activator of EC, inducing disturbance of the endothelial cell barrier, release of inflammatory mediators, adhesion of leukocytes on EC, and release of VWF from WPB[347–349]. In these experiments, thrombin treatment of vessel explants led to significant loss of endothelial VWF demonstrating that the EC in the vessel explants remain functional and capable of responding to stimulation.

To evaluate whether a DIVI-like phenotype could be generated in our *ex vivo* vessel model four drugs that have been reported to cause DIVI in animal models were tested: bosentan, fenoldopam, minoxidil, and rolipram (refer to **Introduction**, **Table 1.1**). The length of treatment (24 hours) was selected to recapitulate the time course of injury seen *in vivo*[200]. Shorter postdosing intervals demonstrated that drug-induced damage in the mesenteric artery did not always occur, in a rat study regardless of the dose, DIVI was only evident when fenoldopam was infused for longer than 12 hours[100].

Bosentan, fenoldopam and minoxidil caused significant loss of VWF from the CD31+ endothelium, to a comparable extent to the positive control, thrombin. In contrast, rolipram had no effect. Importantly, the endothelium remained intact following each of the drug treatments. Therefore, VWF loss is more likely to be a marker of activation rather than death of the endothelium. This however should be confirmed by staining for apoptotic markers (such as activated caspase-3). It should be noted that degradation as opposed to release may be responsible for the loss of VWF in these assays. There are reasons for the loss of expression which could be irrespective of VWF release. For example, endothelial autophagosomes contain abundant VWF protein and the drugs could increase degradation of VWF. Degradation of VWF has been described in the **Introduction 1.6.2**.

It may be expected that VWF would be re-synthesised during the 24 hour treatment, such that increased release would be masked in our model, since total intracellular VWF was detected. Re-synthesis could be for example be measured by quantitative polymerase chain reaction (qPCR), which monitors the amplification of targeted DNA molecules in real-time. Conversely, since EC have limited VWF storage capacity[204,350,351], repeated EC activation may cause depletion of the cytoplasmic pool of VWF from WPB. In this study, rolipram was the only drug that did not cause a reduction in VWF. However, although there are reports regarding VWF release with fenoldopam and a K^+ channel opener in preclinical animals[200], this is the first data investigating VWF expression after stimulation with bosentan and rolipram.

Although previous histopathological imaging of arteries injured *in vivo* showed an accumulation of VWF in the SMC region[200], the drugs used in this study did not induce retention of VWF within the SMC region in the *ex vivo* model. However, the VWF

accumulation observed in previous reports may represent plasma-derived VWF extravasating in the tunica media[199], a level of complexity absent from this model. It is also known that the shear stress induced by blood flow (which was not present in this experiment) can alter the expression and release of proteins within EC and it is possible that VWF release and distribution are also affected[352]. Indeed, the absence of plasma and flow is a limitation of this *ex vivo* model.

These data suggest that an *ex vivo* model could be used to evaluate whether early development compounds may cause EC activation. In this approach, several drugs were tested on the mesenteric artery of a single rat, significantly reducing the number of animals required for this assessment. Although time course and dose-response studies have not been conducted in this project, with this positive proof-of-concept work, these could also be readily performed. In addition, this method could also be used to investigate EC activation looking at other biomarkers, such as VCAM-1 and ICAM-1, and to investigate SMC necrosis. In the standard toxicology studies, each timepoint and dose requires sufficient group numbers to provide statistical power. Surely, this model would not replace toxicology studies, but it still may be relevant for informing on dose and time.

There are several important differences to consider between an *ex vivo* approach and an *in vivo* drug dose. The *ex vivo* model does not include blood cells that might contribute to the extent of arterial injury. Leukocytes have been observed adhering to arteries injured *in vivo*[39,61]. Moreover, a characteristic sign of DIVI is focal haemorrhage. The red blood cells (RBC) that bleed into the vessel wall may promote further damage and inflammation as they break down[39]. The *ex vivo* model also lacks the contribution of haemodynamic forces, and the absence of flow (as mentioned above) is another limitation of this system. *In vivo*, the endothelium of the artery will be subjected to blood flow and wall shear stress. Vasodilatation and a local increase in blood flow have been proposed as major physical factors in the development of DIVI[38]. For example, significant increases in rat mesenteric blood flow have been observed with fenoldopam[101] and with the PDE IV inhibitor CI-1044[353] at doses that induce DIVI. It has been hypothesised that alterations in shear stress might be the mechanism for the development of the injury[75]. The endothelium is subjected to either a laminar or a turbulent force, and responds accordingly (refer to **Introduction**, section **1.7**)[354]. EC exposed

to a laminar flow adopt a quiescent anti-inflammatory, anti-thrombotic and anti-apoptotic phenotype[355,356], whereas EC exposed to turbulent flow display an activated phenotype implicated in the pathogenesis of vascular injury by promoting expression of proteins involved in inflammation, coagulation and proliferation[356–358].

Some studies have attempted to add flow to EC to mimic *in vivo* hemodynamic and create a more physiological model. For instance, the American company HemoShear created a co-culture platform with rat primary EC and SMC where the endothelium is exposed to *in vivo*-derived hemodynamic waveforms. They found that a high dose (100 µM) of fenoldopam in the presence of drug-induced hemodynamic significantly increased vascular permeability and elevated several inflammatory pathways, suggesting that flow is important in the study of DIVI.

This model did not involve blood and the data may suggest that an increase in blood flow is not required for DIVI, since three drugs produced an effect. Nonetheless, blood flow may contribute to the extent of the damage, in particular the status of the smooth muscle layer, which is known to be necrotic in DIVI. However, it could also be proposed that flow was important for fenoldopam, minoxidil and bosentan to induce release of VWF. In fact, even though the model did not involve flow, the vessel explants originally developed under flow and adapted to it in the animal. As a consequence, EC have been shear-conditioned in this model. It could be that rolipram needs flow during the drug treatment to generate a DIVI-related phenotype, which did not happen in this model, or perhaps it is just altered flow that is important. However, it could also be that it is the drug specific mechanism of action that caused rolipram to not induce VWF release in this model.
If flow is not a prerequisite for DIVI, this means that it is possible to take a step further in a NC3Rs approach to reproduce the model totally *in vitro.* This will be explained in the next chapter.

In summary, it was successfully demonstrated that VWF is a sensitive morphological marker of EC activation in a rat model of DIVI, it is released from EC following stimulation. These experiments have also demonstrated that these drugs are active and induce a significant reduction of VWF expression in the vessel endothelium. The next chapters will explore VWF release in a human *in vitro* model under static conditions.

4. Investigating DIVI *in vitro*

4.1 Introduction

The primary aim of this chapter was to investigate whether it is possible to recapitulate DIVI *in vitro*. This *in vitro* set up would use human-derived primary cells that would eliminate species specificity translatability issues[359]. To investigate whether DIVI would occur in humans, EC and SMC from human pooled donors were used. Firstly, the effect of the drugs on VWF release was investigated, as loss of VWF from the endothelium in the rat vessel explants was clearly defined in all DIVI drugs except for rolipram (**chapter 3**). Subsequently, other known features of DIVI, such as cell death, vascular permeability and inflammation were investigated.

4.2 Results

HUVEC were selected as the source of EC, since they have been extensively characterised in the literature[341]. HCASMC were used as the source of arterial vascular SMC as they have also been widely described[342]. When grown to confluency, HUVEC had a cobblestone appearance, whereas HCASMC were characterised by an elongated appearance (**Figure 4.1**, A and B).

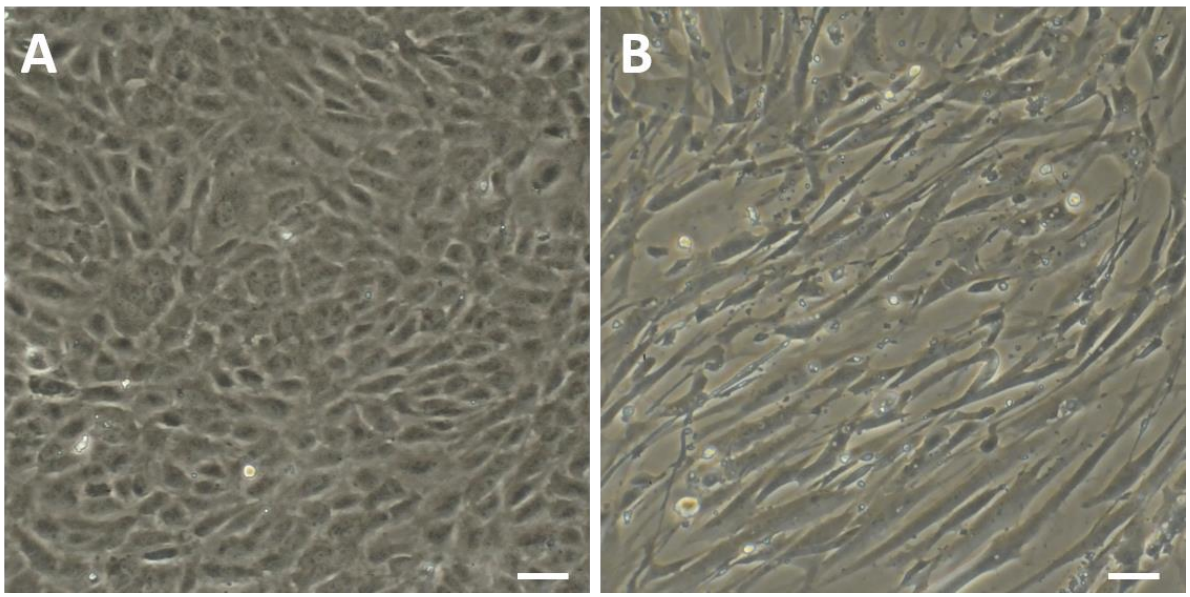

Figure 4.1 Bright field images of EC and SMC. HUVEC are shown in A, and HCASMC in B. Cultured cells were imaged at passage 6. Scale bars represent 50 µM. Images were taken with a bright field microscope. 10x.

The junctional protein VE-cadherin, important in maintaining the integrity of the endothelium, was used as specific EC marker[360,361]. Calponin, a calcium-binding protein that is involved in the modulation of contraction by interaction with actin and inhibition of actomyosin Mg-ATPase activity, was used as a specific marker of SMC[362]. HUVEC stained positive for VE-cadherin (**Figure 4.2**, A and B), however no calponin was identified (C and D). By contrast, HCASMC showed positive expression of calponin (**Figure 4.2**, G and H), but an absence of VE-cadherin (E and F). DAPI was used to stain the cell nuclei (**Figure 4.2**).

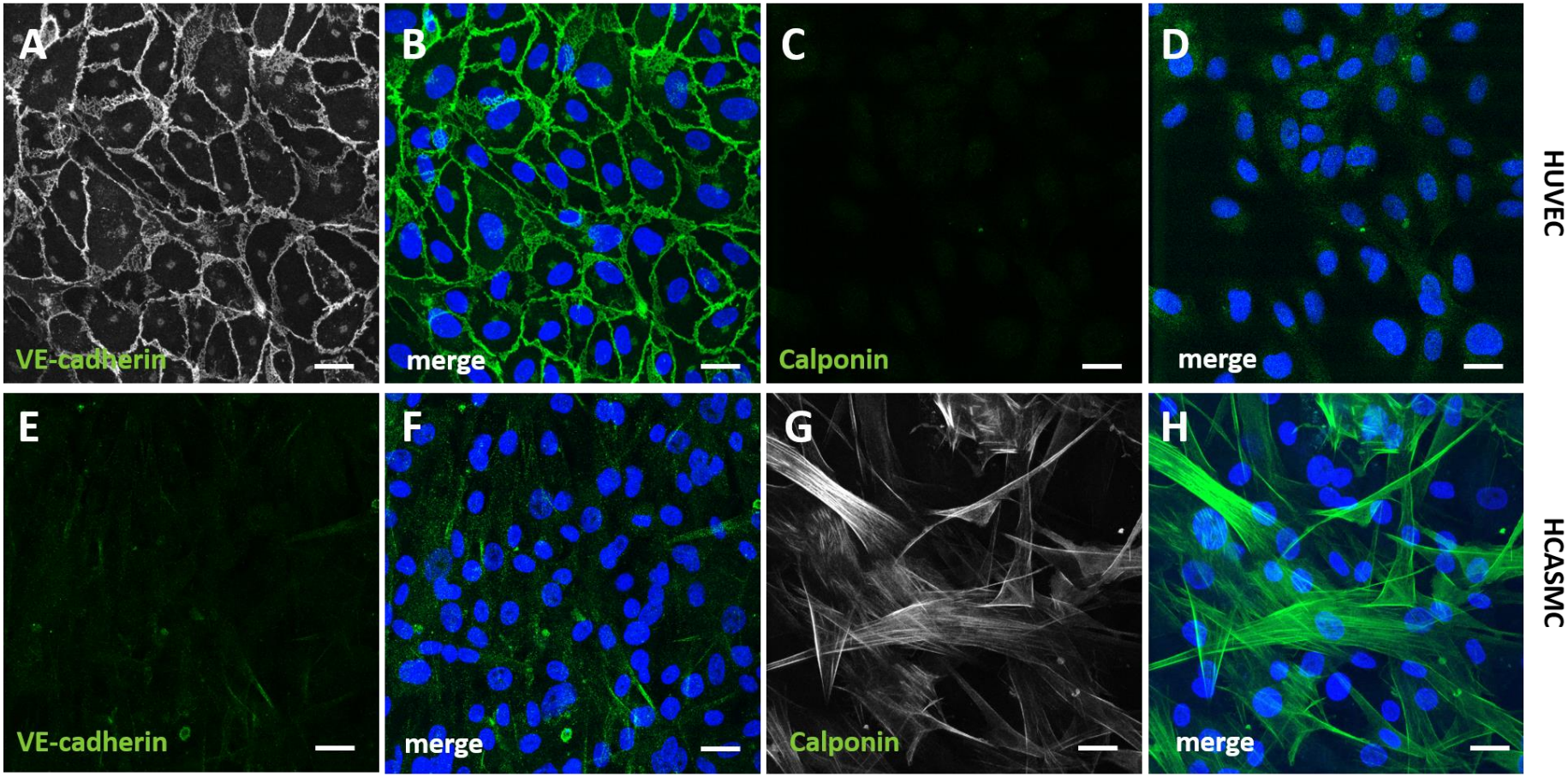

Figure 4.2 Representative confocal images of specific HUVEC and HCASMC markers. VE-cadherin stain is positive in HUVEC (A and B) and negative in HCASMC (E and F). Calponin was detected in SMC (G and H) and was absent in HUVEC (C and D). DAPI (blue) was used to stain the nuclei. Scale bars represent 20 µM. 63x.

4.2.1 VWF release with DIVI-related drugs in HUVEC

Firstly, VWF release from the endothelium was monitored, to understand if the observations in rat mesenteric artery explants in **chapter 3** could be recapitulated in human EC *in vitro*. HUVEC were seeded in ibidi slides at 100,000 cells/well, grown for 24 hours, and treated with 100 μM fenoldopam mesylate, minoxidil sulfate, bosentan and rolipram. Two time points were selected: 1 hour, to assess a short-term effect (acute) and 24 hours, to reflect the time point of the vessel experiment. Thrombin 1 U/ml was used as a positive control in the experiments. Vehicle control cells were treated with 0.1 % v/v DMSO. Following treatment, cells were fixed with 4 % v/v PFA for 10 minutes then permeabilised for 5 minutes with 0.1 % v/v Triton X-100. Specific antibodies were used to detect VWF and CD31 (to mark cell junctions), and DAPI was used to label the nuclei. Cells were imaged with a confocal microscope using a 63x objective. Six images were taken for each treatment per repeat, four experiments were conducted in total.

*4.2.1.1 DIVI-related drugs induce VWF **release** after 1 hour and 24 hours*

VWF release was analysed (**Figure 4.3**, **4.4**). Images in the green channel (VWF) were thresholded to remove background noise. Cells were counted as VWF-positive if they had 3 or more spots/cell. This cut off point was selected as 3 was the minimum number of spots present when the positive control thrombin was analysed. DMSO control cells did not show 100 % positivity, but rather around 80 % both at 1 and 24 hours. This was expected, as VWF is also secreted spontaneously from unstimulated cells through the constitutive secretory pathway[363] (refer to **Introduction**, section **1.6.2.4.2**).

Thrombin 1 U/ml was chosen as positive control to match VWF release *ex vivo* (refer to **chapter 3**). Thrombin induced significant release of VWF compared to DMSO control after 1 hour (% VWF-positive cells was reduced to 41.6 ± 5.5, N=4, $p < 0.01$) and after 24 hours (% VWF-positive cells was reduced to 55.8 ± 2.9, N=4, $p < 0.001$), (**Figure 4.5**). The mean percentages of cells that remained positive for VWF following thrombin stimulation at 1 and 24 hours were not significantly different (41.6 vs 55.8).

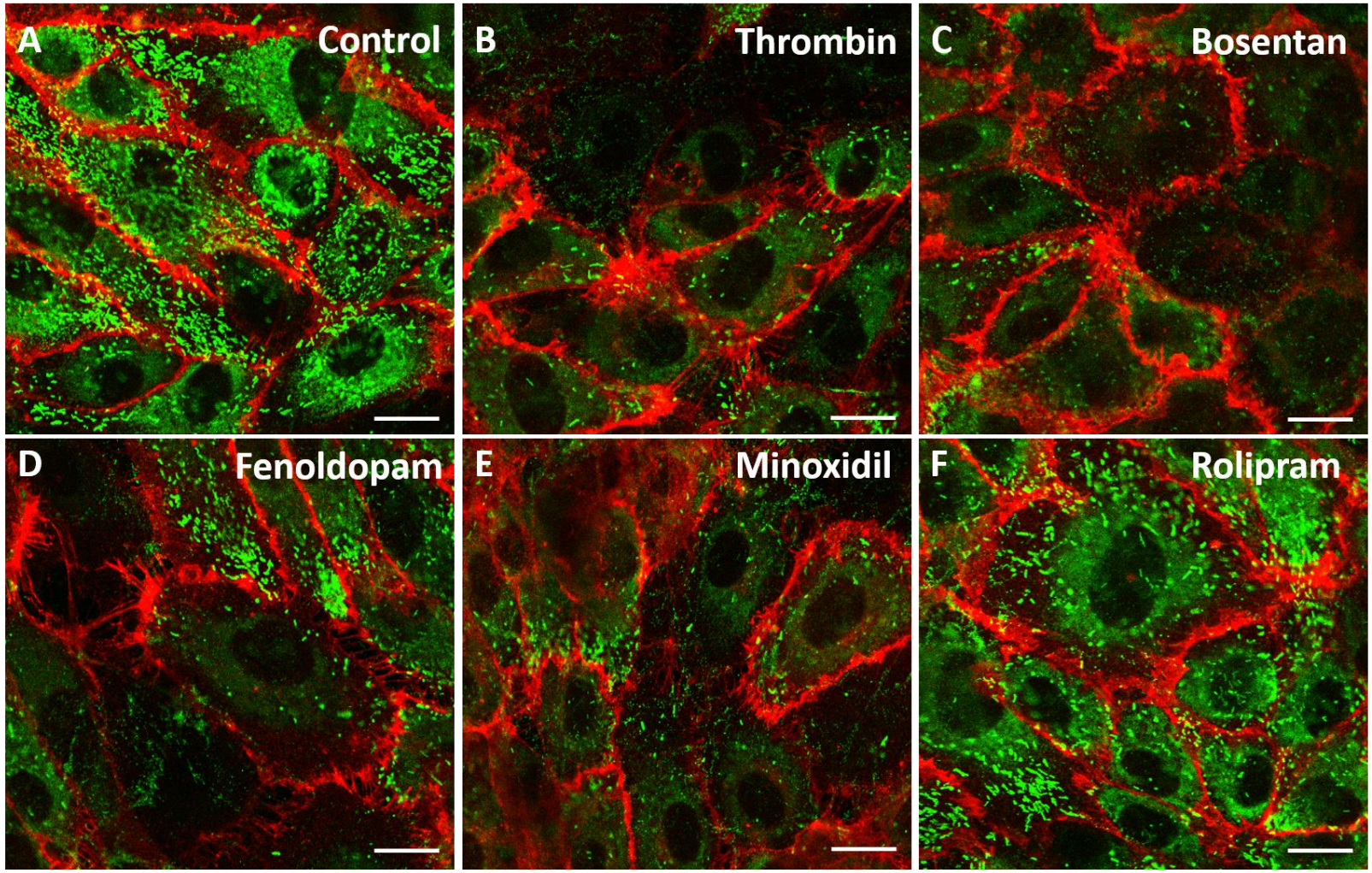

Figure 4.3 Representative confocal pictures of VWF release in HUVEC at 1 hour. HUVEC were grown for 24 hours and then VWF (green) release was detected with a specific antibody after treatment with DIVI-related drugs for 1 hour. Arrows in (A) point at WPB which contain VWF. Arrow in (B) points at a cell which has secreted VWF. Cell junctions are stained with CD31 (red). Scale bars represent 20 μm.

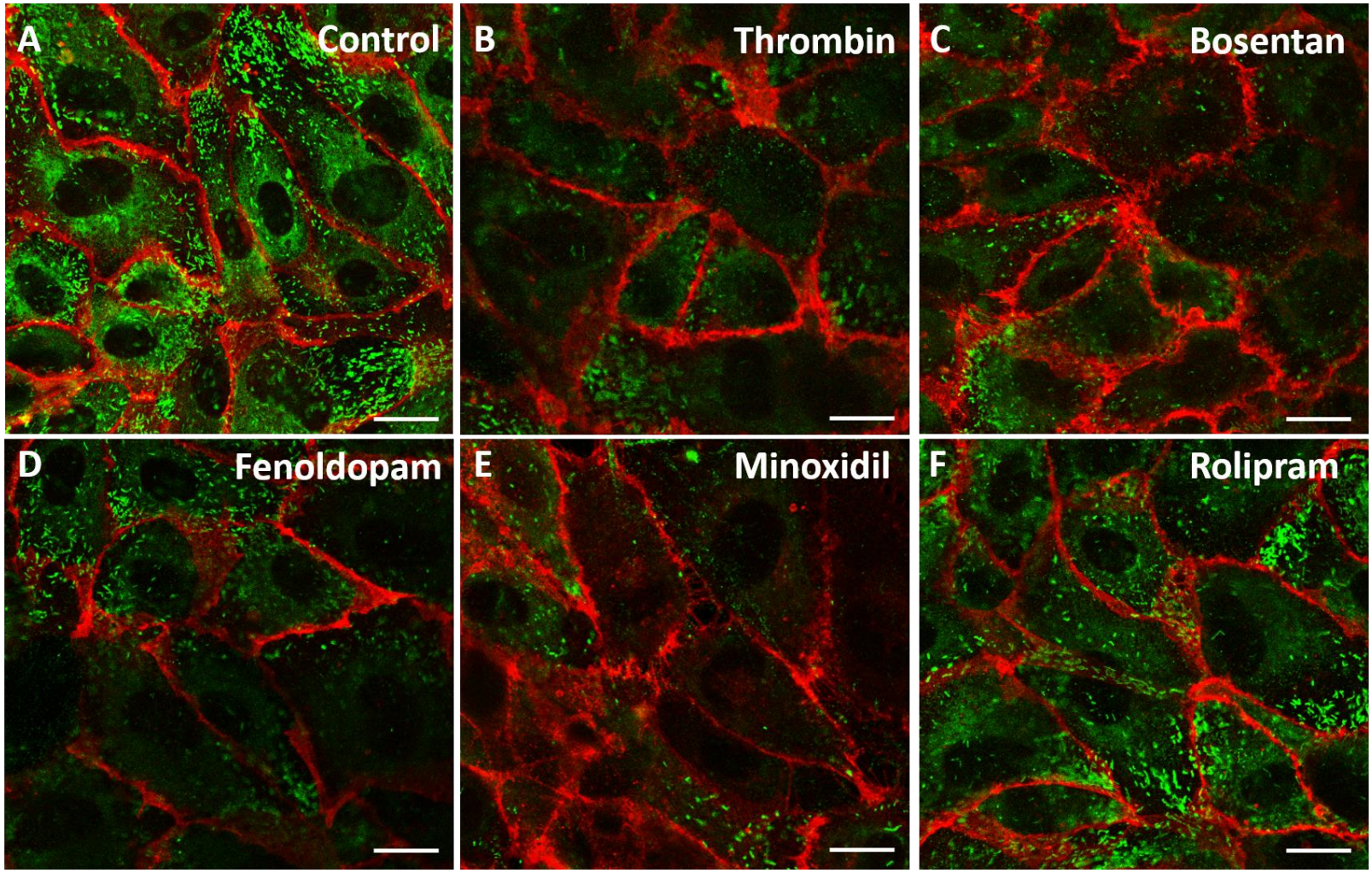

Figure 4.4 Representative confocal pictures of VWF release in HUVEC at 24 hours. HUVEC were grown for 24 hours and then VWF (green) release was detected with a specific antibody after treatment with DIVI-related drugs for 24 hours. Cell junctions are stained with CD31 (red). Scale bars represent 20 μm.

Bosentan induced significant VWF release after 1 hour (% VWF-positive cells was reduced to 51.7 ± 2.6, $p < 0.05$) and 24 hours (reduction to 53.3 ± 6.9, $p < 0.001$). Similarly, fenoldopam caused significant VWF release at both time points. Minoxidil showed a trend but the release was not significant at 1 hour. However, at 24 hours minoxidil significantly expelled VWF (% VWF-positive cells was reduced to 63.5 ± 4.73, $p < 0.01$). Rolipram did not cause VWF release. All represent N=4 (**Figure 4.5**, A and B).

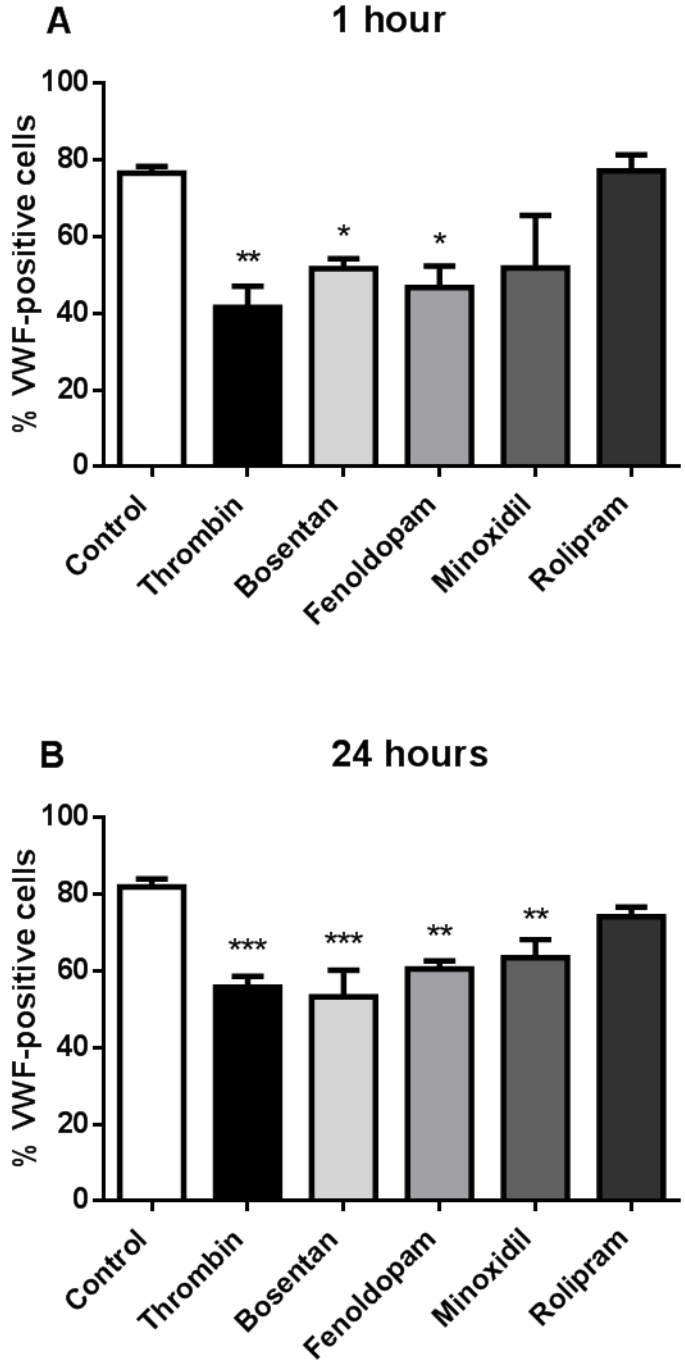

Figure 4.5 VWF release after 1 and 24 hours in HUVEC. HUVEC were treated with 1 U/ml thrombin and DIVI-related drugs at 100 μM for 1 and 24 hours. Data are expressed as % of VWF-positive cells out of all cells in the field of view (six random fields of view per treatment), and represent mean ± SEM of 4 independent experiments, analysed by one-way ANOVA followed by Dunnett's post test. *$p < 0.05$, **$p < 0.01$, ***$p < 0.001$.

4.2.1.2 The particle size of WPB does not differ across treatments

In order to analyse the particle size of WPB, which store VWF, images were thresholded to remove the background, made binary and then the total area of particles larger than 0.3 μm^2 was counted automatically. Using this method, all particles are counted, including the ones outside the cells and therefore this approach does not discriminate whether VWF has been released from the cell. The particle size of WPB did not differ across treatments at 1 hour or 24 hours (**Figure 4.6**, A and B).

These data showed that DIVI-related drugs (except for rolipram) induce significant VWF release compared to control both *ex vivo* in rat vessel explants and *in vitro* in human EC. VWF release is induced acutely (after 1 hour) and the effect is retained after 24 hours. In both experiments, thrombin caused VWF release, proving to be a robust positive control.

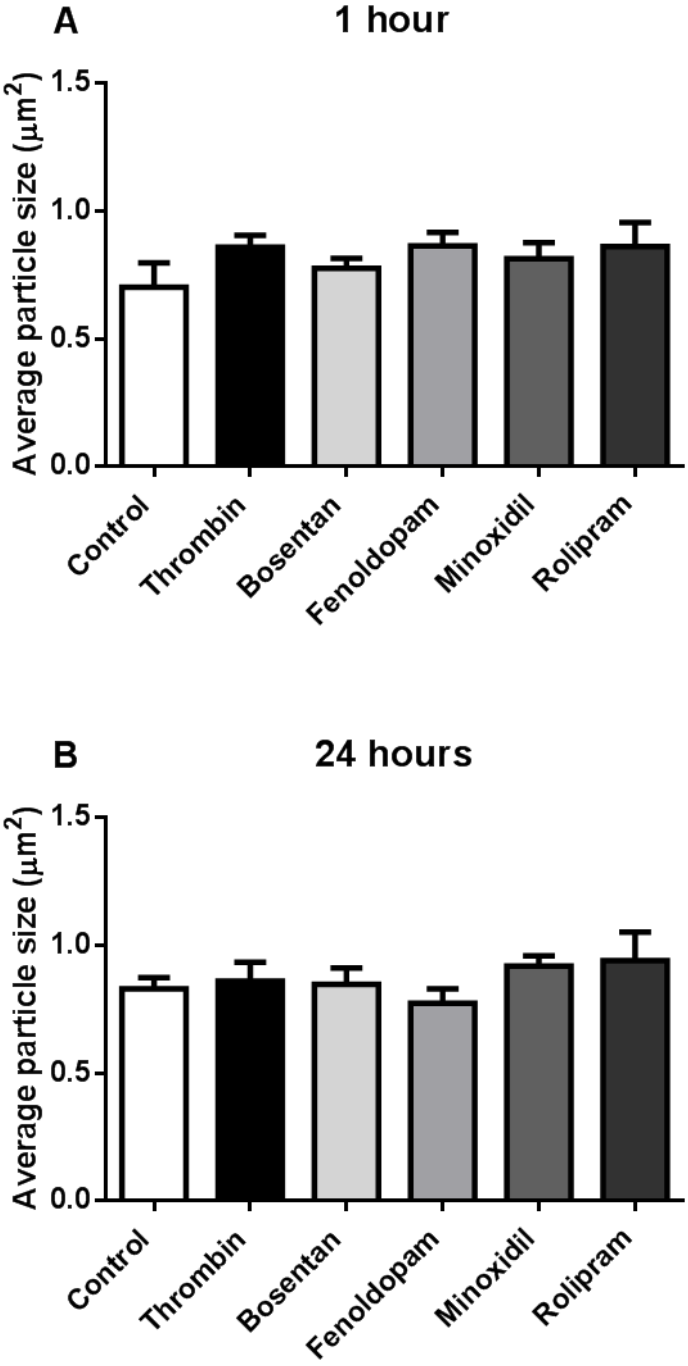

Figure 4.6 Average particle size of WPB at 1 and 24 hours. HUVEC were treated with 1 U/ml thrombin and DIVI-related drugs at 100 μM for 1 and 24 hours. Data are expressed as area of WPB particles in the field of view (six random fields of view per treatment), and represent mean ± SEM of 4 independent experiments, analysed by one-way ANOVA followed by Dunnett's post test.

4.2.2 Assessment of disruption to EC monolayer

Drug-induced disruption to the HUVEC monolayer was assessed via confocal microscopy, using CD31 to mark junctional integrity and disruption. The experiment was conducted as explained in section **4.2.1**. Images taken with a confocal microscope at a 63x objective were processed using ImageJ software. 6 images were taken per treatment per repeat. Images were thresholded in order to remove background noise and enable clear visualisation of the junctions. The image was then converted to binary and the median fluorescence intensity (MFI) of the black pixels enumerated. The larger the area of black the greater disruption to EC monolayer (**Figure 4.7, 4.8**).

4.2.2.1 Fenoldopam induces junctions disruption at 1 hour and minoxidil at 24 hours

Thrombin 1 U/ml was used as positive control for inducing disruption in the junctions. Thrombin significantly disrupted the junctions at 1 hour (mean of 7.5 ± 1.2, $p < 0.01$), and the effect was reversed after 24 hours treatment (mean of 3.2 ± 1.7), (**Figure 4.9**).

All drugs were tested at 100 µM and disruption was assessed at 1 (**Figure 4.7**, **4.9**, A) and 24 hours (**Figure 4.8**, **4.9**, B). Fenoldopam significantly increased junction disruption at 1 hour (mean of 7.9 ± 3.3, $p < 0.01$), however the effect was not observed at 24 hours (mean of 1.2 ± 0.6). Minoxidil showed a trend to increase disruption at 1 hour (mean of 9.3 ± 3.4), and the effect reached significance at 24 hours (mean of 11.5 ± 1.9, $p < 0.01$). Bosentan and rolipram had no effect on junction disruption at 1 hour (mean of 2.1 ± 0.7 and mean of 0.9 ± 0.3, respectively) or 24 hours (mean of 2.7 ± 1.7). All data represent N=4.

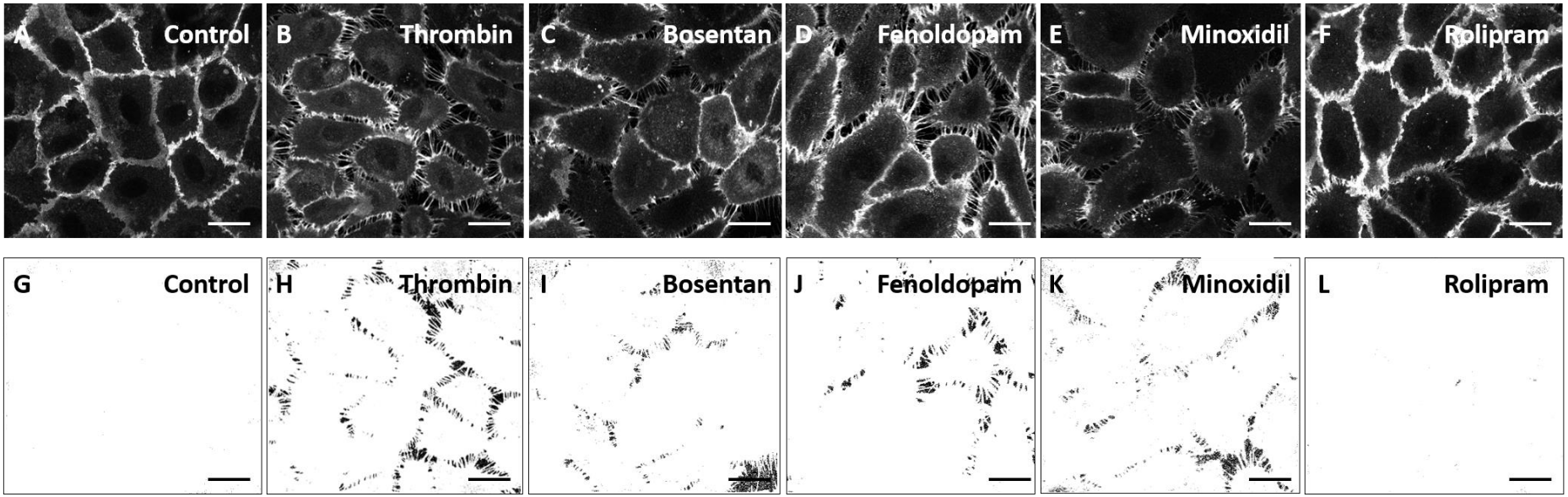

Figure 4.7 Assessment of EC junctional integrity with DIVI-related drugs at 1 hour. HUVEC were grown for 24 hours and then junctional disruption was analysed after treatment with DIVI-related drugs for 1 hour. Cell junctions are stained with CD31. Scale bars represent 30 µm.

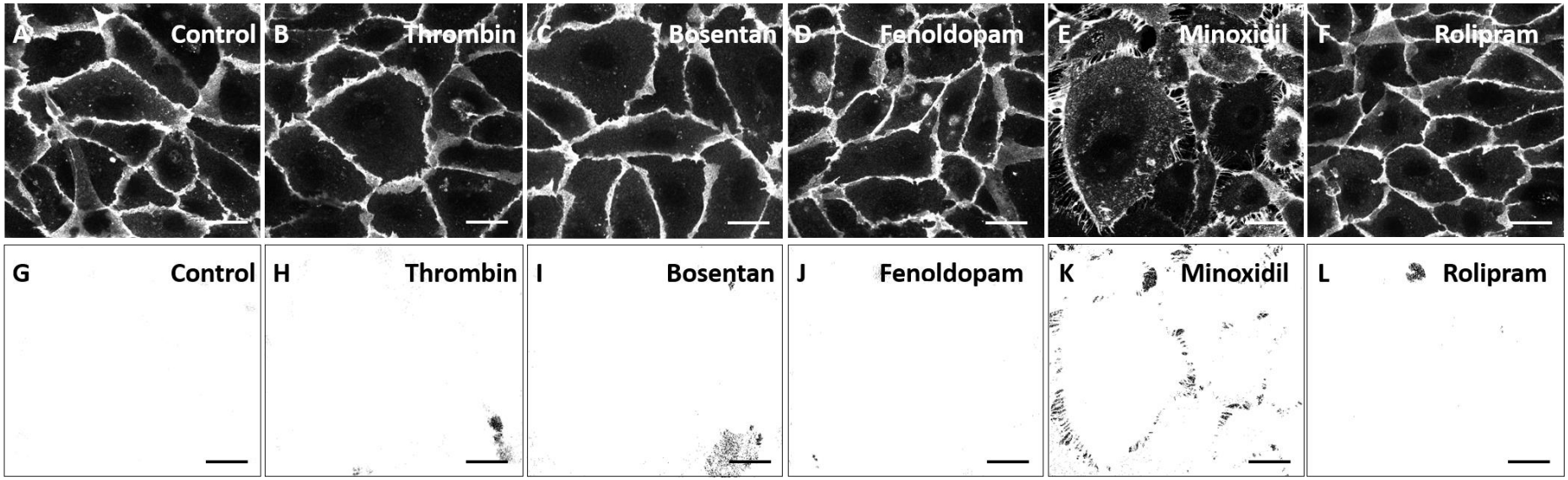

Figure 4.8 Assessment of EC junctional integrity with DIVI-related drugs at 24 hours. HUVEC were grown for 24 hours and then junctional disruption was analysed after treatment with DIVI-related drugs for 24 hours. Cell junctions are stained with CD31. Scale bars represent 30 µm.

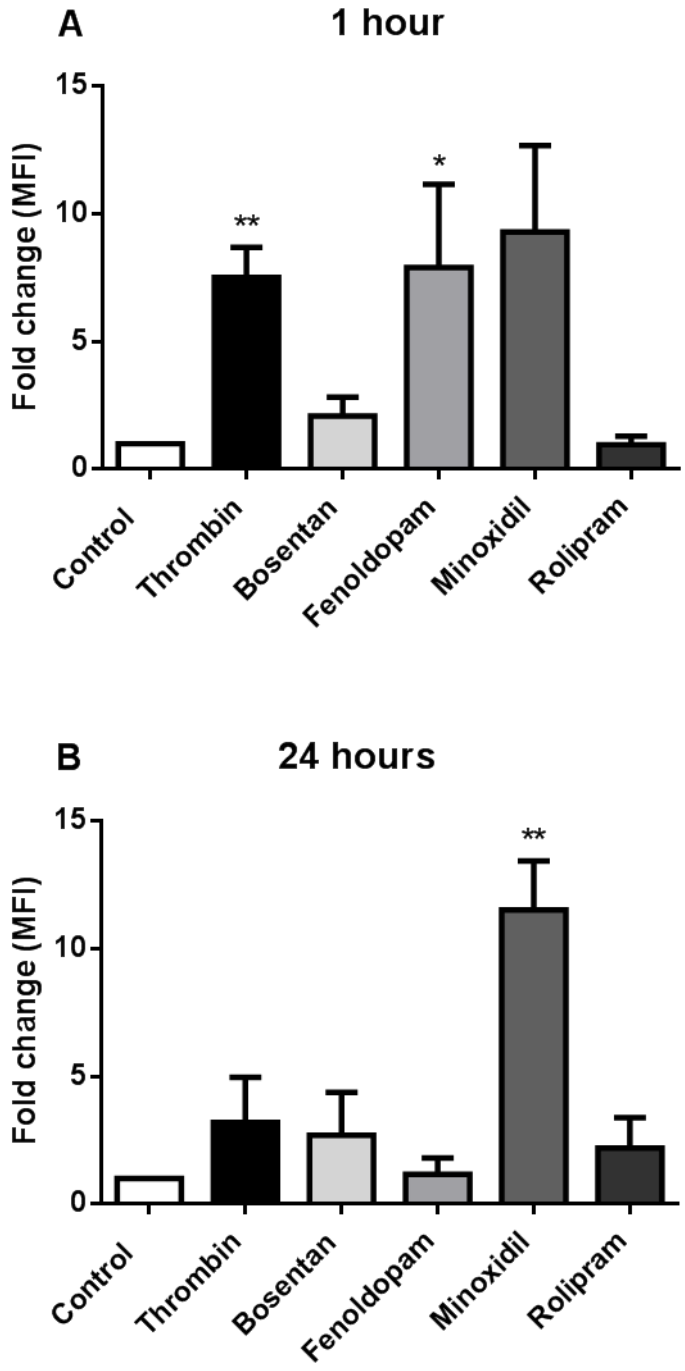

Figure 4.9 Quantification of EC junctional disruption. HUVEC were grown for 24 hours and then junctional disruption was analysed after treatment with DIVI-related drugs at 1 ad 24 hours. Data are normalised to DMSO control and expressed as MFI fold change and represent mean ± SEM of 4 independent experiments, analysed by one-way ANOVA followed by Dunnett's post test. *$p < 0.05$, **$p < 0.01$.

4.2.3 Investigating cell death with an ATP viability assay

A key feature of DIVI is cell death, which was assessed next. DIVI-related drugs have been shown to cause necrosis of the tunica media[170]. Furthermore, investigation of EC death has been suggested as potential biomarker of DIVI[35].

The ATP assay was used to measure the number of viable cells in culture. Cell injury and death leads to membrane permeability and results in a rapid decrease in cytoplasmic ATP, incubation of the substrate with viable cells results in a signal that is proportional to the number of viable cells present. The luminescence assay used here was selected because of its high sensitivity.

Cells were seeded in 96 well plates at 15,000 cells/well and left to grow for 24 hours. They were treated with fenoldopam, minoxidil, bosentan, and rolipram. Four concentrations were used: 0.1, 1, 10, and 100 μM. Saponin, a detergent that dissolves lipids in the cell membrane making it permeable, was used as positive control[364]. Three time points (1, 4 and 24 hours) were chosen. The assay was performed on HUVEC and HCASMC. The luminescence was detected by a plate reader (refer to **methods**, section **2.2.6** for a detailed description of the protocol).

4.2.3.1 Fenoldopam causes cell death after 24 hours in HUVEC

The luminescence for the vehicle was measured to ensure that DMSO would not induce cell death. No significant difference was observed at 1, 4 and 24 hours (**Figure 4.10**). For example, at 1 hour DMSO-treated HUVEC had a mean survival of 97.0 ± 0.6 % and HUVEC treated with media alone had a mean survival of 98.7 ± 0.9 % (N=5, ns).

The positive control saponin induce a significant decrease in cell survival compared to control at all time points. At 1 hour, saponin reduced HUVEC survival by 89.0 ± 0.7 %. Similar effects were seen at 4 and 24 hours.

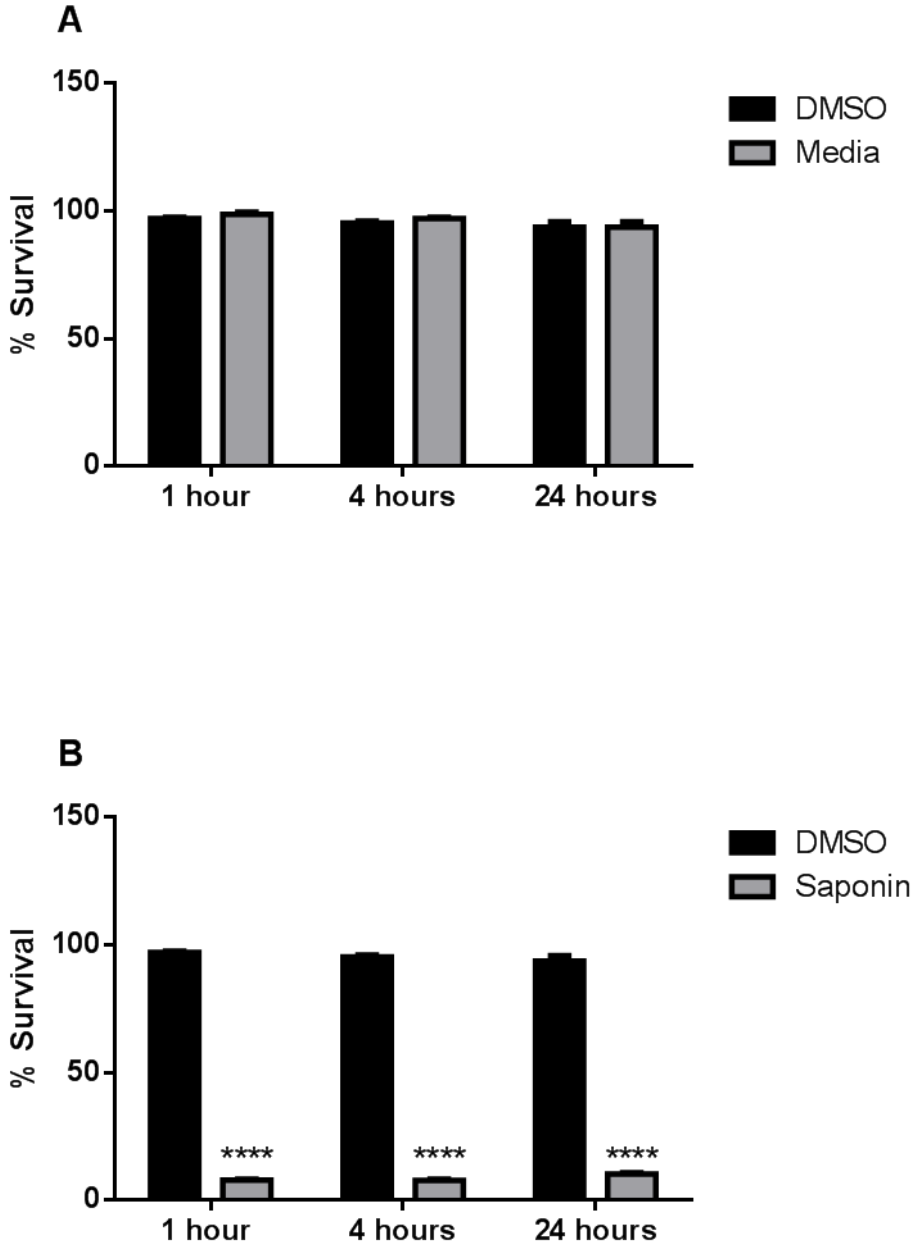

Figure 4.10 Investigating cell death with the ATP viability assay. HUVEC were grown for 24 hours, and luminescence was measured using a plate reader at three time points. DMSO was used as the vehicle for the drugs. The detergent saponin was used as positive control for cell death. Data represent mean ± SEM of 5 independent experiments, analysed by two-way ANOVA followed by Dunnett's post test. **** $p < 0.0001$.

Across the drugs, only 100 μM fenoldopam had a significant effect, inducing approximately 50 % HUVEC cell death at 24 hours (mean survival, 48.4 ± 6.1 %; N=5, $p < 0.05$) (**Figure 4.11**). 10 μM Fenoldopam induced only a small amount of death, displaying a mean of 89.2 ± 2.7, whereas 1 μM showed a mean of 93.3 ± 7.3, and 0.1 μM a mean of 94.8 ± 6.5 (N=5, ns). None of the drugs showed an effect on cell proliferation. In HCASMC none of the drugs had an effect on cell death (**Figure 4.12**).

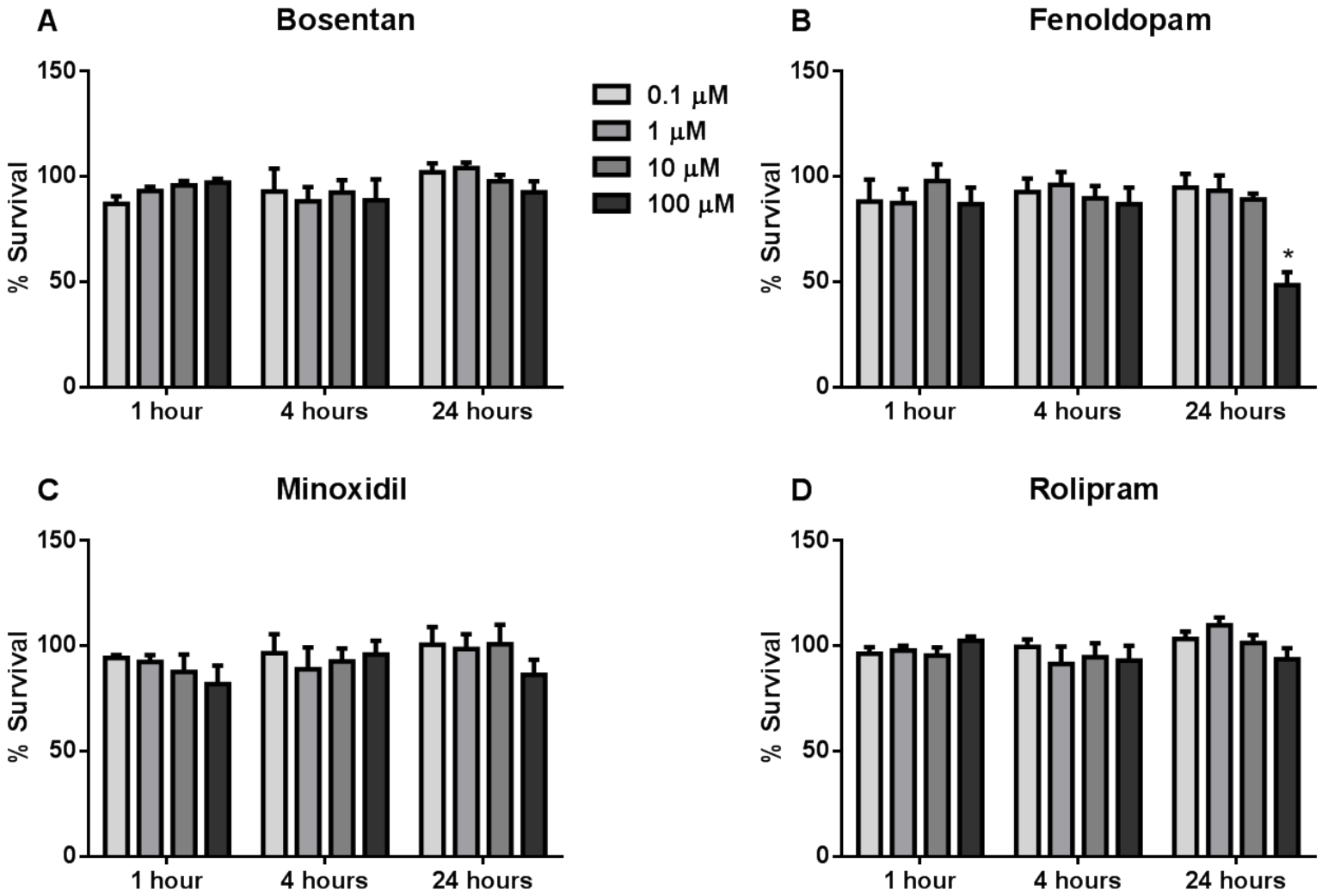

Figure 4.11 ATP viability assay in HUVEC. HUVEC were grown for 24 hours, treated with DIVI-related drugs at 0.1, 1, 10, 100 μM for 1, 4 and 24 hours. Luminescence was detected using a plate reader. Data are expressed as % survival compared to control. 100 % represents no death. Data represent mean ± SEM of 5 independent experiments, analysed by two-way ANOVA followed by Dunnett's post test. *$p < 0.05$.

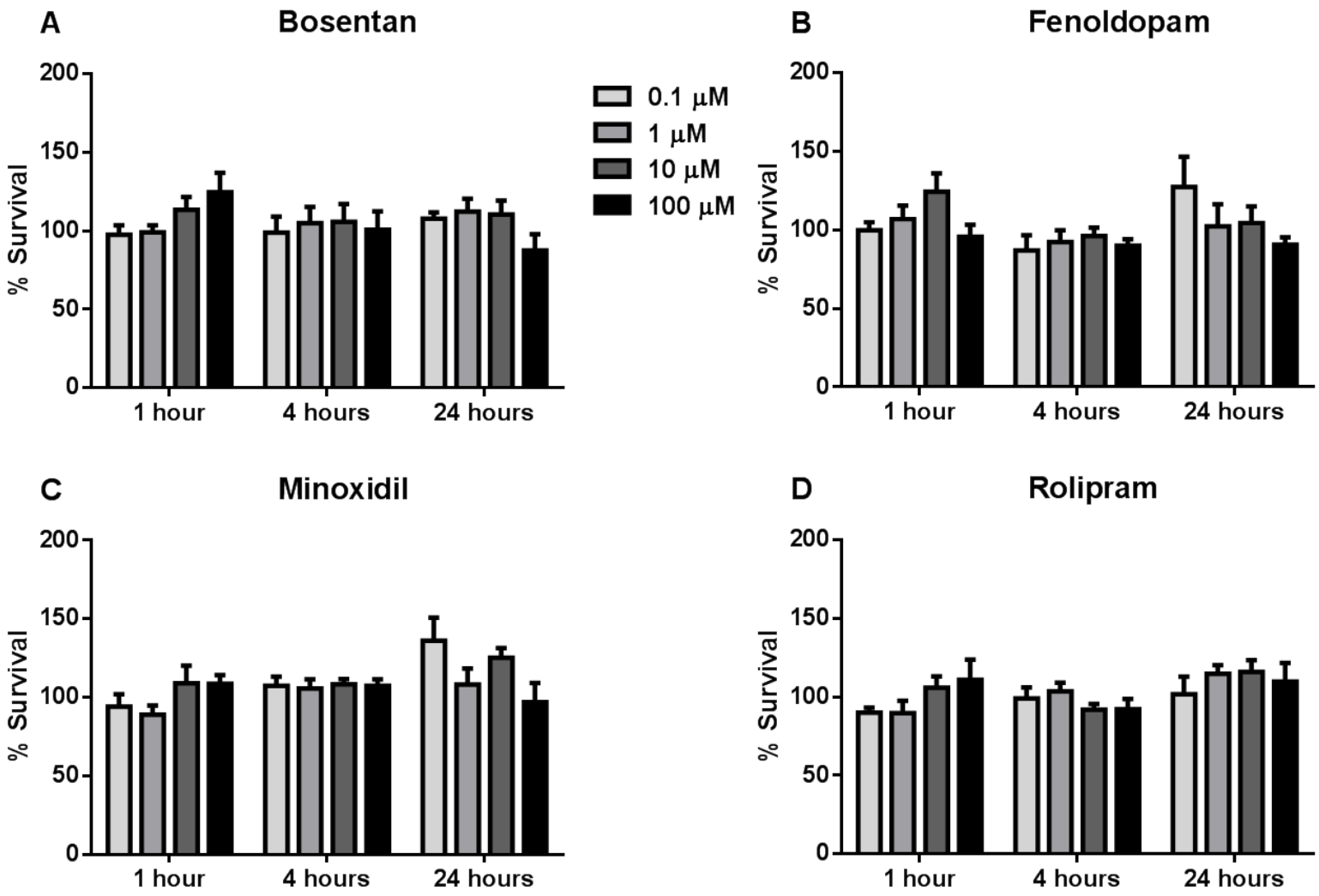

Figure 4.12 ATP viability assay in HCASMC. HCASMC were grown for 24 hours, treated with DIVI-related drugs at 0.1, 1, 10, 100 μM for 1, 4 and 24 hours. Luminescence was detected using a plate reader. Data are expressed as % survival compared to control. 100 % represents no death. Data represent mean ± SEM of 5 independent experiments, analysed by two-way ANOVA followed by Dunnett's post test. *$p < 0.05$.

4.2.4 Exploring inflammation in DIVI

Inflammation and leukocyte recruitment to the injuried artery wall has been extensively indicated as a hallmark of DIVI[35,170,202]. It was therefore tested whether DIVI drugs induced inflammation in EC. VCAM-1 and ICAM-1 were selected as markers of inflammation as they are upregulated in reponse to inflammatoty stimuli and are required for leuckoyte adhesion to the inflamed vessel wall.

HUVEC were grown for 24 hours in 24-well plates, and treated with the drugs or TNF-α as a positive control for 24 hours. HUVEC were then washed with EDTA and incubated with accutase for cell detachment. Accutase was neutralised with M199 containing 20 % v/v FBS, cells were harvested, centrifuged and stained with specific antibodies (**Methods**, **Table 2.3**) and analysed by flow cytometry.

4.2.4.1 TNF-α induces VCAM-1 and ICAM-1 expression in HUVEC in a concentration-dependent manner

HUVEC were gated using forward and side scatter (**Figure 4.13**, A). The cells stained positive for CD31, a specific marker for EC[365] (B). An IgG isotype control was used to remove the non-specific staining from the gating. TNF-α (10 U/ml) induced ICAM-1 and VCAM-1 expression in HUVEC after 24 hours (C and D), as seen by the shift to the right in the MFI.

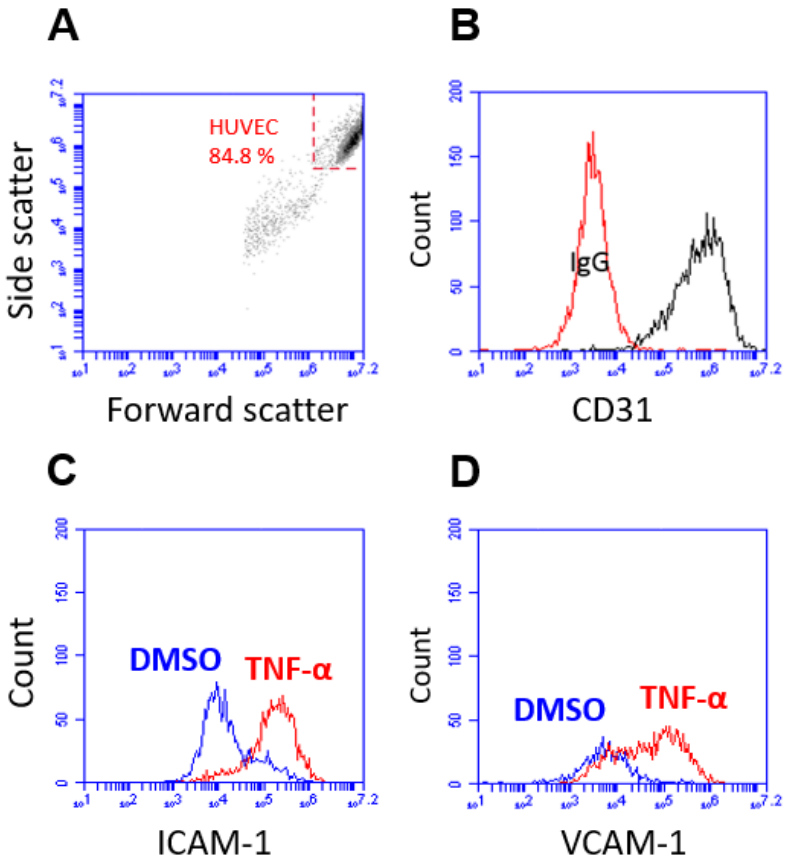

Figure 4.13 ICAM-1 and VCAM-1 expression in HUVEC. HUVEC were grown for 24 hours in 24-well plates, and treated with the drugs or TNF-α as a positive control for 24 hours. Cells were detached with accutase, stained with CD31 (specific EC marker), ICAM-1 and VCAM-1, and analysed by flow cytometry. IgG represents the isotype control.

To establish a suitable concentration of TNF-α to use as a postive control in subsequent experiments to investigate inflammation, HUVEC were treated with various concentrations of TNF-α for 24 hours (1-100 U/ml) (**Figure 4.14**, A, B; data are expressed as MFI fold change compared to control cells). TNF-α induced ICAM-1 and VCAM-1 expression in a concentration-dependent manner. TNF-α 1 U/ml did not significantly increase ICAM-1 (mean fold change of 1.3 ± 0.1, N=5, ns) nor VCAM-1 expression (mean of 1.0 ± 0.1, N=5, ns). TNF-α 5 U/ml significantly increased only ICAM-1 expression (mean of 3.6 ± 0.5, N=5, $p < 0.01$). TNF-α 10, 20, 50 and 100 U/ml significantly increased both ICAM-1 and VCAM-1 expression. For example TNF-α 100 U/ml showed a mean of 12.6 ± 1.1 for ICAM-1 (N=5, $p < 0.001$) and 7.1 ± 1.2 for VCAM-1 (N=5, $p < 0.001$). TNF-α 10 U/ml was the lowest dose to induce a significant effect on both VCAM-1 and ICAM-1 and was therefore chosen as positive control for the next experiment with the drugs (sections **4.2.4.2** and **4.2.4.3**). This concentration was selected, rather than the much stronger stimulation seen with 100 U/ml TNF-α, as it was considered that the DIVI drugs might have relatively weak effects on inflammation and this would be reflected in the control.

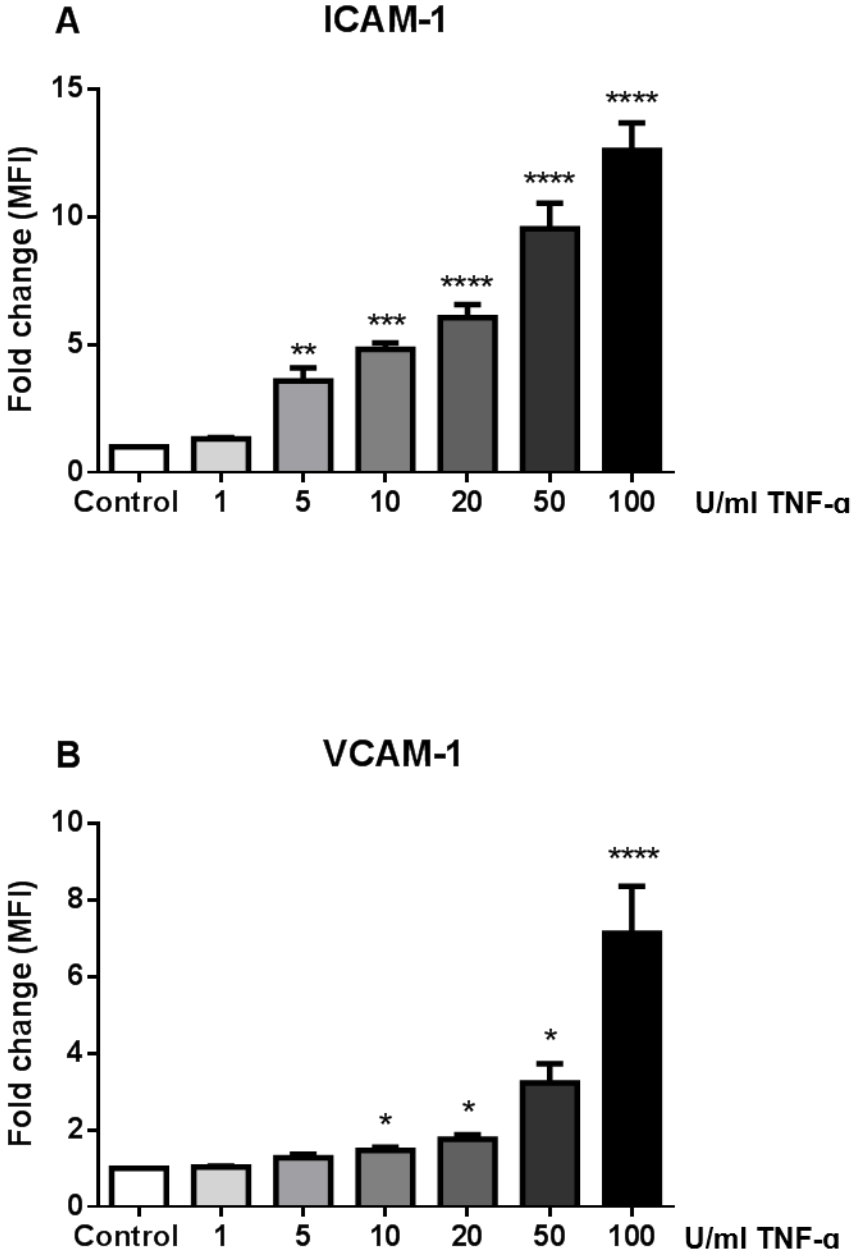

Figure 4.14 ICAM-1 and VCAM-1 expression in HUVEC after treatment with increasing concentrations of TNF-α. HUVEC were grown for 24 hours in 24-well plates, and treated with increasing concentrations of TNF-α for 24 hours. Cells were detached with accutase, stained with CD31 (specific EC marker), ICAM-1 and VCAM-1, and analysed by flow cytometry. Data are expressed as MFI fold change compared to unstimulated control, and represent mean ± SEM of 5 independent experiments, analysed by one-way ANOVA followed by Dunnett's post test. *$p < 0.05$, ** $p < 0.01$, ***$p < 0.001$, ****$p < 0.0001$.

4.2.4.2 Bosentan and fenoldopam induce ICAM-1 and VCAM-1 expression in HUVEC

To test whether the DIVI-related drugs under investigation could induce inflammatory responses in EC, HUVEC were treated with each of the drugs (100 µM) for 24 hours. Bosentan significantly increased ICAM-1 expression after 24 hours with a mean fold change in MFI of 1.8 ± 0.1 (N=5, $p < 0.05$) compared to control (**Figure 4.15**). However, the increase was not to the same extent as TNF-α 10 U/ml (mean fold change of of 5.0 ± 0.3). Bosentan also significantly increased VCAM-1 expression, with a mean of 1.5 ± 0.1 (N=5, $p < 0.01$), showing a similar increase as TNF-α (mean of 1.6 ± 0.2, N=5, $p < 0.001$). Fenoldopam significantly increased only VCAM-1 expression (mean of 1.3 ± 0.1, N=5, $p < 0.05$), with no significant effect on ICAM-1 expression. These data suggest that although some DIVI drugs can induce increased expression of ICAM-1 or VCAM-1 in HUVEC *in vitro*, their effects are relatively weak since even at 100 µM their effects are similar to (or less than) a threshold concentration of TNF-α.

4.2.4.3 ICAM-1 and VCAM-1 expression is increased by bosentan under inflammatory conditions

It has been suggested that DIVI might be facilitated by underlying inflammatory conditions[35,202]. In order to test this hypothesis, HUVEC were treated with the drugs alone at 100 µM (no TNF-α) or in combination with the threshold concentration of TNF-α (10 U/ml) for 24 hours to mimic underlying inflammatory conditions that could facilitate DIVI (**Figure 4.16**). It was observed that bosentan and TNF-α had an additive effect on ICAM-1 expression (mean of 8.3 ± 0.5, compared to 5.3 ± 0.1 of TNF-α alone, N=5, $p < 0.01$). The effect was greater than the sum of TNF-α alone and bosentan alone. However, the effect of bosentan with TNF-α on VCAM-1 expression was not statistically significant (mean of 2.6 ± 0.5, compared to 1.7 ± 0.4 of TNF-α alone, N=5, ns). The other drugs did not induce an additive effect on ICAM-1 or VCAM-1 when co-incubated with the threshold concentration of TNF-α.

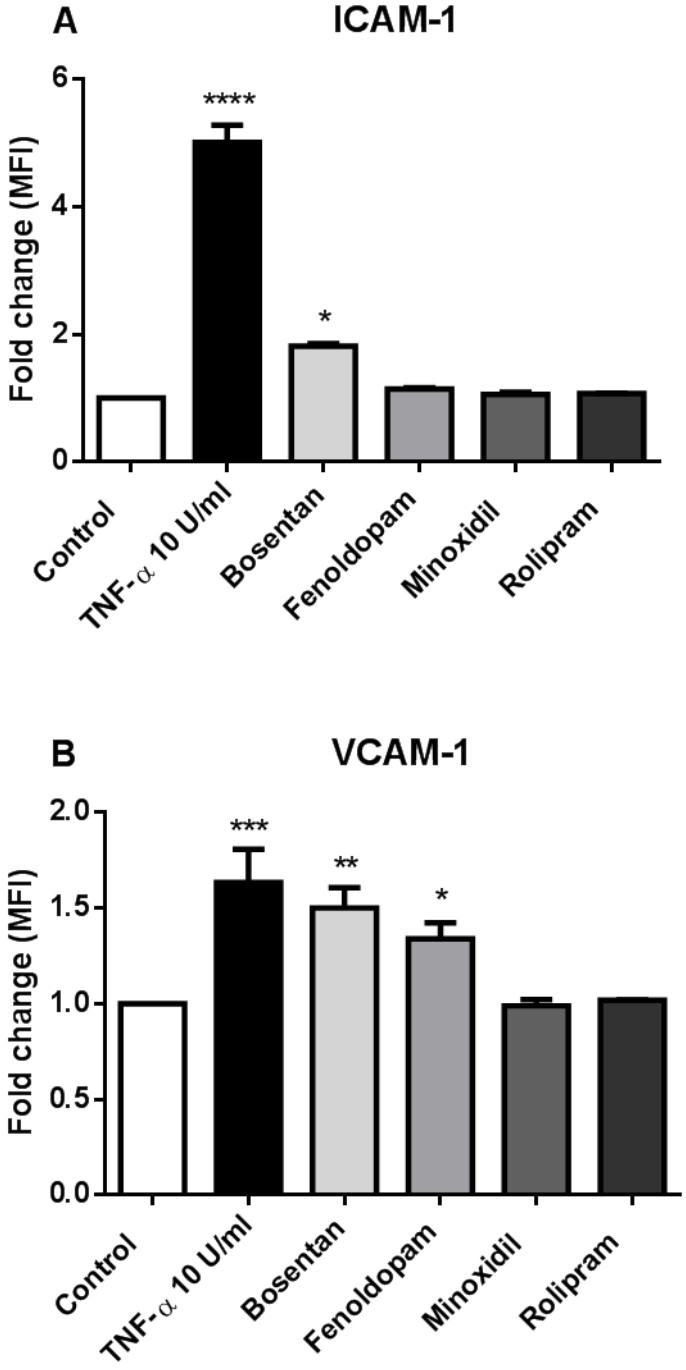

Figure 4.15 Quantification of ICAM-1 and VCAM-1 expression in HUVEC. Data are expressed as fold change compared to control and represent mean ± SEM of 5 independent experiments, analysed by one-way ANOVA followed by Dunnett's post test. *p < 0.05, ** p < 0.01, ***p < 0.001, ****p < 0.0001.

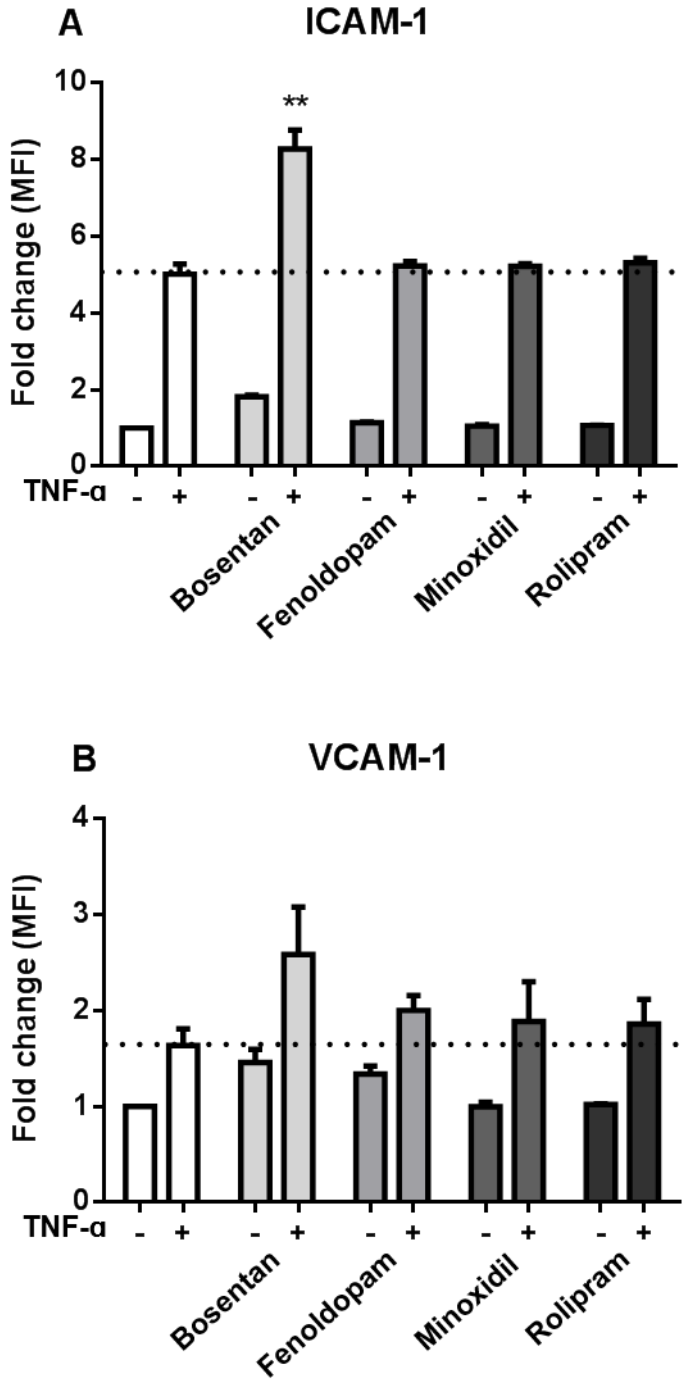

Figure 4.16 ICAM-1 and VCAM-1 expression mimicking underlying inflammatory conditions. HUVEC were incubated with the drugs alone (no TNF-α) or together with TNF-α 10 U/ml for 24 hours. Cells were stained with CD31 (specific EC marker), ICAM-1 and VCAM-1 and analysed by flow cytometry. Data are expressed as MFI fold change compared to unstimulated control and represent mean ± SEM of 5 independent experiments, analysed by two-way ANOVA followed by Dunnett's post test. **$p < 0.01$ compared to TNF-α alone.

4.2.4.4 Bosentan only at high concentrations increases ICAM-1 and VCAM-1 expression

The effect of bosentan on ICAM-1 expression with underlying inflammatory conditions was investigated further, since it was the only drug that had an effect on ICAM-1 expression under inflammatory conditions. The next step was to find the concentration of TNF-α that induced an effect on both VCAM-1 and ICAM-1 when incubated with bosentan, (since bosentan with TNF-α 10 U/ml showed an effect only on ICAM-1). The other were not investigated as these did not induce any effect in sections **4.2.4.2** and **4.2.4.3**, and fenoldopam only induced an effect on VCAM-1 but not on ICAM-1.

Various concentrations of TNF-α (0, 1, 5, 10, 20, 50, 100 U/ml) were tested to identify the concentration that had the greatest effect on induction of ICAM-1 and VCAM-1 expression when incubated with 100 µM bosentan for 24 hours (**Figure 4.17**). The concentrations that produced an effect on both ICAM-1 and VCAM-1 were 20 and 50 U/ml and these were therefore used in the subsequent experiments.

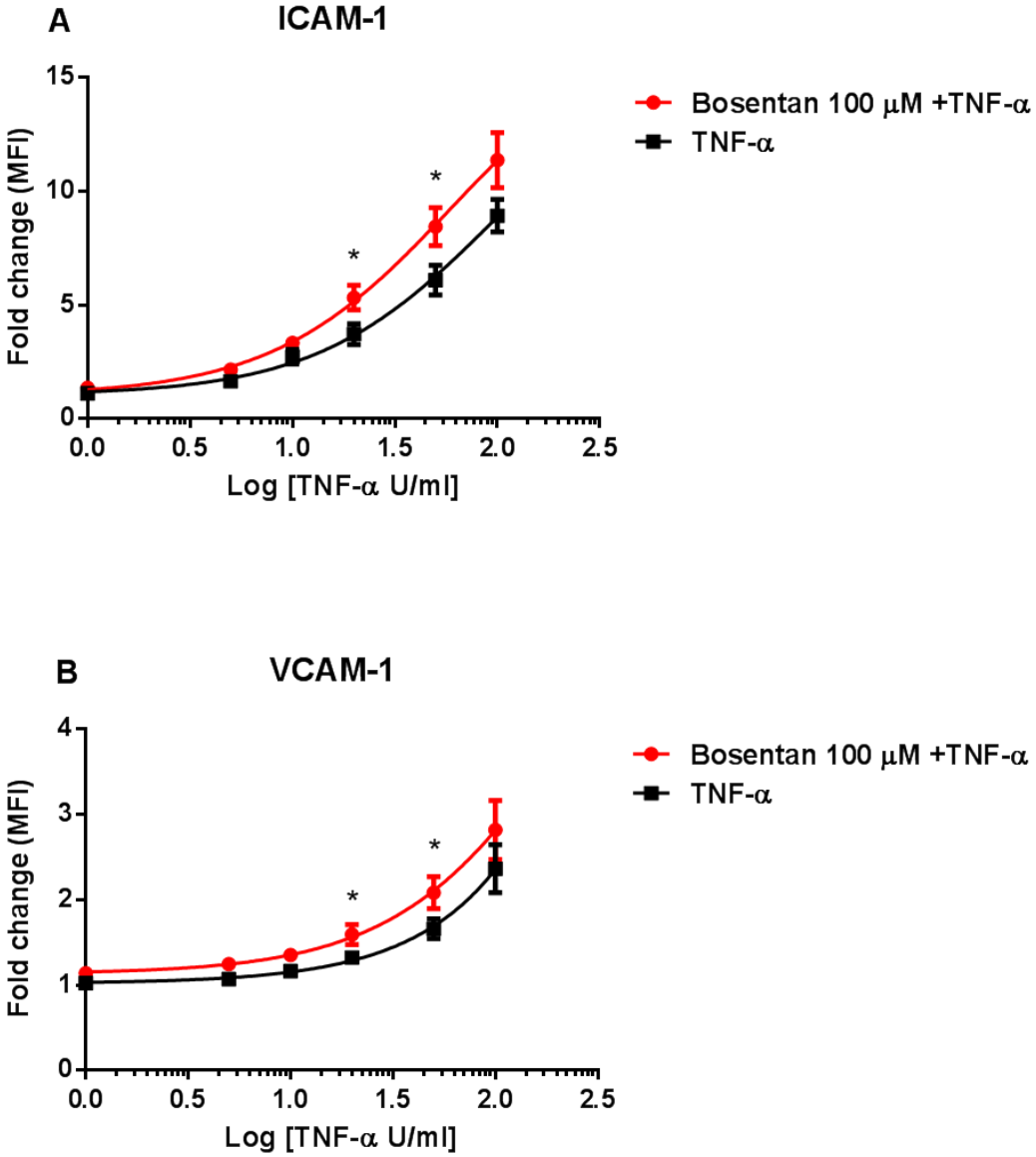

Figure 4.17 Increasing concentrations of TNF-α incubated with bosentan 100 µM on ICAM-1 and VCAM-1 expression in HUVEC. HUVEC were grown for 24 hours in 24-well plates, and treated with bosentan and TNF-α or TNF-α alone for 24 hours. Cells were detached with accutase, stained with CD31 (specific EC marker), ICAM-1 and VCAM-1, and analysed by flow cytometry. Data are expressed as MFI fold change compared to control on a logarithmic scale of concentrations of TNF-α (1, 5, 10, 20, 50, 100 U/ml). Data represent mean ± SEM of 5 independent experiments, analysed by one-way ANOVA followed by Dunnett's post test. *$p < 0.05$.

Having identified the concentrations of TNF-α that induced an effect on ICAM-1 and VCAM-1 expression with bosentan, lower concentrations of bosentan were subsequently investigated. Bosentan (1, 10 and 100 μM) were incubated with TNF-α 20 or 50 U/ml (**Figure 4.18**). As shown previously, TNF-α 20 U/ml significantly increased ICAM-1 (mean of 5.1 ± 0.1, N=5, $p < 0.001$) and VCAM-1 expression (mean of 1.9 ± 0.1, N=5, $p < 0.01$). TNF-α 50 U/ml also significantly increased ICAM-1 (mean of 7.8 ± 0.2, N=5, $p < 0.0001$) and VCAM-1 expression (mean of 3.1 ± 0.1, N=5, $p < 0.001$). Stars are not indicated on the graph as this effect was shown in the previous figures.

HUVEC treated with bosentan (100 μM) and TNF-α (20 U/ml) showed significantly increased ICAM-1 (mean of 8.8 ± 0.5, N=5, $p < 0.001$) and VCAM-1 expression (mean of 3.9 ± 0.2, N=5, $p < 0.001$) compared to TNF-α 20 U/ml alone. Also, bosentan (100 μM) incubated with TNF-α 50 U/ml increased ICAM-1 (mean of 11.4 ± 0.4, N=5, $p < 0.001$) compared to TNF-α 50 U/ml alone and VCAM-1 expression (mean of 4.7 ± 0.1, N=5, $p < 0.0001$). However, lower concentrations of bosentan did not have any effect on VCAM-1 and ICAM-1 expression. These data suggest that although co-stimulation with TNF-α increases the magnitude of the effect of bosentan, it does not increase the sensitivity of HUVEC to bosentan.

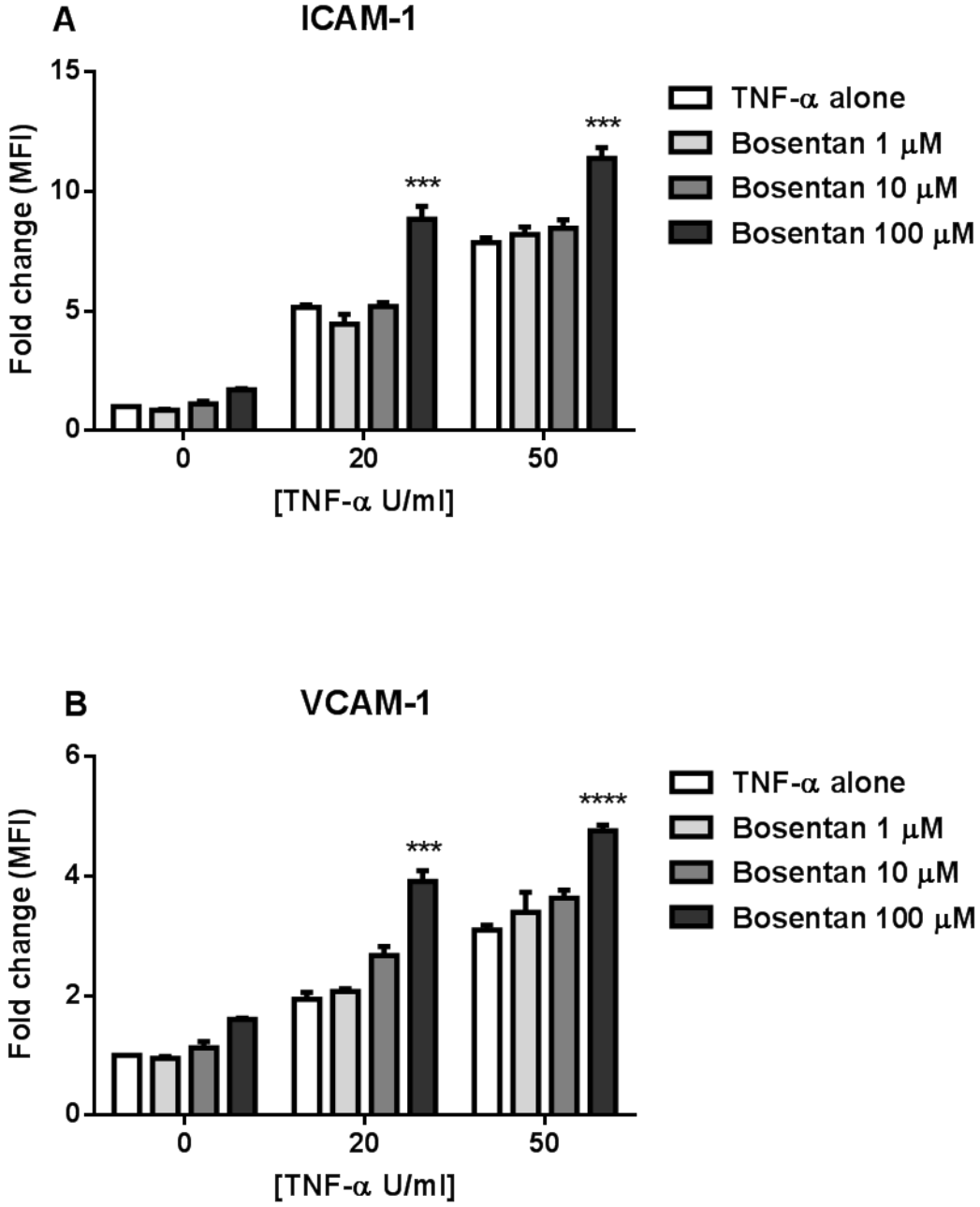

Figure 4.18 Increasing concentrations of bosentan on VCAM-1 and ICAM-1 expression. HUVEC were grown for 24 hours in 24-well plates, and treated with bosentan 1, 10, 100 μM and TNF-α 20 or 50 U/ml for 24 hours. Cells were detached with accutase, stained with CD31 (specific EC marker), ICAM-1 and VCAM-1, and analysed by flow cytometry. Data are expressed as MFI fold change compared to unstimulated control and represent mean ± SEM of 5 independent experiments, analysed by two-way ANOVA followed by Dunnett's post test. ***$p < 0.001$, ****$p < 0.0001$.

4.2.4.5 Bosentan effect on ICAM-1 and VCAM-1 does not depend on ET receptor antagonism

To understand the mechanism by which bosentan induces the effect on VCAM-1 and ICAM-1 expression, interaction with the target receptors was investigated to determine whether the response depends on its primary target or is alternatively an off-target effect. Bosentan is an ET receptor antagonist, acting non-selectively on both ET_A and ET_B[366]. Therefore, cells were treated with the ET_A selective antagonist, BQ123, and the ET_B selective blocker, BQ788, both at 1 µM[367,368]. Neither BQ123 nor BQ788 produced a comparable effect to bosentan 100 µM (**Figure 4.19**). For example, bosentan incubated with TNF-α 20 U/ml increased the fold change in ICAM-1 MFI by 6.9 ± 0.4, whereas BQ123 or BQ788 plus TNF-α led to a fold change in MFI of 3.5 ± 0.1 or 3.2 ± 0.7, respectively. This suggested that the effect does not depend on a selective antagonism of ET_A nor ET_B.

To understand whether the effect of bosentan is through a combined non-selective action on ET_A and ET_B, BQ123 and BQ788 were incubated together but again they did not have a comparable effect to that observed with bosentan alone.

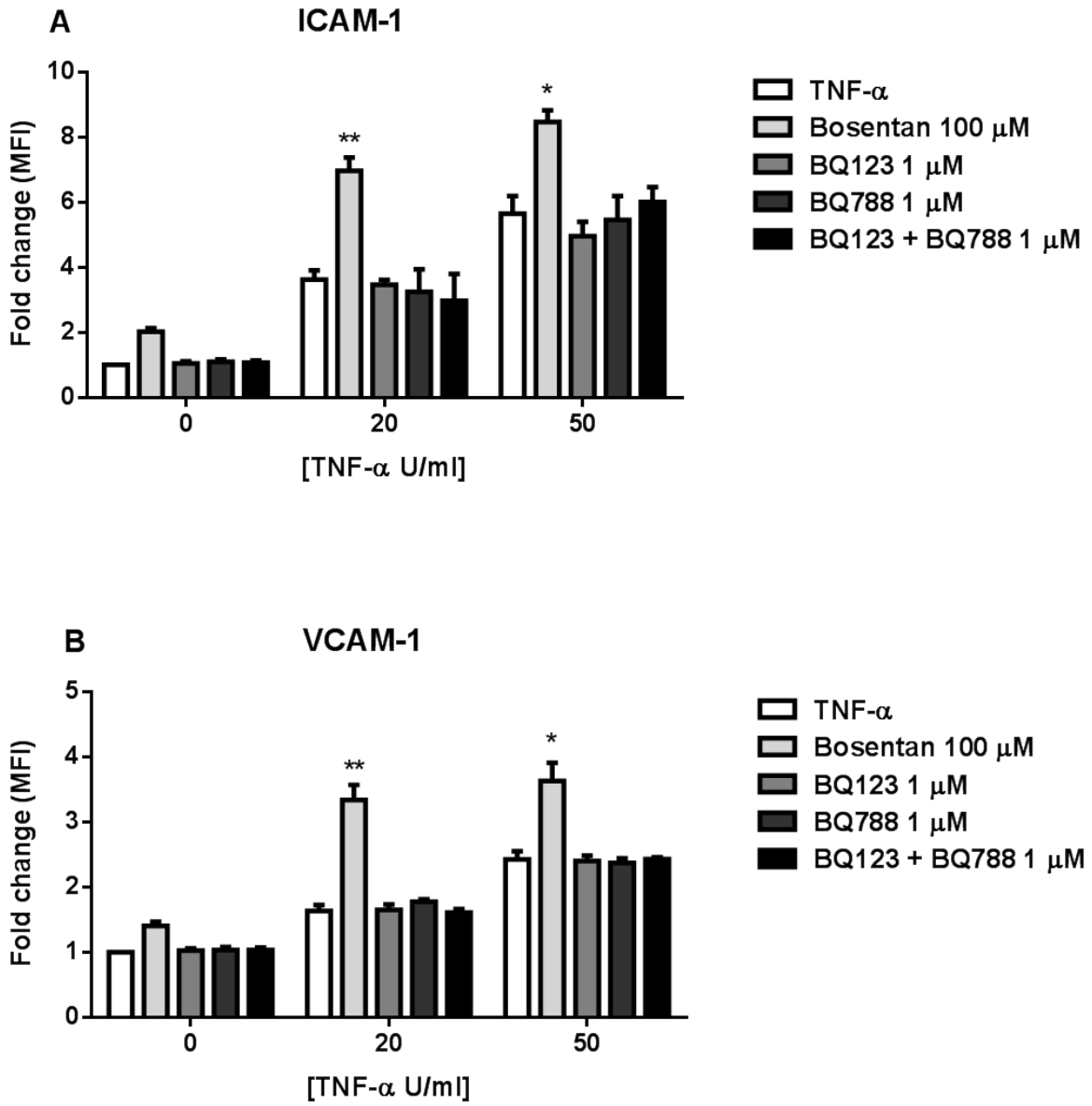

Figure 4.19 ET receptor antagonism effect on ICAM-1 and VCAM-1 expression. HUVEC were grown for 24 hours in 24-well plates, and treated with bosentan 100 μM, BQ123 1 μM, BQ788 1 μM and TNF-α 20 or 50 U/ml for 24 hours. Cells were detached with accutase, stained with CD31 (specific EC marker), ICAM-1 and VCAM-1, and analysed by flow cytometry. Data are expressed as MFI fold change compared to unstimulated control and represent mean ± SEM of 5 independent experiments, analysed by two-way ANOVA followed by Dunnett's post test. *$p < 0.05$, **$p < 0.01$.

4.3 Discussion

In this chapter monocultured EC and SMC were investigated for DIVI-related phenotypes. Monocultured HUVEC and HCASMC were used. It is important to note that observations described in this chapter may differ across different vascular beds and further studies should be directed at investigating those differences. Specifically, HUVEC are derived from veins from immune-naïve foetal tissue and show differences from adult vascular endothelium.

VWF release was measured *in vitro* in HUVEC. The cells were permeabilised to allow VWF intracellular levels to be measured. Thrombin was used as positive control. Thrombin induces VWF release in HUVEC[369–371]. Here, thrombin caused a significant VWF release at 1 hour and 24 hours compared to DMSO (vehicle)-treated cells. The release of VWF from cells is not uniform in the field of view, and some control cells had completely released VWF. This could be explained as newly synthesised VWF is also secreted spontaneously from unstimulated cells through the constitutive secretory pathway[363] (refer to **Introduction**, section **1.6.2.4.2**). In addition, the HUVEC were derived from pooled donors and were at different stage of growth, which may also explain the non-uniformity between cells in the field of view. Using a single donor would have certainly decreased variability between cells and perhaps VWF expression in DMSO controls would have been more uniform but it would have been less useful and less representative of a large population. The way this could have been addressed would have been to use several single donor populations and compare VWF expression and release with pooled donors, as well as how VWF expression alters during the EC lifespan, but it would have been costly and not time efficient.

Fenoldopam, bosentan and minoxidil caused significant VWF release at 24 hours, reflecting the effects observed in the rat mesenteric artery explant (**chapter 3**). Rolipram did not show VWF release, again recapitulating the vessel work. This might depend on the specific rolipram mechanism of action, but further experiments are required to prove this. Bosentan and fenoldopam also caused release of VWF after 1 hour in HUVEC, suggesting that the effect of the drug is acute and it would have been interesting to assess VWF release at this time point *ex vivo* to understand how it compared.

Fenoldopam has been previously shown to promote VWF release *in vivo*[198,200]. VWF levels were measured in rat plasma in these studies after 2, 6 and 24 hours post treatment. It was found that fenoldopam caused release of VWF acutely, but levels returned to baseline after 24 hours. In a study from the same group in dogs, a K^+ channel opener has also been found to increase plasma VWF levels acutely[200]. This transient increase might depend on differences between *ex vivo*/*in vitro* and *in vivo* work[372].

The average particle size of WPB containing VWF was measured to make sure the difference in VWF was only in the extent of release rather than a change in the shape or size. In line with this, results showed that the size of the particles did not change across treatments. This suggests that WPB do not fuse together. However, it was noticed (data not shown) that the intracellular location of the WPB changes across treatment and after treatment with thrombin WPB migrate towards the periphery of the cell. This may suggest that the drugs cause VWF release through a different mechanism compared to thrombin, as this was not observed with any of the DIVI drugs. It would be interesting to understand this more in detail, investigating the signalling pathways of the drugs by blocking receptors. Importantly, the change in WPB size was not observed with the positive control thrombin either. It is therefore unclear whether how valid these findings are without a control that significantly impacts on WPB size. For example, statins have been reported to decrease the size significantly and could have been used as a positive control. This is something that is worth investigation in the future.

Following assessment of VWF release, other potential markers of DIVI were investigated. EC junctional integrity, as an indirect measure of permeability which is a feature of DIVI (refer to **Introduction**), was assessed by CD31 staining of the cell junctions. Junctional permeability could have been also studied using other approaches, e.g. VE-cadherin phosphorylation (Y658) or IP-IB with catenins. In this thesis, cells were defined as 'permeable' if there was disruption of the junctions, which led to an evident empty area between cells and a larger black area during the analysis. CD31 has been used as a marker to determine EC permeability. The rationale behind this relates to the extensive usage of CD31 to mark EC junctions to assess their integrity. Thrombin has been used as positive control for EC junctional disruption[373]. The mechanism by which thrombin causes disruption is well described and is dependent on

activation of protease-activated receptor (PAR)-1, a G protein-coupled receptor[347]. PAR-1 activation is coupled to G-proteins, including G_i, which in turn causes a decrease in intracellular cAMP level, G_q, which leads to an increase in intracellular Ca^{2+} and diacylglycerol (DAG) concentration, and $G_{12/13}$, which lead to activation of the small GTPase, Rho. Ca^{2+}/calmodulin-dependent activation of myosin light chain kinase (MLCK) promotes phosphorylation of myosin light chains, together with Rho kinase-dependent inactivation of myosin phosphatases, stimulates stress fiber formation and triggers actomyosin contraction[347]. In our experiments, thrombin-induced disruption was observed at 1 hour. It may have occurred earlier than this, as thrombin-induced barrier disruption has been reported to occur more rapidly[142]. The time points in this study did not allow to look at this in detail and it is something worth investigating in the future, but it was beyond the scope of this study. The effect on the junctions was restored after 24 hours, suggesting that thrombin has only a rapid and reversible action on permeability. The reversible effect of thrombin on permeability has been previously shown[374].

The effect of fenoldopam was similar to the observed thrombin response, in that, following fenoldopam treatment gaps could be observed in the endothelial monolayer within 1 hour, which had reversed by 24 hours. A previous *in vitro* study, in which rat aortic EC were co-cultured with SMC and exposed to *in vivo*-derived hemodynamics, showed that fenoldopam 100 µM caused endothelial permeability[79]. Although not assessed here, future studies to investigate whether fenoldopam can induce similar intracellular signalling to thrombin would be interesting.

In contrast, these studies showed that minoxidil induces a trend toward endothelial junctional disruption at 1 hour, which reached statistical significance at 24 hours. These results suggest that minoxidil has an effect on cell junctions that persists for at least 24 hours, however high variability in this data suggests additional experiments would be required for confidence. Of the drugs tested, minoxidil alone induced endothelial barrier disruption at 24 hours suggesting that potentially there may be differences in the intracellular signalling pathways triggered by minoxidil, fenoldopam and thrombin[53,80,154].

Rolipram, a PDE inhibitor, did not affect HUVEC junctions in these studies. Indeed, this is in agreement with previous studies that have suggested that PDE inhibitors may protect

endothelial barrier integrity. For example, a study in rats reported that the PDE IV inhibitor roflumilast suppressed histamine-induced permeability in rat mesenteric microvasculature[373]. In these experiments, rats were firstly administered FITC-labelled bovine albumin and roflumilast was given for 1 hour. The mesenteric artery was the superfused *in situ* with buffer supplemented with histamine (potent trigger of endothelial permeability) and the extent of leakage assessed by FITC-derived fluorescence. Roflumilast reversed histamine-induced extravasation of FITC-albumin by approximately 85 %. Notably, the same effect could also be observed *in vitro*, where permeability was measured using a transwell assay. HUVEC were preincubated with the roflumilast, rolipram and another PDE IV inhibitor (cilomilast) at a range of concentrations (10 pM - 100 µM) for 15 minutes, and permeability was elicited by thrombin treatment (1 U/ml). The permeation of horseradish peroxidase was assessed after 1 hour. In these assays all compounds were able to restore the HUVEC barrier integrity impaired by thrombin indicating that rolipram may have a repair function on cell contraction. The ability of PDE IV and PDE III inhibitors in protecting the EC barrier *in vitro* is supported in other studies[375,376]. These data demonstrate that rolipram does not have any effect on EC barrier permeability, either acutely or after 24 hours stimulation.

It is possible that the effect of PDE inhibitors is due to an elevation in cAMP concentration. cAMP is involved in protecting the integrity of the EC junctions, through the involvement of protein kinase A and the exchange protein (Epac) that is directly activated by cAMP[377–379]. Epac-1/Rap1 and protein kinase A activate Rac resulting in an improvement of the integrity of the EC barrier. Other mechanisms are also involved, such as protein kinase A-dependent myosin light chain kinase (MLCK) phosphorylation and RhoA inactivation[380].

Bosentan did not disrupt endothelial junctions, despite being as effective as thrombin and fenoldopam at triggering the release of VWF. This suggests that there is a difference in the intracellular signalling pathway activated by bosentan treatment compared with fenoldopam or thrombin.

In summary, endothelial junction disruption cannot be considered a robust indicator of DIVI *in vitro*, as only fenoldopam and minoxidil had an effect but all of them induce DIVI. It can be speculated that the effect of these drugs on EC junctions does not depend on the on-target mechanism of the compounds and is rather an off-target action that needs further investigation.

One of the features associated with DIVI is cell death, specifically SMC necrosis[170]. To investigate cell death a high-throughput assay was utilised, whereby ATP release from cells was used as an indirect measure for cell viability. The high-throughput ATP assay was ideal for detecting cell proliferation and cytotoxicity[381–383].

None of the drugs tested in these studies induced cell death at either 1 or 4 hours in HUVEC or HCASMC. However, ~50 % cell death in HUVEC was observed after 24 hours with fenoldopam at the highest concentration. There was no observed effect on cell death at lower concentrations.

There is no evidence in the literature of cell death induced by fenoldopam or the other drugs used in these experiments. On the contrary minoxidil has been shown to promote cell proliferation in dermal papilla cells of human hair follicle. This has been shown to be regulated by activation of the ERK and Akt pathways, and by inhibiting cell death through increasing the ratio of Bcl-2/Bax[384]. As minoxidil had no effect on vascular cell proliferation this could possibly be attributed to the phenotypic differences in the cell types used, since dermal cells are highly proliferative cells.

SMC necrosis is a feature of DIVI however none of these drugs were cytotoxic to SMC at any of the time points or concentrations in this study. This may be because a more physiologically relevant system is required to elicit this response, whereby for example EC and SMC interact together as a co-culture and/or are exposed to flow/shear stress[385].

In addition, these data showed that these drugs did not induce cell proliferation. However, it had been observed in the literature that minoxidil can inhibit proliferation of SMC both *in vivo* and *in vitro*[386] and bosentan was reported to inhibit proliferation of pulmonary artery SMC[387]. In these experiments the cells were seeded to confluency and this may have limited the ability to accurately assess effects on proliferation. Perhaps seeding the cells at lower density would have allowed for the observation of growth curves in the presence and absence of treatment. It would be useful to compare cell death in these *in vitro* experiments with the vessel explant in **chapter 3** to understand if translation occurs *ex vivo*/*in vitro*. From a qualitative point of view, these drugs did not appear to induce EC death. Although the endothelium was intact after all drug treatments, including fenoldopam, it was difficult to assess from confocal imaging whether the cells were functional. Moreover, SMC death cannot be ruled out in the

ex vivo worked conducted, since α-SMA was only used to detect the size of the smooth muscle layer but was not quantified.

Finally, HUVEC were stained for markers of inflammation. It has been suggested that DIVI-related drugs may promote inflammation through expression of adhesion molecules such as E-selectin, VCAM-1 and ICAM-1, as well as other cytokines and chemokines[388]. VCAM-1 and ICAM-1 aid in leukocytes recruitment and their expression represent a robust markers of EC activation during inflammation[389–391]. TNF-α is a powerful inducer of these adhesion molecules both *in vivo* and *in vitro* and was therefore chosen as positive control[392–394].

Treatment of cells with TNF-α for 24 hours increased the expression of ICAM-1 and VCAM-1 in a concentration-dependent manner. Bosentan and fenoldopam increased VCAM-1 expression after 24 hours treatment, and bosentan also increased ICAM-1 expression under the same conditions. It is interesting how fenoldopam only affects one of the cell adhesion molecules and not the other. The mechanism of action of the two compounds is very different, and this effect might depend on transcription factors and protein regulation. For example, it has been suggested that regulation of VCAM-1 gene expression may be coupled to oxidative stress through specific reduction-oxidation sensitive transcriptional or posttranscriptional regulatory factors[395]. Fenoldopam has been shown to act through the NO pathway, since the incidence and severity of fenoldopam-induced vascular injury were decreased when an NOS inhibitor or a scavenger of NO-generated free radicals were coadministered with fenoldopam[100]. Therefore, it is possible that VCAM-1 expression induced by fenoldopam depends on the drug producing free radicals through an increase in NO generation.

The data presented here are in contrast with literature reports about the anti-inflammatory effects of bosentan[396–398]. However, the experimental differences (first of all *in vivo* versus *in vitro*) could account for the observed differences. They were also studies in patients with systemic sclerosis, making the experiments difficult to fully compare. Lower concentrations of bosentan were investigated for VCAM-1 and ICAM-1 activation but they did not show any effect.

DIVI has been suggested to be facilitated when underlying inflammatory conditions are present[35,202]. To recapitulate this inflammatory state, cells were incubated with TNF-α with the drugs at the highest concentration (100 μM) for 24 hours. Of the drugs tested, bosentan showed an additive effect on ICAM-1 expression when incubated together with TNF-α for 24 hours. The other drugs showed no effect and were therefore not investigated further. These data suggest that underlying inflammatory conditions might enhance the effect of bosentan, by perhaps summation of signalling pathways, but this does not apply to the rest of DIVI-related drugs. Further experiments investigating the signalling pathways of bosentan may help shed a light on this.

The mechanism of the inflammatory effect observed with bosentan was investigated with respect to ET receptors antagonism or an off-target effect. To address this, BQ123, a selective ET_A antagonist and BQ788, a selective ET_B blocker, were used but they did not show a comparable effect in terms of ICAM-1 and VCAM-1 expression to bosentan, suggesting that this mechanism might be driven by an off-target effect. Using tools such as the Swiss Target Prediction from the Swiss Institute of Bioinformatics it is possible to predict the targets of small molecules. Apart from ET receptors, serotonin receptors and $P2Y_1$ receptors, activated by ADP[399], have been indicated to be the secondary target with the highest probability and could be investigated in the future in the same way used here.

In conclusion, in this chapter, potential markers of DIVI were investigated *in vitro*. A summary of the effects of DIVI-related drugs is shown in **Table 4.1**. It was identified that VWF release *in vitro* was induced by the same drugs that induced VWF release *ex vivo* in the vessel explants (**chapter 3**), implying that the effect of DIVI-inducing drugs on VWF release can be successfully recapitulated *in vitro*. However, rolipram that has been classified as DIVI-related drug failed to show an effect in the vessel explant and *in vitro* in these studies. Therefore, it is possible to conclude that VWF release cannot be the only biomarker assessed to assess DIVI.

DIVI is described as an event that induces vascular permeability, cell death and endothelial cell inflammation. However, these features were not observed ubiquitously in all drug

treatments. Perhaps this is due to the reductive approach of this *in vitro* work, which is a simple model and not necessarily indicative of an *in vivo* system. In the following chapter we shall increase the complexity of this *in vitro* assay to encompass physical and paracrine communications between SMC and EC. Furthermore, we will investigate whether endothelial cells respond differently to these drugs using a pharmacological agent to mimic shear stress, providing a more physiologically relevant model.

Effect	Time course (hours)	Bosentan	Fenoldopam	Minoxidil	Rolipram
VWF release	1	✓	✓	×	×
	24	✓✓✓	✓✓	✓✓	×
EC junctional breakage	1	×	✓	×	×
	24	×	×	✓✓	×
Cell death	1	×	×	×	×
	4	×	×	×	×
	24	×	✓ (on EC)	×	×
Inflammation	24				
ICAM-1		✓	×	×	×
VCAM-1		✓✓	✓	×	×

Table 4.1 Summary of the effects of DIVI-related drugs *in vitro*. Attributes of DIVI were investigated in this chapter: (1) VWF release from EC; (2) disruption to EC monolayer was measured by disruption of the intercellular junctions; (3) EC and SMC death; and (4) inflammation, shown as increased expression of ICAM-1 and VCAM-1 in EC. ✓✓✓= very significant effect ($p < 0.001$); ✓✓= very significant effect ($p < 0.01$); ✓= significant effect ($p < 0.05$); ×= no effect.

5. Exploring the effects of DIVI-related drugs in whole blood

5.1 Introduction

The objective of this chapter was to determine whether bosentan, fenoldopam mesylate, minoxidil sulfate salt, and rolipram directly activate blood cells. DIVI has been reported to increase inflammation, through upregulation of cell adhesion molecules, including endothelial ICAMs and VCAMs, and the release of secreted factors, for example, NO, cytokines, cellular enzymes, and acute phase proteins[2,34,124,400,401]. Inflammation promotes the adhesion of leukocytes, particularly neutrophils, macrophages and lymphocytes[2] to the vessel wall and into the perivascular space, which may contribute to the DIVI phenotype. It has been reported that leukocytes adhere to endothelial junctions, and erythrocytes and platelets extravasate into the perivascular space contributing to the progression of the lesions[76] (refer to **Introduction,** section **1.3**). However, it is not clear whether these events are a consequence of the drug action on EC, or as a result of an additional direct activation of leukocytes or platelets that contribute to the progression of the injury. In this chapter, flow cytometry was used to specifically characterise platelet and leukocyte activation. This simplistic monoculture experimental design will establish whether interaction directly between blood cells and drug is sufficient to induce cell activation or whether a more complex physiological system is required.

5.2 Methods

Blood was taken from healthy volunteers from the Department of Pharmacology in 75 µM PPACK, a synthetic peptide derivative that irreversibly and specifically inhibits thrombin-mediated platelet activation by binding with high affinity to the active site of thrombin and is therefore used as an anticoagulant. Blood was promptly stimulated with the drugs or positive controls at room temperature to avoid artefactual platelet activation. Following stimulation, blood was stained with the appropriate antibodies and then fix-lysed. This step allows lysis of only red blood cells (RBC) so that the other fixed blood components (platelets and leukocytes) can be easily visualised and quantified. Samples were then analysed by flow cytometry. Prior to the analysis, each channel was compensated to correct for fluorescence bleed-through. A detailed description of the protocol, compensation and antibodies concentrations are given

in **Methods**, section **2.2.3**. The drugs were used at three different concentrations: 1, 10 and 100 μM. Two time points were selected at 20 and 60 minutes as blood cell activation happens rapidly and within this timeframe. As positive controls, the leukocyte-specific agonist fMLP at 10 μM and the protease-activated receptor-1 (PAR-1) agonist TRAP-6 amide at 100 μM were used to induce leukocyte and platelet activation, respectively. It is accepted that some leukocytes (mainly monocytes and macrophages[402]) also express PAR-1, to a lesser extent compared to platelets[403], and will also be activated by TRAP-6 amide.

Platelet P-selectin expression (a marker of platelet granule secretion, which contributes to leukocyte recruitment via PSGL-1[404]) and integrin $\alpha_{IIb}\beta_3$ activation (a receptor for fibrinogen and VWF, monitored by PAC-1 antibody) were used to assess platelet activation. CD11b activation (monitored by CBRM1/5 antibody, which binds to the activated form of CD11b known as $\alpha_M\beta_2$, or Mac-1, involved in the migration of monocytes and neutrophils, as well as adhesion and phagocytosis[405,406]) served to assess neutrophil and monocyte activation. Refer to **Introduction**, section **1.6.5.3** for a detailed description of these molecules. Analysis was performed separately for each group of cells, using the median fluorescence intensity (MFI) as a measure for cell activation.

5.3 Results

5.3.1 TRAP-6 amide activates platelets, as shown by $\alpha_{IIb}\beta_3$ activation and increased P-selectin surface expression

Figure 5.1 shows the acquisition and gating of platelets. Forward scatter (representing cell size) versus side scatter (representing cell granularity) of fix-lysed whole blood are shown in A (unstimulated) and C (blood stimulated with TRAP-6 amide). In this process RBC have been lysed. Platelets were identified using forward scatter and CD41 expression, a general surface marker for platelets but not expressed on leukocytes (B). After activation with TRAP-6 amide, there is an increase in size of platelets (C, D) compared to unstimulated blood (A, B), which likely indicates platelet aggregation. Histograms (E and F) show activation with TRAP-6 amide, which causes a shift to the right, in comparison to an unstimulated control sample, as indicated by $\alpha_{IIb}\beta_3$ activation and P-selectin surface expression.

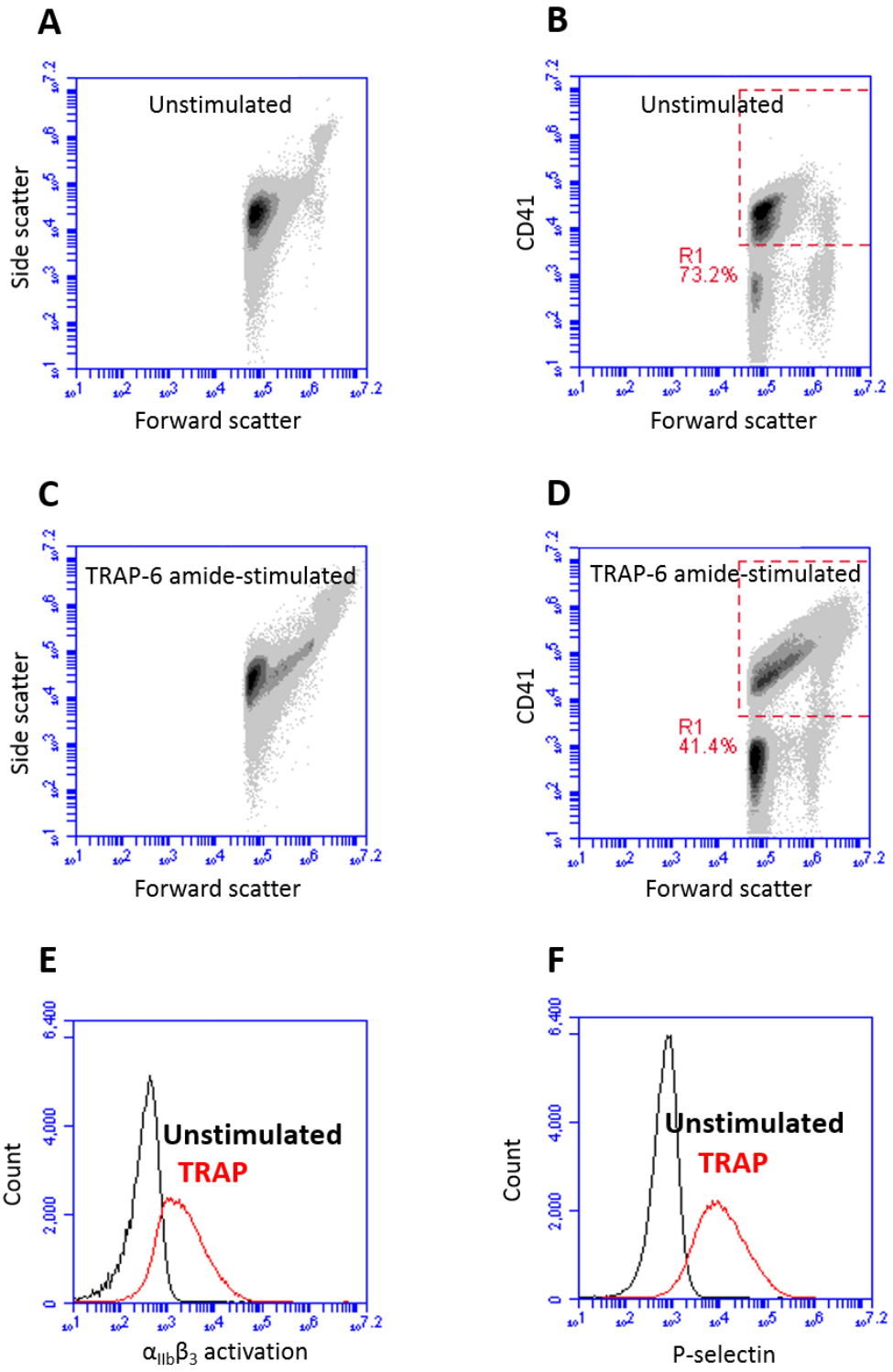

Figure 5.1 Acquisition of platelets with flow cytometer. Whole blood was collected from healthy volunteers and stimulated for 20 or 60 minutes with TRAP-6 amide 100 μM as positive control for platelet activation. A and C show forward scatter and side scatter plot of unstimulated (A) and TRAP-6 amide-stimulated (C) whole blood. Platelets were identified using forward scatter and CD41 expression (B and D). D shows platelets gated in a TRAP-6 amide-stimulated sample. E and F show histograms representing platelet activation, as indicated by $\alpha_{IIb}\beta_3$ activation and P-selectin surface expression in unstimulated (black) and stimulated (red) blood.

5.3.2 fMLP activates leukocytes, as indicated by CD11b activation

Figure 5.2 shows the acquisition and gating of leukocytes. Forward scatter versus side scatter of fix-lysed unstimulated whole blood are shown in A. Leukocytes were subdivided into monocytes (CD14+) and neutrophils (CD15+) (B). Histograms show CD11b activation of monocytes and neutrophils in unstimulated and fMLP-stimulated blood (C and D). Stimulation with fMLP causes a shift to the right which represents CD11b activation.

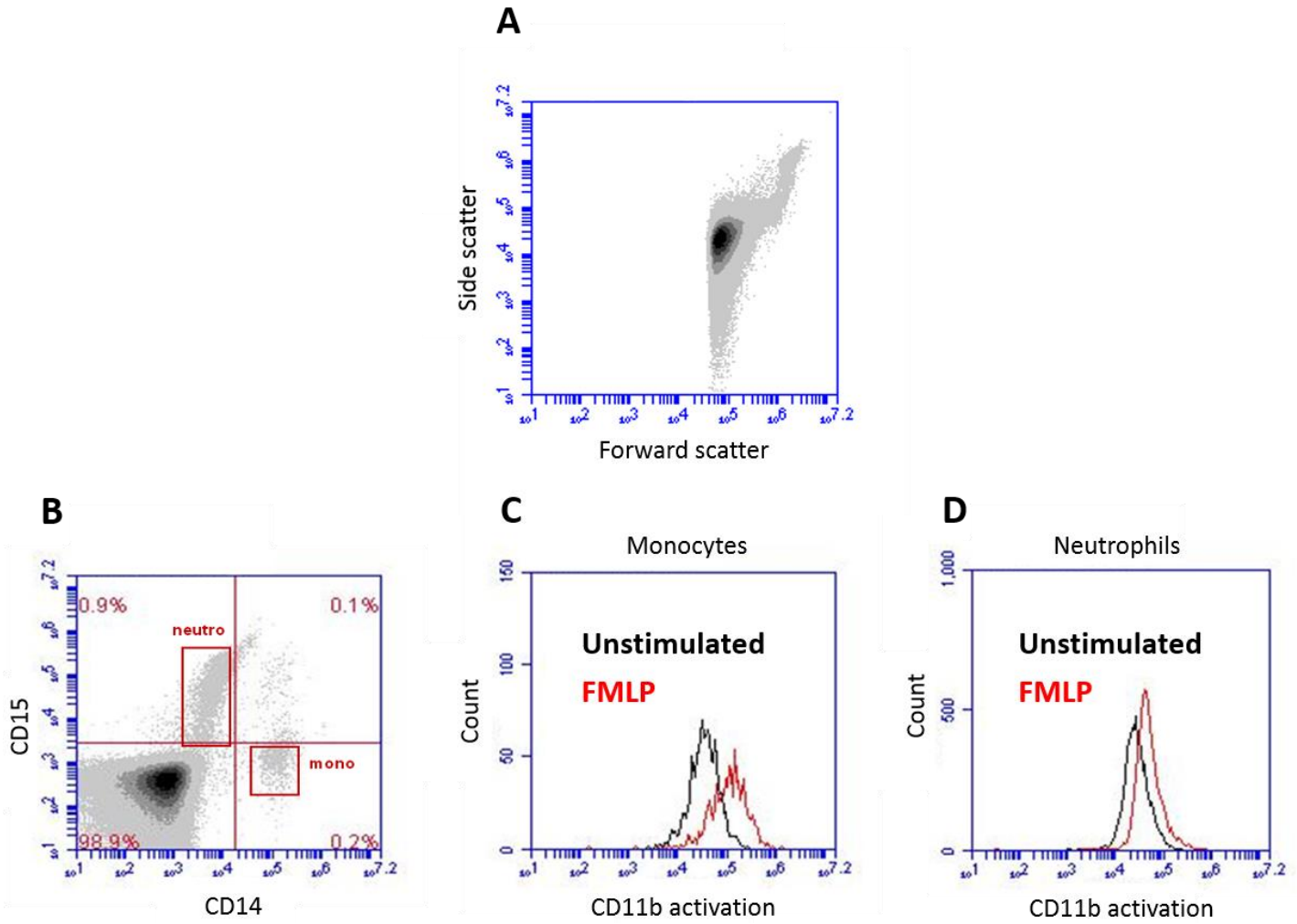

Figure 5.2 Acquisition and analysis of leukocytes with flow cytometer. Whole blood was collected from healthy volunteers and stimulated for 20 or 60 minutes with fMLP 10 μM as positive control for leukocyte activation. A represents forward and side scatter of a whole blood sample. Neutrophils and monocytes are identified by CD15 and CD14 expression, respectively (B). C and Dare histograms showing unstimulated (black) and fMLP-stimulated blood (red). Stimulation with fMLP causes an increase in CD11b activation in monocytes (C) and neutrophils (D).

5.3.3 DIVI drugs do not activate platelets, as shown by P-selectin expression and $\alpha_{IIb}\beta_3$ activation

TRAP-6 amide is used as positive control for platelet activation in whole blood[407]. TRAP-6 amide markedly increased platelet integrin $\alpha_{IIb}\beta_3$ activation, with a difference between means of 1003 ± 206 compared to unstimulated samples after 20 minutes (N=5, $p < 0.001$) and 477.4 ± 63.4 after 60 minutes stimulation (N=5, $p < 0.01$) (**Figure 5.3**). TRAP-6 amide markedly increased P-selectin expression (8465 ± 840) compared to unstimulated samples after 20 minutes (N=5, $p < 0.001$) and 6400 ± 974 after 60 minutes stimulation (N=5, $p < 0.001$). The effect is not significantly reduced after 60 minutes. fMLP did not induce platelet activation, as expected (**Figure 5.4**).

Whole blood was treated with four drugs, as described in **chapters 3** and **4**, at 1, 10, and 100 µM for 20 and 60 minutes. A total of 5 healthy volunteers were used in these experiments (N=5). Fenoldopam, bosentan, minoxidil and rolipram did not induce platelet activation, as no integrin $\alpha_{IIb}\beta_3$ activation or increase in P-selectin expression was observed at any concentration.

For example, for the integrin $\alpha_{IIb}\beta_3$ activation, fenoldopam 1, 10, 100 µM is comparable to the unstimulated mean at 20 minutes: unstimulated is 257.5 ± 9.190, TRAP-6 amide is 1261 ± 206.1, fMLP is 269.9 ± 9.341, fenoldopam 1 µM is 307.0 ± 45.19, 10 µM is 286.1 ± 30.49, and 100 µM is 318.2 ± 65.18 (N=5, ns) (**Figure 5.3**). At 60 minutes fenoldopam 1, 10 and 100 µM mean is comparable to controls. All other drugs produced a comparable effect.

For P-selectin at 20 minutes, unstimulated is 95.30 ± 12.36, TRAP-6 amide is 8560 ± 840.0, fMLP is 96.20 ± 29.18, fenoldopam 1 µM is 110.0 ± 28.96, 10 µM is 104.2 ± 23.25, and 100 µM is 109.9 ± 25.85 (N=5, ns). The other drugs produced a comparable effect. At 60 minutes fenoldopam 1, 10 and 100 µM mean is comparable to controls (**Figure 5.4**). Similar means were produced with the other drugs. These data show that no effect is produced with the drugs tested and that the experimental conditions were optimal as the positive control induced an effect.

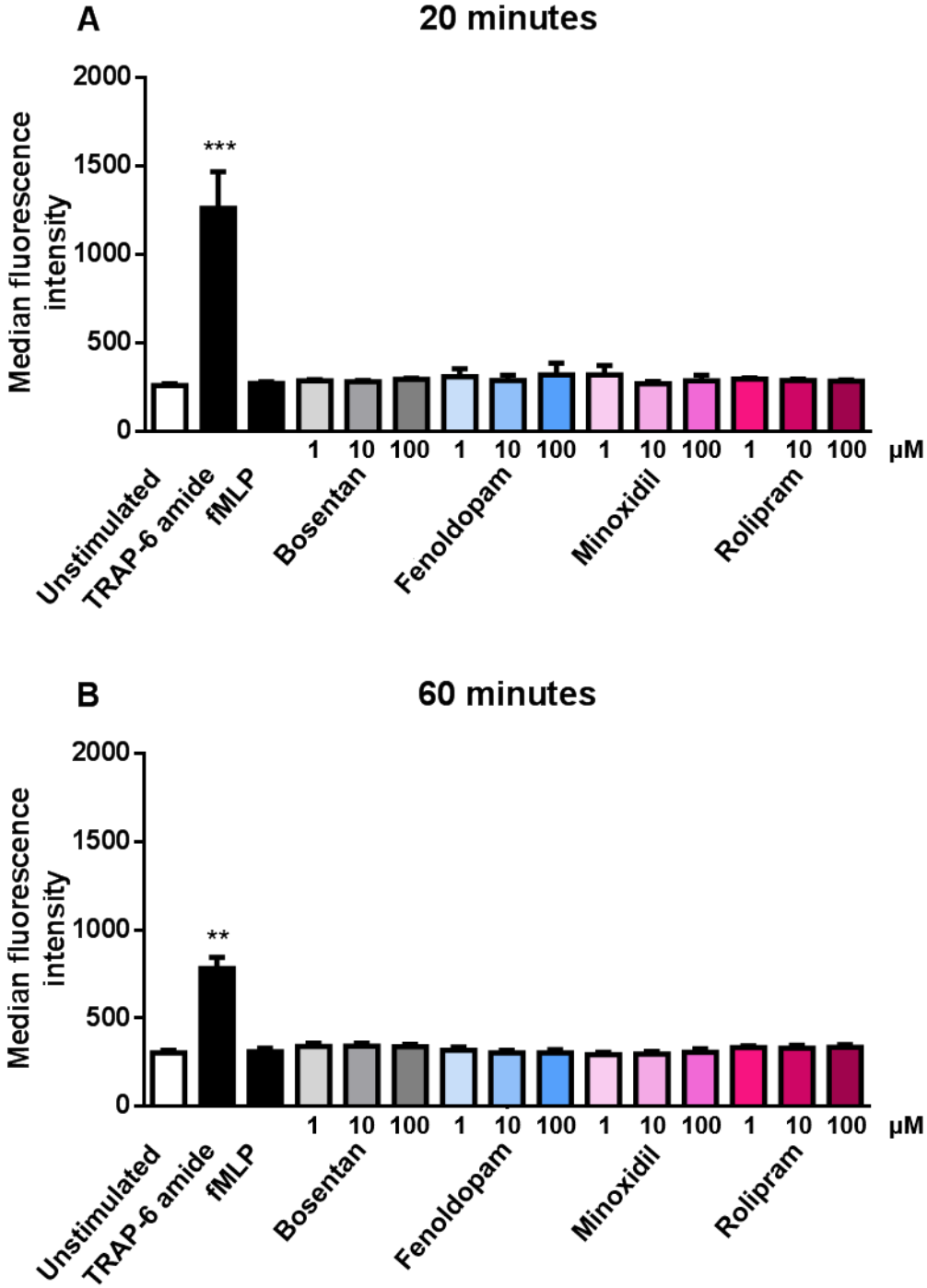

Figure 5.3 Effects of the drugs on platelet integrin $\alpha_{IIb}\beta_3$ activation. Whole blood was collected from healthy volunteers and stimulated for 20 or 60 minutes with TRAP-6 amide 100 µM, fMLP 10 µM, and DIVI-related drugs 1, 10, 100 µM. Data are expressed as median fluorescence intensity and represent mean ± SEM of 5 independent experiments, analysed by one-way ANOVA followed by Dunnett's post test. ***$p < 0.001$, **$p < 0.01$.

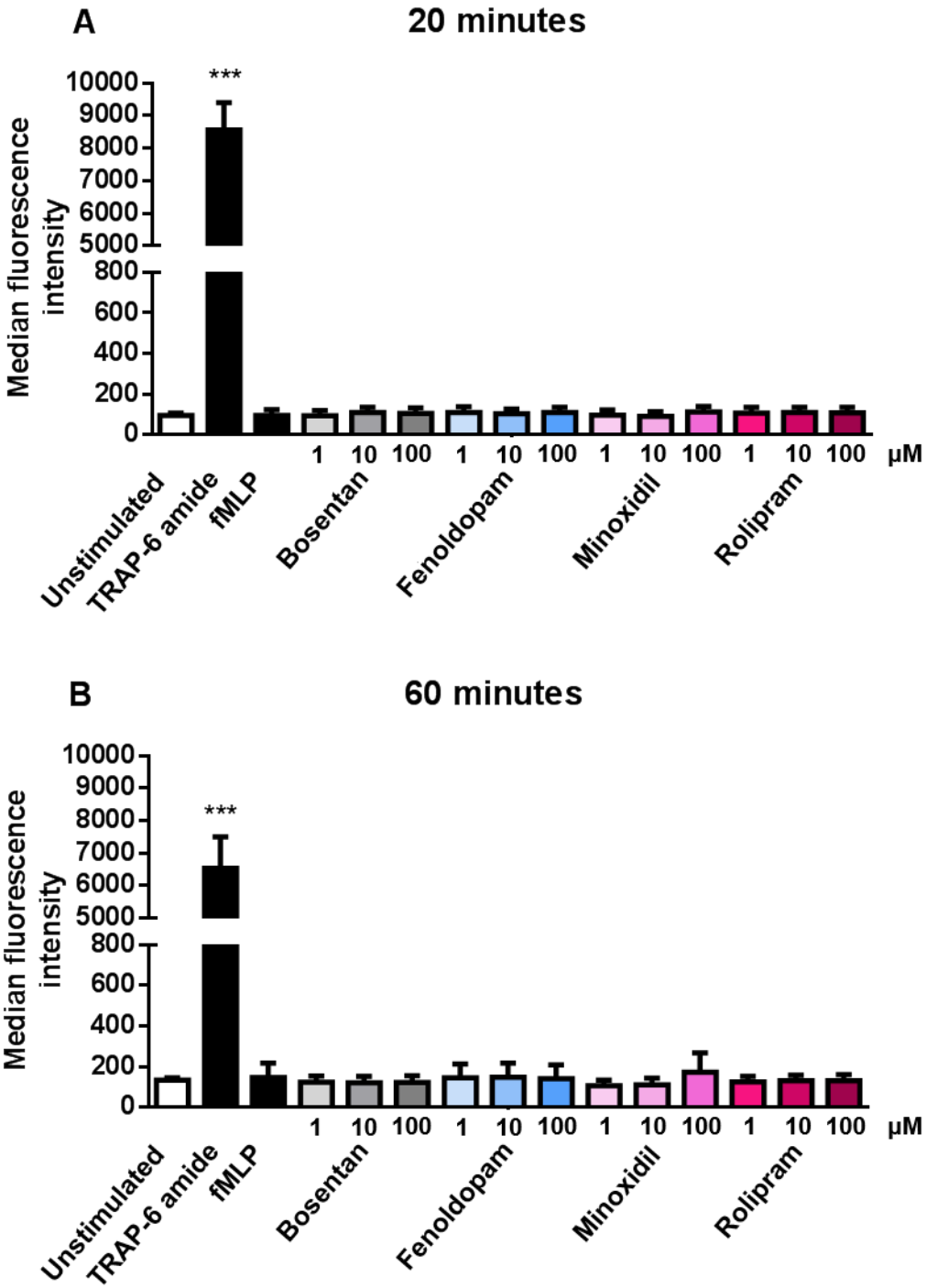

Figure 5.4 Effects of the drugs on platelet P-selectin expression. Whole blood was collected from healthy volunteers and stimulated for 20 or 60 minutes with TRAP-6 amide 100 µM, fMLP 10 µM, and DIVI-related drugs 1, 10, 100 µM. Data are expressed as median fluorescence intensity and represent mean ± SEM of 5 independent experiments, analysed by one-way ANOVA followed by Dunnett's post test. ***$p < 0.001$.

5.3.4 Minoxidil and bosentan activate leukocytes, as indicated by CD11b activation

fMLP was used as positive control because it specifically stimulates neutrophils and monocytes but not lymphocytes and platelets[408]. CD11b was selected as a marker for leukocyte activation. CD11b forms a complex with CD18 called membrane-activated complex 1 (Mac-1). Mac-1 binds ICAM-1 on EC[409] and is therefore important for leukocyte attachment to EC and transmigration (refer to **Introduction**, section **1.6.5.3**). TRAP-6 amide and fMLP induced a significant leukocyte activation at 20 and 60 minutes, as shown by increased CD11b expression (**Figure 5.5**). TRAP-6 amide increased CD11b activation after 20 minutes, with a difference between means compared to unstimulated samples of 18020 ± 2155 (N=5, $p < 0.01$), and 60 minutes, with a difference of 19790 ± 5395 (N=5, $p < 0.001$). fMLP significantly increased activation after 20 minutes, with a difference between means of 32300 ± 2810 compared to unstimulated samples (N=5, $p < 0.001$), and 60 minutes stimulation, with a difference of 42720 ± 4254 (N=5, $p < 0.001$) (**Figure 5.5**). As above, these data indicate that the experimental conditions were optimal as the positive control induced an effect.

Bosentan increased CD11b activation at 60 minutes stimulation at both 100 µM (mean of 52555 ± 6691 and at 10 µM (mean of 54239 ± 8406) (N=5, $p < 0.05$).

Minoxidil significantly activated leukocytes, as shown by increased CD11b activation at 20 and 60 minutes (**Figure 5.5**). There is a concentration-dependent effect, where 10 and 100 µM significantly affected leukocyte activation at 20 minutes (100 µM: mean of 34737 ± 2329) compared to unstimulated (20128 ± 1180) and 100 µM also at 60 minutes (46135 ± 2162) compared to unstimulated (33470 ± 2377) (N=5, $p < 0.01$).

Fenoldopam did not significantly activate leukocytes. However, there is a trend towards activation at 20 minutes only. Rolipram had no effect on leukocyte CD11b activation.

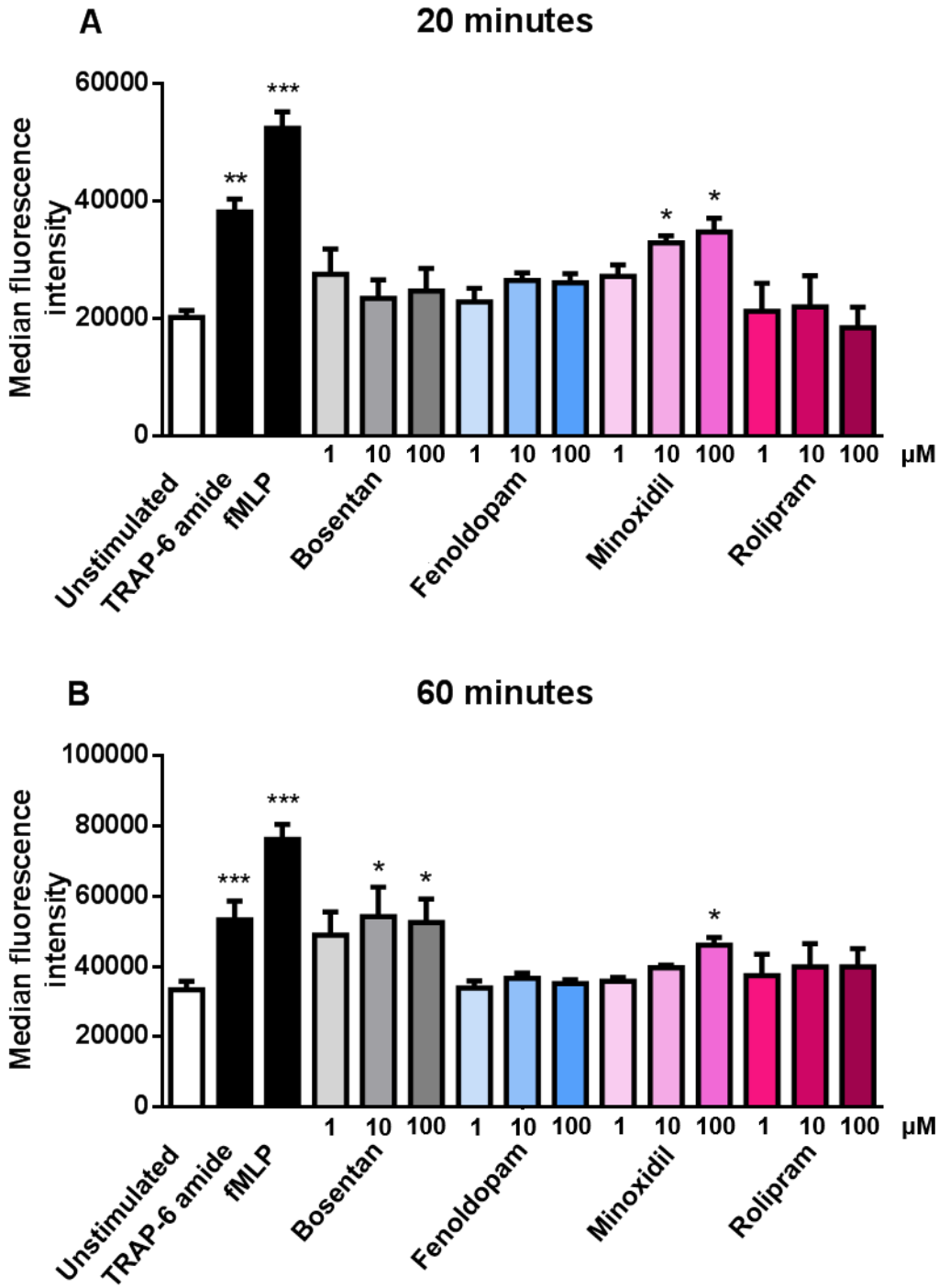

Figure 5.5 Effects of the drugs on leukocyte activation. Whole blood was collected from healthy volunteers and stimulated for 20 or 60 minutes with TRAP-6 amide 100 µM, fMLP 10 µM, and DIVI-related drugs 1, 10, 100 µM. Data are expressed as median fluorescence intensity and represent mean ± SEM of 5 independent experiments, analysed by one-way ANOVA followed by Dunnett's post test. *$p < 0.05$, **$p < 0.01$, ***$p < 0.001$.

5.3.4.1 Minoxidil and bosentan activate neutrophils and not monocytes

To identify whether the observed effect was in neutrophils, monocytes or both, the two groups of cells were separated during the analysis. In single cell populations, TRAP-6 amide increased CD11b expression in neutrophils, with a difference between means of 22580 ± 3030 after 20 minutes (N=5, $p < 0.01$) and 25600 ± 4646 after 60 minutes stimulation (N=5, $p < 0.001$). fMLP increased CD11b expression after 20 minutes with a difference between means of 35490 ± 3455 (N=5, $p < 0.001$), and after 60 minutes, with a difference of 46840 ± 6134 (N=5, $p < 0.001$) (**Figure 5.6**).

It was identified that the effect of bosentan and minoxidil on leukocyte activation was neutrophil driven, not monocytes (**Figures 5.6**). Bosentan (100 µM) activated neutrophils at 60 minutes (N=5, $p < 0.05$). Minoxidil activated neutrophils at 20 minutes at 10 µM (N=5, $p < 0.05$) and 100 µM (N=5, $p < 0.01$) compared to unstimulated. At 60 minutes stimulation, only 100 µM activated neutrophils (N=5, $p < 0.05$). The activation at both time points however is not of the same extent as fMLP nor TRAP-6 amide.

TRAP-6 amide increased CD11b expression in monocytes only at 60 minutes, with a difference between means compared to unstimulated samples of 29760 ± 8975 (N=5, $p < 0.05$). The effect was not significant at 20 minutes. fMLP increased CD11b expression in monocytes after 20 minutes with a difference between means of 17140 ± 2641 (N=5, $p < 0.05$), and after 60 minutes, with a difference of 45640 ± 12080 (N=5, $p < 0.001$) (**Figure 5.7**).

Bosentan and minoxidil did not activate monocytes, however there is a trend towards activation for minoxidil at the highest concentration (**Figure 5.7**).

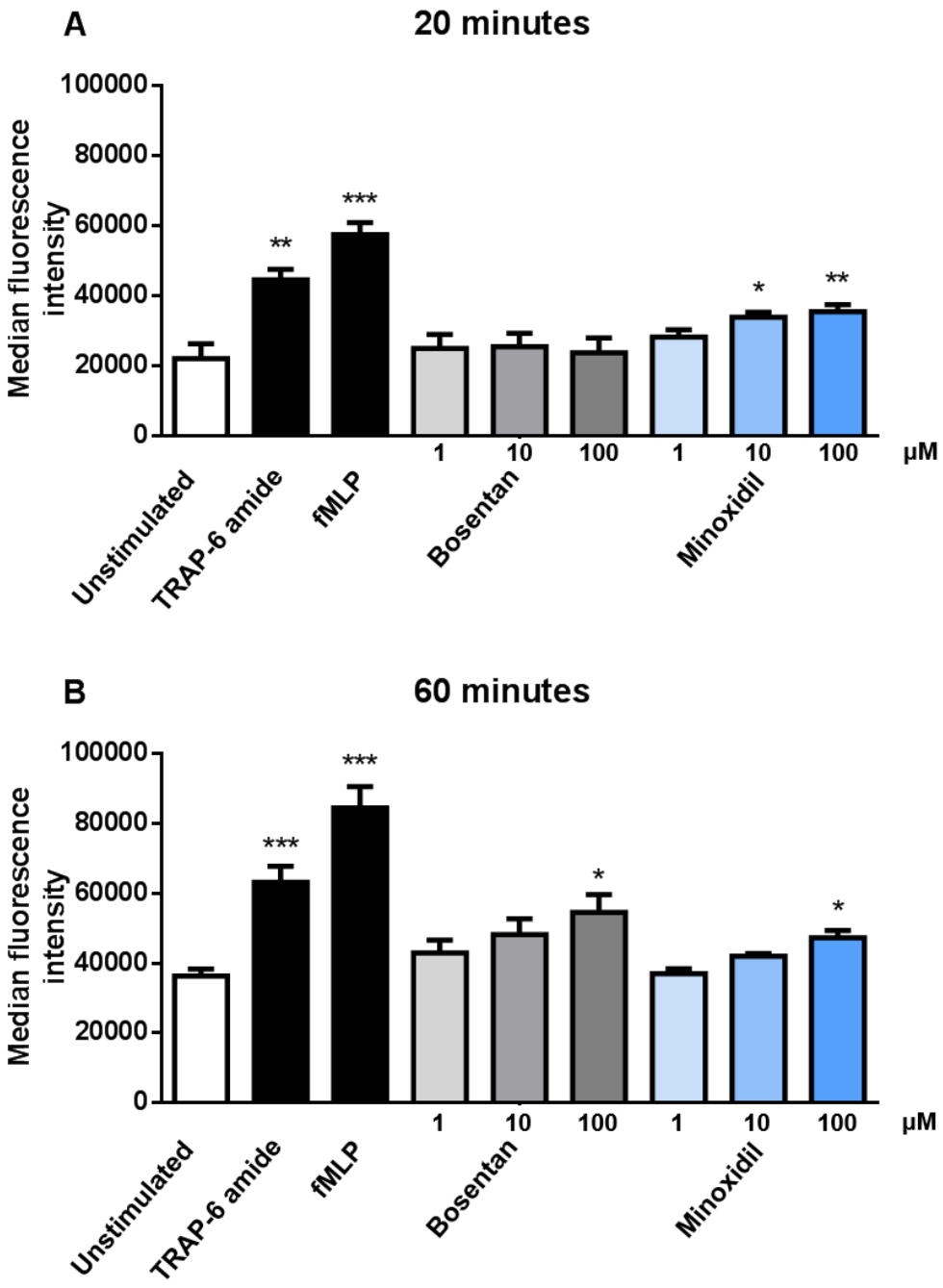

Figure 5.6 Effects of bosentan and minoxidil on neutrophils. Whole blood was collected from healthy volunteers and stimulated for 20 or 60 minutes with TRAP-6 amide 100 µM, fMLP 10 µM, bosentan and minoxidil 1, 10, 100 µM. Data are expressed as median fluorescence intensity and represent mean ± SEM of 5 independent experiments, analysed by one-way ANOVA followed by Dunnett's post test. *$p < 0.05$, **$p < 0.01$, ***$p < 0.001$.

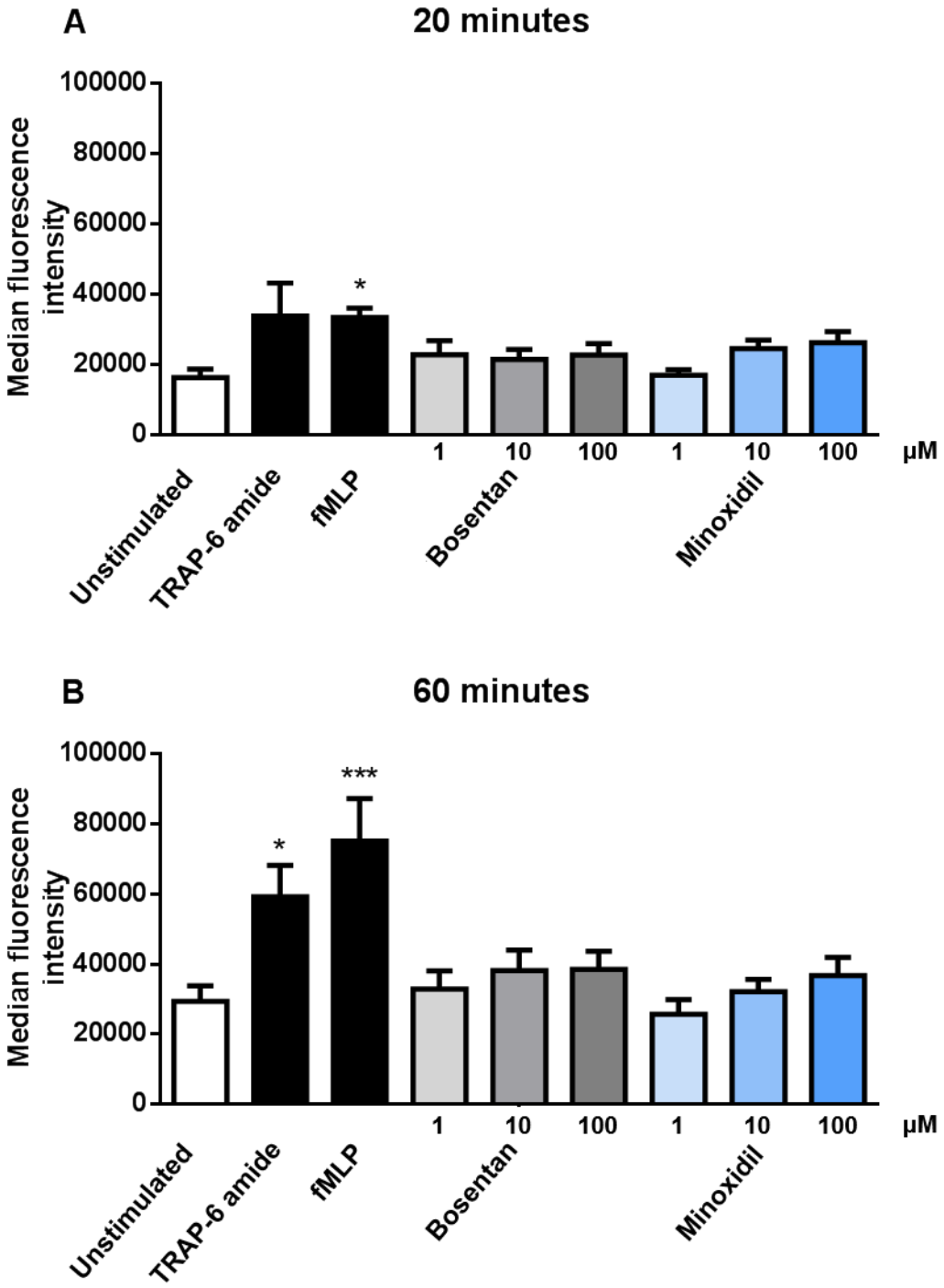

Figure 5.7 Effects of bosentan and minoxidil on monocytes. Whole blood was collected from healthy volunteers and stimulated for 20 or 60 minutes with TRAP-6 amide 100 μM, fMLP 10 μM, bosentan and minoxidil 1, 10, 100 μM. Data are expressed as median fluorescence intensity and represent mean ± SEM of 5 independent experiments, analysed by one-way ANOVA followed by Dunnett's post test. *$p < 0.05$, ***$p < 0.001$.

5.4 Discussion

The aim of these experiments was to determine whether DIVI-related drugs would activate discrete blood cell populations. There are several reports of increased levels of inflammatory factors in DIVI[2,124,400,401]. Secretion of these factors during the inflammatory response would promote the recruitment of inflammatory cells in the vascular wall and perivascular space which contribute to the DIVI phenotype. This evidence would provide data that would enable to select and develop the ideal *in vitro* model for DIVI.

The positive controls worked, as TRAP-6 amide and fMLP induced platelet and leukocyte activation, respectively. TRAP-6 amide markedly increased platelet P-selectin expression and integrin $\alpha_{IIb}\beta_3$ activation which was expected, since this has been previously reported by others via binding to PAR-1 and triggering downstream signalling causing α-granule fusion with the plasma membrane[410]. This effect is still significant but is reduced after 60 minutes. The activation of the integrin is dependent on intracellular Ca^{2+} release and transient fluctuations might cause this decrease.

A previous study reported that minoxidil prevented platelet aggregation in response to ADP and arachidonic acid and reduced the synthesis of prostaglandin E2 (PGE2) and thromboxane B2 (TxB2)[411]. These data showed that the effect on platelet aggregation was not associated with increased cyclic adenosine monophosphate synthesis. Therefore, it has been suggested that minoxidil functions primarily as a cyclooxygenase inhibitor in platelet metabolism. These data support these findings, in that, there was no observed platelet activation in the presence of drug treatment in these studies.

Bosentan acts as an antagonist to both ET_A and ET_B. However the action on platelets has yet to be established with some studies reporting an activation of platelets and others inhibition of platelets[412–414]. The data in this chapter showed that bosentan had no effect on platelet function.

A previous study used rolipram treatment to investigate platelet aggregation *ex vivo*[415]. Pre-treatment of anaesthetised rabbits with rolipram did not impair the platelet aggregation

induced by ADP, collagen, arachidonic acid or thrombin. Furthermore in vitro studies demonstrated that fenoldopam had no effect on platelets following an *in vitro* study on whole blood[416]. Therefore, the data presented in this study are in agreement with these findings as rolipram and fenoldopam had no observed effect on platelets in these experiments.

Leukocytes would be expected to be elevated in DIVI as there are reports of increased levels of inflammatory factors in DIVI[2,124,400,401] and leukocytes are recruited during the inflammatory response.TRAP-6 amide caused activation of neutrophils and monocytes, as indicated by increased CD11b activation. However, it is unclear whether this is a direct response to TRAP-6 amide, or an indirect effect via activation of platelets which in turn activate leukocytes. fMLP induced marked activation of neutrophils and monocytes but no platelet activation. The effect of the positive controls was observed at two time points (20 and 60 minutes). These time points were selected because DIVI studies reported that the effect of the drugs is generally acute and occurs within hours of administration[34]. In addition, 60 minutes is considered a maximal amount of time for platelet degranulation[417]. Additionally, by selecting this time point, assessment of the effect of drugs on protein synthesis in leukocytes could be undertaken. Furthermore, this time interval is sufficient to assess autocrine activation of cellular subsets. At 60 minutes, CD11b expression was greater than at 20 minutes both for neutrophils and monocytes. This might be related to leukocytes sticking to the plastic of the tubes, or because the experiment was run in non-sterile conditions[418].

Minoxidil had an effect on leukocyte activation at both 20 minutes and 60 minutes. Interestingly, two doses of minoxidil (10 and 100 µM) induced the effect at 20 minutes and only the high dose at 60 minutes, indicating that minoxidil acts rapidly. There are no previous reports of using minoxidil in whole blood experiments. By identifying the distinct cell populations, the effect of minoxidil was determined to be on neutrophils and not on monocytes. This possibly depends on the specific mechanism of action of the drug and perhaps a different distribution of K^+ channels on neutrophils and monocytes[419]. Minoxidil is a K^+ channel opener and a vasodilator, which opens K_{IR} (inward rectifier) 6.X ATP sensitive K^+ channels. The mechanism by which DIVI is induced is unclear. These data and that presented from previous chapters suggests that minoxidil acts on both EC and circulating blood cells.

However, it is unclear whether it is the leukocyte activation that leads to the development of the vascular damage or rather the leukocyte recruitment is a secondary event to the initial damage. A study reported an anti-inflammatory effect of minoxidil, as evidenced by significant downregulation of IL-1α gene expression in human keratinocytes[420]. A further study showed that minoxidil has been found to not cause T-cells to infiltrate into skin upon topical application for alopecia[421]. However, it is difficult to compare these findings with ours, as there are differences in the cell types used and in the route of administration.

Activation was observed following 60 minute treatment with bosentan. The effect, similarly to minoxidil, was on neutrophils and not monocytes. A previous *in vivo* study reported a reduction in leukocyte adhesion and inflammation in a mice in response to bosentan[422]. Another study observed anti-inflammatory effects of bosentan in mice[423]. The observed difference may be related to species-specificity (human vs. mice) or as a consequence of a lack of communication between blood cells and EC for example *in vitro*[424].

An *in vivo* study found that selective inhibition of PDE IV (the mechanism of action of rolipram) significantly reduced neutrophil recruitment at the site of vascular damage[425]. In addition, it has been reported in the same study that the effect of PDE IV inhibition on neutrophil adhesion was primarily mediated by downregulation of P-selectin-induced activation of Mac-1. It has also been observed[426] found that rolipram inhibited leukotriene B_4 (LTB_4) synthesis in neutrophils, produced from leukocytes in response to inflammation *in vitro*[427,428]. The compounds were inactive when LTB_4 was triggered by the calcium ionophore A23187, suggesting that the compounds induce a receptor-mediated event. The compounds also inhibited TNF-α synthesis in monocytes suggesting that rolipram has an anti-inflammatory effect. The data presented in this chapter recapitulate these findings, as no activation of neutrophils nor monocytes was observed. Fenoldopam did not activate nor inhibit leukocytes.

Additionally, other markers of leukocyte activation that have been reported in DIVI could have been investigated, for example IL-6, IL-8 and C-reactive protein[2]. Other biomarkers of inflammation include shedding of L-selectin, macrophage inflammatory protein-3β (MIP-3β), monokine induced by gamma interferon (MIG) and stromal cell-derived factor 1 (SDF1).

Longer time points could have been investigated, to monitor how the drugs affect protein processing, however storing whole blood for long periods of time is problematic as platelets and neutrophils get activated and degrade spontaneously with time *in vitro*[429]. One method would be to fractionate the blood or use white blood cells lines.

As reported previously, platelets and leukocytes may form platelet-leukocyte aggregates mainly via platelet-expressed P-selectin and its receptor PSGL-1, as well as via fibrinogen bridging between integrin $\alpha_{IIb}\beta_3$ and CD11b/CD18[430]. However, data on platelet-leukocyte aggregation were not collected but it is something that could be investigated in the future.

Collectively, these data suggest that DIVI-related drugs mostly affect vascular cells (EC and SMC) rather than circulating blood cells. One proposed mechanism is that the drug effect on blood cells is an indirect process following EC activation. EC would then induce the cascade of events whereby leukocytes are recruited to initiate the inflammatory response, and platelets activated triggering the typical DIVI phenotype. In the previous chapter (**chapter 4**, section **4.2.4.2**), it was found that fenoldopam and bosentan increase VCAM-1 expression on EC. This would likely lead to more leukocyte adhesion and possibly more transmigration.

To finitely address whether the drugs affect blood cells in an *ex vivo* setup, the next step would be to cannulate blood vessels and perfuse blood inside the lumen. The drug treatment could happen before cannulation (as a pre-treatment), or during perfusion. It is possible to choose whether to perfuse human blood or animal blood from the different species affected, and then image leukocyte adhesion to the vessel wall or monitor released inflammatory factors in the perfused blood collected from the outlet.

In conclusion, the effect of DIVI-related drugs was investigated in single EC and SMC (in **chapter 4**) and here on circulating blood cells (**Table 5.1**). The next chapter will assess whether a more physiological system, where EC and SMC interact together in a co-culture system, is important to elicit a DIVI phenotype.

Effect		Time course (minutes)	Bosentan	Fenoldopam	Minoxidil	Rolipram
Platelets	Integrin $\alpha_{IIb}\beta_3$ activation	20	×	×	×	×
		60	×	×	×	×
	P-selectin expression	20	×	×	×	×
		60	×	×	×	×
Leukocytes	Neutrophil CD11b activation	20	×	×	✓✓	×
		60	✓	×	✓	×
	Monocyte CD11b activation	20	×	×	×	×
		60	×	×	×	×

Table 5.1 Summary of the effects of DIVI-related drugs *in vitro* on blood cells. ✓✓= very significant effect ($p < 0.01$); ✓= significant effect ($p < 0.05$); ×= no effect.

6. Investigating DIVI in a co-culture system

6.1 Introduction

The aim of this chapter was to assess whether interaction between EC and SMC is required to give a DIVI-like phenotype *in vitro*. In the previous chapter, several biomarkers of DIVI were investigated in monocultured human EC and SMC. This chapter will address whether the presence of physical contact between EC and SMC increases the effect of the drugs, by culturing these two cell types in co-culture. Two hallmarks of DIVI, as described in **chapter 4** were also selected to be investigated in the co-culture system. These are (1) release of VWF and (2) cell death. VWF release was selected as in the experiments presented in the preceding **chapters 3 and 4** this was altered by all DIVI-related drugs except for rolipram. Therefore, these experiments aimed to assess whether rolipram induces VWF release from EC when SMC are present. Cell death was measured as SMC necrosis has been extensively described in DIVI. However, data shown in **chapter 4** demonstrated that SMC death was not induced by any of the drugs. It is possible that interaction between EC and SMC may alter the cellular response to drug treatment.

There are a number of published methods for co-culture of EC and SMC: (1) culture of SMC and EC on opposite sides of a porous membrane to facilitate cell separation but allow cells communication through paracrine signalling[431–434]; (2) culture of EC on the surface of collagen or fibrin gels that contain embedded SMC[435,436]; (3) culture of EC directly layered over SMC to replicate the geometry *in vivo* in arteries and veins[437,438]; (4) culture of EC and SMC side-by-side where EC and SMC are heterogeneously mixed together[439,440].

The system chosen in this chapter was to culture EC and SMC side-by-side. This was in order to have a rapid (in terms of both the optimisation and the experiment) way of assessing whether SMC are necessary for DIVI development. This co-culture system also allows physical communication and effective paracrine signalling by reducing diffusion distances of molecules between the cell types and is advantageous in the assessment of acute drug treatments.

6.2 Methods

6.2.1 Optimisation of co-culture cell density

The following protocol was used to optimise the seeding density for the co-culture system. HUVEC and HCASMC at passage 6 were grown in flasks separately until confluent. Cell trackers were used to visualise the two cell types. SMC were tracked with a deep red cell tracker, while EC were tracked in green with 5-chloromethylfluorescein diacetate. These tracking probes freely pass through the membrane into the cell and they are transformed into cell-impermeant reaction products after loading. The green tracker contains a chloromethyl group that reacts with thiol groups, utilizing a glutathione S-transferase–mediated reaction, and the deep red tracker contains a succinimidyl ester reactive group, which reacts with amine groups present on proteins. The unique excitation/emission spectra for the two trackers allowed clear visualisation of the two cell types (green excites at 492 and emits at 517 nm, deep red excites at 630 and emits at 650 nm). The key features of the cell trackers are they; 1) are passed to dividing cells but do not transfer to neighbouring cells upon contact, 2) are stable, nontoxic to cells at working concentrations and 3) are brightly fluorescent. The working concentration was within the range suggested by the manufacturer, such that it would produce a bright enough signal to be imaged but would not be toxic to cells.

Cells were washed with RPMI and incubated for 20 minutes with the trackers at 37 °C. Excess dye was removed, the cells seeded in ibidi slides for 24 hours, followed by fixation in 4 % v/v PFA before imaging (refer to **Methods**, section **2.2.2.2)** for a detailed description of the protocol).

Various seeding densities were tested to assess the number of cells per ibidi well and also the ratio between EC and SMC such that the EC would form a confluent monolayer and the cells would maintain viability (**Figure 6.1**). In this system, a proportion of SMC grew on top/bottom of the EC, but this did not appear to affect the results. Following optimisation 500,000 cells/ml were used in all subsequent experiments (**Figure 6.1**, B). At lower and higher densities the cells were either growing too sparsely or were too tightly packed, respectively (**Figure 6.1**, A and C). The optimal ratio between EC and SMC was found to be 2:1 because EC did not survive

when in a 1:1 ratio with SMC (**Figure 6.1**, D). This is may be due to differences in growth rates of EC and SMC and using the 2:1 ratio proved to be an efficient way to limit overgrowth of SMC. The cells were grown in their respective media until plated together, at such time EC media was used, it was observed that SMC could survive in EC media but not vice versa, potentially because the EC media contains VEGF and other growth factors that are essential for EC division and these were not present in SMC media.

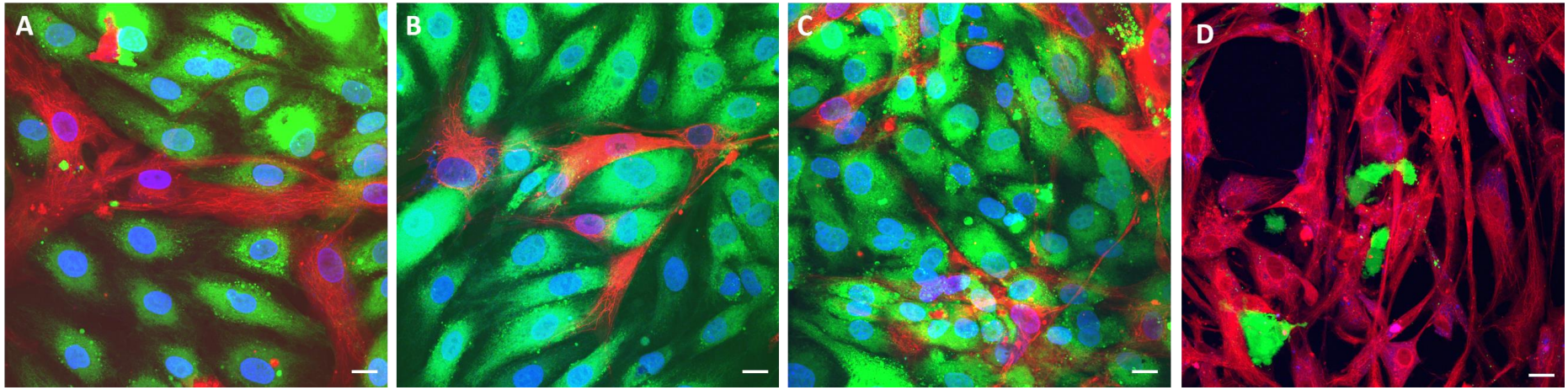

Figure 6.1 Optimisation of co-culture seeding density. EC and SMC were seeded at 375,000 (A), 500,000 (B), or 750,000 cells/ml (C). B represents the optimal density, where SMC occupy the spaces between EC. Cells were seeded at a ratio 2:1 (EC to SMC) because when plated in equal ratio the EC survival was reduced (D). Images are representative confocal pictures taken with a 63x objective. Scale bars represent 20 µm.

6.3 Results

6.3.1 Characterisation of EC and SMC in co-culture

The first step was to assess whether EC morphology would be affected by co-culture with SMC (**Figure 6.2**). This was because previous reports have suggested that EC cultured with SMC changed the EC from the normal polygonal morphology to an elongated shape[435].

In order to assess this, cells were analysed in morphology using parameters related to the cell shapes. EC and SMC were evaluated according to the following descriptors in ImageJ: i) area, in square pixels; and ii) circularity, calculated as 4π*area/perimeter^2 where a value of 1.0 indicates a perfect circle and 0.0 an elongated shape. Analysis was conducted on the brightfield images in ImageJ. The field of view was randomly selected to avoid bias, cell shape was manually defined with the freehand tool and the area and circularity were calculated.

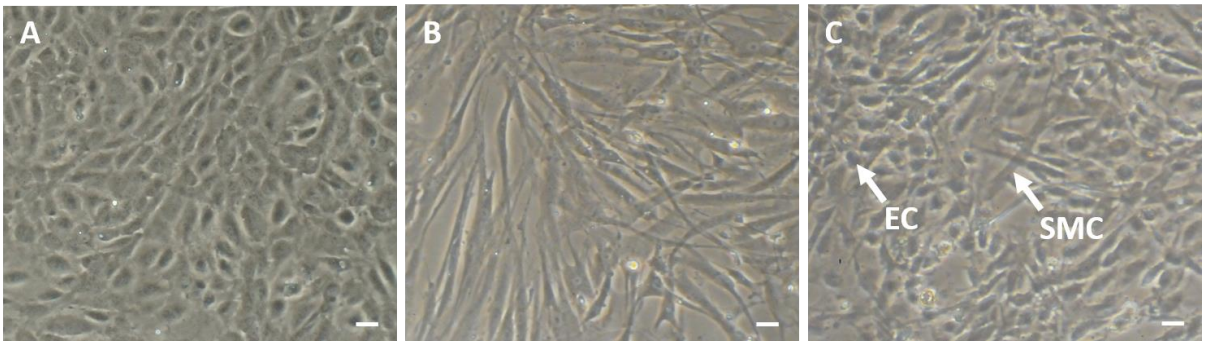

Figure 6.2 Bright field image of monocultured EC and SMC and cells in co-culture. Monocultured HUVEC and HCASMC are shown in A and B, respectively; C shows cells in co-culture. Cultured cells were at passage 6. Arrows point at either EC or SMC in co-culture. Scale bars represent 50 µM. Images were taken with a bright field microscope. 10x.

Monocultured EC did not differ from EC in co-culture in terms of area (difference between means of 0.1 ± 4.1, ns) or circularity (0.1 ± 0.1, ns). SMC also did not differ in co-culture, neither in area nor in circularity, suggesting that the method provided in this chapter does not alter EC-SMC morphology (**Figure 6.3**).

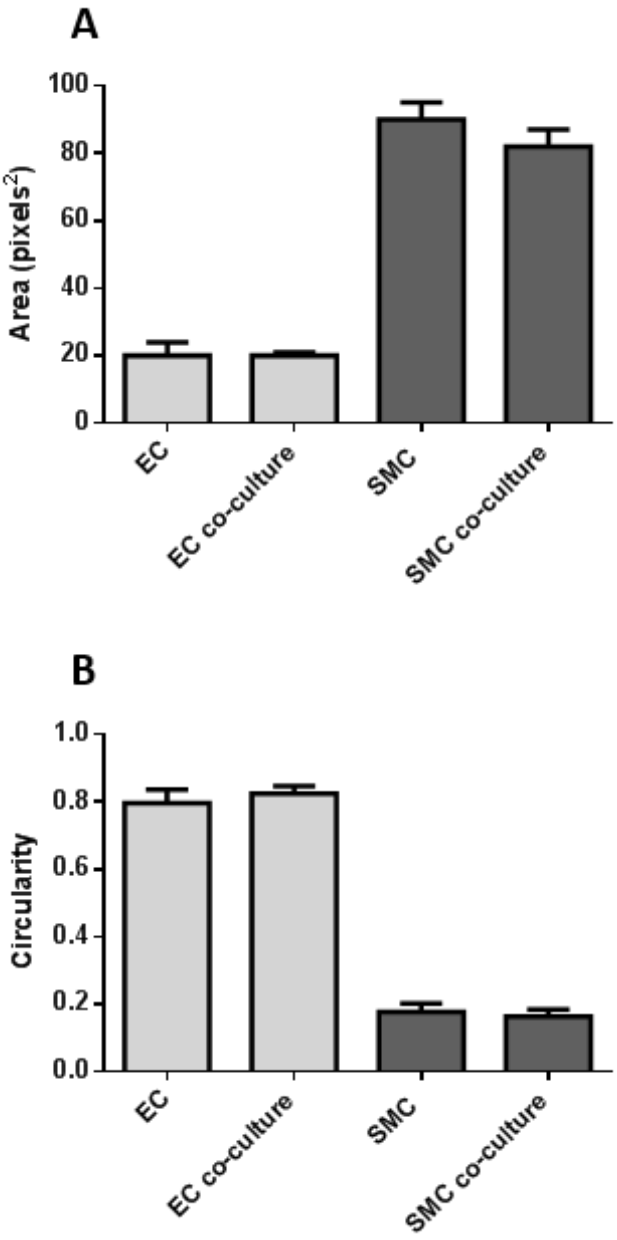

Figure 6.3 Shape descriptors in a co-culture of EC and SMC. The area (A) and circularity (B) of the cells. Data represent mean ± SEM of 4 independent experiments, analysed by one-way ANOVA followed by Dunnett's post test.

6.3.2 VWF release with DIVI-related drugs in co-culture

VWF release was assessed with the same drugs tested in the rat vessel explant (**chapter 3**) and in monocultured HUVEC (**chapter 4**): bosentan, fenoldopam mesylate, minoxidil sulfate and rolipram, at the highest concentration (100 µM). The same time points were chosen: 1 hour to assess a short-term effect and 24 hours, to reflect the time point used in the *ex vivo* vessel experiment. Thrombin 1 U/ml was used as a positive control in the experiments to enable the comparison of VWF release *ex vivo* and *in vitro* in monocultured HUVEC. Vehicle control cells were treated with 0.1 % v/v DMSO. Prior to treatment, HCASMC were tracked with the deep red cell tracker, seeded together with HUVEC and grown for 24 hours. HUVEC were not tracked due to a lack of sufficient fluorescence channels in the confocal microscope. VWF is uniquely produced by EC and not SMC[441] so tracking EC was not essential. Following treatment, cells were fixed with 4 % v/v PFA for 10 minutes, permeabilised for 5 minutes with 0.1 % v/v Triton X-100 and a specific antibody was used to detect VWF (refer to **Methods, Table 2.3**) for antibody concentrations. The permeabilisation step was necessary to visualise VWF intracellularly, as in **chapter 4**. The deep red cell tracker allows cells to be permeabilised but still retain the tracker intracellularly, as the succinimidyl ester reactive group that it contains reacts with amine groups present on intracellular proteins, making the dye persist post fixation and permeabilisation. In addition, to avoid bleed-through and ensure the deep red tracker would only stain SMC, the excess stain was removed by repeated wash steps.

DAPI was used to label all nuclei from both EC and SMC. Cells were imaged with a confocal microscope using a 63x objective. Six images were taken for each treatment per repeat, four experiments were conducted in total. Images were taken as a z-stack of 2 µm/slice to make sure all EC and SMC were all in focus and counted in the analysis.

VWF release was analysed in EC cultured with SMC using the same parameters described in **chapter 4**: (1) the % VWF-positive cells; and (2) the particle size of WPB. As in **chapter 4**, the MFI was analysed (data not shown), but it did not prove to be representative of VWF release. For example, the MFI in thrombin-stimulated cells is expected to be low because VWF has been released, but sometimes this was detected and comparable to DMSO treated cells,

either because of fluorescent non-specific agglomerates or because an automated system cannot differentiate between intra or extracellular VWF.

In order to count the % VWF-positive cells, an additional step was conducted compared to **chapter 4** to account for the presence of SMC. It was assessed that SMC did not express VWF (**Figure 6.4**). Images from the different stacks were merged together as a maximum projection and separated into the different channels. Images in the green channel (VWF) were thresholded to remove background noise. SMC in the red channel were identified using the freehand tool in ImageJ and the contour was added into the region of interest manager. The selection was then opened in the correspondent image in the green channel. SMC were counted as VWF-positive if they showed more than 3 green spots/cell. It was found that SMC only expressed a very low % of VWF (around 2-3 %) and there was no difference across treatments. This was expected since VWF is uniquely produced by EC and platelets[348].

To assess VWF release from EC, the total nuclei (EC and SMC) were automatically counted. This was carried out by thresholding the images to remove the background and allow particles greater than 15 μm^2 to be counted as nuclei. The three channels were merged back together, SMC nuclei were counted manually and subtracted from the total nuclei to calculate only EC nuclei. EC were determined VWF-positive if they showed more than 3 spots/cell in the green channel. This was conducted as described previously, after thresholding to remove background noise.

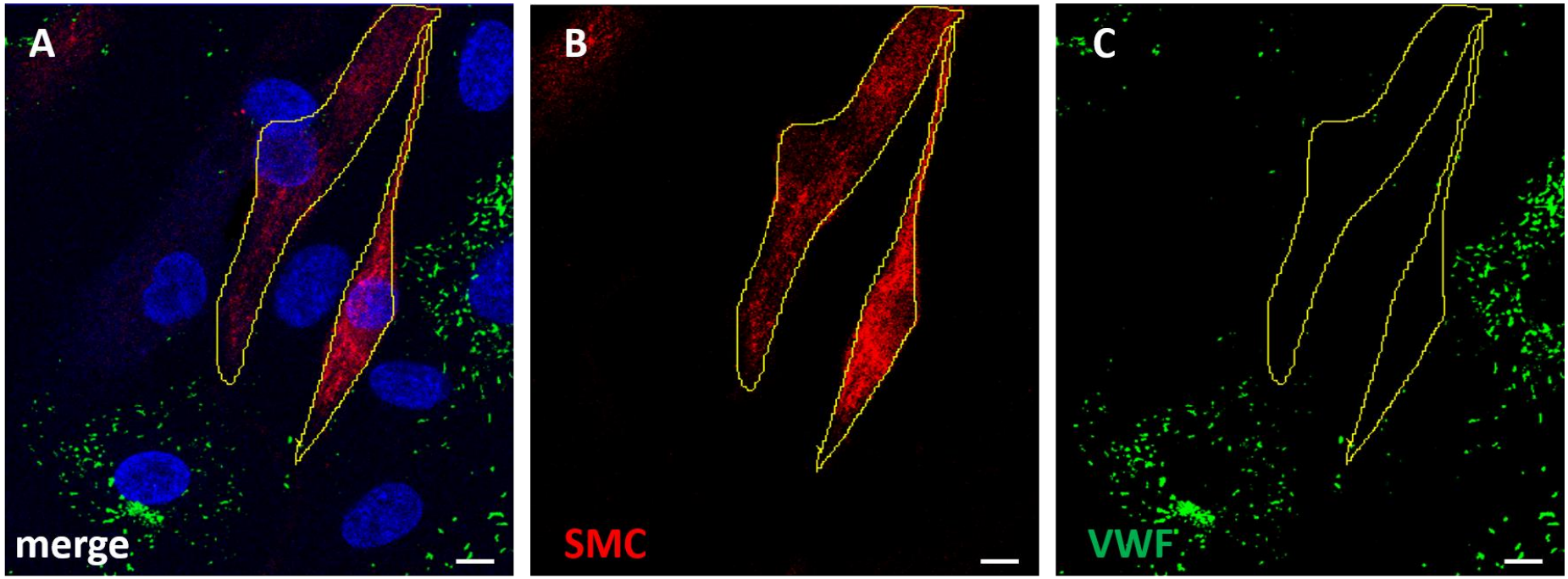

Figure 6.4 Assessment of VWF expression in SMC. HCASMC were tracked with a deep red cell tracker and seeded together with HUVEC, grown for 24 hours and then VWF (green) release at 1 and 24 hours was detected with a specific antibody. Six images of random field of view were taken for each treatment per repeat, four experiments were conducted in total. Images are representative confocal maximum projections pictures taken with a 63x objective. Scale bars represent 10 µm.

6.3.2.1 DIVI-related drugs induce VWF release in co-culture after 1 hour and 24 hours

As observed in **chapter 4**, in these experiments the DMSO treated control did not demonstrate 100 % VWF-positive cells, but rather around 86 % at 1 hour and 88 % at 24 hours. This was expected since unstimulated cells release VWF through a constitutive pathway[363]. In addition, it may have also been due to the use of pooled donor cells, which show some variability in phenotype and growth characteristics, so also VWF expression might be different[442]. In addition, the prolonged treatment up to 24 hours did not affect this.

Thrombin (1 U/ml) was used as a positive control to match VWF release *ex vivo* (refer to **chapter 3**). Thrombin induced significant release of VWF compared to DMSO control after 1 hour (% VWF-positive cells was reduced to 54.4 ± 5.2, N=4, $p < 0.01$) and after 24 hours (% VWF-positive cells was reduced to 51.7 ± 3.9, N=4, $p < 0.001$), (**Figure 6.5, 6.6, 6.7**). The mean percentage of cells that were positive for VWF following thrombin stimulation at 1 and 24 hours were not significantly different (54.4 ± 5.2 vs 51.7 ± 3.9) suggesting that the release is at constant rate or that VWF released at 1 hour does not get resynthesized and released.

Bosentan induced significant VWF release after 1 hour (% VWF-positive cells was reduced to 68.3 ± 3.8, $p < 0.05$) and 24 hours (% VWF-positive cells was reduced to 62.8 ± 3.7, $p < 0.01$). Similarly, fenoldopam caused significant VWF release at both time points (% VWF-positive cells was reduced to 57.9 ± 5.1 at 1 hour $p < 0.01$, and to 54.2 ± 3.2 at 24 hours, $p < 0.001$). A similar effect with these drugs was found in monocultured HUVEC in **chapter 4**. The effect with minoxidil was not statistically significant at 1 hour. However, at 24 hours minoxidil treated cells significantly released VWF (% VWF-positive cells was reduced to of 54.5 ± 8.8, $p < 0.001$). These data correlate with the minoxidil effect observed in **chapter 4**, whereby monocultured HUVEC treated with minoxidil exhibited significant release at 24 hours. Rolipram did not cause VWF release in these experiments. All represent N=4.

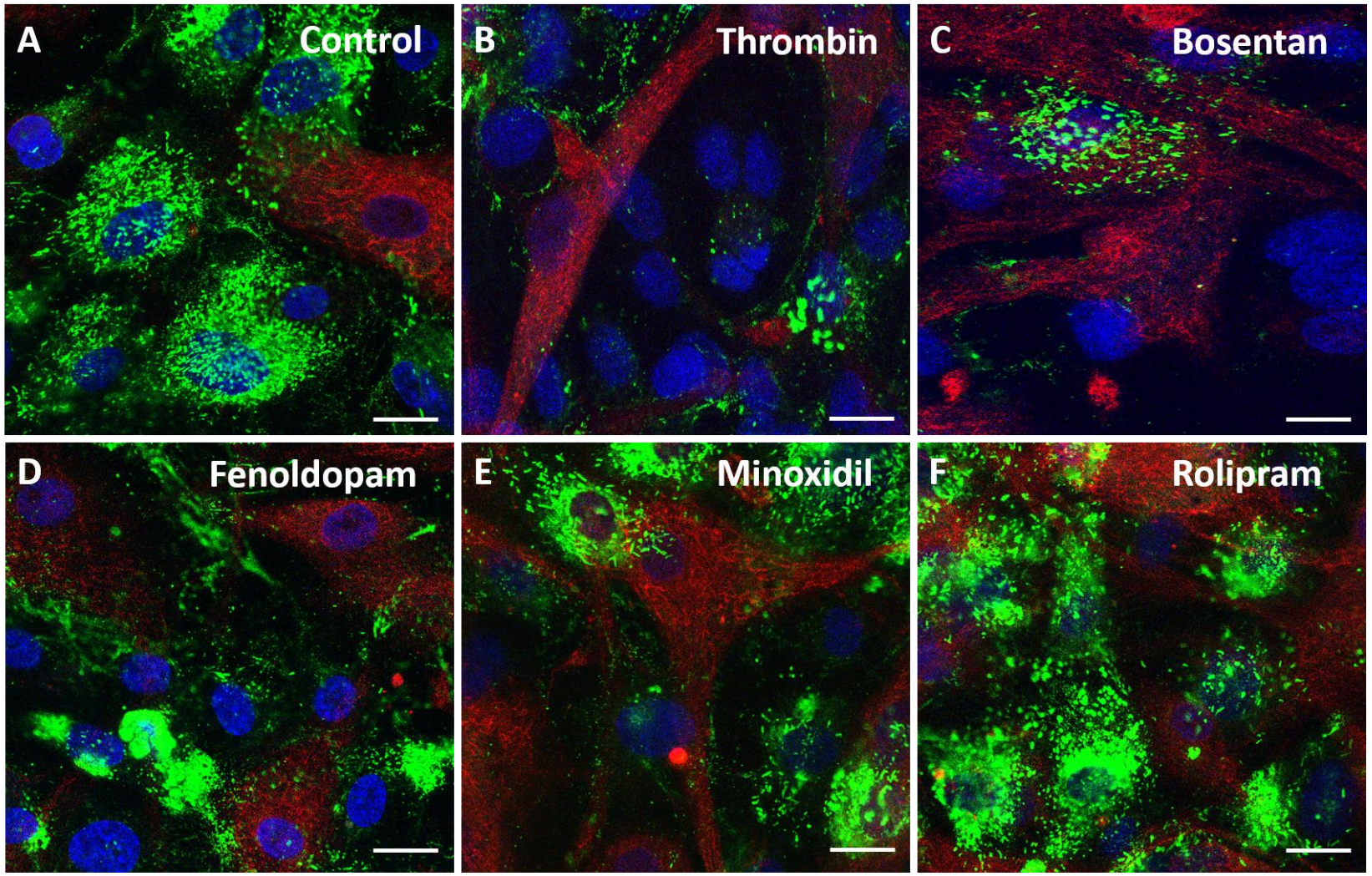

Figure 6.5 Representative confocal images of VWF release in EC and SMC co-culture at 1 hour. HCASMC were labelled with a deep red cell tracker and seeded together with HUVEC, grown for 24 hours and then VWF (green) release was detected with a specific antibody after treatment with DIVI-related drugs at 1 hour. Six images of random field of view were taken for each treatment per repeat, four experiments were conducted in total. Images are maximum projections, taken with a 63x objective. Scale bars represent 20 μm.

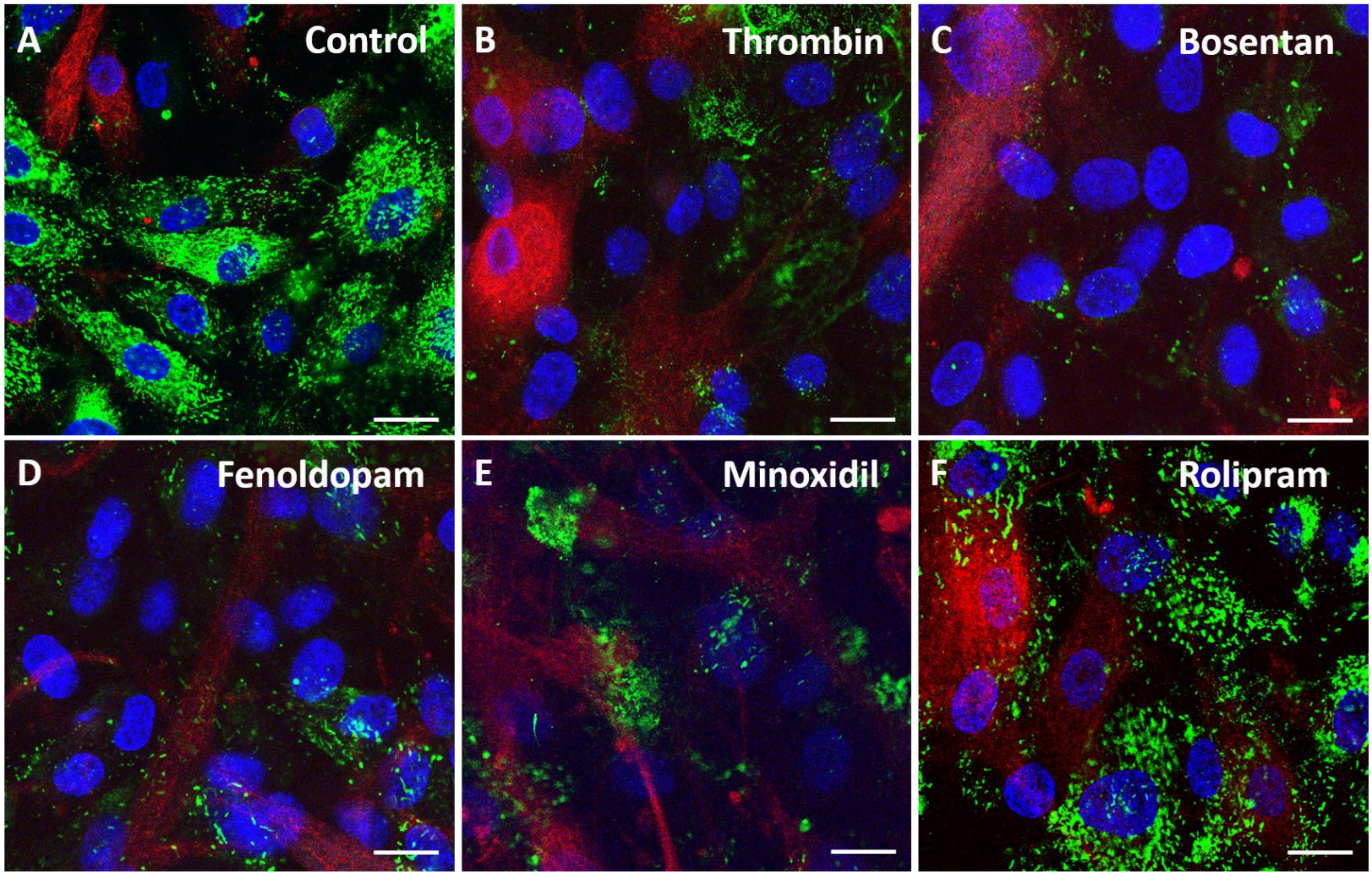

Figure 6.6 Representative confocal pictures of VWF release in EC and SMC co-culture at 24 hours. HCASMC were labelled with a deep red cell tracker and seeded together with HUVEC, grown for 24 hours and then VWF (green) release was detected with a specific antibody after treatment with DIVI-related drugs at 24 hours. Six images of random field of view were taken for each treatment per repeat, four experiments were conducted in total. Images are maximum projections, taken with a 63x objective. Scale bars represent 20 μm.

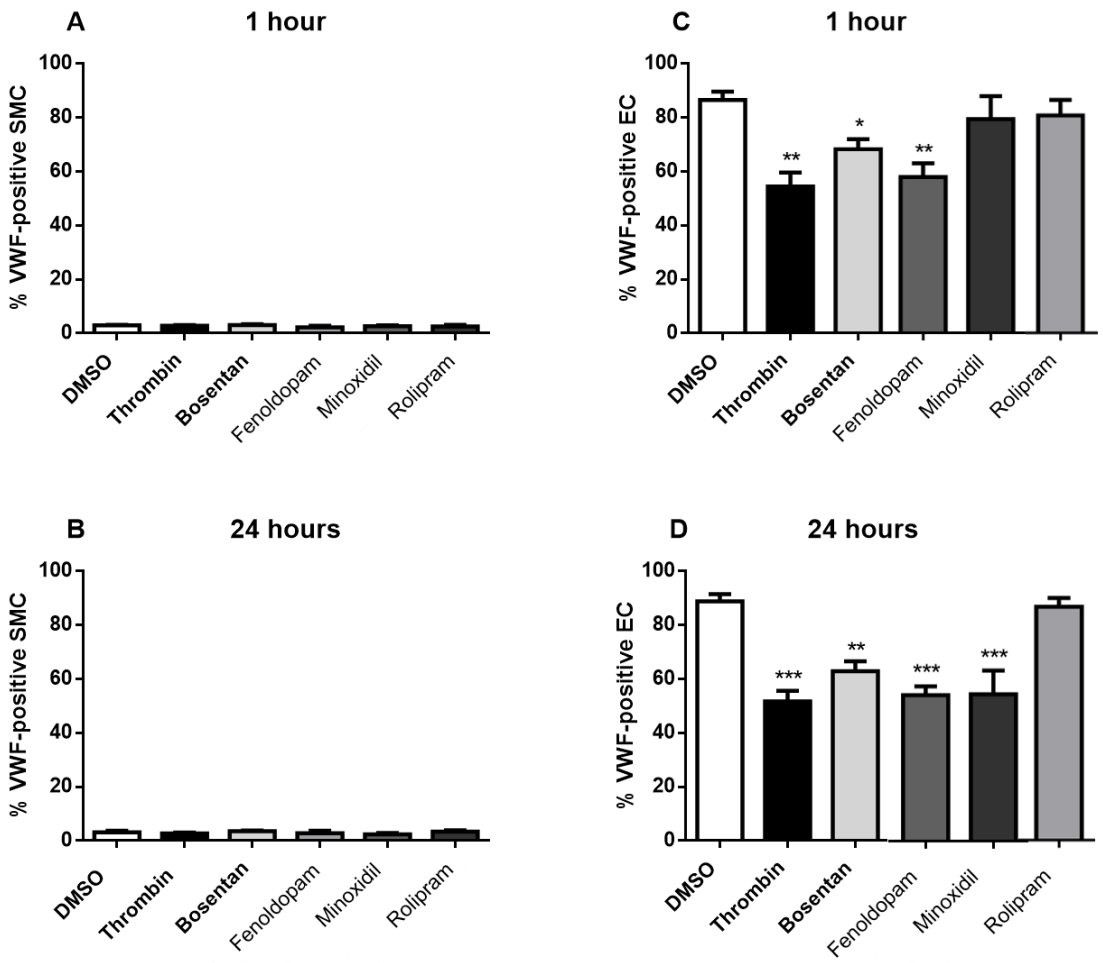

Figure 6.7 VWF release from SMC and EC in co-culture after 1 and 24 hours treatment with DIVI drugs. VWF release from SMC (A and B), and EC (C and D). HCASMC were labelled with a deep red cell tracker and seeded with HUVEC, grown for 24 hours and then VWF release was detected with a specific antibody after treatment with DIVI-related drugs. Data are expressed as % of VWF-positive SMC or EC as a proportion of total cells in the field of view, and represent mean ± SEM of 4 independent experiments, analysed by one-way ANOVA followed by Dunnett's post test. *$p < 0.05$, **$p < 0.01$, ***$p < 0.001$.

These data demonstrate that VWF release from EC in co-culture is similar to the levels observed in monocultured HUVEC, whereby the same drugs induced VWF release at 1 and 24 hours. Therefore co-culturing EC with SMC did not influence VWF release.

6.3.2.2 The particle size of WPB does not differ across treatments

To analyse the particle size of WPB, which contain VWF, images were thresholded to remove the background noise, made binary and then the total area of particles bigger than 0.3 μm^2 was automatically counted. With this method, all particles are counted, including the ones outside the cells and therefore this approach does not discriminate between whether VWF has been released from the cell. The particle size of WPB did not differ across treatments at 1 hour or 24 hours (**Figure 6.8**, A and B), indicating that WPB do not fuse together at the plasma membrane. The particle size is similar to the observations made in monoculture (see **chapter 4**).

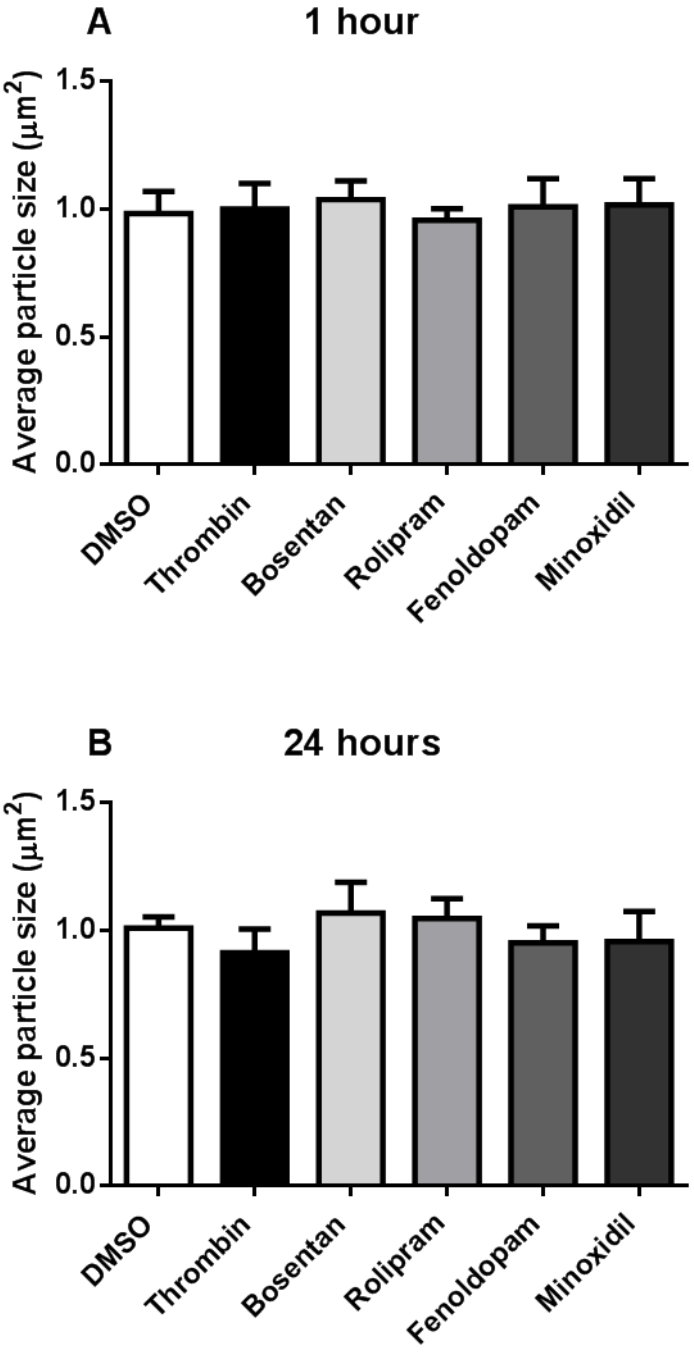

Figure 6.8 Average particle size of WPB at 1 and 24 hours. Data are expressed as area of WPB particles in the field of view (six random fields of view per treatment), and represent mean ± SEM of 4 independent experiments, analysed by one-way ANOVA followed by Dunnett's post test.

6.3.3 Investigating cell death by flow cytometry

Subsequent experiments focussed on assessing DIVI in the context of cell death. Cell death in co-culture was assessed by flow cytometry. The ATP luminescent assay used in **chapter 4** would be unable to discriminate between changes in EC and SMC populations. Therefore, propidium iodide (PI) was used to assess cell death. PI is a membrane impermeant dye that is excluded from viable cells, that have intact membranes, and was therefore used to stain cells with damaged and permeable membranes. PI binds to double stranded DNA by intercalating between base pairs. PI is excited at 488 nm and emits at a maximum wavelength of 617 nm, these spectral characteristics mean that PI can be used in combination with other fluorochromes excited at 488 nm such as FITC. As a result, in these experiments EC were stained with CD31-FITC. As the size and granularity of cells change as cells die (live cells are larger and less granular) these will appear higher in forward and lower in side scatter and will have low PI fluorescence[443].

HCASMC were labelled with a deep red dye, and then HUVEC and HCASMC were seeded in a 2:1 mixture in 24 well plates, incubated for 24 hours and subsequently treated with the DIVI-related drugs used previously at 100 µM for 24 hours. Monocultured HUVEC and monocultured HCASMC were also seeded in parallel to serve as a control. Cisplatin (50 µM) was used as a positive control for cell death in both EC and SMC. Following treatment, cells were washed with EDTA and incubated with accutase for cell detachment. Accutase was neutralised with M199 containing 20 % v/v FBS, cells were harvested, centrifuged and and stained with PI 10 µg/ml. HUVEC were also stained with CD31. Cells were analysed by flow cytometry.

6.3.3.1 Gating strategy

Cells were gated using forward and side scatter using a log scale to gate out cellular debris (**Figure 6.9**). SMC were labelled with the red cell tracker, and EC were stained with the specific marker, CD31[365]. PI was used to assess cell death. An IgG isotype control was used to remove the non-specific staining from the gating. To prevent bleed-through of the red cell tracker in the other cell population, the samples were washed thoroughly.

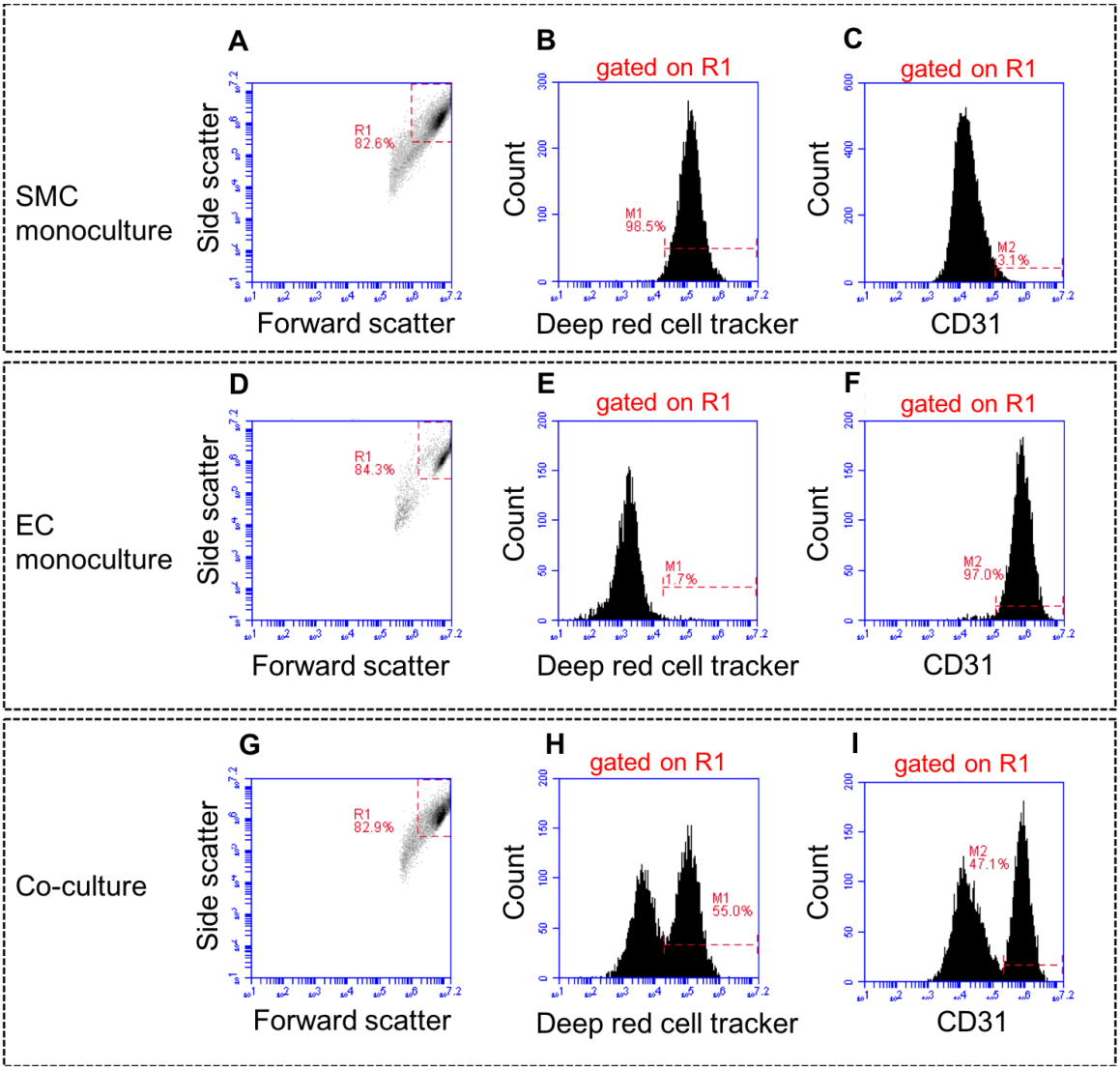

Figure 6.9 Gating of EC and SMC to assess cell death. Monoculture SMC, EC and cells in co-culture show up on forward and side scatter, which represent size and granularity, respectively (A, D, G). SMC are tracked in red (B) and do not show CD31 (C), which is a specific EC marker (F). Cells in co-culture appear as two separate populations, which are detected by a deep red cell tracker for SMC (H) and CD31 for EC (I).

6.3.3.2 Bosentan causes cell death in co-culture

The positive control cisplatin induced death in monocultured EC and SMC (91 ± 3.4 and 94.2 ± 2.3 % death, respectively), and also to the same extent in EC and SMC in co-culture (94.9 ± 2.5 and 94.4 ± 2.3 %) compared to DMSO control. The difference between monoculture and co-culture was not statistically significant. All represent N=4 (**Figures 6.10 and 6.11**).

Bosentan did not cause any death in monocultured EC or SMC and this is in line with data from the ATP viability assay in monocultured HUVEC and HCASMC in **chapter 4**, section **4.2.3.1**. However, in co-culture bosentan induced significant death both in EC and SMC (15.9 + 0.5 % death, $p < 0.05$ and 16.6 + 0.5 % death, $p < 0.01$, respectively) compared to monocultured EC and SMC (3.9 ± 0.1 % death and 2.6 ± 0.3 % death, respectively). This suggests that the effect of bosentan on cell death is altered under co-culture conditions.

Fenoldopam caused significant death in monocultured EC (8.6 ± 1.1 % death compared to 3.3 ± 0.1 % in DMSO control), similarly to ATP viability data shown in **chapter 4,** section **4.2.3.1**, where fenoldopam induced death in monocultured HUVEC. However, the effect of fenoldopam was not affected by the co-culture. Rather, fenoldopam seemed to have a protective effect on EC death in co-culture, as it caused only 1.8 % EC death in co-culture compared to 8.6 % in monocultured EC (there is a trend, but the effect is not significant). Also on SMC the difference between monoculture and co-culture was not significant. The other drugs did not induce cell death, either in monoculture or co-culture.

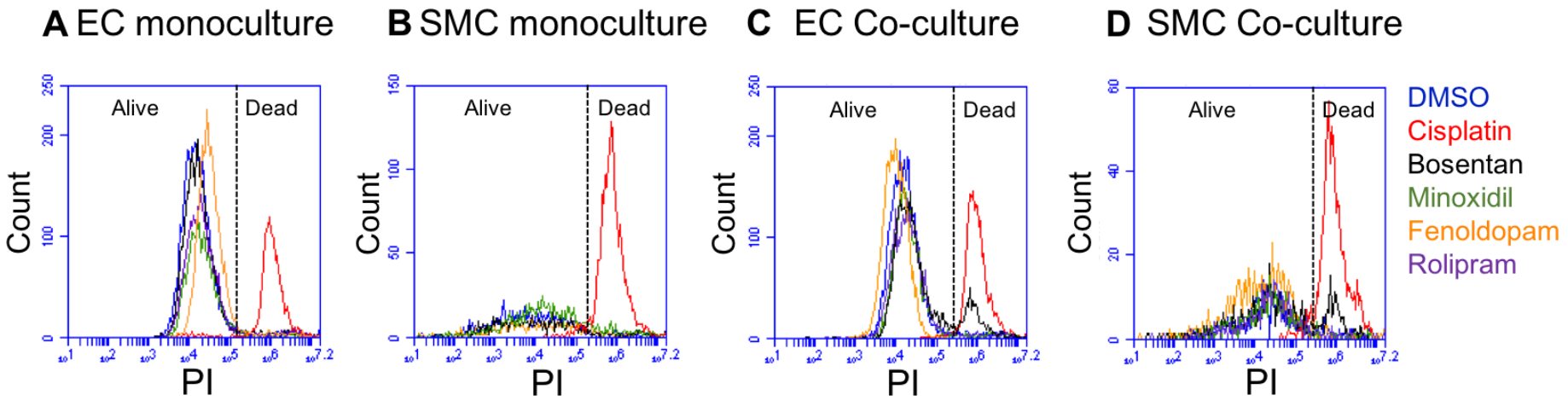

Figure 6.10 Propidium iodide (PI) is used to assess cell death. Death was assessed in monocultured EC (A), monocultured SMC (B), in EC in co-culture (C) and in SMC in co-culture (D) and analysed by flow cytometry. Cisplatin (red) caused cell death in monoculture and in co-culture, as shown by a shift to the right in the PI MFI. Among the drugs, only bosentan (black) induced cell death in EC and SMC in co-culture.

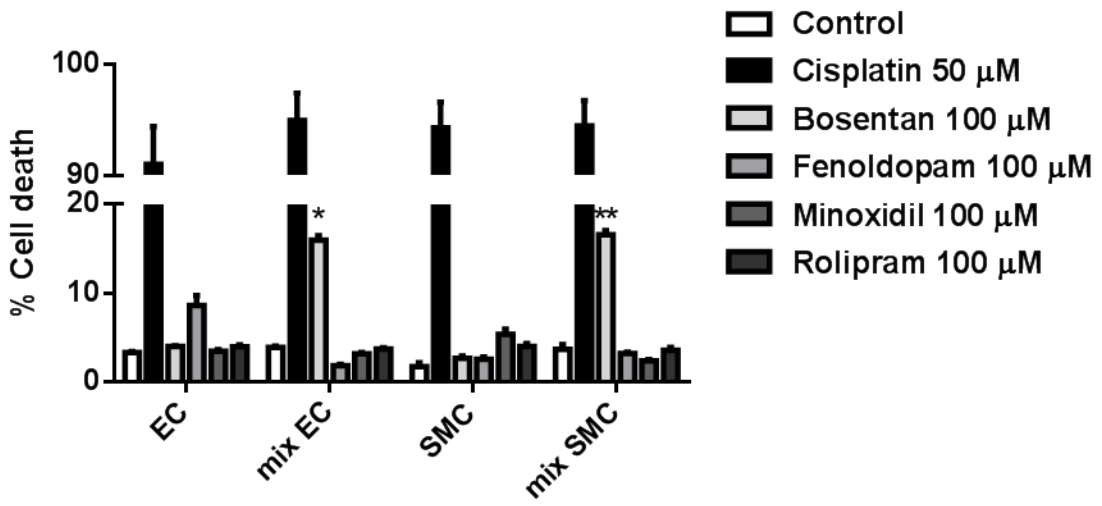

Figure 6.11 Cell death induced by DIVI-related drugs and analysed by flow cytometry using PI. Summary of the data from the previous figure (**6.10**). Data are expressed as % cell death after treatment with DIVI-related drugs for 24 hours. 100 % represents no death. Data represent mean ± SEM of 5 independent experiments, analysed by one-way ANOVA followed by Dunnett's post test. *$p < 0.05$, **$p < 0.01$.

6.4 Discussion

Several hallmarks of DIVI have been explored, however as not all the drugs investigated in this study caused DIVI with the same mechanism they produced different phenotypes. Potentially, the processes regulating DIVI cannot be fully recapitulated in isolated cell models and a more complicated, physiologically relevant model that mimics the anatomy of the vessel wall is required. As a step toward achieving this, a more complex co-culture model was developed, whereby EC and SMC are mixed together in a side-by-side model.

This method has several advantages; firstly, EC are in close proximity to SMC and therefore have physical and paracrine contact. This eliminates issues arising from some co-culture methods where EC are separated from SMC by a membrane and the direct contact between cells is prevented by the thickness of the membranes[431]. This model also allowed evaluation of the role of EC-SMC interaction in DIVI without characterising and optimising a complicated setup. Furthermore, this system could be easily be replicated and standardised allowing quick screening of drugs.

However, it is accepted that there are some limitations to using this co-culture model. First of all, this system does not closely mimic the *in vivo* architecture where EC grow as a single monolayer on top of SMC layers. Here, the ratio of EC to SMC does not resemble a physiological setting, where the SM layer represents the majority of the vascular cells and the endothelium only forms a thin monolayer. However, this is the ratio that allows EC to survive in the presence of SMC in this system and it is a simple setup that can be easily replicated. It would have been interesting to use the data from the mesenteric artery in **chapter 3** to investigate how this system matches to a physiological setting.

A more sophisticated system that resembles the *in vivo* vessel architecture, would be, for example, tissue engineered blood vessels, which closely mimic the *in vivo* geometry[444]. An elegant co-culture system has been developed for the *in vitro* study of DIVI, where EC are cultured on top of SMC separated by a porous membrane mimicking the internal elastic lamina, and cells are exposed to *in vivo*-derived hemodynamics[114] (refer to **Introduction**, section **1.8.1**, where this model has been described in detail). Although this system allows retention of many of the *in vivo* features of a blood vessel, it is a complex and low throughput

model, which also has a high variability. Although the complexity and physiological relevance would have been optimal for the characterisation of DIVI, for the purposes of this study the goal was to optimise a vascular model in a less complex system.

Several *in vitro* models of EC and SMC co-culture have been reported in the literature, which demonstrate the importance of EC-SMC interaction in the study of vascular diseases. It has been reported that EC co-cultured with quiescent SMC (differentiated) have a reduced inflammatory response to TNF-α compared with EC cultured alone, which is due in part to the EC interactions with the SMC-produced extracellular matrix (ECM)[445]. In addition, direct contact co-culture increases the expression of the EC-specific transcription factor KLF-2, which promotes an anti-oxidant and anti-inflammatory EC phenotype.

Other models have also been described, that involved culturing EC and SMC on opposite sides of a microporous membrane in transwell models[446,447]. One of these studies showed that SMC co-cultured with EC exhibited a significant increase in the number of adherent and spreading cells, and greater messenger ribonucleic acid (mRNA) and protein expression of β1-integrin compared to SMC cultured alone[447].

Review of the literature has shown that the co-culture conditions can produce different results. For example, it has been reported that direct co-culture of EC on top of SMC leads to a reduction in the responsiveness of EC to TNF-α, whereas the effect is reduced when the cells are grown on the opposite sides of a porous membrane[445]. In addition, transforming growth factor-β1 (TGF-β1) release is greater when EC and SMC are cultured together in a single layer than on opposite sides of a membrane. It would be interesting to observe whether the results described in this chapter would be altered by a different co-culture system.

EC and SMC morphology was analysed to understand whether the co-culture system affected these parameters. It has been reported that EC in co-culture tend to elongate, which is more representative of their morphology in vessels *in vivo*, as opposed to a polygonal morphology that is observed in the absence of SMC[435]. This is interesting, as it suggests that shear stress from blood flow is not the only determinant of the elongated EC morphology *in vivo*. In our system, the shape of EC and SMC was not altered when grown in a co-culture system perhaps

suggesting that the technical approach to co-culture can affect the phenotype of the EC and SMC. Cell density, the ratio between EC and SMC, culture medium constituents, and the type of EC and SMC are all likely to have an impact[448].

VWF release was assessed with the same drugs tested in the rat vessel explant and *in vitro* in monoculture. SMC did not express WPB containing VWF, and VWF released from EC did not adhere to SMC nor was it internalised by SMC. This is consistent with the data from the rat vessel explant shown in **chapter 3**, where VWF was not also retained within the smooth muscle region. Unstimulated (DMSO-treated) control cells were not 100 % VWF-positive. This was similar to monocultured HUVEC in **chapter 4**. VWF is constitutively released from unstimulated cells[363] (refer to **Introduction**, section **1.6.2.4.2**). Furthermore, cells were from pooled donors and at different stages of growth.

In these experiments, thrombin served as a positive control for VWF release. Thrombin induced VWF release at 1 hour and 24 hours and it proved to be a robust positive control in the co-culture system, as it had been in isolated EC.

Thrombin induced the release of VWF from approximately 30 % of EC after 1 hour and 35 % after 24 hours compared to no release from DMSO-treated control. The release was greater at 24 hours compared to monocultured cells, where thrombin induced release of approximately 25 % at 24 hours. This perhaps suggests that the interaction between EC and SMC plays a role in the mechanism of thrombin in releasing VWF. The signalling pathways could be investigated, by knocking down the receptor on these cell types and then look at the effect of thrombin on VWF release.

In the *ex vivo* experiment thrombin stimulation reduced endothelial VWF intensity, indicative of release, by around 60 % compared to control. This suggests that the effect *ex vivo* is greater than *in vitro* in monoculture, and that studying DIVI *in vitro* might be too reductionist. However, it is hard to directly compare *ex vivo* with *in vitro* in this case, because the starting expression levels in the vessels compared with the cellular model are unknown, the thrombin might stick to the plastic, the expression levels of the thrombin receptor might be different, and also the serum used in cell culture may affect the release.

The same drugs that induced VWF release in **chapter 4**, caused a similar effect in co-culture experiments. Specifically, bosentan and fenoldopam induced release at 1 hour and 24 hours.

Minoxidil caused VWF release only at 24 hours that was similar to the observed effect in monocultured HUVEC. Likewise, rolipram showed no effect on VWF release in either cells or the vessel. This might suggest that rolipram might need to be injected in the animal in order to produce injury or it might work with different mechanisms in different species.

It would have been interesting to assess EC junctional integrity as in **chapter 4**. However, the setup of the co-culture model was not suitable as EC did not form complete intercellular junctions when cultured with SMC. This could have been addressed for example by using transwell assays where EC are cultured on an insert lateral to SMC. This system would allow EC junctions to be intact that could be visualised and analysed. Studies have reported that co-culture of EC with SMC produced increased localisation of tight junction proteins to the junctions and increased permeability in a similar way to the effect of cAMP, indicating that SMC play a critical role in regulating EC permeability[431,449]. This may have been of particular interest for rolipram. In these studies, no DIVI related effects for rolipram have been observed, despite it being reported as an effective inducer of DIVI *in vivo*. As it is a PDE inhibitor, it would be expected to increase cAMP and so may have affected EC junctions. To confirm this, cAMP levels could be assessed after administration of rolipram and determine whether these are being altered.

More complex studies conducted by HemoShear identified that fenoldopam (100 µM) in combination with *in vivo*-derived hemodynamics increase vascular permeability in a rat mesentery co-culture system[79] and that fenoldopam treatment altered several inflammatory pathways. In order to understand the mechanism of DIVI, it would also be interesting to study inflammation to see whether the effect of bosentan and fenoldopam described in **chapter 4** is amplified in a co-culture system. For example, a co-culture flow system was developed to investigate the adhesion of flowing leukocytes, which have a crucial role in inflammation (refer to **Introduction**, section **1.6.5.3**) to EC co-cultured with SMC[432,450,451]. It was demonstrated that co-culture of EC with SMC at opposite sides of a porous membrane markedly increased the adhesion of flowing leukocytes to EC and that the response of co-cultured EC to TNF-α stimulation was amplified.

Furthermore, it would have been useful to also assess the phenotype of SMC in co-culture before and after drug treatment. Within mature blood vessels, SMC usually have contractile

functions and express SMC-specific contractile markers such as calponin[452] and α-SMA[453] (refer to **Introduction**, section **1.6.3**). In disease states, for example in atherosclerosis, SMC repress expression of these genes and express a more proliferative, synthetic phenotype (**Figure 6.12**).

It has been shown that EC can influence SMC phenotype expression, proliferation and migration[454,455]. For example, EC maintain SMC in a more contractile phenotype compared with SMC cultured alone. In addition, EC inhibit SMC type I collagen synthesis and promote SMC migration and proliferation in co-culture[456].

In response to injury, SMC switch from contractile to a proliferative phenotype capable of dividing in response to several mitogens, including platelet-derived growth factor (PDGF) and basic fibroblast growth factor (bFGF) and they also synthesise extracellular matrix components such as collagen, elastin, and proteoglycans[457,458]. Adhesion proteins such as fibronectin and laminin play an important role in determining the basic phenotypic state of the cells and exert their effects via integrin receptors[458]. Assessing whether the drug treatment alters the SMC phenotype could also be done in the future, both on monocultured SMC and in co-culture. This could be achieved by assessing the expression of SMC specific phenotypic markers by Western blot or measuring RNA levels of those proteins in untreated and stimulated samples.

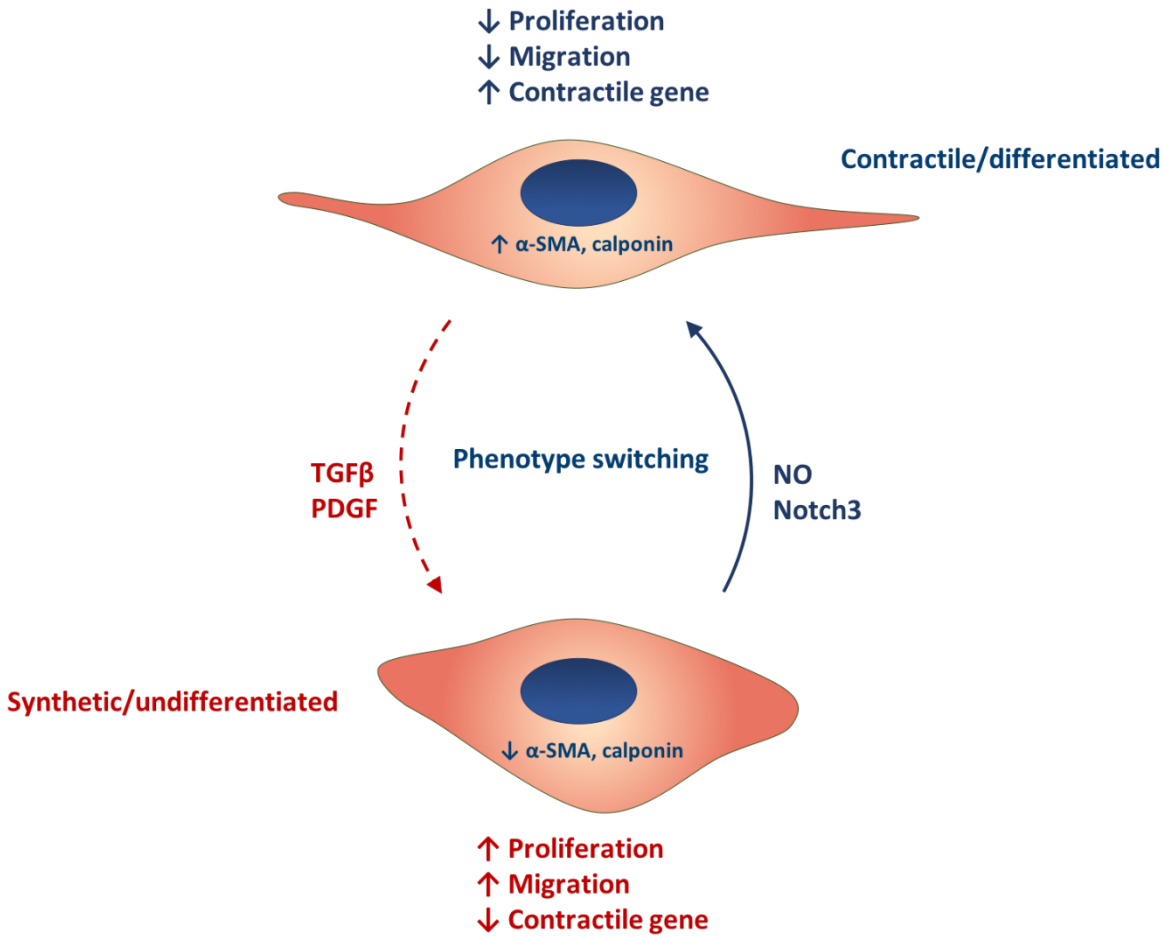

Figure 6.12 Phenotype switching in SMC. Mature and healthy SMC show a contractile and differentiated phenotype, expressing markers like α-SMA and calponin. However, in disease states increased expression of TGFβ and PDGF can induce SMC switch to a synthetic and undifferentiated phenotype, characterised by high proliferation and migration of SMC. This phenotype can be promoted by and is characterised by decreased expression of α-SMA and calponin. Author's own drawing.

Finally, cell death was investigated in co-culture by flow cytometry. This technique was used because it was an effective way to analyse separate EC and SMC populations in the same sample and could be used to rapidly analyse sufficient cells to make statistically powered conclusions[459]. SMC necrosis is a clear feature of DIVI, however the ATP viability assay in **chapter 4** did not show death in monocultured SMC. Therefore, cell death was investigated in co-culture to understand whether the presence of EC would affect SMC death. PI has been reported to be a robust method to assess the viability of cells[443]. PI is considered a cell death indicator because loss of cell membrane integrity is a common event in all forms of cell death, however this method cannot be used to detect dying cells or to distinguish between different types of death[460,461]. Alternative methods can differentiate between necrosis and apoptosis, including caspase activation, cytochrome c release and oligonucleosomal DNA fragmentations (apoptotic parameters).

Cisplatin was used as positive control for inducing cell death. It is well known that cisplatin akin to other antitumor drugs induces apoptosis primarily by damaging the DNA, whereby a nuclear signal generated in the initiation phase is directed to the cytoplasm subsequently returning to the nucleus to produce internucleosomal DNA degradation[462]. As expected, cisplatin induced monocultured SMC and EC death.

Bosentan did not cause death in monocultures of EC and SMC, recapitulating what was observed in the ATP viability assay in **chapter 4**. However, unexpectedly bosentan caused EC and SMC cell death in co-culture, indicating that potentially the interaction between cells is an important effect of bosentan. How this could be happening remains to be explored, as well as whether it is an off-target effect, which is likely. As demonstrated in **chapter 4**, the effects of bosentan at this concentration may not be through its primary targets, the endothelin (ET) receptors. It is possible to hypothesise that bosentan activates EC to release a signalling molecule that acts on the SMC.

Fenoldopam induced around 10 % death in monocultured EC and no additive effects was observed in co-culture. Of the other drugs tested no effect was observed in respect of cell death.

In summary, these data demonstrated that co-culturing EC and SMC is not sufficient to alter (increase or decrease) an existing or induce a novel DIVI phenotype for any of the drugs. Only bosentan caused both VWF release and EC and SMC death of all the drugs (**Table 6.1**). As it was not possible to induce features common to all DIVI-related drugs in this *in vitro* system perhaps this adds to the evidence from previous chapters suggesting a more complex physiological model needs to be explored. Co-culture flow systems that allow variation of flow and pressure to model physiological conditions may advance the understanding of the role of these factors in regulating DIVI. Indeed, work conducted by HemoShear has developed an EC-SMC co-culture platform where the cells are separated by a synthetic internal elastic lamina and the endothelium is exposed to *in vivo*-derived hemodynamics[79]. In the proceeding chapters the role of flow in regulating EC function in DIVI will be investigated.

Effect	Time course (hours)	Bosentan	Fenoldopam	Minoxidil	Rolipram
VWF release	1	✓	✓	×	×
	24	✓	✓	✓	×
Cell death	24	✓	×	×	×

Table 6.1 Summary of the effects of DIVI-related drugs in co-culture. Attributes of DIVI were investigated in this chapter: (1) VWF release from EC and SMC; (2) EC and SMC death. ✓= significant effect ($p < 0.05$); ×= no effect.

7. The role of flow in DIVI

7.1 Introduction

In this thesis the impact of four drugs known to induce DIVI has been investigated to elucidate their effects in a rat vessel explant, blood cells, monocultured EC and SMC, and finally in a direct co-culture system. Several biomarkers including VWF release from EC, EC junctional disruption, inflammation and cell death were investigated but no common DIVI associated features were indicative of all the drugs. Indeed, bosentan was the only drug that had an effect on both VWF release and cell death in co-culture and conversely, rolipram failed to show a DIVI phenotype in any of the assays tested.

It has been suggested that shear stress plays a role in the mechanism of DIVI and that localised changes in coronary blood flow is involved in the pathogenesis of DIVI (refer to **Introduction**, section, **1.5.1**)[203]. Each of the drugs tested in these studies are vasodilators (though not all cause a drop in main arterial blood pressure) (**Introduction**, **Table 1.1**), and therefore investigating the effect of shear stress was the next step considered important in assessing the onset of DIVI.

Although DIVI has been mostly studied *in vivo* in dog and rodents, one report of investigating DIVI *in vitro* is by HemoShear, who developed a system where EC and SMC are cultured on top of each other, separated by a membrane and EC are directly exposed to *in vivo*-derived hemodynamics through a miniaturised cone-an-plate viscometre[79]. Intellectual property restrictions have limited the information regarding the shear rate and time period over which the cells are exposed to flow. However, these studies showed that with hemodynamic regulation, fenoldopam (100 μM) elicited effects on several parameters that are affected by flow, increasing EC layer permeability as measured by VE-cadherin expression, inflammation, oxidative stress, promotes cell death and cell remodelling. These findings demonstrate the potential importance of shear stress in the study of DIVI[79].

Several methods have been developed to apply shear stress to EC *in vitro*, such as microfluidics, parallel-plate flow chambers, cone-and-plate viscometers, and orbital shakers[463]. However, these systems are complicated and costly. One of the primary aims of

the thesis was to characterise a "simplistic" *in vitro* model that could derisk DIVI, therefore providing the closest physiological environment was important. A simple high-throughput screening model would mean that other laboratories could use this assay, reducing variability and increasing reproducibility, providing a robust methodology for safety assessment.

Recently, Piezo-1 channels expressed on EC were identified as fundamental regulators in sensing the shear stress caused by changes in blood flow[464]. Piezo-1 are stretch-activated calcium permeable channels, that serve as sensors of mechanical stress in EC[465]. Complete knock down of Piezo-1 in mice is embryonic lethal, with embryos displaying vascular remodelling deficiencies[336]. The importance of this protein in transducing shear stress to a biological effect was displayed in gene silencing studies in HUVEC, where Piezo-1 -/- cells cannot align effectively in response to shear stress[336]. Therefore, this last chapter explores the addition of Yoda-1, which activates Piezo-1, as a potential 'flow-mimetic' that could be used as an alternative over more complicated microfluidics. Yoda-1 is a synthetic small molecule, which selectively activates Piezo-1 and not Piezo-2 channels (also expressed on EC[464]) was used. Yoda-1 activates Piezo-1 by stabilising channel in an open conformation without the mechanical stimulation of flow[466]. Yoda-1 has a binding affinity to the purified Piezo-1 protein in the range of 10-50 µM. The selectivity of Yoda-1 for Piezo-1 channels was demonstrated in artificial lipid bilayers, where Yoda-1 activated Piezo-1 without other accessory proteins[467,468]. Furthermore, activation of eNOS by shear stress on EC can be mimicked by acute administration of Yoda-1[338]. Besides Piezo channels, prior evidence supports a role for integrins as mechanotransuders in the endothelium by promoting phosphorylation of different targets though the activation of focal adhesion kinase[464]. Furthermore, different structures of EC, mainly primary cilia are also involved in mechanotransduction.

In the previous chapters, the DIVI-causing drugs *ex vivo* in a rat vessel explant, *in vitro* in monocultured cells and in co-culture of EC and SMC did not produce a phenotype that was common to all the drugs. In this chapter, Yoda-1's capability as a flow-mimetic was examined, comparing HUVEC phenotypes while stimulated under Yoda-1 against HUVEC experiencing laminar shear stress. Subsequently, EC and SMC VWF release and death were assessed in the presence of both Yoda-1 and the candidate drug. The hypothesis was that shear stress might

contribute and enhance the effects of the drugs. Although shear stress has been reported to have a protective effect from several damaging stimuli[469,470], it can also increase cell toxicity in response to certain drugs. For example, it has been recently shown in our laboratory that Yoda-1 and laminar shear stress both enhanced cytotoxicity of doxorubicin in EC[340].

7.2 Methods

In this chapter, the same four drugs tested previously (**chapter 3-6**) were assessed for hallmarks of DIVI. Cells were grown for 24 hours and pre-treated with Yoda-1. Subsequently, cells were then incubated with DIVI-related drugs. Refer to the **Methods** and to the specific sections in this chapter for a detailed description of the protocol (concentrations and time points) depending on each assay.

7.3 Results

7.3.1 Establishing a working concentration of Yoda-1

Firstly, a working concentration of Yoda-1 was established. A concentration of Yoda-1 was required that would be present during long-term cell culture (24-48 hours), that produced no cytotoxic effects, and would thus model EC under continued shear. Cytotoxicity was conducted using two methods, the ATP luminescence assay (used in the previous chapters) and confocal imaging. The ATP assay was performed on HUVEC treated with Yoda-1 for 1, 4 or 24 hours in a range between 0.1 μM and 100 μM (**Figure 7.1**). 1 μM was the concentration that did not cause cell death at any of the time points and thus was used in the subsequent experiments, whereas higher concentrations (10-100 μM) were substantially toxic to HUVEC, especially at longer periods of time.

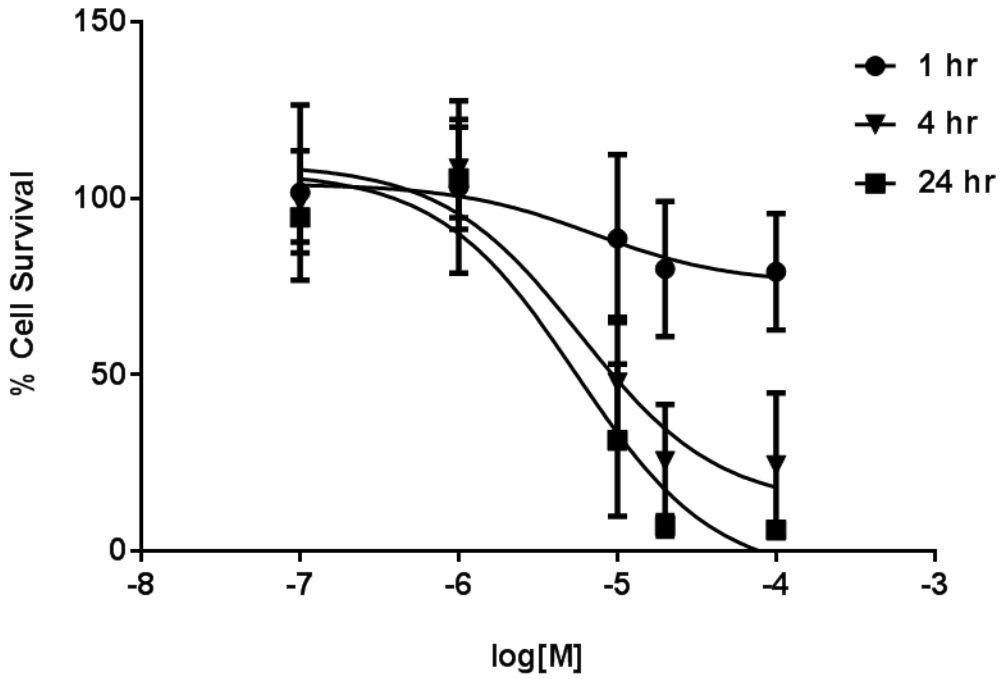

Figure 7.1 Assessment of cytotoxicity using an ATP viability assay. HUVEC were treated with increasing concentrations of Yoda-1 for 1, 4 or 24 hours. Data represent mean ± SEM of 5 independent experiments.

To assess cell death using confocal imaging, HUVEC were treated with Yoda-1 for 24 hours and incubated with a cell viability dye (blue) prior to fixation (**Figure 7.2**). Nuclei (red) were stained with DAPI and cell junctions with VE-cadherin (green), a protein that maintains intact intercellular junctions. The detergent Triton X-100 was used as a positive control, to cause cell membrane disruption and ultimately cell lysis. After treatment with Triton X-100, the viability dye enters the nuclei and co-localises with the nuclei stain. None of the concentrations of Yoda-1 tested (up to 2 μM) induced cell death after 24 hours, thereby confirming results from the ATP assay (described above). A working range of 0.05-2 μm was established. Additionally, in these experiments Yoda-1 did not alter cell division (**Figure 7.2**, C), as the number of the nuclei in random fields of view showed no difference.

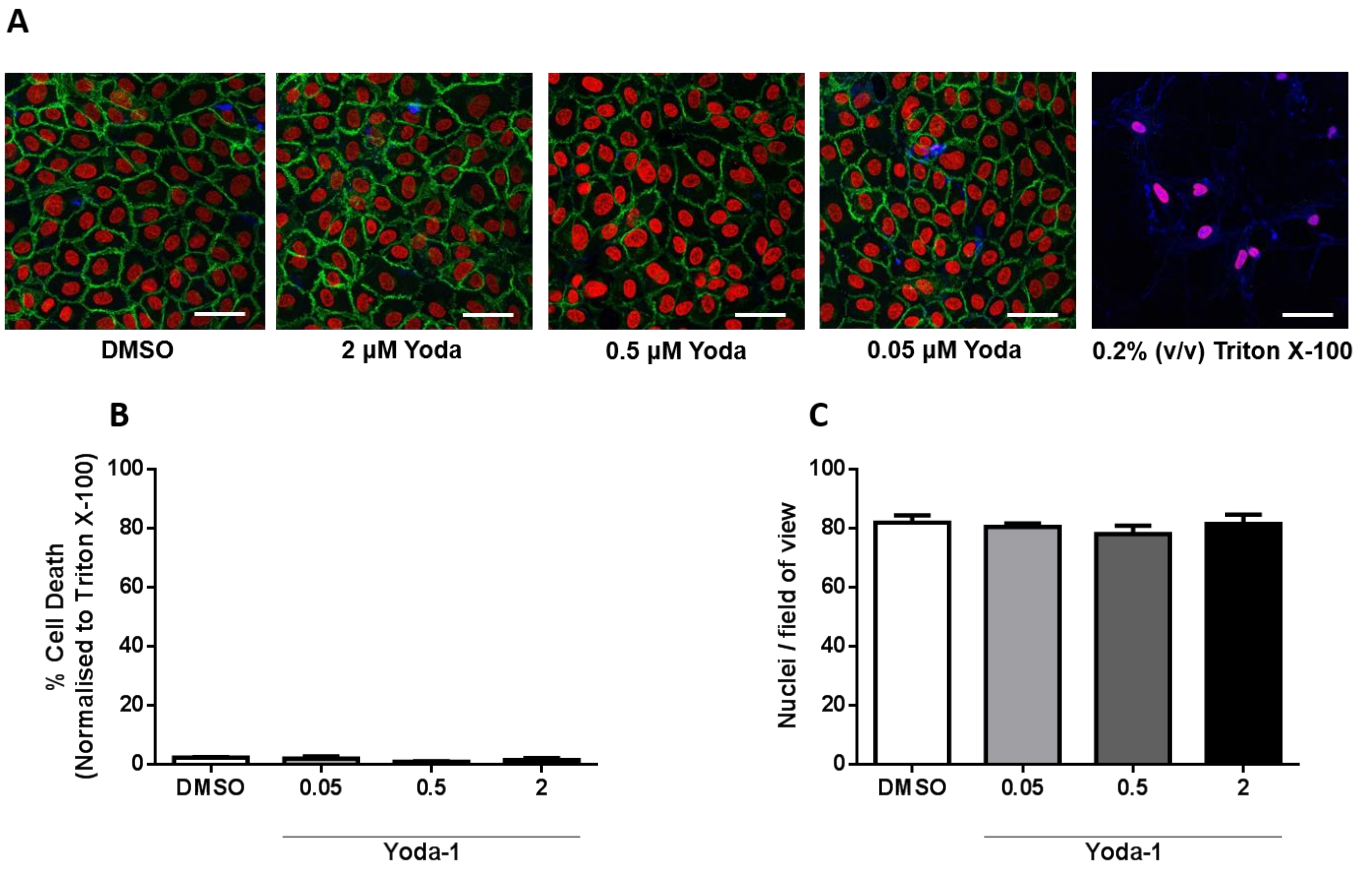

Figure 7.2 Assessment of cytotoxicity using immunofluorescence. Representative confocal pictures show HUVEC incubated for 24 hours with varying concentrations of Yoda-1. Nuclei were stained with DAPI (red), and EC junctions with VE-cadherin (green). Cell death was monitored through a fluorescent cell viability stain (blue) (A). B represents % dead cells normalised against 0.2 % v/v Triton X-100. C represents cell nuclei per field of view. Six random fields of view were quantified for each repeat, three independent experiments were conducted. Scale bars in A represent 20 µm. Data in B and C represent mean ± SEM of 5 independent experiments, analysed by one-way ANOVA followed by Dunnett's post test.

7.3.2 Yoda-1 mimics the effect of flow in static EC

A working concentration range of Yoda-1 was used to assess whether phenotypes commonly observed under shear stress conditions could be observed. Incubation of HUVEC with Yoda-1 (at concentration range between 0 and 2 μM) for 24 hours increased the surface expression of ICAM-1 to 1.45 ± 0.11 fold higher than the DMSO control (N=5, $p < 0.05$) (**Figure 7.3**, B). This increase was not observed with the surface molecule, VCAM-1 (D). It was considered appropriate to model Yoda-1 effects to HUVEC under 5 dyn/cm^2 shear stress, as HUVEC are derived from a vein, and this is the shear stress measured in small veins and post capillary venules[471,472].Under flow (5 dyn/cm^2), expression of ICAM-1 (A) but not VCAM-1 (C) significantly increased, in a similar way to that observed with Yoda-1 (1 μM). This has been previously reported, but following shorter incubation periods to those used in this study[473].

Phosphorylation of eNOS and its upstream kinase Akt (**Figure 7.4**) was also observed in Yoda-1 (1 μM) stimulated HUVEC at 24 hours. HUVEC cultured under flow (5 dyn/cm^2) for 24 hours displayed a comparable level of phosphorylation to those cells treated with 1 μM Yoda-1. This effect was maintained for 24 hours. It has been previously described that Yoda-1 induces Akt and eNOS phosphorylation, and this effect is strongly reduced after knockdown of Piezo-1[338]. However, previous studies did not investigate the effect of Yoda-1 for periods exceeding 30 minutes[338]. It was important to assess that the response to Yoda-1 response would be maintained post 24 hours in order to allow comparison with previous experiments conducted for this study. All the experiments described below were conducted at 24 hours.

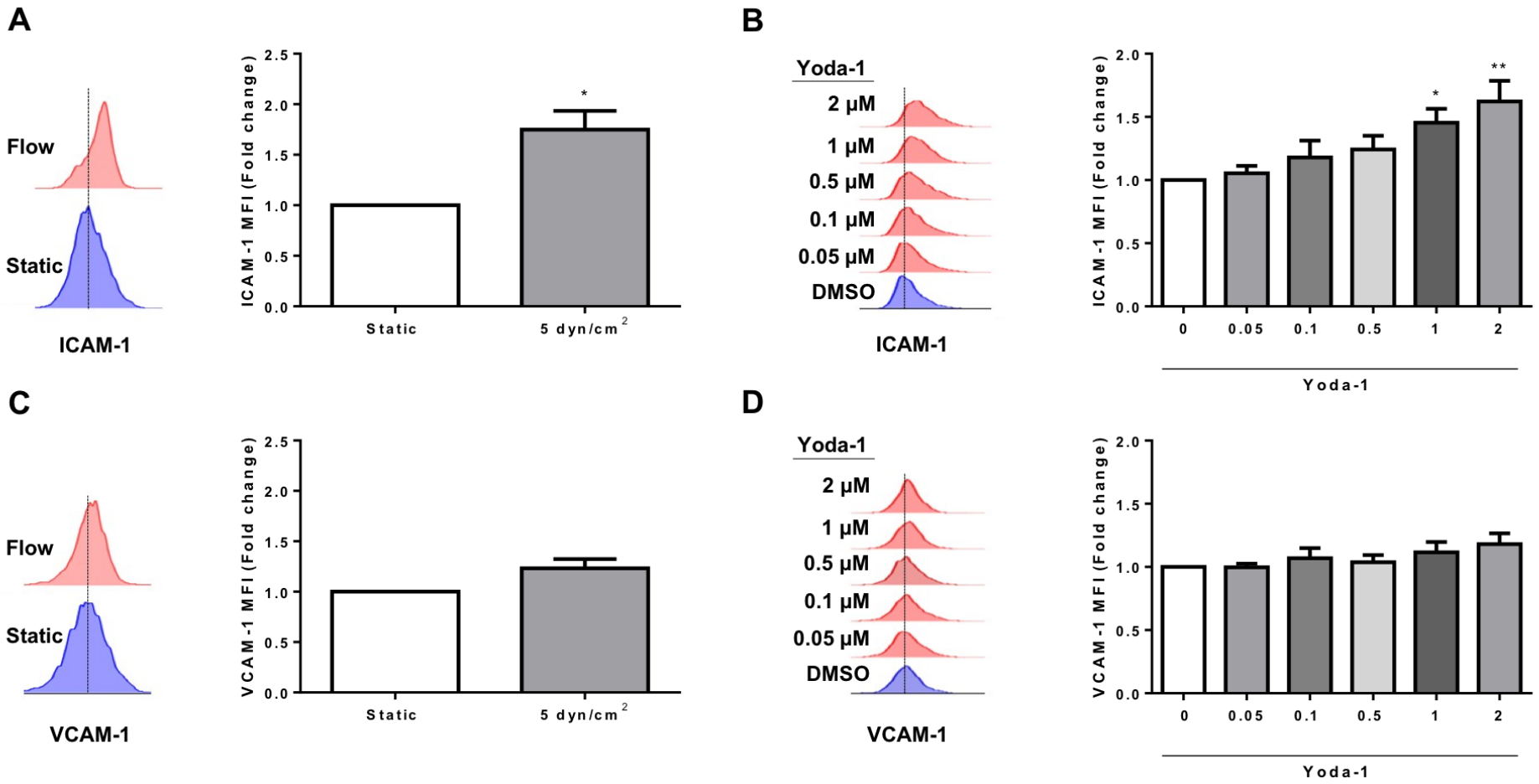

Figure 7.3 ICAM-1 and VCAM-1 expression in HUVEC under flow or using the flow-mimetic Yoda-1. Expression under flow (A and C), and static conditions (B and D) using a concentration range of Yoda-1 for 24 hours. Representative histograms from a single experiment are shown, followed by MFI normalised to their appropriate static culture control. Data represent mean ± SEM of 5 independent experiments, analysed by two-tailed non-parametric test and one-way ANOVA followed by Dunnett's post test. *$p < 0.05$, ** $p < 0.01$.

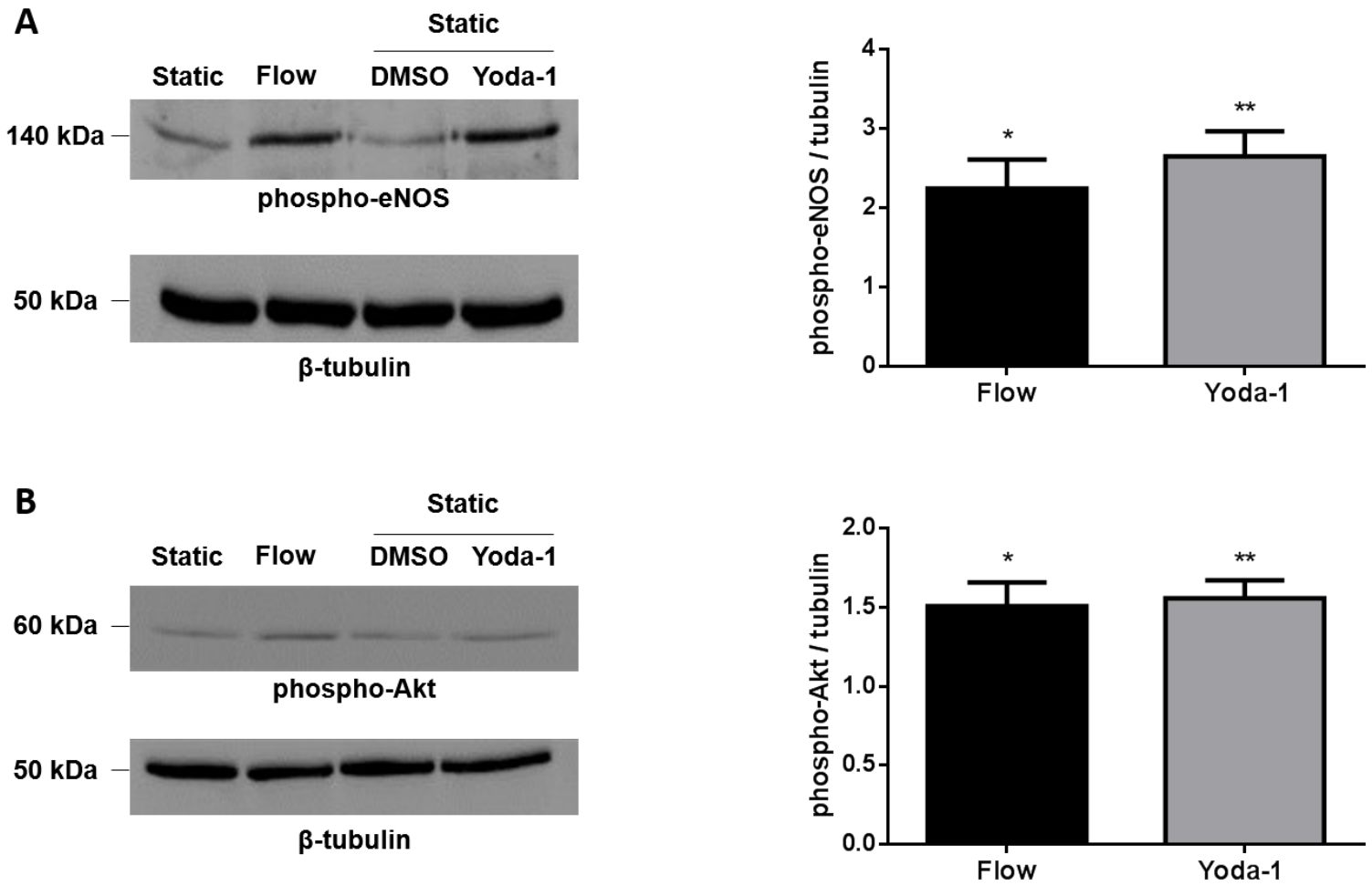

Figure 7.4 Representative blots and quantification by densitometric analysis of phospho-eNOS and phospho-Akt. Phosphorylation of eNOS (A) and Akt (B) is shown under flow or in static conditions after 1 μM Yoda-1 treatment for 24 hours. Data are normalised against their appropriate static (no Yoda-1) control lysate and represent mean ± SEM of 5 independent experiments, analysed by one-way ANOVA followed by Tukey's post test. *$p < 0.01$, **$p < 0.001$.

These results indicate EC cultured under shear stress conditions compared to Yoda-1. The effect of Yoda-1 on HUVEC treated with DIVI-related compounds was then assessed. 1 μM Yoda-1 was preincubated 24 hours prior to drug treatment to model a shear pre-conditioned endothelium, a phenomenon that would occur *in vivo*[474]. In all subsequent experiments when Yoda-1 was added it was at a concentration of 1 μM.

7.3.3 DIVI-related drugs in the presence of Yoda-1 do not induce VWF release

First, VWF release from the endothelium was assessed, to identify if the effect of the drugs observed in previous chapters could be altered by exposing HUVEC to the flow-mimetic. HUVEC were seeded in ibidi slides at 100,000 cells/well, grown for 24 hours, treated with 1 μM Yoda-1 for 24 hours and then treated with bosentan, fenoldopam mesylate, minoxidil sulfate, and rolipram all at 100 μM. The same two time points from **chapters 4** and **5** were chosen: 1 hour, to assess a short-term effect and 24 hours, to reflect the time point used in the vessel experiment. 0.1 % v/v DMSO was the vehicle for all the drugs. Following treatment, cells were fixed with 4 % v/v PFA for 10 minutes and then permeabilised for 5 minutes with 0.1 % v/v Triton X-100. Specific antibodies were used to detect VWF and CD31 (to mark cell junctions), and DAPI was used to label the nuclei. Cells were imaged with a confocal microscope using a 63x objective. Six images were taken for each treatment per repeat. Four experiments were conducted in total.

Over 24 hours, VWF release was not significantly different in control cells, where 87.4 ± 2.8 % were VWF-positive and at 24 hours this was relatively unchanged at 93.0 ± 1.5 % (**Figure 7.5**, **7.6, 7.7**). This observation was consistent with the release observed in previous chapters.

Yoda-1 control-treated cells induced some VWF release at 1 hour, as the % of VWF-positive cells was 79.5 ± 6.0 %, and the release was significantly increased at 24 hours to 63.9 ± 1.90 %. Shear stress has been shown to release VWF from the endothelium, this could explain these findings[471,472]. However, none of the drugs appeared to increase the VWF release from EC following pretreatment with Yoda-1 at either 1 hour or 24 hour time periods. In the previous chapters (**chapter 4** and **chapter 5**), bosentan and fenoldopam showed a significant effect and induced VWF release in monocultured HUVEC and in HUVEC in co-culture at 1 hour

and at 24 hours, whereas in these studies this effect was not apparent. Yoda-1 may be masking the effect of the drugs in inducing VWF release.

Rolipram showed a trend for a reduction in VWF release, but the effect was not significant. Again, these results are in contrast with previous **chapters 4** and **5**, where bosentan, fenoldopam and minoxidil induced a significant VWF release at 24 hours. All represent N=4.

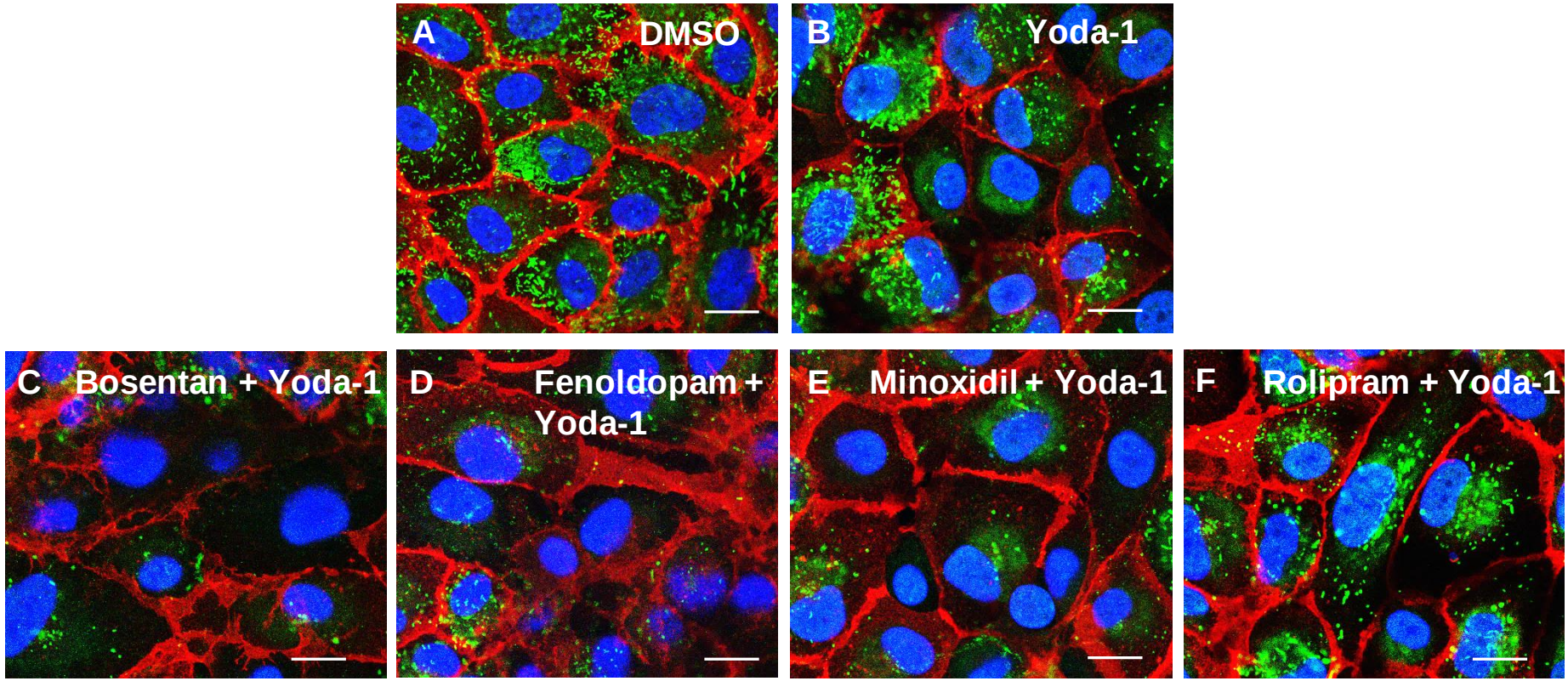

Figure 7.5 Representative confocal pictures of VWF release in HUVEC pre-treated with Yoda-1 1 μM at 1 hour. HUVEC were grown for 24 hours, treated with Yoda-1 (1 μM) for 24 hours and then the drugs at 100 μM. VWF (green) release was assessed at 1 hour. Cell junctions are stained with CD31 (red), and nuclei with DAPI (blue). Six images were taken in random fields of view, four experiments were conducted in total. Scale bars represent 20 μm. 63x.

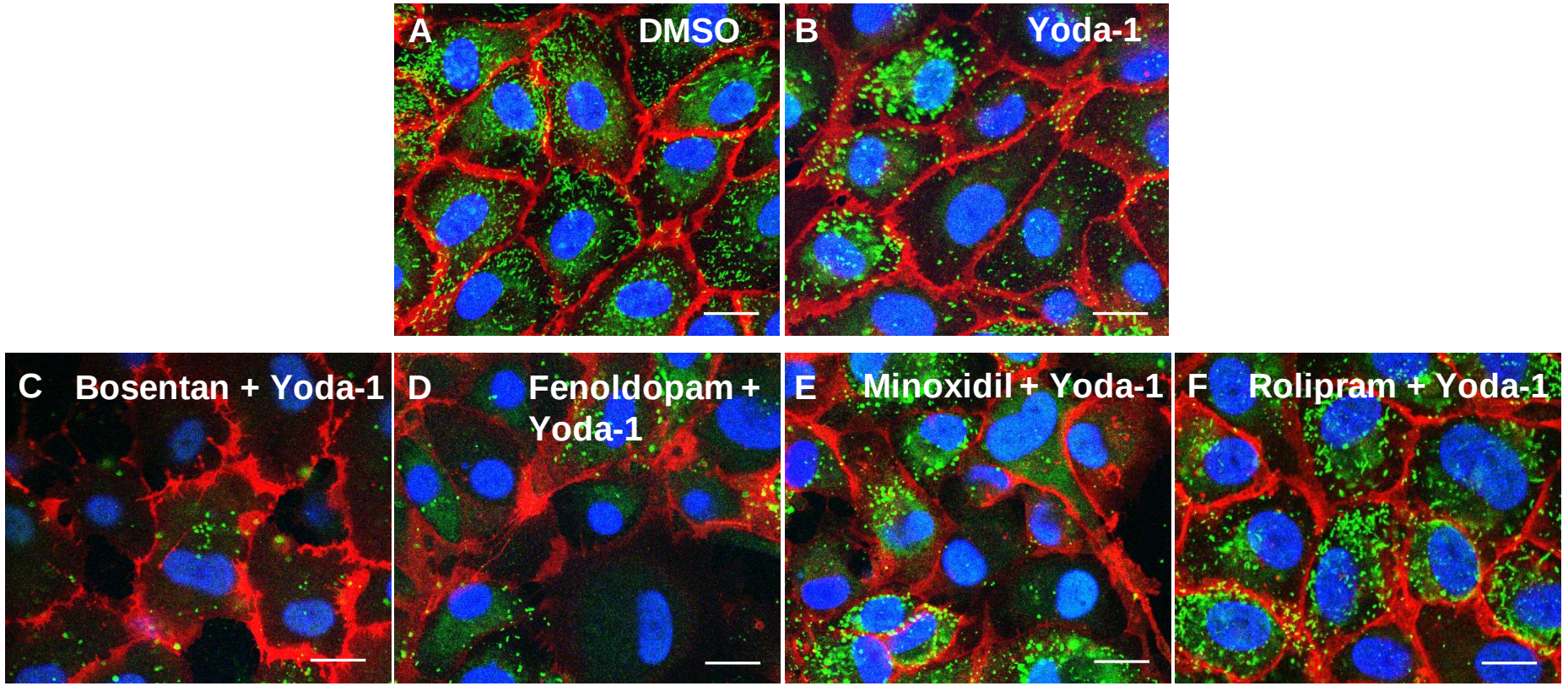

Figure 7.6 Representative confocal pictures of VWF release in HUVEC pre-treated with Yoda-1 at 24 hours. HUVEC were grown for 24 hours, treated with Yoda-1 1 μM for 24 hours and then the drugs at 100 μM. VWF (green) release was assessed at 24 hours. Cell junctions are stained with CD31 (red), and nuclei with DAPI (blue). Six images were taken in random fields of view, four experiments were conducted in total. Scale bars represent 20 μm. 63x.

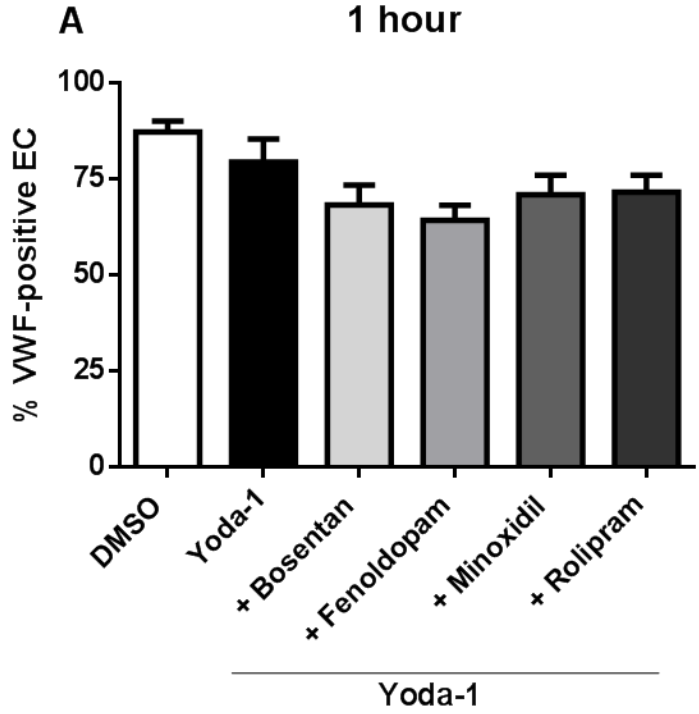

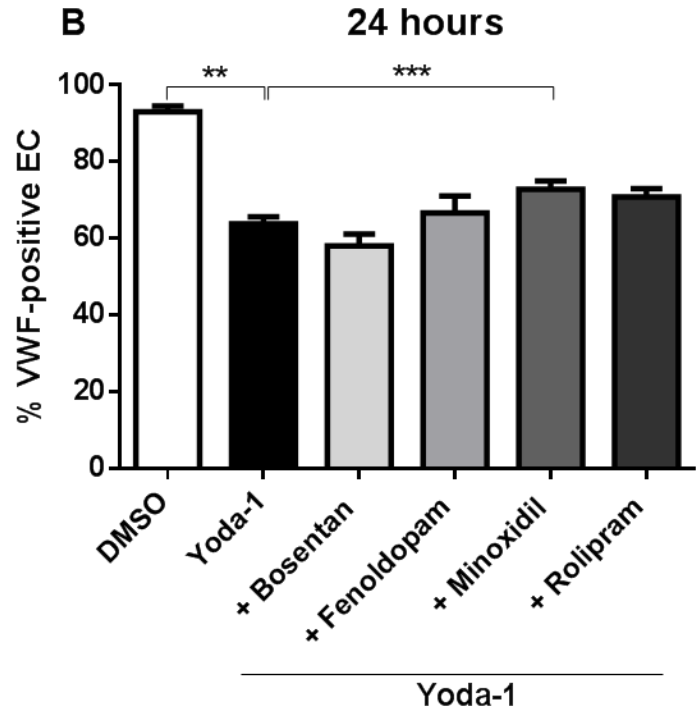

Figure 7.7 VWF release after 1 (A) and 24 (B) hours in HUVEC pre-treated with Yoda-1 1 µM. HUVEC were grown for 24 hours, treated with Yoda-1 1 µM for 24 hours and then with the drugs at 100 µM for 1 and 24 hours. Data are expressed as % of VWF-positive cells out of all cells in the field of view (six random fields of view per treatment), and represent mean ± SEM of 4 independent experiments, analysed by one-way ANOVA followed by Dunnett's post test. **p < 0.01, ***p < 0.001, compared to Yoda-1.

7.3.4 The particle size of VWF does not differ across treatments

The particle size of intracellular VWF was monitored to understand if Yoda-1 affected the packaging and distribution of VWF into WPB. The size was analysed as described in **chapter 4**, section **4.2.2**. The particle size of VWF did not differ across treatments at 1 hour or 24 hours (**Figure 7.8**, A and B), indicating that WPB do not fuse together at the plasma membrane. This is consistent with findings from monocultured HUVEC and also co-culture, where the average particle size did not alter with treatments.

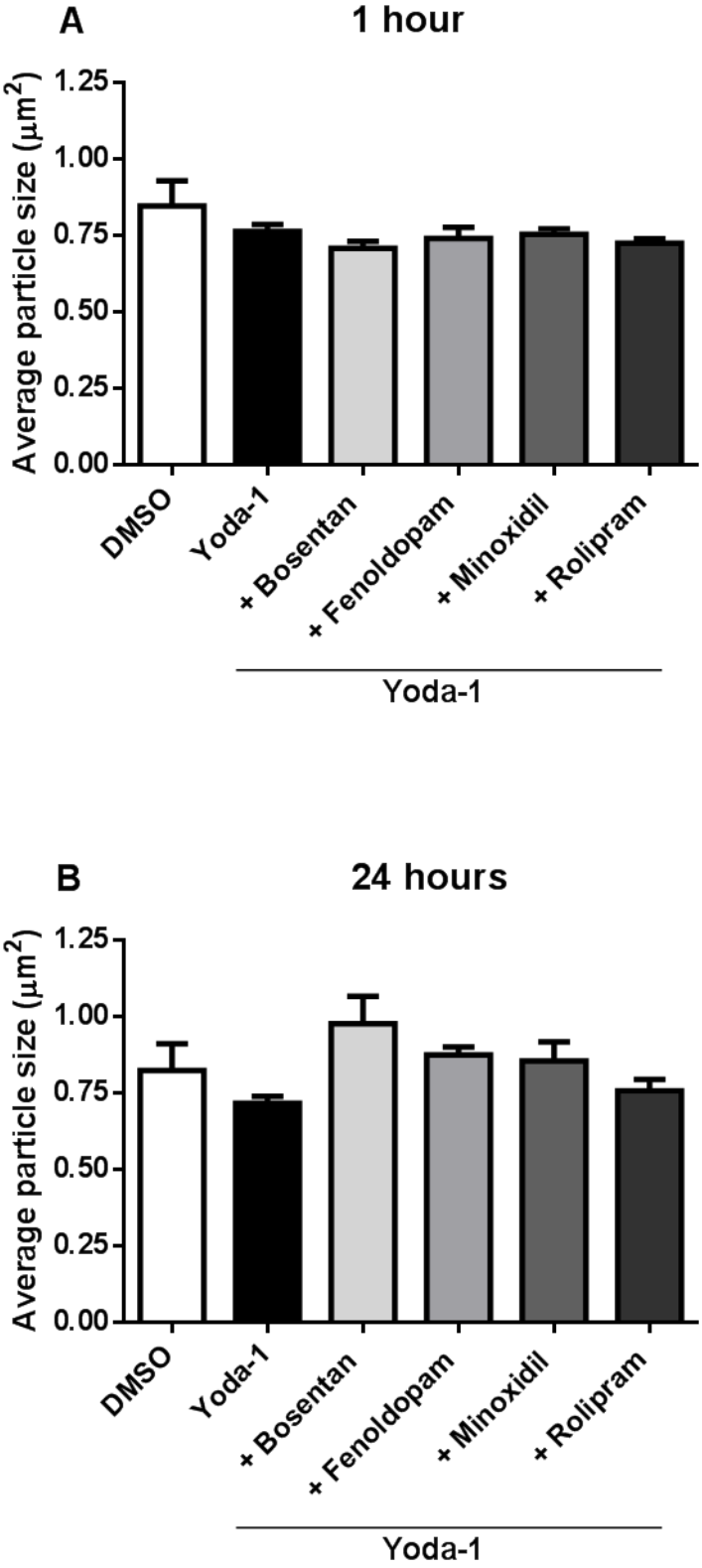

Figure 7.8 Average particle size of VWF at 1 (A) and 24 hours (B). HUVEC were grown for 24 hours, treated with Yoda-1 (1 µM) for 24 hours and then with the drugs at 100 µM for 1 and 24 hours. Data are expressed as area of VWF particles in the field of view (six random fields of view per treatment), and represent mean ± SEM of 4 independent experiments, analysed by one-way ANOVA followed by Dunnett's post test compared to Yoda-1.

7.3.5 The drugs do not affect EC junctional integrity

Drug-induced disruption to the HUVEC monolayer was assessed using confocal microscopy as described in **chapter 4**, section **4.2.2**, using CD31 to visualise junctional integrity and disruption. The experiment was conducted as described in this **chapter**, section **7.3.3**. The greater the black area, the more disruption to the EC monolayer (**Figure 7.9**). Cells were pre-treated with Yoda-1 and the effect of the drugs was assessed at 1 and 24 hours (**Figures 7.9**, **7.10** and **7.11**). The MFI for each drug treatment was measured and normalised against the Yoda-1 control. At 1 hour, Yoda-1 control significantly disrupted the junctions as shown by a larger black area between cells (and a higher MFI) compared to DMSO control (mean of 0.45 ± 0.07; N=4, $p < 0.05$). The drugs did not significantly affect the junctions, however bosentan, fenoldopam and minoxidil showed a trend towards disruption (score for bosentan, fenoldopam and minoxidil compared to Yoda-1 control were 4.9 ± 2.8, 7.7 ± 4.9, and 3.4 ± 2.0, respectively). Previously, in monoculture experiments, in the absence of Yoda-1, fenoldopam induced significant disruption of the junctions at 1 hour, and minoxidil at 24 hours (refer to **chapter 4**, section **4.2.2.1**).

After 24 hours, Yoda-1 control induced significant EC monolayer disruption compared to DMSO control, which showed a mean of 0.3 ± 0.04 (N=4, $p < 0.01$). This is not surprising as flow can affect the EC permeability, allowing the exchange of molecules with the tissues. Among all the drugs, only bosentan showed a trend towards disruption but it was not deemed significant (mean of 21.0 ± 5.0, N=4, ns).

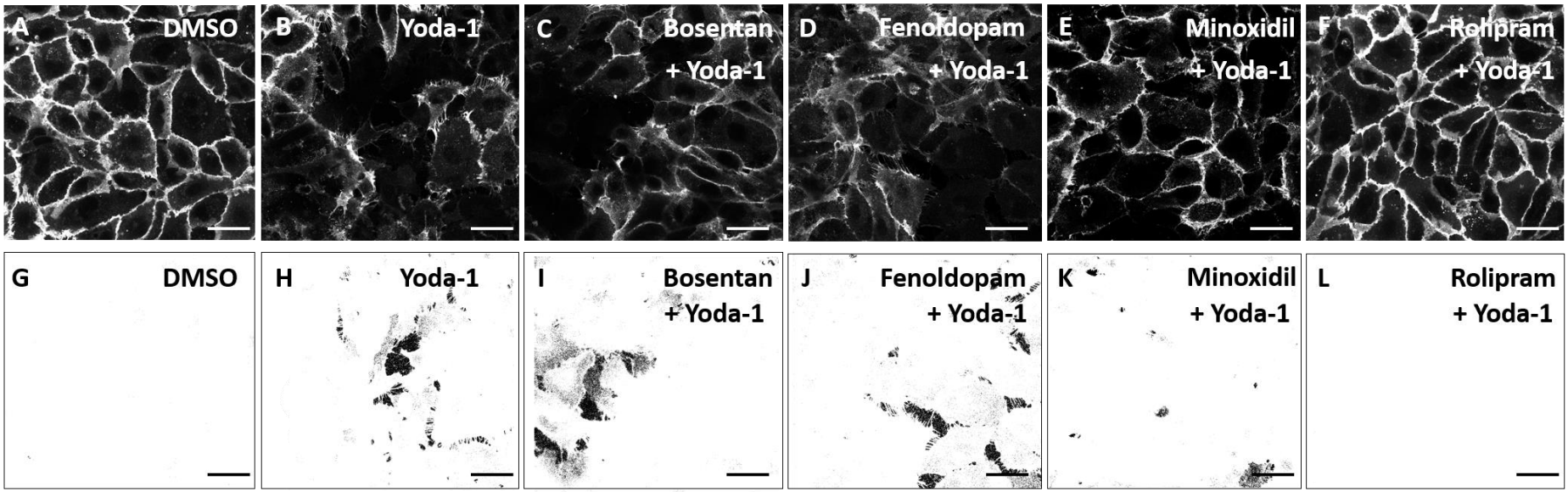

Figure 7.9 Representative confocal pictures of assessment of EC junctional integrity with DIVI-related drugs in the presence of Yoda-1 (1 µM) at 1 hour. HUVEC were grown for 24 hours, treated with Yoda-1 1 µM for 24 hours and then with the drugs at 100 µM for 1 hour. Cell junctions are stained with CD31. Six images were taken in random fields of view, four experiments were conducted in total. Scale bars represent 20 µm. 63x.

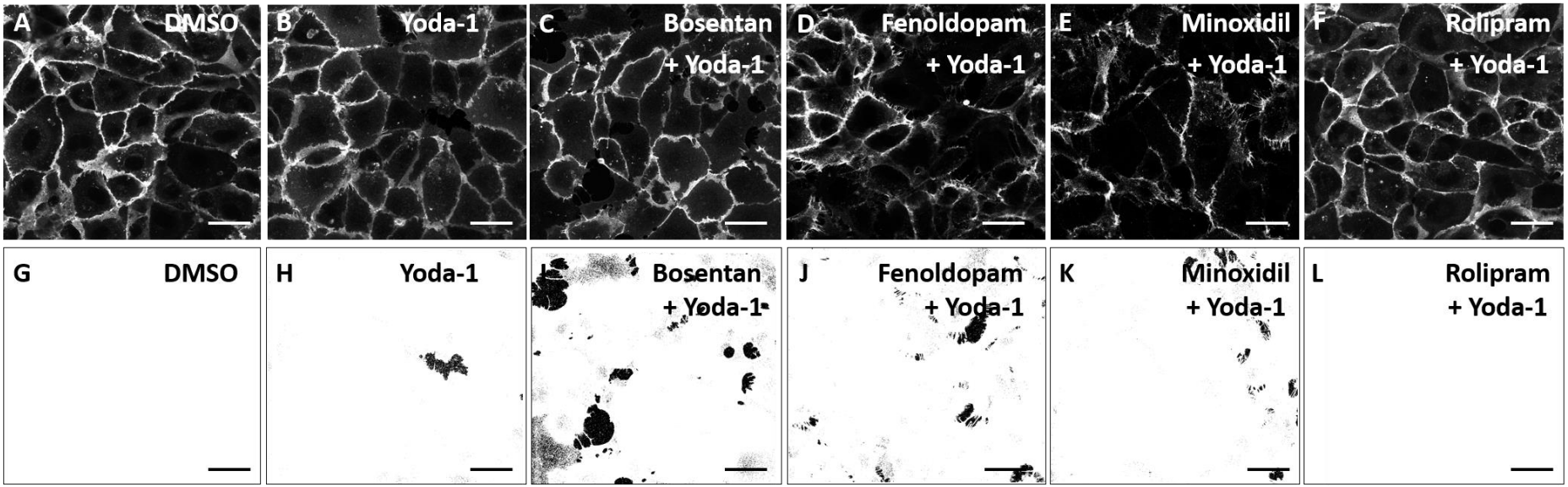

Figure 7.10 Representative confocal pictures of assessment of EC junctional integrity with DIVI-related drugs in the presence of Yoda-1 1 µM at 24 hours. HUVEC were grown for 24 hours, treated with Yoda-1 1 µM for 24 hours and then with the drugs at 100 µM for 24 hours. Cell junctions are stained with CD31. Six images were taken in random fields of view, four experiments were conducted in total. Scale bars represent 20 µm. 63x.

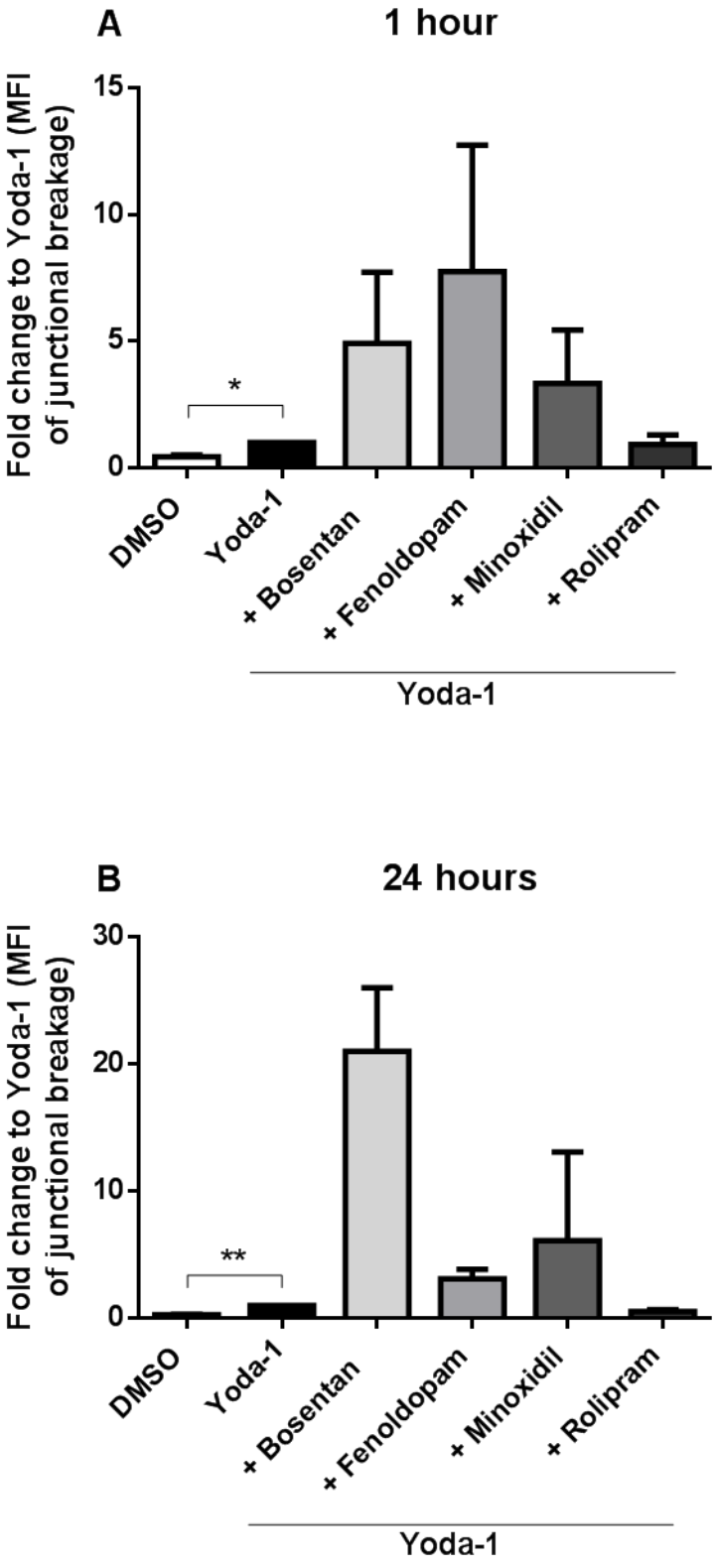

Figure 7.11 Assessment of junctional disruption at 1 hour (A) or 24 hours (B) in HUVEC. HUVEC were grown for 24 hours, treated with Yoda-1 1 µM for 24 hours and then with the drugs at 100 µM for 1 and 24 hours. Data are normalised to Yoda-1 control and expressed as MFI fold change, and represent mean ± SEM of 4 independent experiments, analysed by one-way ANOVA followed by Dunnett's post test. *$p < 0.05$, **$p < 0.01$, compared to Yoda-1.

7.3.6 Bosentan and fenoldopam in the presence of Yoda-1 cause EC but not SMC death

To investigate the effect on cell death, the drugs were incubated with Yoda-1 and the same ATP viability assay used in **chapter 4**, section **4.2.3** was used. The assay was performed using three drug concentrations (1, 10 and 100 µM) at 24 hours, as data from **chapter 4** showed no effect at shorter time points. The same protocol used in **chapter 4** was used with the exception that cells were pre-treated with Yoda-1. Cells were seeded in a 96 well plate and grown for 24 hours. Then they were treated with Yoda-1 (1 µM) for 24 hours and then drugs for a further 24 hours.

In EC, 100 µM bosentan (in the absence of Yoda-1) induced 17.6 ± 2.4 % cell death ($p < 0.001$, N=5) (**Figure 7.12**). This differs from data observed in monocultured HUVEC, where bosentan did not induce cell death. Bosentan with Yoda-1 caused 37.1 ± 3.8 % cell death ($p < 0.01$, N=5). This is novel and suggests that the effect of the drug is enhanced by flow. Bosentan was also the only drug causing an effect on cell death on both EC and SMC when co-cultured.

Fenoldopam at 100 µM alone induced 24.1 ± 2.9 % cell death compared to DMSO control ($p < 0.0001$, N=5). This aligns with data in single HUVEC from **chapter 4**, section **4.2.3**. Fenoldopam with Yoda-1 induced 72.6 ± 4.9 % cell death ($p < 0.0001$, N=5), indicating that the effect of fenoldopam is greatly increased by flow. Fenoldopam was not found to increase cell death on EC and SMC in co-culture. The other drugs had no effect on cell death.

In SMC, none of the drugs induced cell death at 24 hours (**Figure 7.13**). This is in line with data from **chapter 4**, section **4.2.3** where in single cells none of the drugs was cytotoxic to SMC.

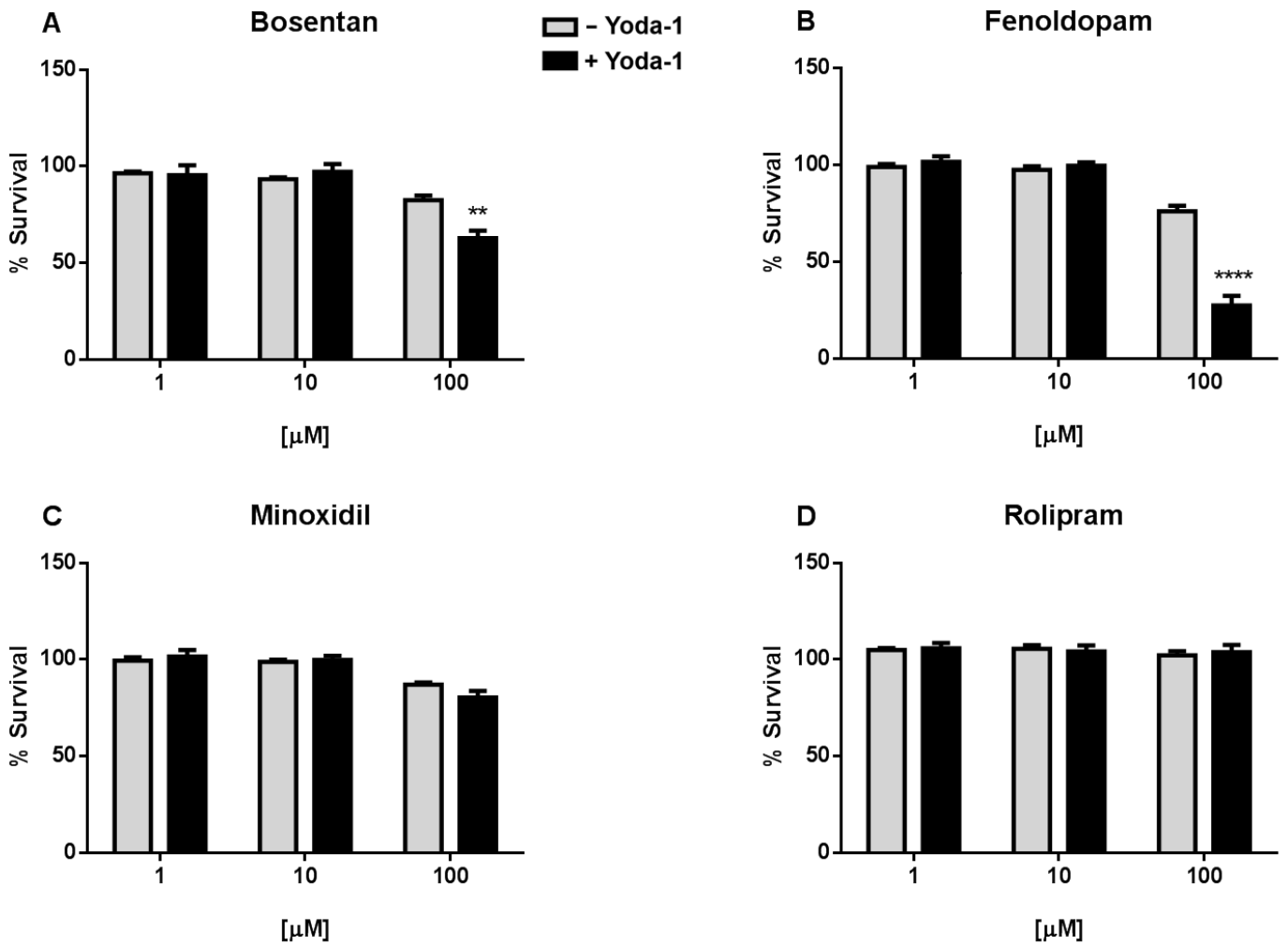

Figure 7.12 Assessment of cell death using an ATP assay in HUVEC pre-treated with Yoda-1 1 µM. HUVEC were grown for 24 hours, pre-treated with Yoda-1 1 µM and then treated with the drugs at 1, 10 and 100 µM for 24 hours. Data are expressed as % survival compared to control. 100 % represents no death. Data represent mean ± SEM of 5 independent experiments, analysed by two-way ANOVA followed by Dunnett's post test. **p < 0.01, ****p < 0.0001.

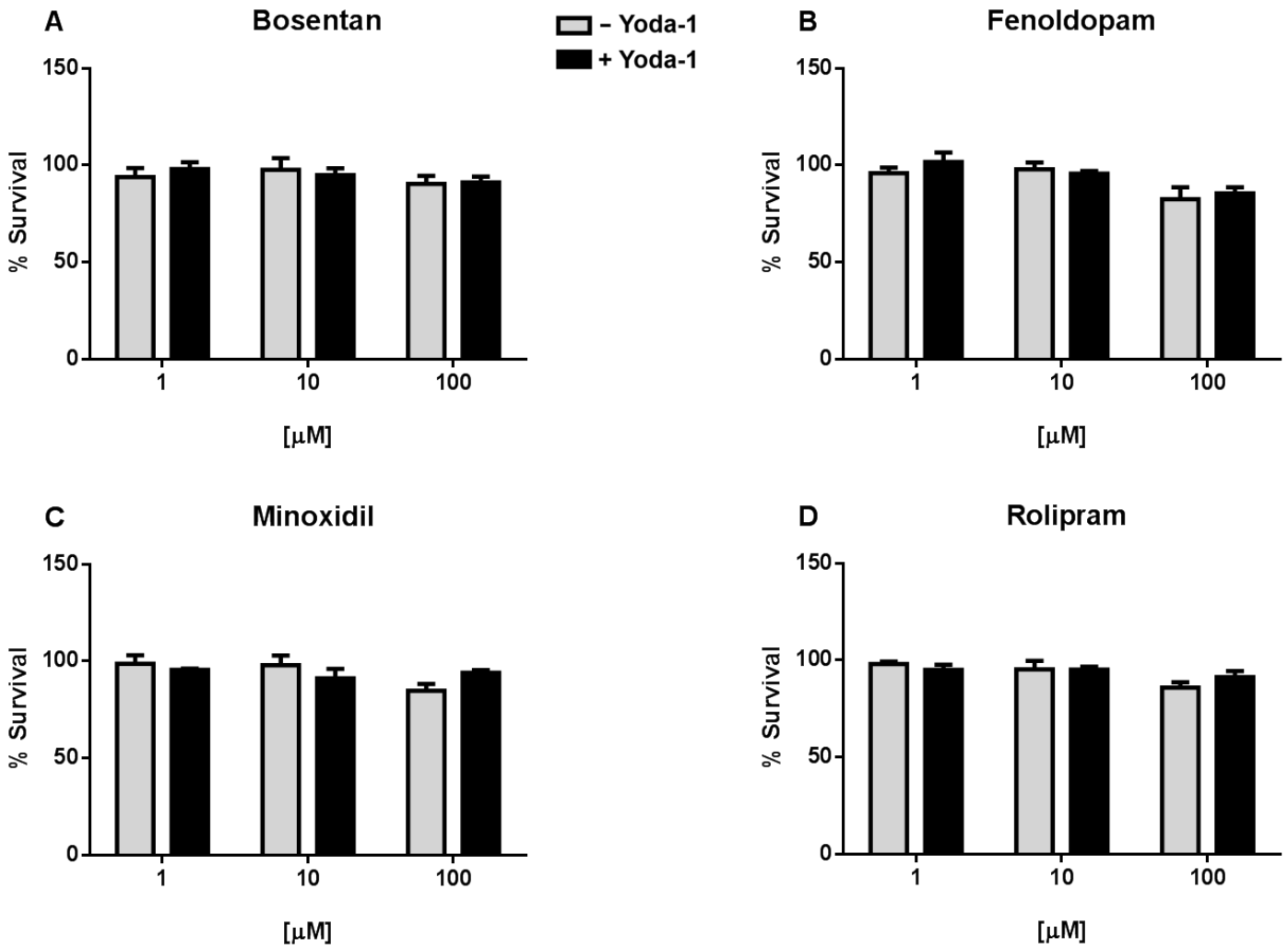

Figure 7.13 Assessment of cell death using an ATP assay in HCASMC pre-treated with Yoda-1 1 μM. HUVEC were grown for 24 hours, pre-treated with Yoda-1 1 μM and then treated with the drugs at 1, 10 and 100 μM for 24 hours. Data are expressed as % survival compared to control. 100 % represents no death. Data represent mean ± SEM of 5 independent experiments, analysed by two-way ANOVA followed by Dunnett's post test.

In summary, these data have demonstrated that flow affects only bosentan and fenoldopam and not the other drugs.

7.4 Discussion

In this final chapter, the effects of DIVI-related drugs were investigated in HUVEC in the presence of a molecule, Yoda-1, that mimics shear stress, the frictional force that blood flow exerts on EC in the vessel (refer to **Introduction**, section **1.7**). It has been suggested that shear stress plays a role in DIVI[203]. Alterations in shear stress can result in leukocyte adhesion, endothelial junctional breaks, breakdown of the vessel wall integrity, breaks in the internal elastic lamina, and haemorrhage[475,476].

Flow is studied *in vitro* using microfluidic devices, which have three-dimensional complexity, enable cell-cell interactions and the relevant extracellular environment that is typical of living tissues. These devices, composed of submillimetre-scale channels through which liquid flows in a controlled manner, are an attractive way for the investigation of blood vessel function[477]. Precast three-dimensional micro networks can be engineered using different polymers and EC seeded on top of which blood flow can be mimicked and regulated. For example, in the production of a system that replicated aspects of angiogenesis, where micro vessels when activated produced new branches and recruited mural cells previously seeded in the device[478]. Nonetheless, although these models resemble the cellular arrangement and responses of *in vivo* vessels, for drug discovery in early safety these may not be optimal.

Complicated *in vitro* models have also used a parallel plate design[479]. An innovative co-culture model utilising a combination of parallel plates with flow and a transwell with EC and SMC co-culture has also been developed[480]. In this study, EC were either cultured alone or co-cultured with SMC under static conditions or subjected to normal levels of laminar shear stress of 15 dyn/cm^2 by using a parallel-plate co-culture flow chamber system. It was demonstrated that both shear stress and SMC could increase EC migration, and was associated with the increased expression of histone deacetylase 6 (HDAC6) and low level of acetylated tubulin. Another system focussed on the study of platelet aggregation by flowing whole blood and RBC and

leukocyte entry into the underlying tissue. It has been shown in the same study that adding a pro-inflammatory stimulus induced EC activation, promoted platelet aggregation and the formation of a blood clot[339].

All these models are complicated to construct and difficult to be standardised across different laboratories. The scope of this thesis is to create a simple *in vitro* system to allow quick screening of a large set of compounds. Therefore Yoda-1, a small molecule activator of Piezo-1 cation channels, was used to mimic flow. Piezo-1 mediates flow-induced release of ATP from EC, leading to the activation of the G_q/G_{11}-coupled purinergic $P2Y_2$ receptor and subsequent phosphorylation of Akt and eNOS leading to NO production[338]. siRNA-mediated knockdown of Piezo-1 was shown to inhibit shear stress-induced increases in Ca^{2+} and also blocked phosphorylation of Akt and eNOS in response to shear stress in human umbilical arterial EC (HUAEC)[338]. In addition, several studies demonstrated that EC fail to align to the direction of flow when Piezo-1 is knocked down or partially removed[336,337,481,482].

Yoda-1 was chosen because 1) it selectively activates Piezo-1 channels, which have been shown to be important in the regulation of shear stress on EC; 2) it mimics *in vivo* flow without requiring a complex flow device.

Yoda-1 induces effects similar to those generated by Piezo-1 in response to flow[338]. Yoda-1 increases Ca^{2+} and the effect is reduced after knockdown of Piezo-1. Yoda-1 also induces Akt and eNOS phosphorylation, increases nitrate formation and causes ATP release, similarly to the effects of Piezo-1 in response to flow. All these responses are reduced after knockdown of Piezo-1. In addition, it was confirmed that Yoda-1-induced effects were dependent on ATP[338]. Knockdown of $P2Y_2$ or G_q/G_{11} or incubation of HUAEC with apyrase, the enzyme that degrades ATP, or with an antagonist of $P2Y_2$ receptors resulted in inhibition of Ca^{2+} increases and Akt/eNOS phosphorylation. These experiments demonstrate that Yoda-1-induced signalling pathways align with Piezo-1-mediated pathways induced by flow and involve $P2Y_2$ and G_q/G_{11}.

The first step was to find a working concentration of Yoda-1 that could be used in investigating hallmarks of DIVI. This was carried out using two methods: 1) the ATP luminescent assay used

in the previous chapters; and 2) confocal imaging, to have an additional confirmation. The ATP luminescent assay showed that 1 μM Yoda-1 is not toxic to the cells at 1, 4 or 24 hours, however higher concentrations did cause cell death in HUVEC. Using immunofluorescence, concentrations up to 2 μM were tested and were found to be non-cytotoxic in HUVEC.

It was then confirmed that Yoda-1 mimicked the effects seen with shear stress *in vivo* reported in the literature. An important step was also to make sure that Yoda-1 would have a continued and sustainable effect (for 24 hours or more), similar to those seen in EC undergoing long term flow conditioning[483]. VWF endothelial release and cell death were assessed at this time point. In accordance with the literature[338], it was observed that phospho-eNOS and phospho-Akt levels were increased by Yoda-1 treatment, to a similar degree to the shear stress control experiments. It was also confirmed that Yoda-1 increases expression of ICAM-1 and not VCAM-1 similarly to flow. In the control experiments shear stress has a similar effect on these proteins and these results had been previously reported[473].

Subsequent experiments focussed on investigating the same hallmarks of DIVI described in previous chapters in the presence of the flow mimetic, Yoda-1. There is evidence that VWF release is modulated by flow and it has been shown that laminar shear stress increases VWF release within few hours of exposure[484,485]. As such, VWF release from EC was measured and showed that Yoda-1 caused a slight VWF release at 1 hour and a significant release at 24 hours compared to DMSO control. The drugs that had in previous experiments induced significant VWF release both acutely and at 24 hours did not induce an effect in the presence of the flow-mimetic. In monocultured HUVEC in the absence of Yoda-1 and in co-culture with SMC bosentan and fenoldopam caused VWF release. Interestingly, in the presence of shear stress the effect of these drugs on VWF release is reduced. This discrepancy with data from monocultured HUVEC in the absence of Yoda-1 (chapter 4) could relate to variability in the assay, an effect driven by the low n values used in the study.

Similarly to what has been discussed in **chapter 4**, the change in WPB size was not observed with the drugs nor with the positive control thrombin. It would have been useful to add a control e.g. statins which are reported to significantly decrease the size of WPB and this is something that is worth investigation in the future.

Following assessment of VWF release, focus was redirected to investigating endothelial junction integrity. Yoda-1 induced significant EC junctional disruption at 1 hour and 24 hours compared to DMSO control monolayers. As discussed earlier, flow affects EC permeability[486] however in these studies none of the drugs caused significant EC monolayer disruption in the presence of Yoda-1. Although an observed trend to increase EC disruption was observed for bosentan and fenoldopam at 1 hours, bosentan at 24 hours. This finding differed from monocultured cells in which fenoldopam at 1 hour and minoxidil at 24 hours induced disruption. In these studies, it appears as though Yoda-1 is having a protective effect. This is contradictory to all reported DIVI studies where the lesions were found *in vivo* and had been exposed to flow. This may suggest that SMC play a crucial role in the interaction with EC in generating lesions when exposed to the drugs under physiological flow *in vivo*, or it conversely it may indicate that more evidence is required to demonstrate that DIVI occurs humans.

Finally, the effect of a shear-stress mimetic on cell death was assessed by ATP luminescent assay at three drug concentrations at 24 hours. Bosentan and fenoldopam alone were cytotoxic at the highest concentration. The toxic effect of fenoldopam had been shown previously in EC (**chapter 4**), however fenoldopam induced cell death to a greater extent. Experimental conditions were different, and this may account for the observed differences. It is possible that cell density plays a role in this and growing the cells for one more day to allow pretreatment with Yoda-1 affected this result. To confirm this, assessment of expression markers could be performed to understand if 24 hours more in culture make a difference.

Both fenoldopam and bosentan induced greater cytotoxicity at the highest concentration when incubated with Yoda-1 compared with when they were administered alone. This suggests that flow plays an important role in their mechanism of action, by inducing cell markers that alter the response to these drugs.

Bosentan did affect SMC cell death in co-culture. This suggests that the EC-SMC interaction plays a fundamental role in bosentan mechanism of causing DIVI and has a stronger influence on determining SMC cell death than flow.

The observation that bosentan induced cytotoxicity to both EC and SMC in co-culture indicates that the effect of bosentan is greatly influenced by EC-SMC interaction and flow. Conversely, as no SMC cytotoxicity was observed following treatment with fenoldopam it is possible to summarise that flow is a more important regulator of this effect than the presence of SMC.

A summary of the effects of the drugs under flow is given in **Table 7.1**. The addition of the flow-mimetic failed to show an effect with rolipram and as for the co-culture it was not able to elicit the same DIVI phenotype for all the drugs. It is accepted that the experimental approach explored in these studies may be too reductionist, in terms of model complexity, and in the future there might be the need of investigating more complete systems (this will be discussed in **chapter 8**). However, using more complex systems was beyond the scope and aims of this work. In the general discussion (**chapter 8**), other approaches will be explored in order to find a physiological model that is simple enough so that would allow quick screening of drugs in development.

Effect	Time course (hours)	Bosentan	Fenoldopam	Minoxidil	Rolipram
VWF release	1	×	×	×	×
	24	×	×	×	×
EC junctional breakage	1	×	×	×	
	24	×	×	×	×
Cell death	24	✓✓	✓✓✓✓	×	×

Table 7.1 Summary of the effects of DIVI-related drugs in the presence of the flow-mimetic Yoda-1. The following hallmarks have been investigated in this chapter: (1) VWF release from EC, (2) disruption of the EC monolayer and (3) EC and SMC death. ✓✓✓✓= very significant effect ($p < 0.0001$); ✓✓= very significant effect ($p < 0.01$); ×= no different to Yoda-1 treatment alone.

8. General Discussion

The aim of this PhD thesis was to define a toxicological limit around which the therapeutic index (TI) of a drug can be set, in order to reduce in the future the number of DIVIs seen in the clinic.

Within this body of work, DIVI has been investigated in monocultured EC and SMC, in co-culture (EC-SMC) and in a model that mimics flow *in vitro* under static conditions. However, no classical model could be developed that consistently recapitulated the major features of DIVI (apoptosis, barrier permeability, adhesion molecule upregulation) using drugs with a range of mechanisms of action that are known to cause DIVI in pre-clinical animal models. Importantly, DIVIs are likely to be mediated by an off-target toxicity rather than an on-target action of the drug. This is suggested by the fact that DIVI-related drugs have all different mechanisms of action and investigation on which off-target receptors might be implicated still has to be conducted. The drugs have been tested in the assays presented within this thesis at a limit concentration (100 µM) that would not be administered to humans but was important to define limits of off-target toxicity. In the future, more studies should be aimed at confirming the on vs. off-target effects either by using other compounds with comparable mechanism of actions but developed from different chemical templates or antagonism of specific sites of action.

This **Discussion** will consider some of the factors that may have contributed to these findings, and the learnings that can be applied to our understanding of DIVI, and suggest directions for future research that may be to address these issues.

8.1 VWF release with DIVI-related drugs *ex vivo* and *in vitro*

DIVI is an *in vivo* phenotype in specific blood vessels described in pre-clinical studies. One reason for the difficulties in generating a reductionist, humanised model *in vitro* might thus have been cross species translatability. It was therefore necessary to first recapitulate DIVI *ex vivo* in relevant animal tissue, in a vessel in which DIVI has been widely described. For this, the rat mesentery artery was chosen as it has been reported as a site of DIVI by numerous groups[124,198,203,400]. Four drugs each with different mechanisms of action (refer to **Introduction**, **Table 1.1**), were selected from compounds that are known to cause DIVI in preclinical species, that are approved in the clinic.

Here, vessel explants were treated with the drugs and investigated for features of DIVI. Endothelial release of VWF was used as a DIVI biomarker, since its release signifies both EC activation and damage. It has often been described in the literature as a potential marker of DIVI in animals and a possible marker of vascular injury in patients[35,198,201,203]. Additionally, other properties make it a suitable target biomarker include the release into the blood that allows assessment through routine blood monitoring, and a short half-life (12 hours) that gives a definitive timestamp for acute damage.

Most DIVI studies involve drug treatment *in vivo*, with separate animals for control and drug treatment, which requires four animals per group for the study to produce power. In this study however, for each replicate an explant from one animal was sectioned to enable multiple drug conditions to be carried out in parallel. This greatly reduced experimental variation and produced a more accurate vehicle control response.

Using this technique, it was demonstrated that a response seen *in vivo* (VWF release from EC into plasma) can be reproduced *ex vivo* (albeit not release into plasma but loss from EC) for three of the drugs tested (bosentan, fenoldopam and minoxidil) however this was not observed following rolipram treatment.
VWF release in the *ex vivo* experiments appeared similar between all three drugs excluding rolipram, as subsequent expression of VWF within the tunica media as localised by the SMC stain α-SMA was not present.

Rolipram has previously been reported to effectively enter HUVEC. Incubation for 2 minutes with 50 µm of rolipram induced a 85 % increase in cAMP production[487]. The inability of rolipram to release VWF is surprising given that both rises in cAMP and cytosolic calcium have been documented to stimulate WBP membrane fusion[488]. Perhaps for a rolipram-dependent VWF release in these experiments, complementary cellular signals are required, for example, shear stress has been documented to increase cAMP levels in cultured HUVEC[489]; it is plausible that this synergistic effect is necessary to induce release.

Previous studies have described acute VWF release (monitoring within initial 24 hours) *in vivo* with fenoldopam and ZD6169, a K^+ channel opener[198,201]. Conversely, bosentan and rolipram

VWF release *in vivo* has never been reported (**Table 8.1**). In fact, bosentan was reported to not affect VWF release in patients with systemic sclerosis and pulmonary hypertension[397], a condition characterised by high levels of VWF[490]. However, in these trials, VWF plasma levels were monitored as an end stage, perhaps after resolution, following 12 months of bosentan treatment, which makes the comparison with the study reported here more challenging.

Studies have reported that fenoldopam induced VWF release into plasma at 2 hours and 6 hours, but returned to baseline at 24 hours when lesions were identified by immunohistochemistry *in vivo* in rats[198],[201]. Minoxidil has not been investigated for VWF release but another K^+ channel opener that released VWF in dogs is ZD6169[201]. ZD6169 was associated with transient increases in VWF plasma levels at 1, 3 and 6 hours post-dosing in dogs. However, plasma VWF levels declined at all doses, in all dogs, 24 hours post-dose when histopathology confirmed morphologic evidence of medial necrosis and haemorrhage.

There are several implications from the observations in this *ex vivo* model. First, it is possible to recapitulate at least one feature of DIVI with some drugs in a rat vessel explant. This *ex vivo* model uses the most relevant tissue, rat mesenteric artery, but lacks two potentially important *in vivo* features, namely drug-induced increases in local blood flow, and the actions of leukocytes, erythrocytes and platelets. In addition, there is no nervous system influences in this model, which may alter the vascular physiology (e.g. blood pressure). As described in the **Introduction**, section **1.5.1**, one hypothesis regarding the mechanism of DIVI suggests that global or local increases in blood flow lead to vascular damage, with direct toxic effect of the drug on the vessel cells themselves. However, these data indicate a direct effect of three drugs on the EC themselves in the absence of changes in blood flow, at least for VWF release. Other key features of DIVI may still require increased blood flow, and this deserves further attention in the future. One approach may be to use cannulated, perfused vessels (as used in pressure myography, for example). A limitation with a significant increase in the complexity of the model however is a reduction in the throughput for drug screening, a consequence we were keen to avoid. A second implication of the data present with this *ex vivo* model is that, even with what was considered to be the most relevant tissue/animal model, this DIVI phenotype could not be recapitulated following rolipram treatment. It is possible that a local increase in blood flow is a necessary prerequisite for the effects of rolipram therefore making

it unlikely that the rolipram phenotype could be mimicked in an *in vitro* model – exactly as was ultimately found in the models tested in these studies. A further implication is that there must be some mechanistic difference between DIVI induced by rolipram, and DIVI induced by the other drugs that were tested, as rolipram was the only drug that induced no effect in all the assays tested, *ex vivo* and *in vitro*. Consequently, it may be difficult to ever generate a screening model that will reliably predict all drugs that cause DIVI. However, pharmaceutical industries generally aim for a 70 % accuracy in their safety screens, and it is unlikely to produce a biological assay that is 100 % accurate. In assay development, sensitivity and specificity are the most important factors.

Following *ex vivo* investigation of DIVI, the drugs were tested for endothelial VWF release *in vitro*, using (1) monocultured EC; (2) a co-culture of EC-SMC; and (3) monocultured EC exposed to the flow-mimetic Yoda-1. These effects are summarised in **Table 8.1**. The experiments conducted within this thesis are highlighted in the red box, to compare with previous *in vivo* studies showing VWF release in animals or patients.

It was observed that for bosentan, VWF release at 1 hour is not affected by more complex *in vitro* systems. In fact, using monocultured EC, co-culture or the flow-mimetic Yoda-1 did not increase VWF secretion. In monoculture and co-culture, but not when Yoda-1 was added, bosentan induced VWF release from EC acutely. At 24 hours, bosentan induced VWF release in monoculture and co-culture, the monocultured EC produced a higher (around 25 % reduction in % VWF-positive cells at 1 hour and 25 % at 24 hours compared to DMSO control) effect compared to co-culture (15 % reduction at 1 hour and 25 % at 24 hours compared to DMSO control), suggesting that interaction with SMC does have a role in reducing the VWF released from EC. Interestingly, Yoda-1 did not induce release (acutely or at 24 hours) when added with bosentan. Thus, perhaps it is possible to infer that EC-SMC interaction plays a more important role in bosentan induced VWF release than flow.

Drug	Time course (hours)	*In vivo* (previous studies)	*Ex vivo*	*In vitro*		
			Rat vessel explant	Monocultured EC	Co-culture EC-SMC	EC with Yoda-1
Bosentan	1	No change in patients with systemic sclerosis[397]	n/a	✓	✓	×
	24		✓	✓✓✓	✓✓	×
Fenoldopam	1	Release at 2,4,6 hours in rats[198,201]	n/a	✓	✓✓	×
	24		✓	✓✓	✓✓✓	×
Minoxidil	1	Release at 1,3,6 hours with ZD6169[201]	n/a	×	×	×
	24		✓	✓✓	✓✓✓	×
Rolipram	1	n/a	n/a	×	×	×
	24		×	×	×	×

Table 8.1 Comparative effects of VWF release seen *in vivo* in previous studies with *ex vivo* and *in vitro* investigation conducted within this thesis. ✓✓ ✓= very significant effect ($p < 0.001$); ✓✓= very significant effect ($p < 0.01$); ✓= significant effect ($p < 0.05$); ×= no effect.

Fenoldopam induced VWF release acutely in monoculture and co-culture, but not in the presence of Yoda-1, with the greatest effect observed in a co-culture model, suggesting that EC-SMC interaction plays an important role in its mechanism. At 24 hours, VWF secretion was induced again only in monocultured EC and in co-culture, but not with Yoda-1.

Minoxidil did not induce VWF secretion in monoculture, nor in co-culture at 1 hour, release was seen however at the 24 hour time point. As observed for the other drugs, Yoda-1 caused no significant release compared to the Yoda-1 control.

Rolipram did not induce VWF secretion in any of the biological systems. It may be useful to use a different compound in the same pharmacological class as rolipram, such as the PDE IV inhibitor cilomilast, to understand whether absence of VWF release with rolipram relates uniquely to this drug or is a common factor for the entire class.

Unfortunately, the rat vessel explant was only tested at 24 hours because of limited availability of tissue, and thus a comparison with the acute *in vitro* studies cannot be determined. At 24 hours the *in vitro* systems replicated the effect on VWF release observed in the vessel, except for when Yoda-1 was added, as Yoda-1 *in vitro* at 1 or 24 hours in combination with the drugs did not induce significant release compared to the Yoda-1 control.

In order to build on our understanding, the next steps would be to undertake these experiments in a true shear stress environment. Furthermore, using *in vitro* assays to investigate DIVI resolution would also add to our understanding. Drug could be incubated for the above 24 hour period, then removed and after 7 days of culture VWF release from the endothelium re-probed.

The vessels used in the rat explant had been conditioned by flow in the animal, however during the *ex vivo* drug treatment experiments flow was absent. Release of NO, which occurs when EC are exposed to flow (and also when EC are exposed to Yoda-1[340]), affects VWF secretion[491]. It has been suggested that endogenously produced NO may dampen the regulated pathway (i.e. stimulus-induced) of VWF secretion. In a study in humans, healthy subjects received placebo or an infusion of the NOS inhibitor N-monomethyl-k-arginine (L-

NMMA), which decreases the production of endogenous NO[491]. After this pre-treatment all volunteers received a histamine infusion and blood samples were collected for determination of VWF plasma levels. It was demonstrated that the stimulatory action of histamine on VWF release could be induced *in vivo*, as demonstrated by the increased plasma VWF-antigen levels, and that it may be inhibited by endogenous production of NO, as shown by an enhanced effect of histamine-induced VWF release during NOS inhibition. Given this finding, it is possible that stimulation of NO production by Yoda-1 on EC inhibits drug-induced VWF release. The vessel explant, where flow is absent and thus production of NO may also be reduced, induced VWF release. However, this has not been investigated and would need confirmation.

It may be then questioned as to why previous *in vivo* studies (thus under flow) have been able to demonstrate VWF release in rats and dogs with the same drugs tested here[198,201] (**Table 8.1**). These studies showed that release occurred only acutely up to 6 hours after drug treatment and that VWF plasma levels returned to baseline at 24 hours, when vascular damage was also detected histologically. These *in vivo* studies could suggest that either physiological flow (rather than a flow-mimetic) is required, or perhaps both flow and a co-culture are needed *in vitro* to accurately determine DIVI risk.

In the experiments presented in this thesis continuous VWF release, which would help understand how the drugs affect the kinetics of the release, was not monitored and is something worth investigation in the future. Cells could be either treated with inhibitors of the clathrin-mediated exocytosis pathway or treated with inhibitors of protein synthesis to prevent *de novo* production of VWF[214,492]. Finally, VWF secretion could be tested using drugs from the same families, to understand whether there is a common mechanism underlying one entire class of compounds or whether it is a drug-specific effect.

8.2 Investigation of other markers of DIVI *in vitro*

Next, the reported features of DIVI was investigated *in vitro* using human cells model systems. Clear histopathological features of DIVI, as mentioned in **1.3.1**, are (1) activation and injury of

EC and SMC; (2) inflammation; and (3) extravasation of RBC due to disruption of vascular integrity. Cell activation (measured by assessment of EC junctional integrity), inflammation and death have been investigated in monocultured EC and SMC, in circulating blood cells and in co-culture. The third feature, extravasation of RBC, is something worth investigating in the future and will be discussed in **section 8.3**.

8.2.1 EC junctional breakage

As mentioned in the **Introduction**, section **1.6.1**, under physiological conditions the endothelium forms a selective barrier with adherens, tight and gap junctions. However, this selective membrane can be altered in pathological situations and the monolayer disrupted. A marker investigated in DIVI in monocultured EC and in EC using the flow-mimetic Yoda-1 was EC junctional breakage and a summary of the effects of the drugs is depicted in **Table 8.2**, where also the responses of the drugs in previous *in vitro/vivo* studies are presented. Disruption of the EC barrier can facilitate transendothelial migration of immune cells to the arterial intima and induction of vascular inflammation. Depending on the stimulus, activated EC can return to the quiescent non-activated phenotype or can progress to apoptosis.

Drug	Time course (hours)	*In vitro/vivo* (previous studies)	*In vitro*	
			Monocultured EC	EC with Yoda-1
Bosentan	1	No effect in humans[493]	×	×
	24		×	×
Fenoldopam	1	Increased permeability *in vitro*[79]	✓	×
	24		×	×
Minoxidil	1	Increased permeability *in vivo* and *in vitro*[494]	× (trend)	×
	24		✓✓	×
Rolipram	1	Inhibition permeability induced by thrombin *in vitro*[373]	×	×
	24		×	×

Table 8.2 Comparative effects of EC junctional breakage seen *in vitro/vivo* in previous studies with *in vitro* investigation conducted within this thesis. ✓✓= very significant effect ($p < 0.01$); ✓= significant effect ($p < 0.05$); ×= no effect.

In these studies, bosentan did not cause EC junctional breakage in monocultured EC with, or without Yoda-1. Bosentan has been shown *in vivo* to not induce significant changes in capillary permeability assessed in patients with systemic sclerosis using laser Doppler fluxmetry combined with iontophoresis and fluorescence microscopy[493]. The data presented here are in line with these reports.

In monocultured EC, fenoldopam caused breakage of the junctions acutely at 1 hour. However, the effect was not observed at 24 hours and this pattern mimicked the response of the positive control thrombin, which also caused disruption at 1 hour but not at 24 hours. This suggests that fenoldopam acts rapidly on EC junctions but its effect is short lived. Fenoldopam at a high concentration (100 μM), combined with *in vivo*-derived hemodynamics, has been shown *in vitro* to increase permeability at 28 and 48 hours using a co-culture of rat EC and SMC[79]. Unfortunately, because of intellectual property the details of the study are not available. The addition of Yoda-1 inhibited the effect on junctional breakage seen at 1 hour with fenoldopam, suggesting that flow may exert a protective effect.

Minoxidil showed a trend toward junction disruption in monocultured EC at 1 hour but the effect was not significant. However at 24 hours, minoxidil caused a significant response (more than 10-fold compared to DMSO control) on junctional disruption, suggesting that the mechanism of action may require hours to induce EC monolayer disruption but the effect is sustained for at least one day. This suggests that secondary pathways and downstream effectors may be regulating the observed effect. These data are agreement with previous *in vivo* observations in rodents and *in vitro* in Caco-2 cells, where minoxidil was found to increase permeability[494].

To understand DIVI resolution, which is still unclear, it would be interesting to know whether the effect of minoxidil is irreversible on the junctions. However, this is not likely to be the case because, as mentioned above, irreversible EC activation would lead to cell death and in the cell death assays (discussed in section **8.2.3 and 8.2.4**) minoxidil did not cause any EC nor SMC death. Interestingly, Yoda-1 inhibited the effect on the junctions at 24 hours.

Rolipram did not cause EC monolayer disruption in monocultured EC and this was unaltered with the addition of Yoda-1. Rolipram has been reported *in vitro* in HUVEC to restore the EC

barrier after disruption with thrombin[373]. Roflumilast, a PDE IV inhibitor like rolipram, was reported *in vivo* in rats to restore the EC monolayer in a similar manner[373]. These experiments are discussed in detail in **chapter 4**.

8.2.2 EC inflammation

The drugs were then tested for their ability to induce inflammation in EC, which is a marker of DIVI[170]. **Table 8.3** summarises the effects seen in this thesis.

Bosentan increased both ICAM-1 and VCAM-1, compared with fenoldopam that only increased VCAM-1 expression at 24 hours. However, these effects were relatively small when compared with the ICAM-1 and VCAM-1 expression induced by TNF-α. Previous studies have suggested that bosentan has no effect on VCAM-1 or ICAM-1 expression in patients with systemic sclerosis[493,495]. This discrepancy with previous reports may be related to differences between *in vivo* and *in vitro* studies[372], where binding to plastic, binding to proteins and interaction between the culture medium and the cells are factors that may affect the results. In addition, patients with systemic sclerosis have very different vasculature and physiological conditions compared with an *in vitro* model[496].

Fenoldopam has been reported to elevate several inflammatory pathways *in vitro* using a co-culture of rat EC and SMC and *in vivo*-derived hemodynamics[79]. It has been shown that the hyaluronan-related signalling, which plays a key role in inflammation by recruiting inflammatory cells and releasing pro-inflammatory cytokines[496], is upregulated after treatment with fenoldopam.

Drug	Time course (hours)	*In vitro/vivo* (previous studies)	*In vitro*	
			Monocultured EC	
			ICAM-1	VCAM-1
Bosentan	24	No effect in patients with systemic sclerosis[493,495]	✓	✓✓
Fenoldopam	24	Increase in several inflammatory pathways *in vitro*[79]	×	✓
Minoxidil	24	Increased inflammation in dogs[52]	×	×
Rolipram	24	Downregulation of pro-inflammatory cytokines in the central nervous system in rats[497]	×	×

Table 8.3 Comparative effects of EC inflammation seen *in vitro/vivo* in previous studies with *in vitro* investigation conducted within this thesis. ✓✓= very significant effect ($p < 0.01$); ✓= significant effect ($p < 0.05$); ×= no effect.

Minoxidil and rolipram did not affect VCAM-1 nor ICAM-1 expression in EC. There is evidence of inflammation with minoxidil reported in DIVI in dogs in the tunica adventitia in coronary arteries, but these effects have been described only in dogs and not in humans[52]. Rolipram has been shown to have an anti-inflammatory effect in rats in the central nervous system, where it inhibits TNF-α at both the mRNA and protein levels, and downregulates IL-13, a pro-inflammatory cytokine of T cell origin[497]. In addition, rolipram has been found to downregulate antigen-driven proliferation and cytokine gene expression for IL-5 and IFN-γ in human peripheral blood mononuclear cells[497].

8.2.3 EC death

Drug-induced EC death (**Table 8.4**) was investigated using ATP release as a marker for viability. No drug-dependent cell death was observed at the 1 hour and 4 hour time points in monoculture and therefore only the 24 hour time point was investigated in co-culture and in the presence of Yoda-1. Bosentan did not induce toxicity in EC, but did affect EC death in the presence of SMC or Yoda-1. Fenoldopam did induce cell death after 24 hour drug incubation, with approximately 50 % of the cells showing death. Although fenoldopam-induced cytotoxicity has been observed *in vivo* in the rat mesenteric artery, however only 1 in 6 rats tested positive for EC caspase activation after 24 hours of 100 mg/kg dosage[41]. Death may be exaggerated in our *in vitro* set up as catabolism of the drug is severely reduced compared to *in vivo*[372]. In addition, caspase activation (apoptotic cell death) is different to ATP release (viability). In the future, TUNEL and caspase-3 immunohistochemistry could be conducted in the *ex vivo* set up to access EC and SMC specific cell death profiles. Endothelial cytotoxicity was not observed using any of the other 3 drugs.

Uniquely, fenoldopam induced cytotoxicity was significantly increased in the presence of Yoda-1 after 24 hours (75 % death in the presence of Yoda-1 compared to 50 % death alone). The chemotherapy agent doxorubicin also increases cytotoxicity under shear stress and Yoda-1 conditions through increased production of ROS and consequent mitochondrial stress and DNA damage[498]. Perhaps, fenoldopam acts through a similar mechanism since a link between fenoldopam and increased NO production (which stimulates RNS and ROS) has been

reported[100]. Again, to ultimately conclude that this is a biological phenomenon due to mechanosignalling, HUVEC should be treated with fenoldopam under shear stress conditions and monitored for cell viability.

Minoxidil and rolipram were not cytotoxic in either of the systems used. In previous *in vivo* studies in DIVI, these drugs showed mostly necrosis of SMC and not EC[52,53,127].

It is possible that the differences between cytotoxicity observed *in vivo* and *in vitro* could relate to different expression levels of the drugs known protein targets[372]. This could be quantified through western blot and densitometry analysis. Additionally, different cell species may have different off-target effects. One way to monitor this would be to incubate the drugs with the HUVEC in the presence of inhibitors of the protein targets. Further, secondary pharmacology binding assays/proteomics and stable isotope labelling by amino acids in cells culture (SILAC), a powerful method to investigate the proteomic change under differential treatment, could be performed.

Drug	Time course (hours)	*In vitro/vivo* (previous studies)	*In vitro*		
			Monocultured EC	Co-culture EC-SMC	EC with Yoda-1
Bosentan	24	n/a	✖	✓	✓✓
Fenoldopam	24	Increased activated caspase-3 in rats[41]	✓	✖	✓✓✓✓
Minoxidil	24	Necrosis of SMC and not EC[52,53]	✖	✖	✖
Rolipram	24	Necrosis of SMC and not EC[127]	✖	✖	✖

Table 8.4 Comparative effects of EC death seen *in vitro/vivo* in previous studies with *in vitro* investigation conducted within this thesis.
✓✓✓ ✓= very significant effect ($p < 0.0001$); ✓✓= very significant effect ($p < 0.01$); ✓= significant effect ($p < 0.05$); ✖= no effect.

8.2.4 SMC death

SMC death is summarised in **Table 8.5**. None of the drugs caused SMC death in monocultured SMC, and this effect was unaltered by addition of Yoda-1. This is perhaps surprising as a clear histopathological feature of DIVI is apoptosis and necrosis of SMC (refer to **Introduction**, section **1.3.1**).

Bosentan has been suggested to prevent apoptosis and inflammation in rats[499], conversely data presented in this thesis showed a cytotoxic effect of bosentan on SMC when co-cultured with EC. This effect was absent when Yoda-1 was added to monocultured SMC. This might relate to the differences between *in vivo* and *in vitro* models, and especially the complexity of the latter. A previous study in rats with fenoldopam showed evident SMC apoptosis, measured using activated caspase-3 and TUNEL staining[41].

Another study using a PDE IV inhibitor, CI-1018, in rats showed prominent activated caspase-3 and TUNEL staining in SMC, associated with active inflammation[127]. However, it has been suggested that SMC apoptosis may not be a primary event but rather secondary to the inflammatory response[127]. This suggests that the system used in this thesis may be too reductionist and perhaps a more complex system using a combination of EC-SMC interaction and flow, is required. It is known that both EC and SMC are altered by the effects of flow *in vivo*[500,501] and this was absent in the system described here which may have limited the findings.

Drug	Time course (hours)	*In vivo* (previous studies)	*In vitro*		
			Monocultured SMC	Co-culture EC-SMC	SMC with Yoda-1
Bosentan	24	Anti-apoptotic effects in rats[499]	×	✓	×
Fenoldopam	24	Increased activated caspase-3 in rats[41]	×	×	×
Minoxidil	24	Necrosis in dogs shown by H&E staining[53,57]	×	×	×
Rolipram	24	Apoptosis in tunica media in rats with CI-1018[127]	×	×	×

Table 8.5 Comparative effects of SMC death seen *in vitro*/*vivo* in previous studies with *in vitro* investigation conducted within this thesis. ✓= significant effect ($p < 0.05$); ×= no effect.

8.2.5 Platelet and leukocyte activation

Finally, the final DIVI feature investigated was whole blood cell activation following drug treatment. The effects of the drugs are summarised in **Table 8.6**. It has been shown that platelets adhere to EC and also form aggregates with leukocytes in DIVI[199,502]. However, in these experiment the drugs had no effect on platelets and only bosentan and minoxidil induced an effect on neutrophil activation. The effects seen in previous studies have been described in **chapter 5**.

Drug	Time course (hours)	*In vitro/vivo* (previous studies)	*In vitro*			
			Platelets		Leukocytes	
			Integrin $\alpha_{IIb}\beta_3$	P-selectin	Neutrophils	Monocytes
Bosentan	20	Effects on platelets unclear[412–414], reduction in leukocyte adhesion and inflammation in mice[422]	×	×	×	×
	60				✓	
Fenoldopam	20	No effect on platelets[416]	×	×	×	×
	60		×	×	×	×
Minoxidil	20	Prevention of platelet aggregation[411]	×	×	✓✓	×
	60		×	×	✓	×
Rolipram	20	Reduction in neutrophil recruitment *in vivo* and *in vitro*[425]	×	×	×	×
	60		×	×	×	×

Table 8.6 Comparative effects of inflammation seen *in vitro/vivo* in previous studies with *in vitro* investigation conducted within this thesis.
✓✓= very significant effect ($p < 0.01$); ✓= significant effect ($p < 0.05$); ×= no effect.

In summary, the four drugs tested have been reported to cause DIVI in preclinical species, even though the exact mechanisms driving the injury are still unclear. In this study, when investigated *in vitro* for classic biomarkers of DIVI, no common patterns emerged and they each had different effects on the features explored. This suggests that the somewhat simplistic approach taken here is not ideal for the assessment of DIVI and additional elements need to be added to generate a more complex *in vitro* model for DIVI. In addition, it has to be noted that the assays investigated in this thesis are mostly phenotypic and not mechanistic. As such, future investigation should focus on understanding in detail the cellular and mechanistic aspects of DIVI. The subsequent sections will provide hypotheses on markers that could be investigated in the future to increase the understanding of the mechanisms underlying DIVI. The next sections will explore (1) other potential DIVI biomarkers that are worth investigation and (2) the construction of a more complex model system to study DIVI.

8.3 Exploring other potential markers of DIVI *in vitro*

A popular DIVI theory is that these compounds induce lesions by triggering vasodilation (described in **Introduction**, section **1.5.1**). For example, it has been reported that administration of minoxidil, an opener of K_{IR} (inward rectifier) 6.X ATP sensitive K^+ channels, to rats at an equipotent hypotensive dose to SK&F 95654, a PDE III inhibitor, led to arterial lesions that were macroscopically, microscopically, and ultrastructurally identical to those induced by the PDE III inhibitor[76]. This suggests that the lesion may be caused by the haemodynamic effect of these compounds rather than an underlying cytotoxic effect. This finding is important for the understanding of the mechanisms underlying all drugs implicated in DIVI. Both compounds also induce a comparable and long-lasting increase in mesentery blood flow in rats, which is expected to produce an increase in endothelial shear stress.

These observations suggest that a useful potential marker of DIVI that has not been investigated in this thesis is NO, which is fundamental in maintaining vascular tone. Previous studies have implicated NO as a potential regulator involved in the pathogenesis of DIVI[35,100,127,128,171], particularly for phosphodiesterase IV inhibitors, where the upregulation of cAMP causes SMC relaxation[503]. For example, an elevation in eNOS phosphorylation at S615

has been shown after administration of the PDE IV inhibitor CI-1044, accompanied by overproduction of NO and vascular injury[125]. These elevations were higher in the mesenteric arteries in rats compared to the aorta, which is not damaged in response to PDE IV inhibitors. This finding was not specific to PDE IV inhibitors, since each of the other classes of drugs examined (PDE III inhibitor, adenosine agonist and a K^+ channel opener) produced similar results. These findings support the hypothesis that NO may underlie DIVI and it will warrant further investigation.

Transcriptional profiling of specific elements of blood vessels from animal models of vascular toxicity is an approach to gain insight into molecular mechanisms of vascular injury[41]. A study using fenoldopam in rats used laser capture microdissection to assess differential gene expression in the mesenteric arteries. RNA was then isolated, linearly amplified and hybridized to Affymetrix GeneChips®. It was found that fenoldopam resulted in differential expression of 333 versus 458 genes in EC and 371 versus 618 genes in SMC at the 1 hour or 4 hour time point, respectively.

Microarray technology to detect circulating microRNAs is able to screen a large set of components in the plasma and might also be a useful approach to gain insights into DIVI. Further, -omic approaches can be used to assess pathways that change with DIVI-related drugs in the presence or absence of Yoda-1 (such as eNOS and Akt phosphorylation, VCAM-1 and ICAM-1 expression) in the model used here and compare them with traditional flow. Blood vessels on a chip to study DIVI metabolites and biomarkers using BIOCORE analysis of the media/blood that is flowed through the device may also be of help[504].

A model to study extravasation of RBC would also be useful to understand DIVI. It has been described in dogs treated with a PDE III inhibitor that erythrocytes fill the space previously occupied by SMC that undergo necrosis[76]. A microfluidic vascular device where EC and SMC are co-cultured together has been developed to study this phenomenon that is still unclear in DIVI[114]. This *in vitro* system is made using poly(dimethylsiloxane) (PDMS), where primary rat EC and SMC are co-cultured on opposite sides of a porous membrane mimicking the internal elastic lamina and then whole blood perfused in the EC chamber with the possibility of studying extravasation of RBC into the smooth muscle region[114]. The endothelial chamber

was designed to be 200 µM in diameter in order to replicate the size of rat mesentery vessels affected by DIVI. It was found that administration for 8 hours of a candidate drug (CI-1044) known to cause DIVI induced extravasation of RBC, which was suggested to be due to the deleterious effects of the compound on EC junctions or other responses such as vascular oxidant stress and inflammation reported in previous *in vivo* studies with CI-1044.

8.4 The optimum device to study DIVI

A human *in vitro* model of DIVI has been developed in this study, where several markers that play a crucial role in the development and progression of the lesions in DIVI have been investigated. A factor that has not been investigated is the addition of Yoda-1 to EC-SMC co-culture rather than studying the effects of Yoda-1 only on EC. In addition, SMC inflammation has not been explored and is something that is worth doing in the future as inflammation is an important sign of DIVI.

This *in vitro* system provided the following advantages: (1) it is a simple model to construct as the parameters investigated have been well-characterised in the past and are relatively simple and quick to measure; (2) it is a model that can be replicated across different laboratories and does not involve the use of complicated and expensive machinery nor equipment. In drug development the aim is to have reproducibility, low cell number, robust endpoint, plate format, sensitivity and specificity and these requirements have been met with the model presented here.

However, there are a few limitations using this model: (1) absence of flow. Flow might be a crucial component in the development of DIVI and the use of real flow with blood rather than a flow-mimetic would allow the study of RBC extravasation, because although Yoda-1 mimics some of the biological effects of flow, the physical forces are likely the elements that cause RBC extravasation, although this has not been established yet[114]; (2) complexity and physiological relevance. The model did not include the study of the effect of the drugs using a combination of EC-SMC co-culture and flow.

It has been suggested that a key element in RBC extravasation may be the porous internal elastic lamina, where the diameter of its holes is large enough to allow extravasation of RBC[114] as it has been hypothesised that this is their route of passage into the tunica media in DIVI. Therefore consideration in designing an optimal future device would be incorporating a porous membrane that separates the EC and the SMC layer, mimicking the naturally porous internal elastic lamina.

The optimal device would also allow cells to be cultured for long periods of time, in order to investigate the phenomena demonstrated in animals, where drugs are administered for months. This would enable an understanding of the resolution of the lesions that have been observed with some of the drugs that is still a matter for debate (refer to **Introduction**, section **1.3.1**). Moreover, the ideal device would allow isolation of different cell types to perform end stage testing and also to assess whether SMC undergo the phenotype switch to the synthetic or proliferating one, that has been reported in vascular diseases such as atherosclerosis[236]. Isolation of plasma or cell supernatant to monitor biomarkers released from the cells at different time intervals would also be optimal. Investigating DIVI in an assay format has proven to be difficult and perhaps a low throughput/high sensitivity option in a device (rather than a high-throughput/low sensitivity) is the way forward. The benefit of this as opposed to an *in vivo* model would still be the reduction in the use of animals in research.

In summary, this PhD aimed at studying a toxicological event in human cells. Further studies are needed in the future to understand the exact mechanism by which drugs cause vascular injury. Likely, as mentioned previously, the drugs act through off-target actions and possibly the on-target effect has little implication in the development of the injury. Mechanistically, this could be achieved by studying the molecular structure of the drug to understand which receptors could be implicated in the DIVI pathology and then blocking those receptors to assess whether the effect of the drug is reduced. Most likely, one assay will not be sufficient and multiple assays are required for these studies.

8.5 Limitations and concluding remarks

Several limitations affect the studies presented in this thesis. First of all, the low sample size (n=4), which is usually appropriate for initial/pilot experiments, is a very limited number for

in vivo studies. As mentioned in **chapter 2**, previous studies in the field describe similar experiments using a comparable number of animals. In addition, considerations related to the Replacement, Refinement and Reduction of Animals in Research (3Rs) have been made and the number of rats used kept to the minimum.

Furthermore, it would have been ideal to use for the studies endothelial and smooth muscle cell lines originating from arteries usually affected by DIVI. HUVEC are derived from veins from immune-naïve foetal tissue and show differences from adult vascular endothelium. However, HUVEC were selected as the source of EC since they have been extensively characterised in the literature[341] and HCASMC were used as the source of arterial vascular SMC as they have also been widely described[342]. Limitations related to the sensitivity to drugs and shear stress should be taken into considerations and have been described more in detail in the specific chapters sections.

A further limitation relates to the fact that degradation as opposed to release may be responsible for the loss of VWF in the assays presented. There are reasons for the loss of expression which could be irrespective of VWF release. For example, endothelial autophagosomes contain abundant VWF protein and the drugs could increase degradation of VWF. This should be taken into consideration and further investigated in the future.

In conclusion, the aim of the work presented in this thesis was to develop a simple cellular system that would facilitate future screening of a large number of compounds for DIVI risk during drug development. In such an underinvestigated area it has been difficult to develop a predictive assay. A human *in vitro* model has been generated, whereby drugs known to cause DIVI in preclinical animal species were used to identify whether a DIVI phenotype could be detected in human cells. The approach was limited by variability in DIVI features following drug treatment and the utilisation of high doses that poorly correlated with a human efficacious dose.

The limitations associated with the model may indicate that a more complex system needs to be developed for the *in vitro* study of DIVI, or that the absence of DIVI markers in human cell models means that there is limited cross species translation and that this is a pathophysiological effect that only occurs in animals and not humans. In order to fully confirm this hypothesis, in the future improvements must be added to the assay in order to have a

tool that reproduces in the best possible way the *in vivo* physiology, and at the same time is easy to use and cost-effective. Drug attrition at present is still high, and safety assessment is of fundamental importance. Thus, the need for robust predictive assays remains. With further development, this model will have utility as an *in vitro* screening test of candidate drugs for DIVI.

References

1. Dimasi, J. A., Feldman, L., Seckler, A. & Wilson, A. Trends in risks associated with new drug development: Success rates for investigational drugs. *Clinical Pharmacology and Therapeutics* (2010) doi:10.1038/clpt.2009.295.

2. Bendjama, K. *et al.* Translation Strategy for the Qualification of Drug-induced Vascular Injury Biomarkers. *Toxicol. Pathol.* (2014) doi:10.1177/0192623314527644.

3. Lipsky, M. S. & Sharp, L. K. From Idea to Market : The Drug Approval Process FDA : A Historical Perspective. *JABFP* (2001).

4. Kim, J. H. & Scialli, A. R. Thalidomide: The tragedy of birth defects and the effective treatment of disease. *Toxicol. Sci.* (2011) doi:10.1093/toxsci/kfr088.

5. Arrowsmith, J. Trial watch: Phase II failures: 2008–2010. *Nat. Rev. Drug Discov.* (2011) doi:10.1038/nrd3439.

6. Pammolli, F., Magazzini, L. & Riccaboni, M. The productivity crisis in pharmaceutical R&D. *Nat. Rev. Drug Discov.* (2011) doi:10.1038/nrd3405.

7. Kola, I. & Landis, J. Can the pharmaceutical industry reduce attrition rates? *Nat. Rev. Drug Discov.* (2004) doi:10.1038/nrd1470.

8. Ferri, N. *et al.* Drug attrition during pre-clinical and clinical development: Understanding and managing drug-induced cardiotoxicity. *Pharmacology and Therapeutics* (2013) doi:10.1016/j.pharmthera.2013.03.005.

9. Avdeef, a *et al.* Can the pharmaceutical industry reduce attrition rates? *Curr. Opin. Chem. Biol.* (2004) doi:10.1038/nrd1470.

10. Hay, M., Thomas, D. W., Craighead, J. L., Economides, C. & Rosenthal, J. Clinical development success rates for investigational drugs. *Nat. Biotechnol.* (2014) doi:10.1038/nbt.2786.

11. Bunnage, M. E. Getting pharmaceutical R&D back on target. *Nat. Chem. Biol.* (2011) doi:10.1038/nchembio.581.

12. Munos, B. Lessons from 60 years of pharmaceutical innovation. *Nature Reviews Drug Discovery* (2009) doi:10.1038/nrd2961.

13. Kaitin, K. I. & Dimasi, J. A. Pharmaceutical innovation in the 21st century: New drug approvals in the first decade, 2000-2009. *Clin. Pharmacol. Ther.* (2011) doi:10.1038/clpt.2010.286.

14. Organization, W. H. *Handbook of resolutions and decisions of the World Health Assembly and Executive Board*. (1973).

15. Bond, C. A. & Raehl, C. L. Adverse drug reactions in United States hospitals. *Pharmacotherapy* (2006) doi:10.1592/phco.26.5.601.

16. Pirmohamed, M. Adverse drug reactions as cause of admission to hospital: prospective analysis of 18 820 patients. *BMJ* (2004) doi:10.1136/bmj.329.7456.15.

17. Laverty, H. G. *et al.* How can we improve our understanding of cardiovascular safety liabilities to develop safer medicines? *British Journal of Pharmacology* (2011) doi:10.1111/j.1476-5381.2011.01255.x.

18. Shah, R. R. Can pharmacogenetics help rescue drugs withdrawn from the market? *Pharmacogenomics* (2006) doi:10.2217/14622416.7.6.889.

19. Redfern, W. S. *et al.* Relationships between preclinical cardiac electrophysiology, clinical QT interval prolongation and torsade de pointes for a broad range of drugs: Evidence for a provisional safety margin in drug development. *Cardiovascular Research* (2003) doi:10.1016/S0008-6363(02)00846-5.

20. Dieppe, P. A., Ebrahim, S., Martin, R. M. & Jüni, P. Lessons from the withdrawal of rofecoxib: ***. *BMJ* (2004) doi:10.1136/bmj.329.7471.867.

21. Sun, S. X., Lee, K. Y., Bertram, C. T. & Goldstein, J. L. Withdrawal of COX-2 selective inhibitors rofecoxib and valdecoxib: impact on NSAID and gastroprotective drug prescribing and utilization. *Curr. Med. Res. Opin.* (2007) doi:10.1185/030079907x210561.

22. Hanton, G., Eder, V., Rochefort, G., Bonnet, P. & Hyvelin, J.-M. Echocardiography, a non-invasive method for the assessment of cardiac function and morphology in

preclinical drug toxicology and safety pharmacology. *Expert Opin. Drug Metab. Toxicol.* (2008) doi:10.1517/17425255.4.6.681.

23. Radić, M., Martinović Kaliterna, D. & Radić, J. Drug-induced vasculitis: A clinical and pathological review. *Netherlands Journal of Medicine* (2012).

24. Moslehi, J. J. & Deininger, M. Tyrosine kinase inhibitor-associated cardiovascular toxicity in chronic myeloid leukemia. *Journal of Clinical Oncology* (2015) doi:10.1200/JCO.2015.62.4718.

25. Rasmussen, A. L. *et al.* Host genetic diversity enables Ebola hemorrhagic fever pathogenesis and resistance. *Science (80-.).* (2014) doi:10.1126/science.1259595.

26. Ericsson A, C. M. A brief history of animal modeling. *Mo. Med.* **110 (3)**, (2013).

27. Taylor, G. I. & Minabe, T. The angiosomes of the mammals and other vertebrates. *Plast. Reconstr. Surg.* (1992) doi:10.1097/00006534-199202000-00001.

28. Jennings, R. B. & Reimer, K. A. Factors involved in salvaging ischemic myocardium: effect of reperfusion of arterial blood. *Circulation* (1983).

29. Nienaber, C., Gottwik, M., Winkler, B. & Schaper, W. The relationship between the perfusion deficit, infarct size and time after experimental coronary artery occlusion. *Basic Res. Cardiol.* (1983) doi:10.1007/BF01906674.

30. KELLIHER, G. J., DIX, R. K. & SOIFER, B. E. Animal Studies in Artificially Induced Myocardial Infarction. in *Myocardial Infarction and Cardiac Death* (2012). doi:10.1016/b978-0-12-471350-5.50008-4.

31. Maxwell, M. P., Hearse, D. J. & Yellon, D. M. Species variation in the coronary collateral circulation during regional myocardial ischaemia: A critical determinant of the rate of evolution and extent of myocardial infarction. *Cardiovascular Research* (1987) doi:10.1093/cvr/21.10.737.

32. JOHANSSON, S. CARDIOVASCULAR LESIONS IN SPRAGUE-DAWLEY RATS INDUCED BY LONG-TERM TREATMENT WITH CAFFEINE. *Acta Pathol. Microbiol. Scand. Sect. A Pathol.* (1981) doi:10.1111/j.1699-0463.1981.tb00207.x.

33. Bailey, M., Christoforidou, Z. & Lewis, M. C. The evolutionary basis for differences

between the immune systems of man, mouse, pig and ruminants. *Vet. Immunol. Immunopathol.* (2013) doi:10.1016/j.vetimm.2012.09.022.

34. Kerns, W. *et al.* Drug-induced vascular injury - A quest for biomarkers. *Toxicology and Applied Pharmacology* (2005) doi:10.1016/j.taap.2004.08.001.

35. Louden, C. *et al.* Biomarkers and mechanisms of drug-induced vascular injury in non-rodents. *Toxicologic Pathology* (2006) doi:10.1080/01926230500512076.

36. Brott, D. A. *et al.* Current status and future directions for diagnostic markers of drug-induced vascular injury. *Cancer Biomarkers* (2005) doi:10.3233/CBM-2005-1104.

37. Carlson, R. G. & Feenstra, E. S. Toxicologic studies with the hypotensive agent minoxidil. *Toxicol. Appl. Pharmacol.* (1977) doi:10.1016/0041-008X(77)90171-5.

38. Swanson, T. A. *et al.* Hemodynamic Correlates of Drug-induced Vascular Injury in the Rat Using High-frequency Ultrasound Imaging. *Toxicol. Pathol.* (2014) doi:10.1177/0192623314525687.

39. Kerns, W. D. *et al.* Pathogenesis of arterial lesions induced by dopaminergic compounds in the rat. *Toxicol Pathol* (1989) doi:10.1103/PhysRevB.79.125313.

40. Kerns, W.D., E. Arena, and D. G. M. Role of dopaminergic and adrenergic receptors in the pathogenesis of arterial lesions induced by fenoldopam mesylate and dopamine in the rat. *Am J Pathol* **135(2)**, 339–49 (1989).

41. Dalmas, D. A. *et al.* Transcriptional Profiling of Laser Capture Microdissected Rat Arterial Elements: Fenoldopam-induced Vascular Toxicity as a Model System. *Toxicol. Pathol.* (2008) doi:10.1177/0192623307311400.

42. Hanton, G., Le Net, J. L., Ruty, B. & Leblanc, B. Characterization of the arteritis induced by infusion of rats with UK-61,260, an inodilator, for 24 h - A comparison with the arteritis induced by fenoldopam mesylate. *Arch. Toxicol.* (1995) doi:10.1007/s002040050235.

43. Ikegami, H. *et al.* Histopathological and immunohistochemical studies on arteritis induced by fenoldopam, a vasodilator, in rats. *Exp. Toxicol. Pathol.* (2001) doi:10.1078/0940-2993-00158.

44. Nyska, A., Herbert, R. A., Chan, P. C., Haseman, J. K. & Hailey, J. R. Theophylline-induced mesenteric periarteritis in F344/N rats. *Arch. Toxicol.* (1998) doi:10.1007/s002040050567.

45. Daguès, N. *et al.* Altered gene expression in rat mesenteric tissue following in vivo exposure to a phosphodiesterase 4 inhibitor. *Toxicol. Appl. Pharmacol.* (2007) doi:10.1016/j.taap.2006.10.018.

46. Westwood, F. R., Iswaran, T. J. & Greaves, P. Pathologic changes in blood vessels following administration of an inotropic vasodilator (IC1153,110) to the rat. *Toxicol. Sci.* (1990) doi:10.1093/toxsci/14.4.797.

47. Greaves, P. Patterns of drug-induced cardiovascular pathology in the beagle dog: Relevance for humans. *Exp. Toxicol. Pathol.* (1998) doi:10.1016/S0940-2993(98)80008-0.

48. Greaves, P. Patterns of cardiovascular pathology induced by diverse cardioactive drugs. in *Toxicology Letters* (2000). doi:10.1016/S0378-4274(99)00222-2.

49. Detweiler, D. K., Ratcliffe, H. L. & Luginbühl, H. THE SIGNIFICANCE OF NATURALLY OCCURRING CORONARY AND CEREBRAL ARTERIAL DISEASE IN ANIMALS. *Ann. N. Y. Acad. Sci.* (1968) doi:10.1111/j.1749-6632.1968.tb53843.x.

50. Detweiler, D. K. Spontaneous and Induced Arterial Disease in the Dog: Pathology and Pathogenesis . *Toxicol. Pathol.* (2017) doi:10.1177/019262338901700105.

51. Mesfin, G. M., Shawaryn, G. G. & Higgins, M. J. Cardiovascular Alterations in Dogs Treated with Hydralazine. *Toxicol. Pathol.* (1987) doi:10.1177/019262338701500404.

52. Mesfin, G. M. *et al.* Pathogenesis of Cardiovascular Alterations in Dogs Treated with Minoxidil <sup/>. *Toxicol. Pathol.* (1989) doi:10.1177/019262338901700113.

53. Mesfin, G. M., Robinson, F. G., Higgins, M. J., Zhong, W. Z. & DuCharme, D. W. The pharmacologic basis of the cardiovascular toxicity of minoxidil in the dog. *Toxicol. Pathol.* (1995) doi:10.1177/019262339502300406.

54. Mesfin, G. M., Higgins, M. J., Robinson, F. G. & Zhong, W. Z. Relationship between serum concentrations, hemodynamic effects, and cardiovascular lesions in dogs

treated with minoxidil. *Toxicol. Appl. Pharmacol.* (1996) doi:10.1006/taap.1996.0229.

55. Liang, C. S. *et al.* Effects of milrinone on systemic hemodynamics and regional circulations in dogs with congestive heart failure: Comparison with dobutamine. *J. Cardiovasc. Pharmacol.* (1987) doi:10.1097/00005344-198711000-00003.

56. Jones, H. B. *et al.* Endothelin antagonist-induced coronary and systemic arteritis in the Beagle dog. *Toxicol. Pathol.* (2003) doi:10.1080/01926230390204298.

57. Clemo, F. A. S., Evering, W. E., Snyder, P. W. & Albassam, M. A. Differentiating spontaneous from drug-induced vascular injury in the dog. in *Toxicologic Pathology* (2003). doi:10.1080/01926230309769.

58. Enerson, B. *et al.* Acute drug-induced vascular injury in beagle dogs: Pathology and correlating genomic expression. *Toxicol. Pathol.* (2006) doi:10.1080/01926230500512068.

59. Harleman, J. H. *et al.* Cardiotoxicity of a new inotrope/vasodilator drug (SK&F 94120) in the dog. *Arch. Toxicol.* (1986) doi:10.1007/BF00263958.

60. Isaacs, K. R., Joseph, E. C. & Betton, G. R. Coronary Vascular Lesions in Dogs Treated with Phosphodiesterase III Inhibitors . *Toxicol. Pathol.* (2017) doi:10.1177/019262338901700112.

61. Joseph, E. C., Jones, H. B. & Kerns, W. D. Characterization of coronary arterial lesions in the dog following administration of SK&F 95654, a phosphodiesterase III inhibitor. *Toxicol. Pathol.* (1996) doi:10.1177/019262339602400405.

62. Louden, C. S. *et al.* Endothelin receptor subtype distribution predisposes coronary arteries to damage. *Am. J. Pathol.* (2000) doi:10.1016/S0002-9440(10)64524-5.

63. McDuffie, J. E. *et al.* Acute coronary artery injury in dogs following administration of CI-1034, an endothelin a receptor antagonist. *Cardiovasc. Toxicol.* (2006) doi:10.1385/CT:6:1:25.

64. Albassam, M. A., Lillie, L. E., and Smith, G. S. Asymptomatic Polyarteritis in a Cynomolgus Monkey. *Lab. Anim. Sci* **43:628**-**629**, (199AD).

65. Albassam, M. A., Smith, G. S. & Macallum, G. E. Arteriopathy Induced by an

Adenosine Agonist-Antihypertensive in Monkeys. *Toxicol. Pathol.* (1998) doi:10.1177/019262339802600311.

66. Saito, N. & Kawamura, H. The Incidence and Development of Periarteritis Nodosa in Testicular Arterioles and Mesenteric Arteries of Spontaneously Hypertensive Rats. *Hypertens. Res.* (2008) doi:10.1291/hypres.22.105.

67. Kane, G. C. & Keogh, K. A. Involvement of the heart by small and medium vessel vasculitis. *Current Opinion in Rheumatology* (2009) doi:10.1097/BOR.0b013e32831cb94d.

68. Jennette, J. C. *et al.* Nomenclature of systemic vasculitides. Proposal of an international consensus conference. *Arthritis Rheum.* (1994).

69. Bahrami, S., Malone, J. C., Webb, K. G. & Callen, J. P. Tissue eosinophilia as an indicator of drug-induced cutaneous small-vessel vasculitis. *Arch. Dermatol.* (2006) doi:10.1001/archderm.142.2.155.

70. Ramdial, P. K. & Naidoo, D. K. Drug-induced cutaneous pathology. *Journal of Clinical Pathology* (2009) doi:10.1136/jcp.2008.058289.

71. Joseph, E., et al. Pathogenesis of arterial lesions caused by vasoactive compounds in laboratory animals. *Cardiovasc. Toxicol.* 279–307 (1997).

72. Joseph, E. C., Rees, J. A. & Dayan, A. D. Mesenteric Arteriopathy in the Rat Induced by Phosphodiesterase III Inhibitors: AN Investigation of Morphological, Ultrastructural, and Hemodynamic Changes. *Toxicol. Pathol.* (1996) doi:10.1177/019262339602400406.

73. Stephan-Gueldner, M. & Inomata, A. Coronary arterial lesions induced by endothelin antagonists. in *Toxicology Letters* (2000). doi:10.1016/S0378-4274(99)00218-0.

74. Albassam, M. A. *et al.* Studies on coronary arteriopathy in dogs following administration of CI-1020, an endothelin a receptor antagonist. *Toxicol. Pathol.* (2001) doi:10.1080/019262301316905228.

75. Joseph, E. C., Rees, J. A. & Dayan, A. D. Mesenteric Arteriopathy in the Rat Induced by Phosphodiesterase III Inhibitors: AN Investigation of Morphological, Ultrastructural,

and Hemodynamic Changes. *Toxicol. Pathol.* (1996) doi:10.1177/019262339602400406.

76. Joseph, E. C. Arterial lesions induced by phosphodiesterase III (PDE III) inhibitors and DA1agonists. in *Toxicology Letters* (2000). doi:10.1016/S0378-4274(99)00221-0.

77. Louden, C. *et al.* Coronary arterial lesions in dogs treated with an endothelin receptor antagonist. *J. Cardiovasc. Pharmacol.* (1998) doi:10.1097/00005344-199800001-00109.

78. J. Dupuis and M.M. Hoeper. Endothelin receptor antagonists in pulmonary arterial hypertension. *Eur Respir J* **31: 407–41**, (2008).

79. Michael B. Simmers, Banu Cole, Aaron Mackey, David Manka, Brett R. Blackman, B. R. W. Altered Hemodynamics Play a Critical Role in Fenoldopam-Induced Mesenteric Vasculitis in the Rat. *HemoShear, LLC, Charlottesv. VA*.

80. Berkowitz, B. A. & Ohlstein, E. H. Fenoldopam. *Cardiovasc. Drug Rev.* (1987) doi:10.1111/j.1527-3466.1987.tb00511.x.

81. Sobota, J. T. Review of Cardiovascular Findings in Humans Treated with Minoxidil. *Toxicol. Pathol.* (1989) doi:10.1177/019262338901700115.

82. Sica, D. A. Minoxidil: an underused vasodilator for resistant or severe hypertension. *Journal of clinical hypertension (Greenwich, Conn.)* (2004) doi:10.1111/j.1524-6175.2004.03585.x.

83. Larson, J. L., Pino, M. V., Geiger, L. E. & Simeone, C. R. The toxicity of repeated exposures to rolipram, a type IV phosphodiesterase inhibitor, in rats. *Pharmacol. Toxicol.* (1996) doi:10.1111/j.1600-0773.1996.tb00178.x.

84. Kerns, W. D. *et al.* Pathogenesis of Arterial Lesions Induced by Dopaminergic Compounds in the Rat . *Toxicol. Pathol.* (2017) doi:10.1177/019262338901700116.

85. Bugelski, P. J. *et al.* Ultrastructure of an arterial lesion induced in rats by fenoldopam mesylate, a dopaminergic vasodilator. *Br. J. Exp. Pathol.* (1989).

86. Swanson TA, Conte T, Deeley B, Portugal S, Kreeger JM, Obert LA, Joseph EC, Wisialowski TA, Sokolowski SA, Rief C, Nugent P, Lawton MP, E. B. Hemodynamic

correlates of drug-induced vascular injury in the rat using high-frequency ultrasound imaging. *Toxicol Pathol* **42(4)**, 784–91 (2014).

87. Zhang, J. *et al.* Histopathology of vascular injury in Sprague-Dawley rats treated with phosphodiesterase IV Inhibitor SCH 351591 or SCH 534385. *Toxicol. Pathol.* (2008) doi:10.1177/0192623308322308.

88. Losco, P. E. *et al.* The Toxicity of SCH 351591, a Novel Phosphodiesterase-4 Inhibitor, in Cynomolgus Monkeys. *Toxicol. Pathol.* (2004) doi:10.1080/01926230490431493.

89. Firth, J. O. & Ratcliffe, P. J. Organ distribution of the three rat endothelin messenger RNAs and the effects of ischemia on renal gene expression. *J. Clin. Invest.* (1992) doi:10.1172/JCI115915.

90. Anthony P. Davenport, Kelly A. Hyndman, Neeraj Dhaun, Christopher Southan, Donald E. Kohan, Jennifer S. Pollock, D. M. P. & David J. Webb, and J. J. M. Endothelin. *Pharmacol. Rev.* **68:357-418**, (2016).

91. Migneault, A. *et al.* Chronically elevated endothelin levels reduce pulmonary vascular reactivity to nitric oxide. *Am. J. Respir. Crit. Care Med.* (2005) doi:10.1164/rccm.200403-340OC.

92. Awane-Igata, Y., Ikeda, S. & Watanabe, T. Inhibitory effects of TAK-044 on endothelin induced vasoconstriction in various canine arteries and porcine coronary arteries: A comparison with selective ET(A) and ET(B) receptor antagonists. *Br. J. Pharmacol.* (1997) doi:10.1038/sj.bjp.0700925.

93. Dagassan, P. H. *et al.* Up-regulation of endothelin-B receptors in atherosclerotic human coronary arteries. *J. Cardiovasc. Pharmacol.* (1996) doi:10.1097/00005344-199601000-00023.

94. Moreland, S., McMullen, D. M., Delaney, C. L., Lee, V. G. & Hunt, J. T. Venous smooth muscle contains vasoconstrictor ETB-like receptors. *Biochem. Biophys. Res. Commun.* (1992) doi:10.1016/0006-291X(92)91163-K.

95. Brooks DP, DePalma PD, Pullen M, N. P. Characterization of canine renal endothelin receptor subtypes and function. *J Pharmacol Exp Ther* **268:1091–1**, (1994).

96. Karoor V, Shih M, Tholanikunnel B, M. C. Regulating expression and function of G-protein-linked receptors. *Prog Neurobiol* **48:555–568**, (1996).

97. Huggins, J. P., Pelton, J. T. & Miller, R. C. The structure and specificity of endothelin receptors: Their importance in physiology and medicine. *Pharmacology and Therapeutics* (1993) doi:10.1016/0163-7258(93)90041-B.

98. Ohlstein, E. H., Zabko-Potapovich, B. & Berkowitz, B. A. The DA1 receptor agonist fenoldopam (SK & F 82526) is also an α2-adrenoceptor antagonist. *Eur. J. Pharmacol.* (1985) doi:10.1016/0014-2999(85)90143-8.

99. Yuhas, E. M. *et al.* Arterial medial necrosis and hemorrhage induced in rats by intravenous infusion of fenoldopam mesylate, a dopaminergic vasodilator. *Am. J. Pathol.* (1985).

100. Brott, D. A., Richardson, R. J. & Louden, C. S. Evidence for the Nitric Oxide Pathway as a Potential Mode of Action in Fenoldopam-induced Vascular Injury. *Toxicol. Pathol.* (2012) doi:10.1177/0192623312444027.

101. Lappe, R. W., Todt, J. A. & Wendt, R. L. Effects of fenoldopam on regional vascular resistance in conscious spontaneously hypertensive rats. *J Pharmacol Exp Ther* (1986).

102. Houslay, M. D. & Milligan, G. Tailoring cAMP-signalling responses through isoform multiplicity. *Trends in Biochemical Sciences* (1997) doi:10.1016/S0968-0004(97)01050-5.

103. Kim, H. K., Kwon, J. Y., Yoo, C. & Abdi, S. The Analgesic Effect of Rolipram, a Phosphodiesterase 4 Inhibitor, on Chemotherapy-Induced Neuropathic Pain in Rats. *Anesth. Analg.* (2015) doi:10.1213/ANE.0000000000000853.

104. WACHTEL, H. Neurotropic effects of the optical isomers of the selective adenosine cyclic 3',5'-monophosphate phosphodiesterase inhibitor rolipram in rats in-vivo. *J. Pharm. Pharmacol.* (1983) doi:10.1111/j.2042-7158.1983.tb04318.x.

105. Torphy, T. J. & Undem, B. J. Phosphodiesterase inhibitors: New opportunities for the treatment of asthma. *Thorax* (1991) doi:10.1136/thx.46.7.512.

106. Francischi, J. N. *et al.* Anti-inflammatory and analgesic effects of the

phosphodiesterase 4 inhibitor rolipram in a rat model of arthritis. *Eur. J. Pharmacol.* (2000) doi:10.1016/S0014-2999(00)00330-7.

107. Gong, B. *et al.* Persistent improvement in synaptic and cognitive functions in an Alzheimer mouse model after rolipram treatment. *J. Clin. Invest.* (2004) doi:10.1172/JCI22831.

108. Sheth, C. M., Enerson, B. E., Peters, D., Lawton, M. P. & Weaver, J. L. Effects of modulating in vivo nitric oxide production on the incidence and severity of PDE4 inhibitor-induced vascular injury in sprague-dawley rats. *Toxicol. Sci.* (2011) doi:10.1093/toxsci/kfr082.

109. Sandusky, G. E., Means, J. R. & Todd, G. C. Comparative Cardiovascular Toxicity in Dogs Given Inotropic Agents by Continuous Intravenous Infusion. *Toxicol. Pathol.* (1990) doi:10.1177/019262339001800205.

110. Ikegami, H., et al. Immunohistochemical study on inducible type of nitric oxide (iNOS), basic fibroblast growth factor (bFGF) and tumor growth factor-beta1 (TGF-beta1) in arteritis induced in rats by fenoldopam and theophylline, vasodilators. *Exp Toxicol Pathol* **54(1)**, 1–7 (2002).

111. Humphrey, S. J. & Zins, G. R. Whole Body and Regional Hemodynamic Effects of Minoxidil in the Conscious Dog. *J. Cardiovasc. Pharmacol.* (1984) doi:10.1097/00005344-198406060-00001.

112. Chelly, J. E., Doursout, M. F., Begaud, B., Tsao, C. C. & Hartley, C. J. Effects of hydralazine on regional blood flow in conscious dogs. *J Pharmacol Exp Ther* (1986).

113. M.S., A. *et al.* Computation of hemodynamics in the circle of Willis. *Stroke* (2007).

114. Hoganson, D. M. *et al.* A bilayer small diameter in vitro vascular model for evaluation of drug induced vascular injury. *Biomicrofluidics* (2016) doi:10.1063/1.4964814.

115. Bregman, C.L., et al. Single-dose and multiple-dose intravenous toxicity studies of BMY-25282 in rats. *Fundam Appl Toxicol* **9(1)**, 90–109 (1987).

116. Pisoni, R., Ruggenenti, P. & Remuzzi, G. Drug-induced thrombotic microangiopathy: Incidence, prevention and management. *Drug Safety* (2001) doi:10.2165/00002018-

200124070-00002.

117. WANG, S. *et al.* Activation of nuclear factor-κB during doxorubicin-induced apoptosis in endothelial cells and myocytes is pro-apoptotic: the role of hydrogen peroxide. *Biochem. J.* (2002) doi:10.1042/bj20020752.

118. Mikaelian, I. *et al.* Primary endothelial damage is the mechanism of cardiotoxicity of tubulin-binding drugs. *Toxicol. Sci.* (2010) doi:10.1093/toxsci/kfq189.

119. Kumar, D., Hysmith, R. M. & Boor, P. J. Allylamine and β-aminopropionitrile-induced vascular injury: An in vivo and in vitro study. *Toxicol. Appl. Pharmacol.* (1990) doi:10.1016/0041-008X(90)90231-I.

120. Nishida, M., Eshiro, K., Okada, Y., Takaoka, M. & Matsumura, Y. Roles of endothelin ETA and ETB receptors in the pathogenesis of monocrotaline-induced pulmonary hypertension. *J. Cardiovasc. Pharmacol.* (2004) doi:10.1097/00005344-200408000-00007.

121. Pacher, P., Beckman, J. S. & Liaudet, L. Nitric Oxide and Peroxynitrite in Health and Disease. *Physiol. Rev.* (2007) doi:10.1152/physrev.00029.2006.

122. Su, J. B. Vascular endothelial dysfunction and pharmacological treatment. *World J. Cardiol.* (2015) doi:10.4330/wjc.v7.i11.719.

123. Weaver, J. L. *et al.* Biomarkers in peripheral blood associated with vascular injury in Sprague-Dawley rats treated with the phosphodiesterase IV inhibitors SCH 351591 or SCH 534385. *Toxicol. Pathol.* (2008) doi:10.1177/0192623308322310.

124. Weaver, J. L. *et al.* Early events in vascular injury in the rat induced by the phosphodiesterase IV inhibitor SCH 351591. *Toxicol. Pathol.* (2010) doi:10.1177/0192623310374331.

125. Tobin, G. A. M. *et al.* The Role of eNOS Phosphorylation in Causing Drug-induced Vascular Injury. *Toxicol. Pathol.* (2014) doi:10.1177/0192623314522885.

126. Förstermann, U. & Sessa, W. C. Nitric oxide synthases: Regulation and function. *European Heart Journal* (2012) doi:10.1093/eurheartj/ehr304.

127. Slim, R. M., Yunling Song, Albassam, M. & Dethloff, L. A. Apoptosis and Nitrative

Stress Associated with Phosphodiesterase Inhibitor-Induced Mesenteric Vasculitis in Rats. *Toxicol. Pathol.* (2003) doi:10.1080/01926230390241972.

128. Zhang, J. *et al.* Mechanisms and biomarkers of cardiovascular injury induced by phosphodiesterase inhibitor III SK&F 95654 in the spontaneously hypertensive rat. *Toxicol. Pathol.* (2006) doi:10.1080/01926230600588562.

129. Weyand, C. M. & Goronzy, J. J. Pathogenic mechanisms in giant cell arteritis. in *Cleveland Clinic Journal of Medicine* (2002).

130. Sams Jr., W. M. Human hypersensitivity angiitis, an immune complex disease. *J Invest Dermatol* (1985).

131. Vugmeyster, Y. Pharmacokinetics and toxicology of therapeutic proteins: Advances and challenges. *World J. Biol. Chem.* (2012) doi:10.4331/wjbc.v3.i4.73.

132. Janin, A. *et al.* CD95 engagement induces disseminated endothelial cell apoptosis in vivo: Immunopathologic implications. *Blood* (2002) doi:10.1182/blood.V99.8.2940.

133. Baldwin, A. L. & Thurston, G. Mechanics of Endothelial Cell Architecture and Vascular Permeability. *Crit. Rev. Biomed. Eng.* (2001) doi:10.1109/TIME.2009.19.

134. Pries, A. R., Secomb, T. W. & Gaehtgens, P. The endothelial surface layer. *Pflugers Archiv European Journal of Physiology* (2000) doi:10.1007/s004240000307.

135. Dejana, E., Corada, M. & Lampugnani, M. G. Endothelial cell-to-cell junctions. *FASEB J.* (1995) doi:10.1101/cshperspect.a006528.

136. Schnittler, H.-J. Structural and functional aspects of intercellular junctions in vascular endothelium. *Basic Res. Cardiol.* (1998) doi:10.1111/nph.13122.

137. Bazzoni, G., Estrada, O. M. M. & Dejana, E. Molecular structure and functional role of vascular tight junctions. *Trends in Cardiovascular Medicine* (1999) doi:10.1016/S1050-1738(99)00022-5.

138. Vestweber, D. Molecular mechanisms that control endothelial cell contacts. *Journal of Pathology* (2000) doi:10.1002/(SICI)1096-9896(200002)190:3<281::AID-PATH527>3.0.CO;2-Z.

139. Bazzoni, G. & Dejana, E. Endothelial Cell-to-Cell Junctions: Molecular Organization and Role in Vascular Homeostasis. *Physiol. Rev.* (2004) doi:10.1152/physrev.00035.2003.

140. Dejana, E. Endothelial adherens junctions. Implications in the control of vascular permeability and angiogenesis. *Journal of Clinical Investigation* (1996) doi:10.1172/JCI118997.

141. Alexander, J. S. & Elrod, J. W. Extracellular matrix, junctional integrity and matrix metalloproteinase interactions in endothelial permeability regulation. *Journal of Anatomy* (2002) doi:10.1046/j.1469-7580.2002.00057.x.

142. Dejana, E., Orsenigo, F. & Lampugnani, M. G. The role of adherens junctions and VE-cadherin in the control of vascular permeability. *J. Cell Sci.* (2008) doi:10.1242/jcs.017897.

143. Weis, W. I. & Nelson, W. J. Re-solving the Cadherin-Catenin-Actin Conundrum. *J. Biol. Chem.* (2006) doi:10.1074/jbc.R600027200.

144. Corada, M. *et al.* Vascular endothelial-cadherin is an important determinant of microvascular integrity in vivo. *Proc. Natl. Acad. Sci. U. S. A.* (1999).

145. Dejana, E. & Vestweber, D. The role of VE-cadherin in vascular morphogenesis and permeability control. in *Progress in Molecular Biology and Translational Science* (2013). doi:10.1016/B978-0-12-394311-8.00006-6.

146. Küppers, V., Vockel, M., Nottebaum, A. F. & Vestweber, D. Phosphatases and kinases as regulators of the endothelial barrier function. *Cell and Tissue Research* (2014) doi:10.1007/s00441-014-1812-1.

147. Andriopoulou, P., Navarro, P., Zanetti, A., Lampugnani, M. G. & Dejana, E. Histamine induces tyrosine phosphorylation of endothelial cell-to-cell adherens junctions. *Arterioscler. Thromb. Vasc. Biol.* (1999) doi:10.1161/01.ATV.19.10.2286.

148. Angelini, D. J. *et al.* TNF-α increases tyrosine phosphorylation of vascular endothelial cadherin and opens the paracellular pathway through fyn activation in human lung endothelia. *Am. J. Physiol. Cell. Mol. Physiol.* (2006) doi:10.1152/ajplung.00109.2006.

149. Hudry-Clergeon, H., Stengel, D., Ninio, E. & Vilgrain, I. Platelet-activating factor increases VE-cadherin tyrosine phosphorylation in mouse endothelial cells and its association with the PtdIns3′-kinase. *FASEB J.* (2005) doi:10.1096/fj.04-2202com.

150. Esser, S., Lampugnani, M. G., Corada, M., Dejana, E. & Risau, W. Vascular endothelial growth factor induces VE-cadherin tyrosine phosphorylation in endothelial cells. *J. Cell Sci.* (1998).

151. Davis, M. E., Cai, H., Drummond, G. R. & Harrison, D. G. Shear stress regulates endothelial nitric oxide synthase expression through c-Src by divergent signaling pathways. *Circ. Res.* (2001) doi:10.1161/hh2301.100806.

152. Xiao, K. p120-Catenin Regulates Clathrin-dependent Endocytosis of VE-Cadherin. *Mol. Biol. Cell* (2005) doi:10.1091/mbc.e05-05-0440.

153. Weis, S. M. & Cheresh, D. A. Pathophysiological consequences of VEGF-induced vascular permeability. *Nature* (2005) doi:10.1038/nature03987.

154. Bogatcheva, N. V., Garcia, J. G. & Verin, A. D. Molecular mechanisms of thrombin-induced endothelial cell permeability. *Biochemistry. Biokhimiia* (2002) doi:10.1023/A:1013904231324.

155. Vandenbroucke St Amant, E. *et al.* PKCα activation of p120-catenin serine 879 phospho-switch disassembles VE-cadherin junctions and disrupts vascular integrity. *Circ. Res.* (2012) doi:10.1161/CIRCRESAHA.112.269654.

156. Gavard, J., Patel, V. & Gutkind, J. S. Angiopoietin-1 Prevents VEGF-Induced Endothelial Permeability by Sequestering Src through mDia. *Dev. Cell* (2008) doi:10.1016/j.devcel.2007.10.019.

157. Xiao, K. *et al.* Mechanisms of VE-cadherin processing and degradation in microvascular endothelial cells. *J. Biol. Chem.* (2003) doi:10.1074/jbc.M211746200.

158. Dudek, S. M. & Garcia, J. G. N. Cytoskeletal regulation of pulmonary vascular permeability. *J. Appl. Physiol.* (2017) doi:10.1152/jappl.2001.91.4.1487.

159. Mehta, D. & Malik, A. B. Signaling Mechanisms Regulating Endothelial Permeability. *Physiol. Rev.* (2006) doi:10.1152/physrev.00012.2005.

160. Privratsky, J. R. & Newman, P. J. PECAM-1: Regulator of endothelial junctional integrity. *Cell and Tissue Research* (2014) doi:10.1007/s00441-013-1779-3.

161. Biswas, P. *et al.* PECAM-1 affects GSK-3β-mediated β-catenin phosphorylation and degradation. *Am. J. Pathol.* (2006) doi:10.2353/ajpath.2006.051112.

162. Carrithers, M. *et al.* Enhanced susceptibility to endotoxic shock and impaired STAT3 signaling in CD31-deficient mice. *Am. J. Pathol.* (2005) doi:10.1016/S0002-9440(10)62243-2.

163. Privratsky, J. R. *et al.* Relative contribution of PECAM-1 adhesion and signaling to the maintenance of vascular integrity. *J. Cell Sci.* (2011) doi:10.1242/jcs.082271.

164. Tzima, E. *et al.* A mechanosensory complex that mediates the endothelial cell response to fluid shear stress. *Nature* (2005) doi:10.1038/nature03952.

165. Muller, W. A. PECAM-1 is required for transendothelial migration of leukocytes. *J. Exp. Med.* (2004) doi:10.1084/jem.178.2.449.

166. Liao, F. *et al.* Migration of monocytes across endothelium and passage through extracellular matrix involve separate molecular domains of PECAM-1. *J. Exp. Med.* (1995).

167. Bogen, S. Monoclonal antibody to murine PECAM-1 (CD31) blocks acute inflammation in vivo. *J. Exp. Med.* (2004) doi:10.1084/jem.179.3.1059.

168. Wakelin, M. W. An anti-platelet-endothelial cell adhesion molecule-1 antibody inhibits leukocyte extravasation from mesenteric microvessels in vivo by blocking the passage through the basement membrane. *J. Exp. Med.* (2004) doi:10.1084/jem.184.1.229.

169. Nakada, M. T. *et al.* Antibodies Against the First Ig-Like Domain of Human Platelet Endothelial Cell Adhesion Molecule-1 (PECAM-1) That Inhibit PECAM-1-Dependent Homophilic Adhesion Block In Vivo Neutrophil Recruitment. *J. Immunol.* (2000) doi:10.4049/jimmunol.164.1.452.

170. Turk, J. R. In Search of Biomarkers for Drug-Induced Vascular Injury. in *Biomarkers: In Medicine, Drug Discovery, and Environmental Health* (2010).

doi:10.1002/9780470918562.ch11.

171. Zhang, J., Defelice, A. F., Hanig, J. P. & Colatsky, T. Biomarkers of endothelial cell activation serve as potential surrogate markers for drug-induced vascular injury. *Toxicologic Pathology* (2010) doi:10.1177/0192623310378866.

172. Bach, F. H. *et al.* Endothelial Cell Activation and Thromboregulation during Xenograft Rejection. *Immunol. Rev.* (1994) doi:10.1111/j.1600-065X.1994.tb00870.x.

173. Pober, J. S. & Cotran, R. S. The role of endothelial cells in inflammation. *Transplantation* (1990) doi:10.1097/00007890-199010000-00001.

174. Pober, S. Cytokines and Endothelial cell biology. *Physiol. Rev.* (1990) doi:10.1152/physrev.1990.70.2.427.

175. Egan, K. & Fitzgerald, G. A. Eicosanoids and the vascular endothelium. *Handb. Exp. Pharmacol.* (2006) doi:10.1007/3-540-32967-6-6.

176. Stevens, T., Garcia, J. G. N., Shasby, D. M., Bhattacharya, J. & Malik, A. B. Mechanisms regulating endothelial cell barrier function. *Am. J. Physiol. Cell. Mol. Physiol.* (2017) doi:10.1152/ajplung.2000.279.3.l419.

177. Middleton, J. *et al.* Transcytosis and surface presentation of IL-8 by venular endothelial cells. *Cell* (1997) doi:10.1016/S0092-8674(00)80422-5.

178. Birch, K. A., Ewenstein, B. M., Golan, D. E. & Pober, J. S. Prolonged peak elevations in cytoplasmic free calcium ions, derived from intracellular stores, correlate with the extent of thrombin-stimulated exocytosis in single human umbilical vein endothelial cells. *J. Cell. Physiol.* (1994) doi:10.1002/jcp.1041600318.

179. Lorant, D. E. *et al.* Coexpression of GMP-140 and PAF by endothelium stimulated by histamine or thrombin: A juxtacrine system for adhesion and activation of neutrophils. *J. Cell Biol.* (1991) doi:10.1083/jcb.115.1.223.

180. Pober, J. S. & Sessa, W. C. Evolving functions of endothelial cells in inflammation. *Nature Reviews Immunology* (2007) doi:10.1038/nri2171.

181. Gainetdinov, R. R., Premont, R. T., Bohn, L. M., Lefkowitz, R. J. & Caron, M. G. DESENSITIZATION OF G PROTEIN–COUPLED RECEPTORS AND NEURONAL FUNCTIONS.

Annu. Rev. Neurosci. (2004) doi:10.1146/annurev.neuro.27.070203.144206.

182. Goepfert, C. *et al.* CD39 modulates endothelial cell activation and apoptosis. *Mol. Med.* (2000).

183. Pober, J. S. & Cotran, R. S. The role of endothelial cells in inflammation. *Transplantation* (1990).

184. Martin, M. U. & Wesche, H. Summary and comparison of the signalling mechanisms of the Toll/ interleukin 1 receptor family. *Biochim. Biophys. Acta* **1592**, **265**–, (2002).

185. Pober, J. S. *et al.* Activation of cultured human endothelial cells by recombinant lymphotoxin: comparison with tumor necrosis factor and interleukin 1 species. *J. Immunol.* (1987).

186. Petrache, I., Birukova, A., Ramirez, S. I., Garcia, J. G. N. & Verin, A. D. The role of the microtubules in tumor necrosis factor-α-induced endothelial cell permeability. *Am. J. Respir. Cell Mol. Biol.* (2003) doi:10.1165/rcmb.2002-0075OC.

187. Ley, K. & Reutershan, J. Leucocyte-endothelial interactions in health and disease. *Handb. Exp. Pharmacol.* (2006) doi:10.1007/3-540-36028-X-4.

188. Adams, D. H. & Shaw, S. Leucocyte-endothelial interactions and regulation of leucocyte migration. *The Lancet* (1994) doi:10.1016/S0140-6736(94)92029-X.

189. Ballermann, B. J. Endothelial cell activation. *Kidney Int* **53(6)**, 1810–26 (1998).

190. Bach, F. H., Hancock, W. W. & Ferran, C. Protective genes expressed in endothelial cells: A regulatory response to injury. *Immunology Today* (1997) doi:10.1016/S0167-5699(97)01129-8.

191. Kerr, J. F. R., Wyllie, A. H. & Currie, A. R. Apoptosis: A basic biological phenomenon with wide-ranging implications in tissue kinetics. *Br. J. Cancer* (1972) doi:10.1038/bjc.1972.33.

192. Savill, J. & Fadok, V. Corpse clearance defines the meaning of cell death. *Nature* (2000) doi:10.1038/35037722.

193. Bannerman, D. D., Sathyamoorthy, M. & Goldblum, S. E. Bacterial lipopolysaccharide

disrupts endothelial monolayer integrity and survival signaling events through caspase cleavage of adherens junction proteins. *J. Biol. Chem.* (1998) doi:10.1074/jbc.273.52.35371.

194. Bombeli T, Karsan A, Tait JF, H. J. Apoptotic vascular endothelial cells become procoagulant. *Blood* **89**, 2429–42 (1997).

195. Bombeli, T., Schwartz, B. R. & Harlan, J. M. Endothelial cells undergoing apoptosis become proadhesive for nonactivated platelets. *Blood* (1999).

196. Schwartz, B. R., Karsan, A., Bombeli, T. & Harlan, J. M. A novel beta 1 integrin-dependent mechanism of leukocyte adherence to apoptotic cells. *J Immunol* (1999).

197. Winn, R. K. & Harlan, J. M. The role of endothelial cell apoptosis in inflammatory and immune diseases. in *Journal of Thrombosis and Haemostasis* (2005). doi:10.1111/j.1538-7836.2005.01378.x.

198. Newsholme, S. J., Thudium, D. T., Gossett, K. A., Watson, E. S. & Schwartz, L. W. Evaluation of plasma von Willebrand factor as a biomarker for acute arterial damage in rats. *Toxicol. Pathol.* (2000) doi:10.1177/019262330002800508.

199. Jones, H. B., Björkman, J. A. & Schofield, J. Coronary and Systemic Arterial Physiology and Immunohistochemical Markers Related to Early Coronary Arterial Lesions in Beagle Dogs Given the Potassium Channel Opener, ZD6169, or the Endothelin Receptor Antagonist, ZD1611. *Toxicol. Pathol.* (2013) doi:10.1177/0192623312464123.

200. Brott DA, Katein A, Thomas H, Lawton M, Montgomery RR, Richardson RJ, L. C. Evaluation of von Willebrand Factor and von Willebrand Factor Propeptide in Models of Vascular Endothelial Cell Activation, Perturbation, and/or Injury. *Toxicol Pathol* **42 (4)**, 672–83 (2014).

201. Brott, D. A. *et al.* Evaluation of von Willebrand Factor and von Willebrand Factor Propeptide in Models of Vascular Endothelial Cell Activation, Perturbation, and/or Injury. *Toxicol. Pathol.* (2014) doi:10.1177/0192623313518664.

202. Mikaelian, I. *et al.* Nonclinical Safety Biomarkers of Drug-induced Vascular

Injury:Current Status and Blueprint for the Future. *Toxicol. Pathol.* (2014) doi:10.1177/0192623314525686.

203. Brott, D. *et al.* Biomarkers of drug-induced vascular injury. in *Toxicology and Applied Pharmacology* (2005). doi:10.1016/j.taap.2005.04.028.

204. van Mourik, J. A. *et al.* von Willebrand factor propeptide in vascular disorders: A tool to distinguish between acute and chronic endothelial cell perturbation. *Blood* (1999).

205. Borchiellini, A. *et al.* Quantitative analysis of von Willebrand factor propeptide release in vivo: effect of experimental endotoxemia and administration of 1-deamino-8-D-arginine vasopressin in humans. *Blood* (1996).

206. Sadler, J. E. BIOCHEMISTRY AND GENETICS OF VON WILLEBRAND FACTOR. *Annu. Rev. Biochem.* (1998) doi:10.1146/annurev.biochem.67.1.395.

207. Zezos, P. *et al.* Elevated plasma von Willebrand factor levels in patients with active ulcerative colitis reflect endothelial perturbation due to systematic inflammation. *World J. Gastroenterol.* (2005) doi:10.3748/wjg.v11.i48.7639.

208. Seligman, B. G. S., Biolo, A., Polanczyk, C. A., Gross, J. L. & Clausell, N. Increased plasma levels of endothelin 1 and von Willebrand factor in patients with type 2 diabetes and dyslipidemia. *Diabetes Care* (2000) doi:10.2337/diacare.23.9.1395.

209. Federici, A. B. The factor VIII/von Willebrand factor complex: basic and clinical issues. *Haematologica* (2003).

210. Zhou, Y. F. *et al.* Sequence and structure relationships within von Willebrand factor. *Blood* (2012) doi:10.1182/blood-2012-01-405134.

211. Zhou, Y. F. & Springer, T. A. Highly reinforced structure of a C-terminal dimerization domain in von Willebrand factor. *Blood* (2014) doi:10.1182/blood-2013-11-523639.

212. Foster, P. A., Fulcher, C. A., Marti, T., Titani, K. & Zimmerman, T. S. A major factor VIII binding domain resides within the amino-terminal 272 amino acid residues of von Willebrand factor. *J. Biol. Chem.* (1987).

213. Jenkins, P. V, Pasi, K. J. & Perkins, S. J. Molecular modelling of ligand and mutation sites of the Type A domains of human von Willebrand factor and their relevance to

von Willebrand's disease. *Blood* (1998).

214. De Wit, T. R., Rondaij, M. G., Hordijk, P. L., Voorberg, J. & Van Mourik, J. A. Real-time imaging of the dynamics and secretory behavior of Weibel-Palade bodies. *Arterioscler. Thromb. Vasc. Biol.* (2003) doi:10.1161/01.ATV.0000069847.72001.E8.

215. Dong, J. fei *et al.* ADAMTS-13 rapidly cleaves newly secreted ultralarge von Willebrand factor multimers on the endothelial surface under flowing conditions. *Blood* (2002) doi:10.1182/blood-2002-05-1401.

216. Madabhushi, S. R. *et al.* Von Willebrand factor (VWF) propeptide binding to VWF D'D3 domain attenuates platelet activation and adhesion. *Blood* (2012) doi:10.1182/blood-2011-10-387548.

217. Nightingale, T. & Cutler, D. The secretion of von Willebrand factor from endothelial cells; an increasingly complicated story. *Journal of Thrombosis and Haemostasis* (2013) doi:10.1111/jth.12225.

218. Levine, J. D., Harlan, J. M., Harker, L. A., Joseph, M. L. & Counts, R. B. Thrombin-mediated release of factor VIII antigen from human umbilical vein endothelial cells in culture. *Blood* (1982) doi:10.1139/b72-129.

219. Rusu, L. *et al.* G protein-dependent basal and evoked endothelial cell vWF secretion. *Blood* (2014) doi:10.1182/blood-2013-03-489351.

220. Sporn, L. A., Marder, V. J. & Wagner, D. D. Inducible secretion of large, biologically potent von Willebrand factor multimers. *Cell* (1986) doi:10.1016/0092-8674(86)90735-X.

221. Flood, V. H. *et al.* Crucial role for the VWF A1 domain in binding to type IV collagen. *Blood* (2015) doi:10.1182/blood-2014-11-610824.

222. Legendre, P. *et al.* Mutations in the A3 domain of Von Willebrand factor inducing combined qualitative and quantitative defects in the protein. *Blood* (2013) doi:10.1182/blood-2012-09-456038.

223. André, P. *et al.* Platelets adhere to and translocate on von Willebrand factor presented by endothelium in stimulated veins. *Blood* (2000).

224. Savage, B., Shattil, S. J. & Ruggeri, Z. M. Modulation of platelet function through adhesion receptors: A dual role for glycoprotein IIb-IIIa (integrin ??IIb??3) mediated by fibrinogen and glycoprotein Ib-von Willebrand factor. *J. Biol. Chem.* (1992).

225. Koppelman, S. J. *et al.* Requirements of von Willebrand factor to protect factor VIII from inactivation by activated protein C. *Blood* (1996).

226. Fay, P. J., Coumans, J. V. & Walker, F. J. von Willebrand factor mediates protection of factor VIII from activated protein C-catalyzed inactivation. *J. Biol. Chem.* (1991).

227. Meng, H., Zhang, X., Lee, S. J. & Wang, M. M. Von Willebrand Factor Inhibits Mature Smooth Muscle Gene Expression through Impairment of Notch Signaling. *PLoS One* (2013) doi:10.1371/journal.pone.0075808.

228. Levy, G. G., Motto, D. G. & Ginsburg, D. ADAMTS13 turns 3. *Blood* (2005) doi:10.1182/blood-2004-10-4097.

229. Van Schooten, C. J. *et al.* Macrophages contribute to the cellular uptake of Von Willebrand factor and factor VIII in vivo. *Blood* (2008) doi:10.1182/blood-2008-01-133181.

230. Oishi, Y. & Manabe, I. Macrophages in inflammation, repair and regeneration. *International Immunology* (2018) doi:10.1093/intimm/dxy054.

231. Owens, G. K. Regulation of differentiation of vascular smooth muscle cells. *Physiol. Rev.* (2017) doi:10.1152/physrev.1995.75.3.487.

232. Alexander, M. R. & Owens, G. K. Epigenetic Control of Smooth Muscle Cell Differentiation and Phenotypic Switching in Vascular Development and Disease. *Annu. Rev. Physiol.* (2011) doi:10.1146/annurev-physiol-012110-142315.

233. Chamley, J. H., Campbell, G. R. & Burnstock, G. Dedifferentiation, redifferentiation and bundle formation of smooth muscle cells in tissue culture: the influence of cell number and nerve fibres. *J. Embryol. Exp. Morphol.* (1974).

234. Ross, R. The pathogenesis of atherosclerosis: A perspective for the 1990s. *Nature* (1993) doi:10.1038/362801a0.

235. Salmon M, Gomez D, Greene E, S. L. & O. G. Cooperative binding of KLF4, pELK-1, and

HDAC2 to a G/C repressor element in the SM22α promoter mediates transcriptional silencing during SMC phenotypic switching in vivo. *Circ Res* **111**, **685**–**6**, (2012).

236. Gomez, D. & Owens, G. K. Smooth muscle cell phenotypic switching in atherosclerosis. *Cardiovascular Research* (2012) doi:10.1093/cvr/cvs115.

237. House, S. J., Potier, M., Bisaillon, J., Singer, H. A. & Trebak, M. The non-excitable smooth muscle: Calcium signaling and phenotypic switching during vascular disease. *Pflugers Archiv European Journal of Physiology* (2008) doi:10.1007/s00424-008-0491-8.

238. Majesky, M. W. Developmental basis of vascular smooth muscle diversity. *Arteriosclerosis, Thrombosis, and Vascular Biology* (2007) doi:10.1161/ATVBAHA.107.141069.

239. Wang, G., Jacquet, L., Karamariti, E. & Xu, Q. Origin and differentiation of vascular smooth muscle cells. *J. Physiol.* (2015) doi:10.1113/JP270033.

240. Sinha, S., Hoofnagle, M. H., Kingston, P. A., McCanna, M. E. & Owens, G. K. Transforming growth factor-β1 signaling contributes to development of smooth muscle cells from embryonic stem cells. *Am. J. Physiol. Physiol.* (2004) doi:10.1152/ajpcell.00221.2004.

241. Deng, H. B. *et al.* A polymorphism in transforming growth factor-β1 is associated with carotid plaques and increased carotid intima-media thickness in older Chinese men: The Guangzhou Biobank Cohort Study-Cardiovascular Disease Subcohort. *Atherosclerosis* (2011) doi:10.1016/j.atherosclerosis.2010.11.025.

242. Rao, M. *et al.* Transforming growth factor-beta 1 gene polymorphisms and cardiovascular disease in hemodialysis patients. *Kidney Int.* (2004) doi:10.1111/j.1523-1755.2004.00748.x.

243. Saltis, J., Agrotis, A. & Bobik, A. Regulation and interactions of transforming growth factor-β with cardiovascular cells: Implications for development and disease. *Clinical and Experimental Pharmacology and Physiology* (1996) doi:10.1111/j.1440-1681.1996.tb02595.x.

244. Yamamoto, K. *et al.* Ribozyme oligonucleotides against transforming growth factor-β inhibited neointimal formation after vascular injury in rat model: Potential application of ribozyme strategy to treat cardiovascular disease. *Circulation* (2000) doi:10.1161/01.CIR.102.11.1308.

245. Kanzaki, T. *et al.* In vivo effect of TGF-β1: Enhanced intimal thickening by administration of TGF-β1 in rabbit arteries injured with a balloon catheter. *Arterioscler. Thromb. Vasc. Biol.* (1995) doi:10.1161/01.ATV.15.11.1951.

246. AJ, L. Genetics of Atherosclerosis. *Trends Genet.* (2012) doi:10.1016/j.biotechadv.2011.08.021.Secreted.

247. Mallat, Z. *et al.* Inhibition of transforming growth factor-β signaling accelerates atherosclerosis and induces an unstable plaque phenotype in mice. *Circ. Res.* (2001) doi:10.1161/hh2201.099415.

248. Doi, H. *et al.* Notch signaling regulates the differentiation of bone marrow-derived cells into smooth muscle-like cells during arterial lesion formation. *Biochem. Biophys. Res. Commun.* (2009) doi:10.1016/j.bbrc.2009.02.116.

249. High, F. A. *et al.* An essential role for Notch in neural crest during cardiovascular development and smooth muscle differentiation. *J. Clin. Invest.* (2007) doi:10.1172/JCI30070.

250. Noseda, M. *et al.* Smooth muscle α-actin is a direct target of Notch/CSL. *Circ. Res.* (2006) doi:10.1161/01.RES.0000229683.81357.26.

251. Domenga, V. *et al.* Notch3 is required for arterial identity and maturation of vascular smooth muscle cells. *Genes Dev.* (2004) doi:10.1101/gad.308904.

252. Heldin, C.-H. & Westermark, B. Mechanism of Action and In Vivo Role of Platelet-Derived Growth Factor. *Physiol. Rev.* (2017) doi:10.1152/physrev.1999.79.4.1283.

253. Zhao, Y. *et al.* PDGF-induced vascular smooth muscle cell proliferation is associated with dysregulation of insulin receptor substrates. *Am. J. Physiol. Physiol.* (2011) doi:10.1152/ajpcell.00670.2008.

254. Tanizawa, S., Ueda, M., Van Der Loos, C. M., Van Der Wal, A. C. & Becker, A. E.

Expression of platelet derived growth factor B chain and β receptor in human coronary arteries after percutaneous transluminal coronary angioplasty: An immunohistochemical study. *Heart* (1996) doi:10.1136/hrt.75.6.549.

255. Aromatario, C. *et al.* Fluid shear stress increases the release of platelet derived growth factor BB (PDGF BB) by aortic endothelial cells. *Minerva Cardioangiol.* (1997).

256. Chang, Y. S., Yaccino, J. A., Lakshminarayanan, S., Frangos, J. A. & Tarbell, J. M. Shear-induced increase in hydraulic conductivity in endothelial cells is mediated by a nitric oxide-dependent mechanism. *Arterioscler. Thromb. Vasc. Biol.* (2000) doi:10.1161/01.ATV.20.1.35.

257. DeMaio, L., Chang, Y. S., Gardner, T. W., Tarbell, J. M. & Antonetti, D. A. Shear stress regulates occludin content and phosphorylation. *Am. J. Physiol. Circ. Physiol.* (2017) doi:10.1152/ajpheart.2001.281.1.h105.

258. Papadaki, M., Tilton, R. G., Eskin, S. G. & McIntire, L. V. Nitric oxide production by cultured human aortic smooth muscle cells: stimulation by fluid flow. *Am. J. Physiol. Circ. Physiol.* (2017) doi:10.1152/ajpheart.1998.274.2.h616.

259. Gosgnach, W., Messika-Zeitoun, D., Gonzalez, W., Philipe, M. & Michel, J.-B. Shear stress induces iNOS expression in cultured smooth muscle cells: role of oxidative stress. *Am. J. Physiol. Physiol.* (2017) doi:10.1152/ajpcell.2000.279.6.c1880.

260. Garanich, J. S., Pahakis, M. & Tarbell, J. M. Shear stress inhibits smooth muscle cell migration via nitric oxide-mediated downregulation of matrix metalloproteinase-2 activity. *Am. J. Physiol. Circ. Physiol.* (2005) doi:10.1152/ajpheart.00428.2003.

261. Doran, A. C., Meller, N. & McNamara, C. A. Role of smooth muscle cells in the initiation and early progression of atherosclerosis. *Arteriosclerosis, Thrombosis, and Vascular Biology* (2008) doi:10.1161/ATVBAHA.107.159327.

262. Rosner, D. *et al.* Interferon-γ induces Fas trafficking and sensitization to apoptosis in vascular smooth muscle cells via a P13K- and Akt-dependent mechanism. *Am. J. Pathol.* (2006) doi:10.2353/ajpath.2006.050473.

263. Grootaert, M. O. J. *et al.* Vascular smooth muscle cell death, autophagy and

senescence in atherosclerosis. *Cardiovascular Research* (2018) doi:10.1093/cvr/cvy007.

264. Guyton, A. C. & Hall, J. E. *Textbook of medical physiology 11th Edition*. *Elsevier saunders* (2006). doi:10.1136/pgmj.51.599.683-c.

265. Marcelo, K. L., Goldie, L. C. & Hirschi, K. K. Regulation of endothelial cell differentiation and specification. *Circulation Research* (2013) doi:10.1161/CIRCRESAHA.113.300506.

266. Senger, D. R. & Davis, G. E. 16. Angiogenesis. *Cold Spring Harb. Perspect. Biol.* (2011) doi:10.1101/cshperspect.a005090.

267. Andrae, J., Gallini, R. & Betsholtz, C. Role of platelet-derived growth factors in physiology and medicine. *Genes and Development* (2008) doi:10.1101/gad.1653708.

268. Gaengel, K., Genové, G., Armulik, A. & Betsholtz, C. Endothelial-mural cell signaling in vascular development and angiogenesis. *Arteriosclerosis, Thrombosis, and Vascular Biology* (2009) doi:10.1161/ATVBAHA.107.161521.

269. Bergers, G., Song, S., Meyer-Morse, N., Bergsland, E. & Hanahan, D. Benefits of targeting both pericytes and endothelial cells in the tumor vasculature with kinase inhibitors. *J. Clin. Invest.* (2003) doi:10.1172/JCI200317929.

270. Eklund, L., & Saharinen, P. (2013). Angiopoietin signaling in the vasculature. Experimental Cell Research, 319(9), 1271–1280. https://doi.org/10.1016/j.yexcr.2013.03.011Eklund, L. & Saharinen, P. Angiopoietin signaling in the vasculature. *Exp. Cell Res.* (2013) doi:10.1016/j.yexcr.2013.03.011.

271. Chislock, E. M., Ring, C. & Pendergast, A. M. Abl kinases are required for vascular function, Tie2 expression, and angiopoietin-1-mediated survival. *Proc. Natl. Acad. Sci.* (2013) doi:10.1073/pnas.1304188110.

272. Jeansson, M. *et al.* Angiopoietin-1 is essential in mouse vasculature during development and in response to injury. *J. Clin. Invest.* (2011) doi:10.1172/JCI46322.

273. Saharinen, P. *et al.* Angiopoietins assemble distinct Tie2 signalling complexes in endothelial cell-cell and cell-matrix contacts. *Nat. Cell Biol.* (2008)

doi:10.1038/ncb1715.

274. Kono, M., Allende, M. L. & Proia, R. L. Sphingosine-1-phosphate regulation of mammalian development. *Biochimica et Biophysica Acta - Molecular and Cell Biology of Lipids* (2008) doi:10.1016/j.bbalip.2008.07.001.

275. Kono, M. *et al.* The sphingosine-1-phosphate receptors S1P1, S1P2, and S1P3 function coordinately during embryonic angiogenesis. *J. Biol. Chem.* (2004) doi:10.1074/jbc.M403937200.

276. High, F. A. *et al.* Endothelial expression of the Notch ligand Jagged1 is required for vascular smooth muscle development. *Proc. Natl. Acad. Sci.* (2008) doi:10.1073/pnas.0709663105.

277. Heberlein, K. R., Straub, A. C. & Isakson, B. E. The myoendothelial junction: Breaking through the matrix? *Microcirculation* (2009) doi:10.1080/10739680902744404.

278. Sandow, S. L. *et al.* What's where and why at a vascular myoendothelial microdomain signalling complex. *Clinical and Experimental Pharmacology and Physiology* (2009) doi:10.1111/j.1440-1681.2008.05076.x.

279. Johnson, R. G., Herman, W. S. & Preus, D. M. Homocellular and heterocellular gap junctions in Limulus: A thin-section and freeze-fracture study. *J. Ultrasructure Res.* (1973) doi:10.1016/S0022-5320(73)80040-1.

280. Sandow, S. L. & Hill, C. E. Incidence of myoendothelial gap junctions in the proximal and distal mesenteric arteries of the rat is suggestive of a role in endothelium-derived hyperpolarizing factor-mediated responses. *Circ. Res.* (2000) doi:10.1161/01.RES.86.3.341.

281. Li, M., Qian, M., Kyler, K. & Xu, J. Endothelial–Vascular Smooth Muscle Cells Interactions in Atherosclerosis. *Front. Cardiovasc. Med.* (2018) doi:10.3389/fcvm.2018.00151.

282. Buttari, B. *et al.* Erythrocytes from patients with carotid atherosclerosis fail to control dendritic cell maturation. *Int. J. Cardiol.* (2012) doi:10.1016/j.ijcard.2011.12.068.

283. Profumo, E. *et al.* Redox imbalance of red blood cells impacts T lymphocyte

homeostasis: implication in carotid atherosclerosis. *Thromb. Haemost.* (2011) doi:10.1160/th11-02-0110.

284. Minetti, M., Agati, L. & Malorni, W. The microenvironment can shift erythrocytes from a friendly to a harmful behavior: Pathogenetic implications for vascular diseases. *Cardiovascular Research* (2007) doi:10.1016/j.cardiores.2007.03.007.

285. Comporti, M., Signorini, C., Buonocore, G. & Ciccoli, L. Iron release, oxidative stress and erythrocyte ageing. *Free Radic. Biol. Med.* (2002) doi:10.1016/S0891-5849(02)00759-1.

286. Buttari, B. *et al.* Oxidized Haemoglobin–Driven Endothelial Dysfunction and Immune Cell Activation: Novel Therapeutic Targets for Atherosclerosis. *Curr. Med. Chem.* (2013) doi:10.2174/09298673113209990162.

287. Buttari, B. *et al.* Haemoglobin triggers chemotaxis of human monocyte-derived dendritic cells: Possible role in atherosclerotic lesion instability. *Atherosclerosis* (2011) doi:10.1016/j.atherosclerosis.2010.12.032.

288. Silva, G. *et al.* Oxidized hemoglobin is an endogenous proinflammatory agonist that targets vascular endothelial cells. *J. Biol. Chem.* (2009) doi:10.1074/jbc.M109.045344.

289. Yun, S.-H., Sim, E.-H., Goh, R.-Y., Park, J.-I. & Han, J.-Y. Platelet Activation: The Mechanisms and Potential Biomarkers. *Biomed Res. Int.* (2016) doi:10.1155/2016/9060143.

290. Hodivala-Dilke, K. M. *et al.* β3-integrin-deficient mice are a model for Glanzmann thrombasthenia showing placental defects and reduced survival. *J. Clin. Invest.* (1999) doi:10.1172/JCI5487.

291. French, D. L. & Seligsohn, U. Platelet glycoprotein IIb/IIIa receptors and Glanzmann's thrombasthenia. *Arteriosclerosis, Thrombosis, and Vascular Biology* (2000) doi:10.1161/01.ATV.20.3.607.

292. Weyrich, A. S. Platelets: More than a sack of glue. *Hematology* (2014) doi:10.1182/asheducation-2014.1.400.

293. Herter, J. M., Rossaint, J. & Zarbock, A. Platelets in inflammation and immunity.

Journal of Thrombosis and Haemostasis (2014) doi:10.1111/jth.12730.

294. Clemetson, K. J. Platelets and primary haemostasis. *Thrombosis Research* (2012) doi:10.1016/j.thromres.2011.11.036.

295. Ley, K., Laudanna, C., Cybulsky, M. I. & Nourshargh, S. Getting to the site of inflammation: The leukocyte adhesion cascade updated. *Nature Reviews Immunology* (2007) doi:10.1038/nri2156.

296. Kansas, G. S. Selectins and their ligands: current concepts and controversies. *Blood* (1996).

297. Rivera-Nieves, J. *et al.* Critical role of endothelial P-selectin glycoprotein ligand 1 in chronic murine ileitis. *J. Exp. Med.* (2006) doi:10.1084/jem.20052530.

298. McEver, R. P. & Cummings, R. D. Role of PSGL-1 binding to selectins in leukocyte recruitment. *Journal of Clinical Investigation* (1997).

299. Moore, K. L. The Biology and Enzymology of Protein Tyrosine O -Sulfation . *J. Biol. Chem.* (2003) doi:10.1074/jbc.r300008200.

300. Hidalgo, A., Peired, A. J., Wild, M. K., Vestweber, D. & Frenette, P. S. Complete Identification of E-Selectin Ligands on Neutrophils Reveals Distinct Functions of PSGL-1, ESL-1, and CD44. *Immunity* (2007) doi:10.1016/j.immuni.2007.03.011.

301. Eriksson, E. E., Xie, X., Werr, J., Thoren, P. & Lindbom, L. Importance of Primary Capture and L-Selectin–Dependent Secondary Capture in Leukocyte Accumulation in Inflammation and Atherosclerosis in Vivo. *J. Exp. Med.* (2001) doi:10.1084/jem.194.2.205.

302. Sperandio, M. *et al.* P-selectin Glycoprotein Ligand-1 Mediates L-Selectin–dependent Leukocyte Rolling in Venules. *J. Exp. Med.* (2003) doi:10.1084/jem.20021854.

303. Bullard, D. C. Infectious susceptibility and severe deficiency of leukocyte rolling and recruitment in E-selectin and P-selectin double mutant mice. *J. Exp. Med.* (2004) doi:10.1084/jem.183.5.2329.

304. Jung, U. & Ley, K. Mice lacking two or all three selectins demonstrate overlapping and distinct functions for each selectin. *J. Immunol.* (1999).

305. Campbell, I. D. & Humphries, M. J. Integrin structure, activation, and interactions. *Cold Spring Harb. Perspect. Biol.* (2011) doi:10.1101/cshperspect.a004994.

306. Canalli, A. A. *et al.* Participation of Mac-1, LFA-1 and VLA-4 integrins in the in vitro adhesion of sickle cell disease neutrophils to endothelial layers, and reversal of adhesion by simvastatin. *Haematologica* (2011) doi:10.3324/haematol.2010.032912.

307. Conran, N., Gambero, A., Ferreira, H. H. A., Antunes, E. & De Nucci, G. Nitric oxide has a role in regulating VLA-4-integrin expression on the human neutrophil cell surface. *Biochem. Pharmacol.* (2003) doi:10.1016/S0006-2952(03)00243-0.

308. Zarbock, A., Lowell, C. A. & Ley, K. Syk signaling is necessary for E-selectin-induced LFA-1-ICAM-1 association and rolling but not arrest. *Immunity* (2007) doi:10.1016/j.immuni.2007.04.011.

309. Campbell, J. J., Qin, S., Bacon, K. B., Mackay, C. R. & Butcher, E. C. Biology of chemokine and classical chemoattractant receptors: Differential requirements for adhesion-triggering versus chemotactic responses in lymphoid cells. *J. Cell Biol.* (1996) doi:10.1083/jcb.134.1.255.

310. Campbell, J. J. *et al.* Chemokines and the arrest of lymphocytes rolling under flow conditions. *Science (80-.).* (1998) doi:10.1126/science.279.5349.381.

311. Von Hundelshausen, P. *et al.* RANTES deposition by platelets triggers monocyte arrest on inflamed and atherosclerotic endothelium. *Circulation* (2001) doi:10.1161/01.CIR.103.13.1772.

312. Huo, Y. *et al.* Circulating activated platelets exacerbate atherosclerosis in mice deficient in apolipoprotein E. *Nat. Med.* (2003) doi:10.1038/nm810.

313. Phillipson, M. *et al.* Intraluminal crawling of neutrophils to emigration sites: a molecularly distinct process from adhesion in the recruitment cascade. *J. Exp. Med.* (2006) doi:10.1084/jem.20060925.

314. Dunne, J. L., Collins, R. G., Beaudet, A. L., Ballantyne, C. M. & Ley, K. Mac-1, but Not LFA-1, Uses Intercellular Adhesion Molecule-1 to Mediate Slow Leukocyte Rolling in TNF- -Induced Inflammation. *J. Immunol.* (2003) doi:10.4049/jimmunol.171.11.6105.

315. Muller, W. A. Leukocyte-endothelial-cell interactions in leukocyte transmigration and the inflammatory response. *Trends Immunol.* (2003).

316. Vestweber, D. Regulation of endothelial cell contacts during leukocyte extravasation. *Current Opinion in Cell Biology* (2002) doi:10.1016/S0955-0674(02)00372-1.

317. Nourshargh, S., Krombach, F. & Dejana, E. The role of JAM-A and PECAM-1 in modulating leukocyte infiltration in inflamed and ischemic tissues. *J. Leukoc. Biol.* (2006) doi:10.1189/jlb.1105645.

318. Mamdouh, Z., Chen, X., Plerini, L. M., Maxfield, F. R. & Muller, W. A. Targeted recycling of PECAM from endothelial surface-connected compartments during diapedesis. *Nature* (2003) doi:10.1038/nature01300.

319. Feng, D., Nagy, J. A., Pyne, K., Dvorak, H. F. & Dvorak, A. M. Neutrophils emigrate from venules by a transendothelial cell pathway in response to FMLP. *J. Exp. Med.* (1998).

320. Engelhardt, B. & Wolburg, H. Mini review: Transendothelial migration of leukocytes: Through the front door or around the side of the house? *European Journal of Immunology* (2004) doi:10.1002/eji.200425327.

321. Millán, J. *et al.* Lymphocyte transcellular migration occurs through recruitment of endothelial ICAM-1 to caveola- and F-actin-rich domains. *Nat. Cell Biol.* (2006) doi:10.1038/ncb1356.

322. Nieminen, M. *et al.* Vimentin function in lymphocyte adhesion and transcellular migration. *Nat. Cell Biol.* (2006) doi:10.1038/ncb1355.

323. Cinamon, G., Shinder, V., Shamri, R. & Alon, R. Chemoattractant Signals and 2 Integrin Occupancy at Apical Endothelial Contacts Combine with Shear Stress Signals to Promote Transendothelial Neutrophil Migration. *J. Immunol.* (2014) doi:10.4049/jimmunol.173.12.7282.

324. Werr, J., Eriksson, E. E., Hedqvist, P. & Lindbom, L. Engagement of {beta}2 integrins induces surface expression of {beta}1 integrin receptors in human neutrophils. *J. Leukoc. Biol.* (2000).

325. Daguès, N. *et al.* Investigation of the molecular mechanisms preceding PDE4 inhibitor-induced vasculopathy in rats: Tissue inhibitor of metalloproteinase 1, a potential predictive biomarker. *Toxicol. Sci.* (2007) doi:10.1093/toxsci/kfm161.

326. Hahn, C. & Schwartz, M. A. Mechanotransduction in vascular physiology and atherogenesis. *Nature Reviews Molecular Cell Biology* (2009) doi:10.1038/nrm2596.

327. Lee, R. D. B. & Langille, B. L. Arterial adaptations to altered blood flow. *Can. J. Physiol. Pharmacol.* (2011) doi:10.1139/y91-147.

328. Baffert, F. *et al.* Cellular changes in normal blood capillaries undergoing regression after inhibition of VEGF signaling. *Am. J. Physiol. Circ. Physiol.* (2006) doi:10.1152/ajpheart.00616.2005.

329. Wang, N. *et al.* Shear stress regulation of Krüppel-like factor 2 expression is flow pattern-specific. *Biochem. Biophys. Res. Commun.* (2006) doi:10.1016/j.bbrc.2006.01.089.

330. Miao, H. *et al.* Effects of flow patterns on the localization and expression of VE-cadherin at vascular endothelial cell junctions: In vivo and in vitro investigations. *J. Vasc. Res.* (2005) doi:10.1159/000083094.

331. Li, Y. S. J., Haga, J. H. & Chien, S. Molecular basis of the effects of shear stress on vascular endothelial cells. *Journal of Biomechanics* (2005) doi:10.1016/j.jbiomech.2004.09.030.

332. Orr, A. W., Helmke, B. P., Blackman, B. R. & Schwartz, M. A. Mechanisms of mechanotransduction. *Developmental Cell* (2006) doi:10.1016/j.devcel.2005.12.006.

333. Coste, B. *et al.* Piezo proteins are pore-forming subunits of mechanically activated channels. *Nature* (2012) doi:10.1038/nature10812.

334. Ge, J. *et al.* Architecture of the mammalian mechanosensitive Piezo1 channel. *Nature* (2015) doi:10.1038/nature15247.

335. Woo, S. H. *et al.* Piezo2 is required for Merkel-cell mechanotransduction. *Nature* (2014) doi:10.1038/nature13251.

336. Ranade, S. S. *et al.* Piezo1, a mechanically activated ion channel, is required for

vascular development in mice. *Proc. Natl. Acad. Sci.* (2014) doi:10.1073/pnas.1409233111.

337. Li, J. *et al.* Piezo1 integration of vascular architecture with physiological force. *Nature* (2014) doi:10.1038/nature13701.

338. Wang, S. P. *et al.* Endothelial cation channel PIEZO1 controls blood pressure by mediating flow-induced ATP release. *J. Clin. Invest.* (2016) doi:10.1172/JCI87343.

339. Dimmeler, S. *et al.* Activation of nitric oxide synthase in endothelial cells by Akt-dependent phosphorylation. *Nature* (1999) doi:10.1038/21224.

340. Jessica E. Davies, Dora Lopresto, Bonita H.R. Apta, Zhiyuan Lin, W. M. and M. T. H. Using Yoda-1 to mimick laminar flow in vitro. A helpful tool to simplify drug testing.

341. Jaffe, E. A., Nachman, R. L., Becker, C. G. & Minick, C. R. Culture of human endothelial cells derived from umbilical veins. Identification by morphologic and immunologic criteria. *J. Clin. Invest.* (1973) doi:10.1172/JCI107470.

342. Bacakova, L. *et al.* The Role of Vascular Smooth Muscle Cells in the Physiology and Pathophysiology of Blood Vessels. in *Muscle Cell and Tissue - Current Status of Research Field* (2018). doi:10.5772/intechopen.77115.

343. Liao, H. *et al.* Effects of long-term serial cell passaging on cell spreading, migration, and cell-surface ultrastructures of cultured vascular endothelial cells. *Cytotechnology* (2014) doi:10.1007/s10616-013-9560-8.

344. Boneu, B., Abbal, M., Plante, J. & Bierme, R. FACTOR-VIII COMPLEX AND ENDOTHELIAL DAMAGE. *The Lancet* (1975) doi:10.1016/S0140-6736(75)92650-1.

345. Lip, G. Y. H. & Blann, A. von Willebrand factor: A marker of endothelial dysfunction in vascular disorders? *Cardiovascular Research* (1997) doi:10.1016/S0008-6363(97)00039-4.

346. De Groot, P. G. *et al.* Isolation of a storage and secretory organelle containing Von Willebrand protein from cultured human endothelial cells. *Biochim. Biophys. Acta - Mol. Cell Res.* (2003) doi:10.1016/0167-4889(84)90140-x.

347. Bogatcheva, N. V., Garcia, J. G. & Verin, A. D. Molecular mechanisms of thrombin-

induced endothelial cell permeability. *Biochemistry. Biokhimiia* (2002) doi:10.1023/A:1013904231324.

348. Peyvandi, F., Garagiola, I. & Baronciani, L. Role of von Willebrand factor in the haemostasis. *Blood Transfusion* (2011) doi:10.2450/2011.002S.

349. Wagner, D. Cell Biology Of Von Willebrand Factor. *Annu. Rev. Cell Dev. Biol.* (2002) doi:10.1146/annurev.cellbio.6.1.217.

350. Wagner, D. D. *et al.* Divergent fates of von Willebrand factor and its propolypeptide (von Willebrand antigen II) after secretion from endothelial cells. *Proc. Natl. Acad. Sci.* (2006) doi:10.1073/pnas.84.7.1955.

351. Olsen, E. H. N. *et al.* Comparative response of plasma VWF in dogs to up-regulation of VWF mRNA by interleukin-11 versus Weibel-Palade body release by desmopressin (DDAVP). *Blood* (2003) doi:10.1182/blood-2003-01-0290.

352. Davies, P. F. Hemodynamic shear stress and the endothelium in cardiovascular pathophysiology. *Nature Clinical Practice Cardiovascular Medicine* (2009) doi:10.1038/ncpcardio1397.

353. Korkmaz, S. *et al.* An increased regional blood flow precedes mesenteric inflammation in rats treated by a phosphodiesterase 4 inhibitor. *Toxicol. Sci.* (2009) doi:10.1093/toxsci/kfn218.

354. Gimbrone, M. A., Nagel, T. & Topper, J. N. Biomechanical activation: An emerging paradigm in endothelial adhesion biology. *Journal of Clinical Investigation* (1997) doi:10.1172/JCI119346.

355. Malek, A. M., Alper, S. L. & Izumo, S. Hemodynamic shear stress and its role in atherosclerosis. *J. Am. Med. Assoc.* (1999) doi:10.1001/jama.282.21.2035.

356. Chappell, D. C., Varner, S. E., Nerem, R. M., Medford, R. M. & Alexander, R. W. Oscillatory shear stress stimulates adhesion molecule expression in cultured human endothelium. *Circ. Res.* (1998) doi:10.1161/01.RES.82.5.532.

357. Brooks, A. R., Lelkes, P. I. & Rubanyi, G. M. Gene expression profiling of human aortic endothelial cells exposed to disturbed flow and steady laminar flow. *Physiol.*

Genomics (2002) doi:10.1152/physiolgenomics.00075.2001.

358. Davies, P. F., Remuzzi, A., Gordon, E. J., Dewey, C. F. & Gimbrone, M. A. Turbulent fluid shear stress induces vascular endothelial cell turnover in vitro. *Proc. Natl. Acad. Sci. U. S. A.* (1986).

359. Mankoff, S. P., Brander, C., Ferrone, S. & Marincola, F. M. Lost in translation: Obstacles to translational medicine. *J. Transl. Med.* (2004) doi:10.1186/1479-5876-2-14.

360. Fleming, W. H. Endothelial cell-specific markers: Going . . . going . . . gone. *Blood* (2005) doi:10.1182/blood-2005-05-1893.

361. Harris, E. S. & Nelson, W. J. VE-cadherin: At the front, center, and sides of endothelial cell organization and function. *Current Opinion in Cell Biology* (2010) doi:10.1016/j.ceb.2010.07.006.

362. El-Mezgueldi, M. Calponin. *Int. J. Biochem. Cell Biol.* (1996) doi:10.1016/S1357-2725(96)00085-4.

363. Giblin, J. P., Hewlett, L. J. & Hannah, M. J. Basal secretion of von willebrand factor from human endothelial cells. *Blood* (2008) doi:10.1182/blood-2007-12-130740.

364. Jamur, M. C. & Oliver, C. Permeabilization of Cell Membranes. in (2010). doi:10.1007/978-1-59745-324-0_9.

365. Liu, L. & Shi, G. P. CD31: Beyond a marker for endothelial cells. *Cardiovascular Research* (2012) doi:10.1093/cvr/cvs108.

366. Roux, S. & Rubin, L. J. Bosentan: a dual endothelin receptor antagonist. *Expert Opin. Investig. Drugs* (2005) doi:10.1517/13543784.11.7.991.

367. Ishikawa, K. *et al.* Cyclic Pentapeptide Endothelin Antagonists with High ETA Selectivity. Potency- and Solubility-Enhancing Modifications. *J. Med. Chem.* (1992) doi:10.1021/jm00089a028.

368. Okada, M. & Nishikibe, M. BQ-788, A Selective Endothelin ETB Receptor Antagonist. *Cardiovasc. Drug Rev.* (2010) doi:10.1111/j.1527-3466.2002.tb00082.x.

369. Meiring, M., Allers, W. & Le Roux, E. Tissue factor: A potent stimulator of Von Willebrand factor synthesis by human umbilical vein endothelial cells. *Int. J. Med. Sci.* (2016) doi:10.7150/ijms.15688.

370. Langer, F., Morys-Wortmann, C., Küsters, B. & Storck, J. Endothelial protease-activated receptor-2 induces tissue factor expression and von Willebrand factor release. *Br. J. Haematol.* (1999) doi:10.1111/j.1365-2141.1999.01356.x.

371. Storck, J., Küsters, B. & Zimmermann, E. R. The tethered ligand receptor is the responsible receptor for the thrombin induced release of von Willebrand factor from endothelial cells (HUVEC). *Thromb. Res.* (1995) doi:10.1016/0049-3848(95)91612-O.

372. Blaauboer, B. J. Biokinetic modeling and in vitro-in vivo extrapolations. *Journal of Toxicology and Environmental Health - Part B: Critical Reviews* (2010) doi:10.1080/10937404.2010.483940.

373. Sanz, M. J. *et al.* Roflumilast inhibits leukocyte-endothelial cell interactions, expression of adhesion molecules and microvascular permeability. *Br. J. Pharmacol.* (2007) doi:10.1038/sj.bjp.0707428.

374. Rabiet, M. J. *et al.* Thrombin-induced increase in endothelial permeability is associated with changes in cell-to-cell junction organization. *Arterioscler. Thromb. Vasc. Biol.* (1996) doi:10.1161/01.ATV.16.3.488.

375. Suttorp, N. *et al.* Hyperpermeability of pulmonary endothelial monolayer: Protective role of phosphodiesterase isoenzymes 3 and 4. *Lung* (2004) doi:10.1007/bf00173310.

376. Draijer, R., Atsma, D. E., Van Der Laarse, A. & Van Hinsbergh, V. W. M. cGMP and nitric oxide modulate thrombin-induced endothelial permeability: Regulation via different pathways in human aortic and umbilical vein endothelial cells. *Circ. Res.* (1995) doi:10.1161/01.RES.76.2.199.

377. Cullere, X. *et al.* Regulation of vascular endothelial barrier function by Epac, a cAMP-activated exchange factor for Rap GTPase. *Blood* (2005) doi:10.1182/blood-2004-05-1987.

378. Fukuhara, S. *et al.* Cyclic AMP Potentiates Vascular Endothelial Cadherin-Mediated

Cell-Cell Contact To Enhance Endothelial Barrier Function through an Epac-Rap1 Signaling Pathway. *Mol. Cell. Biol.* (2004) doi:10.1128/mcb.25.1.136-146.2005.

379. Kooistra, M. R. H., Corada, M., Dejana, E. & Bos, J. L. Epac1 regulates integrity of endothelial cell junctions through VE-cadherin. *FEBS Lett.* (2005) doi:10.1016/j.febslet.2005.07.080.

380. Birukova, A. A. *et al.* Prostaglandins PGE2 and PGI2 promote endothelial barrier enhancement via PKA- and Epac1/Rap1-dependent Rac activation. *Exp. Cell Res.* (2007) doi:10.1016/j.yexcr.2007.03.036.

381. Petty, R. D., Sutherland, L. A., Hunter, E. M. & Cree, I. A. Comparison of MTT and ATP-based assays for the measurement of viable cell number. *J. Biolumin. Chemilumin.* (1995) doi:10.1002/bio.1170100105.

382. Cree, I. A. *et al.* Methotrexate chemosensitivity by ATP luminescence in human leukemia cell lines and in breast cancer primary cultures: Comparison of the TCA-100 assay with a clonogenic assay. *Anticancer. Drugs* (1995) doi:10.1097/00001813-199506000-00006.

383. Maehara, Y., Anai, H., Tamada, R. & Sugimachi, K. The ATP assay is more sensitive than the succinate dehydrogenase inhibition test for predicting cell viability. *Eur. J. Cancer Clin. Oncol.* (1987) doi:10.1016/0277-5379(87)90070-8.

384. Han, J. H. *et al.* Effect of minoxidil on proliferation and apoptosis in dermal papilla cells of human hair follicle. *J. Dermatol. Sci.* (2004) doi:10.1016/j.jdermsci.2004.01.002.

385. Duval, K. *et al.* Modeling Physiological Events in 2D vs. 3D Cell Culture. *Physiology* (2017) doi:10.1152/physiol.00036.2016.

386. Li, Z., Nater, C., Kinsella, J., Chrest, F. & Lakatta, E. G. Minoxidil inhibits proliferation and migration of cultured vascular smooth muscle cells and neointimal formation after balloon catheter injury. *J. Cardiovasc. Pharmacol.* (2000) doi:10.1097/00005344-200036001-00065.

387. Ogawa, A., Nakamura, K., Akagi, S., Kusano, K. & Ito, H. Abstract 16380: Bosentan

Inhibits Proliferation of Cells Isolated from Patients with Chronic Thromboembolic Pulmonary Hypertension . *Circulation* (2010).

388. Tesfamariam, B. & DeFelice, A. F. Endothelial injury in the initiation and progression of vascular disorders. *Vascular Pharmacology* (2007) doi:10.1016/j.vph.2006.11.005.

389. Videm, V. & Albrigtsen, M. Soluble ICAM-1 and VCAM-1 as markers of endothelial activation. *Scand. J. Immunol.* (2008) doi:10.1111/j.1365-3083.2008.02029.x.

390. Faggiotto, A., Ross, R. & Harker, L. Studies of hypercholesterolemia in the nonhuman primate. I. Changes that lead to fatty streak formation. *Arterioscler. An Off. J. Am. Hear. Assoc. Inc.* (2011) doi:10.1161/01.atv.4.4.323.

391. Iiyama, K. *et al.* Patterns of vascular cell adhesion molecule-1 and intercellular adhesion molecule-1 expression in rabbit and mouse atherosclerotic lesions and at sites predisposed to lesion formation. *Circ. Res.* (1999) doi:10.1161/01.RES.85.2.199.

392. McHale, J. F., Harari, O. a, Marshall, D. & Haskard, D. O. TNF-alpha and IL-1 sequentially induce endothelial ICAM-1 and VCAM-1 expression in MRL/lpr lupus-prone mice. *J. Immunol.* (1999) doi:ji_v163n7p3993 [pii].

393. Burke-Gaffney, A. & Hellewell, P. G. Tumour necrosis factor-α-induced ICAM-1 expression in human vascular endothelial and lung epithelial cells: Modulation by tyrosine kinase inhibitors. *Br. J. Pharmacol.* (1996) doi:10.1111/j.1476-5381.1996.tb16017.x.

394. Iademarco, M. F., Barks, J. L. & Dean, D. C. Regulation of vascular cell adhesion molecule-1 expression by IL-4 and TNF-α in cultured endothelial cells. *J. Clin. Invest.* (1995).

395. Marui, N. *et al.* Vascular cell adhesion molecule-1 (VCAM-1) gene transcription and expression are regulated through an antioxidant-sensitive mechanism in human vascular endothelial cells. *J. Clin. Invest.* (1993) doi:10.1172/JCI116778.

396. Kowalczyk, A., Kleniewska, P., Kolodziejczyk, M., Skibska, B. & Goraca, A. The role of endothelin-1 and endothelin receptor antagonists in inflammatory response and sepsis. *Archivum Immunologiae et Therapiae Experimentalis* (2015)

doi:10.1007/s00005-014-0310-1.

397. Iannone, F. *et al.* Bosentan regulates the expression of adhesion molecules on circulating T cells and serum soluble adhesion molecules in systemic sclerosis-associated pulmonary arterial hypertension. *Ann. Rheum. Dis.* (2008) doi:10.1136/ard.2007.080424.

398. Muller, D. N. *et al.* Effect of bosentan on nf-κb, inflammation, and tissue factor in angiotensin II-induced end-organ damage. *Hypertension* (2000) doi:10.1161/01.HYP.36.2.282.

399. Zhang, D. *et al.* Two disparate ligand-binding sites in the human P2Y<inf>1</inf> receptor. *Nature* (2015) doi:10.1038/nature14287.

400. Jun Zhang, S. A. *et al.* SK&F 95654-Induced Acute Cardiovascular Toxicity in Sprague-Dawley Rats—Histopathologic, Electron Microscopic, and Immunohistochemical Studies. *Toxicol. Pathol.* (2002) doi:10.1080/01926230252824680.

401. Zhang, J. *et al.* Histopathology of vascular injury in Sprague-Dawley rats treated with phosphodiesterase IV Inhibitor SCH 351591 or SCH 534385. *Toxicol. Pathol.* (2008) doi:10.1177/0192623308322308.

402. Swystun, L. L. & Liaw, P. C. The role of leukocytes in thrombosis. *Blood* (2016) doi:10.1182/blood-2016-05-718114.

403. Ramachandran, R., Hansen, K. K. & Hollenberg, M. D. Proteinase-Activated Receptors. in *Encyclopedia of Biological Chemistry: Second Edition* (2013). doi:10.1016/B978-0-12-378630-2.00398-4.

404. Moore, K. L. Structure and function of P-selectin glycoprotein ligand-1. *Leukemia and Lymphoma* (1998) doi:10.3109/10428199809058377.

405. Podolnikova, N. P., Kushchayeva, Y. S., Wu, Y. F., Faust, J. & Ugarova, T. P. The Role of Integrins αMβ2(Mac-1, CD11b/CD18) and αDβ2(CD11d/CD18) in Macrophage Fusion. *Am. J. Pathol.* (2016) doi:10.1016/j.ajpath.2016.04.001.

406. Stewart, M., Thiel, M. & Hogg, N. Leukocyte integrins. *Curr. Opin. Cell Biol.* (1995) doi:10.1016/0955-0674(95)80111-1.

407. Mitrugno, A. *et al.* Potentiation of TRAP-6-induced platelet dense granule release by blockade of P2Y 12 signaling with MRS2395. *Platelets* **29**, 383–394 (2018).

408. Lösche, W., Redlich, H., Krause, S., Heptinstall, S. & Spangenberg, P. Activation of leukocytes in whole blood samples by N-formyl-methionyl-leucyl-phenylalanine (FMLP) enhances platelet aggregability but not platelet P-selectin exposure and adhesion to leukocytes. in *Platelets* (1998). doi:10.1080/09537109876726.

409. Y., W. *et al.* Leukocyte integrin Mac-1 regulates thrombosis via interaction with platelet GPIbα. *Nat. Commun.* (2017) doi:10.1038/ncomms15559.

410. Gremmel, T. *et al.* Is TRAP-6 suitable as a positive control for platelet reactivity when assessing response to clopidogrel. *Platelets* (2010) doi:10.3109/09537104.2010.493587.

411. O'Barr, T. P., Swanson, E. W., Fitzpatrick, J. E. & Corby, D. G. Effect of minoxidil on platelet function and the synthesis of prostaglandins in platelets. *J. Lab. Clin. Med.* (1989).

412. Jagroop, I. A., Daskalopoulou, S. S. & Mikhailidis, D. P. Endothelin-1 and human platelets. *Curr. Vasc. Pharmacol.* (2005).

413. Thiemermann, C., May, G. R., Page, C. P. & Vane, J. R. Endothelin-1 inhibits platelet aggregation in vivo: a study with 111indium-labelled platelets. *Br. J. Pharmacol.* (1990) doi:10.1111/j.1476-5381.1990.tb14699.x.

414. A. Jagroop, D. P. Mikhailidis, I. Effect of endothelin-1 on human platelet shape change: reversal of activation by naftidrofuryl. *Platelets* (2002) doi:10.1080/09537100050129288.

415. Holbrook, M. & Coker, S. J. Effects of zaprinast and rolipram on platelet aggregation and arrhythmias following myocardial ischaemia and reperfusion in anaesthetized rabbits. *Br. J. Pharmacol.* (1991) doi:10.1111/j.1476-5381.1991.tb12362.x.

416. Lorenz, R., Paschke, C., Born, P. & Clemens, R. In vitro effects of the selective dopamine 1-agonist fenoldopam on the coagulation system in native whole blood: Comparison to dopamine and nitroprusside. *Thromb. Res.* (1995) doi:10.1016/0049-

3848(95)90871-C.

417. Chronos, N. A. F., Goodall, A. H., Wilson, D. J., Sigwart, U. & Buller, N. P. Profound platelet degranulation is an important side effect of some types of contrast media used in interventional cardiology. *Circulation* (1993) doi:10.1161/01.CIR.88.5.2035.

418. Baenziger, N. L. & Majerus, P. W. [12] Isolation of Human Platelets and Platelet Surface Membranes. *Methods Enzymol.* (1974) doi:10.1016/0076-6879(74)31015-4.

419. Krause, K. H., Demaurex, N., Jaconi, M. & Lew, D. P. Ion channels and receptor-mediated Ca2+ influx in neutrophil granulocytes. in *Blood Cells* (1993).

420. Pekmezci, E., Turkoğlu, M., Gökalp, H. & Kutlubay, Z. Minoxidil downregulates Interleukin-1 alpha gene expression in HaCaT cells. *Int. J. Trichology* (2018) doi:10.4103/ijt.ijt_18_17.

421. Khoury, E. L., Price, V. H., Abdel-Salam, M. M., Stern, M. & Greenspan, J. S. Topical minoxidil in alopecia areata: No effect on the perifollicular lymphoid infiltration. *J. Invest. Dermatol.* (1992) doi:10.1111/1523-1747.ep12611409.

422. Anthoni, C. *et al.* Bosentan, an endothelin receptor antagonist, reduces leucocyte adhesion and inflammation in a murine model of inflammatory bowel disease. *Int. J. Colorectal Dis.* (2006) doi:10.1007/s00384-005-0015-3.

423. Imhof, A. K. *et al.* Potent anti-inflammatory and antinociceptive activity of the endothelin receptor antagonist bosentan in monoarthritic mice. *Arthritis Res. Ther.* (2011) doi:10.1186/ar3372.

424. Dora, K. A. Cell-cell communication in the vessel wall. *Vascular Medicine* (2001) doi:10.1191/135886301666458055.

425. Totani, L. *et al.* Phosphodiesterase type 4 blockade prevents platelet-mediated neutrophil recruitment at the site of vascular injury. *Arterioscler. Thromb. Vasc. Biol.* (2014) doi:10.1161/ATVBAHA.114.303939.

426. Hatzelmann, A. & Schudt, C. Anti-inflammatory and immunomodulatory potential of the novel PDE4 inhibitor roflumilast in vitro. *J Pharmacol Exp Ther* (2001).

427. Peters-Golden, M., Canetti, C., Mancuso, P. & Coffey, M. J. Leukotrienes:

Underappreciated Mediators of Innate Immune Responses. *J. Immunol.* (2014) doi:10.4049/jimmunol.174.2.589.

428. Flamand, L., Tremblay, M. J. & Borgeat, P. Leukotriene B4 triggers the in vitro and in vivo release of potent antimicrobial agents. *J. Immunol.* (2007).

429. Wong, K. H. K. *et al.* The Role of Physical Stabilization in Whole Blood Preservation. *Sci. Rep.* (2016) doi:10.1038/srep21023.

430. Woollard, K. J. *et al.* Pathophysiological levels of soluble P-selectin mediate adhesion of leukocytes to the endothelium through mac-1 activation. *Circ. Res.* (2008) doi:10.1161/CIRCRESAHA.108.180273.

431. Chiu, J. J. *et al.* Shear stress inhibits adhesion molecule expression in vascular endothelial cells induced by coculture with smooth muscle cells. *Blood* (2003) doi:10.1182/blood-2002-08-2560.

432. Rainger, G. E., Stone, P., Morland, C. M. & Nash, G. B. A novel system for investigating the ability of smooth muscle cells and fibroblasts to regulate adhesion of flowing leukocytes to endothelial cells. *J. Immunol. Methods* (2001) doi:10.1016/S0022-1759(01)00427-6.

433. Fillinger, M. F., Sampson, L. N., Cronenwett, J. L., Powell, R. J. & Wagner, R. J. Coculture of endothelial cells and smooth muscle cells in bilayer and conditioned media models. *J. Surg. Res.* (1997) doi:10.1006/jsre.1996.4978.

434. Nackman, G. B., Bech, F. R., Fillinger, M. F., Wagner, R. J. & Cronenwett, J. L. Endothelial cells modulate smooth muscle cell morphology by inhibition of transforming growth factor-beta1 activation. *Surgery* (1996) doi:10.1016/S0039-6060(96)80318-7.

435. van Buul-Wortelboer, M. F. *et al.* Reconstitution of the vascular wall in vitro. A novel model to study interactions between endothelial and smooth muscle cells. *Exp. Cell Res.* (1986) doi:10.1016/0014-4827(86)90433-7.

436. Ziegler, T., Alexander, R. W. & Nerem, R. M. An endothelial cell-smooth muscle cell co-culture model for use in the investigation of flow effects on vascular biology. *Ann.*

Biomed. Eng. (1995) doi:10.1007/BF02584424.

437. Niwa, K., Kado, T., Sakai, J. & Karino, T. The effects of a shear flow on the uptake of LDL and acetylated LDL by an EC monoculture and an EC-SMC coculture. *Ann. Biomed. Eng.* (2004) doi:10.1023/B:ABME.0000019173.79939.54.

438. Wada, Y. *et al.* In vitro Model of Atherosclerosis Using Coculture of Arterial Wall Cells and Macrophage. *Yonsei Med. J.* (2000) doi:10.3349/ymj.2000.41.6.740.

439. Hirschi, K. K., Rohovsky, S. A. & D'Amore, P. A. PDGF, TGF-β, and heterotypic cell-cell interactions mediate endothelial cell-induced recruitment of 10T1/2 cells and their differentiation to a smooth muscle fate. *J. Cell Biol.* (1998) doi:10.1083/jcb.141.3.805.

440. Powell, R. J., Bhargava, J., Basson, M. D. & Sumpio, B. E. Coculture conditions alter endothelial modulation of TGF-β1 activation and smooth muscle growth morphology. *Am. J. Physiol. Circ. Physiol.* (2017) doi:10.1152/ajpheart.1998.274.2.h642.

441. Jaffe, E. A., Hoyer, L. W. & Nachman, R. L. Synthesis of antihemophilic factor antigen by cultured human endothelial cells. *J. Clin. Invest.* (1973) doi:10.1172/JCI107471.

442. Stoddart, M. J., Geoff Richards, R. & Alini, M. In vitro experiments with primary mammalian cells: To pool or not to pool? *European Cells and Materials* (2012) doi:10.22203/eCM.v024a00.

443. Crowley, L. C. *et al.* Measuring cell death by propidium iodide uptake and flow cytometry. *Cold Spring Harb. Protoc.* (2016) doi:10.1101/pdb.prot087163.

444. Zhang, W. J., Liu, W., Cui, L. & Cao, Y. Tissue engineering of blood vessel: Tissue Engineering Review Series. *J. Cell. Mol. Med.* (2007) doi:10.1111/j.1582-4934.2007.00099.x.

445. Wallace, C. S. & Truskey, G. A. Direct-contact co-culture between smooth muscle and endothelial cells inhibits TNF-α-mediated endothelial cell activation. *Am. J. Physiol. Circ. Physiol.* (2010) doi:10.1152/ajpheart.01029.2009.

446. Rose, S. L. & Babensee, J. E. Complimentary endothelial cell/smooth muscle cell Co-culture systems with alternate smooth muscle cell phenotypes. *Ann. Biomed. Eng.* (2007) doi:10.1007/s10439-007-9311-0.

447. Wang, H. Q., Bai, L., Shen, B. R., Yan, Z. Q. & Jiang, Z. L. Coculture with endothelial cells enhances vascular smooth muscle cell adhesion and spreading via activation of β<inf>1</inf>-integrin and phosphatidylinositol 3-kinase/Akt. *Eur. J. Cell Biol.* (2007) doi:10.1016/j.ejcb.2006.09.001.

448. Bogdanowicz, D. R. & Lu, H. H. Multifunction co-culture model for evaluating cell-cell interactions. *Methods Mol. Biol.* (2014) doi:10.1007/7651-2013-62.

449. Kurzen, H. *et al.* Tightening of endothelial cell contacts: A physiologic response to cocultures with smooth-muscle-like 10T1/2 cells. *J. Invest. Dermatol.* (2002) doi:10.1046/j.1523-1747.2002.01792.x.

450. Rainger, G. E. & Nash, G. B. Cellular pathology of atherosclerosis: Smooth muscle cells prime cocultured endothelial cells for enhanced leukocyte adhesion. *Circ. Res.* (2001) doi:10.1161/01.RES.88.6.615.

451. Nackman, G. B. *et al.* Flow modulates endothelial regulation of smooth muscle cell proliferation: A new model. *Surgery* (1998) doi:10.1016/S0039-6060(98)70141-2.

452. Duband, J. L., Gimona, M., Scatena, M., Sartore, S. & Small, J. V. Calponin and SM22 as differentiation markers of smooth muscle: spatiotemporal distribution during avian embryonic development. *Differentiation* (1993) doi:10.1111/j.1432-0436.1993.tb00027.x.

453. Actin expression in smooth muscle cells of rat aortic intimal thickening, human atheromatous plaque, and cultured rat aortic media. *J. Clin. Invest.* (1984) doi:10.1172/JCI111185.

454. Fillinger, M. F., O'Connor, S. E., Wagner, R. J. & Cronenwett, J. L. The effect of endothelial cell coculture on smooth muscle cell proliferation. *J. Vasc. Surg.* (1993) doi:10.1016/0741-5214(93)90676-D.

455. Powell, R. J., Cronenwett, J. L., Fillinger, M. F., Wagner, R. J. & Sampson, L. N. Endothelial cell modulation of smooth muscle cell morphology and organizational growth pattern. *Ann. Vasc. Surg.* (1996) doi:10.1007/BF02002334.

456. Powell, R. J., Hydowski, J., Frank, O., Bhargava, J. & Sumpio, B. E. Endothelial cell

effect on smooth muscle cell collagen synthesis. in *Journal of Surgical Research* (1997). doi:10.1006/jsre.1997.5045.

457. Rensen, S. S. M., Doevendans, P. A. F. M. & Van Eys, G. J. J. M. Regulation and characteristics of vascular smooth muscle cell phenotypic diversity. *Netherlands Heart Journal* (2007) doi:10.1007/BF03085963.

458. Thyberg, J., Hedin, U., Sjöiund, M., Palmberg, L. & Bottger, B. A. Regulation of differentiated properties and proliferation of arterial smooth muscle cells. *Arterioscler. Thromb. Vasc. Biol.* (1990) doi:10.1161/01.ATV.10.6.966.

459. Lieber, R. L. Statistical significance and statistical power in hypothesis testing. *J. Orthop. Res.* (1990) doi:10.1002/jor.1100080221.

460. Darzynkiewicz, Z. *et al.* Cytometry in cell necrobiology: Analysis of apoptosis and accidental cell death (necrosis). *Cytometry* (1997) doi:10.1002/(SICI)1097-0320(19970101)27:1<1::AID-CYTO2>3.0.CO;2-L.

461. Silva, M. T. Secondary necrosis: The natural outcome of the complete apoptotic program. *FEBS Letters* (2010) doi:10.1016/j.febslet.2010.10.046.

462. Fisher, D. E. Apoptosis in cancer therapy: Crossing the threshold. *Cell* (1994) doi:10.1016/0092-8674(94)90518-5.

463. Bowden, N. *et al.* Experimental Approaches to Study Endothelial Responses to Shear Stress. *Antioxid. Redox Signal.* (2016) doi:10.1089/ars.2015.6553.

464. Xu, X. Z. S. Demystifying Mechanosensitive Piezo Ion Channels. *Neurosci. Bull.* (2016) doi:10.1007/s12264-016-0033-x.

465. Lhomme, A. *et al.* Stretch-Activated Piezo1 Channel in Endothelial Cells Relaxes Mouse Intrapulmonary Arteries. *Am. J. Respir. Cell Mol. Biol.* (2018) doi:10.1165/rcmb.2018-0197oc.

466. Lacroix, J. J., Botello-Smith, W. M. & Luo, Y. Probing the gating mechanism of the mechanosensitive channel Piezo1 with the small molecule Yoda. *Nat. Commun.* (2018) doi:10.1038/s41467-018-04405-3.

467. Syeda, R. *et al.* Chemical activation of the mechanotransduction channel Piezo1. *Elife*

(2015) doi:10.7554/eLife.07369.

468. Syeda, R. *et al.* Piezo1 Channels Are Inherently Mechanosensitive. *Cell Rep.* (2016) doi:10.1016/j.celrep.2016.10.033.

469. Hermann, C., Zeiher, A. M. & Dimmeler, S. Shear stress inhibits H2O2-induced apoptosis of human endothelial cells by modulation of the glutathione redox cycle and nitric oxide synthase. *Arterioscler. Thromb. Vasc. Biol.* (1997) doi:10.1161/01.ATV.17.12.3588.

470. Dimmeler, S., Haendeler, J., Rippmann, V., Nehls, M. & Zeiher, A. M. Shear stress inhibits apoptosis of human endothelial cells. *FEBS Lett.* (1996) doi:10.1016/S0014-5793(96)01289-6.

471. Lipowsky, H. H., Kovalcheck, S. & Zweifach, B. W. The distribution of blood rheological parameters in the microvasculature of cat mesentery. *Circ. Res.* (1978) doi:10.1161/01.RES.43.5.738.

472. Givens, C. & Tzima, E. Endothelial Mechanosignaling: Does One Sensor Fit All? *Antioxid. Redox Signal.* (2016) doi:10.1089/ars.2015.6493.

473. Tsuboi, H., Ando, J., Korenaga, R., Takada, Y. & Kamiya, A. Flow stimulates ICAM-1 expression time and shear stress dependently in cultured human endothelial cells. *Biochem. Biophys. Res. Commun.* (1995) doi:10.1006/bbrc.1995.1140.

474. Ott, M. J. & Ballermann, B. J. Shear stress-conditioned, endothelial cell-seeded vascular grafts: Improved cell adherence in response to in vitro shear stress. *Surgery* (1995) doi:10.1016/S0039-6060(05)80210-7.

475. Nerem, R. M. Hemodynamics and the vascular endothelium. *J. Biomech. Eng.* (1993).

476. Davies, P. F. & Tripathi, S. C. Mechanical stress mechanisms and the cell. An endothelial paradigm. *Circ. Res.* (1993).

477. Schöneberg, J. *et al.* Engineering biofunctional in vitro vessel models using a multilayer bioprinting technique. *Sci. Rep.* (2018) doi:10.1038/s41598-018-28715-0.

478. Zheng, Y. *et al.* In vitro microvessels for the study of angiogenesis and thrombosis. *Proc. Natl. Acad. Sci.* (2012) doi:10.1073/pnas.1201240109.

479. Daculsi, R. *et al.* Unusual transduction response of progenitor-derived and mature endothelial cells exposed to laminar pulsatile shear stress. *J. Biomech.* (2008) doi:10.1016/j.jbiomech.2008.06.003.

480. Wang, Y. H. *et al.* Normal shear stress and vascular smooth muscle cells modulate migration of endothelial cells through histone deacetylase 6 activation and tubulin acetylation. in *Annals of Biomedical Engineering* (2010). doi:10.1007/s10439-009-9896-6.

481. Morley, L. C. *et al.* Piezo1 channels are mechanosensors in human fetoplacental endothelial cells. *Mol. Hum. Reprod.* (2018) doi:10.1093/molehr/gay033.

482. Hyman, A. J., Tumova, S. & Beech, D. J. Piezo1 Channels in Vascular Development and the Sensing of Shear Stress. *Curr. Top. Membr.* (2017) doi:10.1016/bs.ctm.2016.11.001.

483. Chiu, J. J. *et al.* Shear Stress Increases ICAM-1 and Decreases VCAM-1 and E-selectin Expressions Induced by Tumor Necrosis Factor-α in Endothelial Cells. *Arterioscler. Thromb. Vasc. Biol.* (2004) doi:10.1161/01.ATV.0000106321.63667.24.

484. Galbusera, M. *et al.* Fluid shear stress modulates von Willebrand factor release from human vascular endothelium. *Blood* (1997).

485. Penny, W. F., Weinstein, M., Salzman, E. W. & Ware, J. A. Correlation of circulating von Willebrand factor levels with cardiovascular hemodynamics. *Circulation* (1991) doi:10.1161/01.CIR.83.5.1630.

486. Reinhart-King, C. A., Fujiwara, K. & Berk, B. C. Chapter 2 Physiologic Stress-Mediated Signaling in the Endothelium. *Methods in Enzymology* (2008) doi:10.1016/S0076-6879(08)02002-8.

487. Campos-Toimil, M., Keravis, T., Orallo, F., Takeda, K. & Lugnier, C. Short-term or long-term treatments with a phosphodiesterase-4 (PDE4) inhibitor result in opposing agonist-induced Ca 2+ responses in endothelial cells. *Br. J. Pharmacol.* (2008) doi:10.1038/bjp.2008.56.

488. Valentijn, K. M., Sadler, J. E., Valentijn, J. A., Voorberg, J. & Eikenboom, J. Functional

architecture of Weibel-Palade bodies. *Blood* (2011) doi:10.1182/blood-2010-09-267492.

489. Boo, Y. C. & Jo, H. Flow-dependent regulation of endothelial nitric oxide synthase: role of protein kinases. *Am. J. Physiol. Physiol.* (2013) doi:10.1152/ajpcell.00122.2003.

490. Herrick, A. L. *et al.* Von Willebrand factor, thrombomodulin, thromboxane, β-thromboglobulin and markers of fibrinolysis in primary Raynaud's phenomenon and systemic sclerosis. *Ann. Rheum. Dis.* (1996) doi:10.1136/ard.55.2.122.

491. Wegener, G. & Volke, V. Nitric oxide synthase inhibitors as antidepressants. *Pharmaceuticals* (2010) doi:10.3390/ph3010273.

492. Lowenstein, C. J., Morrell, C. N. & Yamakuchi, M. Regulation of Weibel-Palade body exocytosis. *Trends in Cardiovascular Medicine* (2005) doi:10.1016/j.tcm.2005.09.005.

493. Hettema, M. E. *et al.* No effects of bosentan on microvasculature in patients with limited cutaneous systemic sclerosis. *Clin. Rheumatol.* (2009) doi:10.1007/s10067-009-1157-4.

494. Ozawa, M., Tsume, Y., Zur, M., Dahan, A. & Amidon, G. L. Intestinal permeability study of minoxidil: Assessment of minoxidil as a high permeability reference drug for biopharmaceutics classification. *Mol. Pharm.* (2015) doi:10.1021/mp500553b.

495. Sfikakis, P. P. *et al.* Improvement of vascular endothelial function using the oral endothelin receptor antagonist bosentan in patients with systemic sclerosis. *Arthritis Rheum.* (2007) doi:10.1002/art.22634.

496. Petrey, A. C. & de la Motte, C. A. Hyaluronan, a crucial regulator of inflammation. *Frontiers in Immunology* (2014) doi:10.3389/fimmu.2014.00101.

497. Zhu, J., Mix, E. & Winblad, B. The Antidepressant and Antiinflammatory Effects of Rolipram in the Central Nervous System. *CNS Drug Rev.* (2006) doi:10.1111/j.1527-3458.2001.tb00206.x.

498. Tsang, W. P., Chau, S. P. Y., Kong, S. K., Fung, K. P. & Kwok, T. T. Reactive oxygen species mediate doxorubicin induced p53-independent apoptosis. *Life Sci.* (2003).

499. Hong, Y. M., Kwon, J. H., Choi, S. & Kim, K. C. Apoptosis and inflammation associated

gene expressions in monocrotaline-induced pulmonary hypertensive rats after bosentan treatment. *Korean Circ. J.* (2014) doi:10.4070/kcj.2014.44.2.97.

500. Davies, P. How Do Vascular Endothelial Cells Respond to Flow? *Physiology* (2017) doi:10.1152/physiologyonline.1989.4.1.22.

501. Chistiakov, D. A., Orekhov, A. N. & Bobryshev, Y. V. Effects of shear stress on endothelial cells: go with the flow. *Acta Physiologica* (2017) doi:10.1111/apha.12725.

502. Joseph, E. C., Jones, H. B. & Kerns, W. D. Characterization of Coronary Arterial Lesions in the Dog Following Administration of SK&F 95654, a Phosphodiesterase III Inhibitor. *Toxicol. Pathol.* (1996) doi:10.1177/019262339602400405.

503. Lincoln, T. M. & Cornwell, T. L. Towards an Understanding of the Mechanism of Action of Cyclic AMP and Cyclic GMP in Smooth Muscle Relaxation. *J. Vasc. Res.* (1991) doi:10.1159/000158852.

504. Franco, C. & Gerhardt, H. Blood vessels on a chip. *Nature* (2012) doi:10.1038/488465a.

Appendix

The following tables summarise the effect of the drugs in the assays tested.

CHAPTER 3 (Rat vessel)

VWF release (N=4)	**24 hours**
Untreated control	100 %
Thrombin 10 U/ml	39.32 ± 8.52 %
Bosentan 100 µM	39.12 ± 3.46 %
Fenoldopam 100 µM	43.99 ± 6.44 %
Minoxidil 100 µM	46.78 ± 5.92 %
Rolipram 100 µM	89.0 ± 23.20

CHAPTER 4 (Monocultured EC and SMC)

VWF release (N=4)	**1 hour**	**24 hours**
DMSO control	80 %	80 %
Thrombin 1 U/ml	41.6 ± 5.5 %	55.8 ± 2.9 %
Bosentan 100 µM	51.7 ± 2.6 %	53.3 ± 6.9 %

EC junctional disruption (N=4)	**1 hour**	**24 hours**
DMSO control	1	1
Thrombin 1 U/ml	7.5 ± 1.2	3.2 ± 1.7
Bosentan 100 µM	2.1 ± 0.7	2.7 ± 1.7
Fenoldopam 100 µM	7.9 ± 3.3	1.2 ± 0.6
Minoxidil 100 µM	9.3 ± 3.4	11.5 ± 1.9
Rolipram 100 µM	0.9 ± 0.3	-

EC death (N=5)	**1 hour**	**4 hours**	**24 hours**
DMSO control	97.0 ± 0.6 %	-	-
Saponin	11.0 ± 0.7 %	-	-
Fenoldopam 100 µM	-	-	48.4 ± 6.1 %
Fenoldopam 10 µM	-	-	89.2 ± 2.7 %
Fenoldopam 1 µM	-	-	93.3 ± 7.3 %
Fenoldopam 0.1 µM	-	-	94.8 ± 6.5

CHAPTER 5 (Whole blood)

Platelets	**20 minutes**	**20 minutes**
	Integrin (N=5)	**P-selectin (N=5)**
Untreated control	257.5 ± 9.190	95.30 ± 12.36
TRAP-6	1261 ± 206.1	8560 ± 840.0
fMLP	269.9 ± 9.341	96.20 ± 29.18
Fenoldopam 1 µM	307.0 ± 45.19	110.0 ± 28.96
Fenoldopam 10 µM	286.1 ± 30.49	104.2 ± 23.25
Fenoldopam 100 µM	318.2 ± 65.18	109.9 ± 25.85

CHAPTER 6 (EC-SMC co-culture)

VWF release (N=4)	**1 hour**	**24 hours**
DMSO control	86 %	88 %
Thrombin 1 U/ml	54.4 ± 5.2 %	51.7 ± 3.9 %
Bosentan 100 µM	68.3 ± 3.8 %	62.8 ± 3.7 %
Fenoldopam 100 µM	57.9 ± 5.1 %	54.2 ± 3.2 %
Minoxidil 100 µM	-	54.5 ± 8.8 %

Cell death (N=4)	**EC**	**EC mix**	**SMC**	**SMC mix**
	24 hours		**24 hours**	
DMSO control	3.3 ± 0.1 %	-	-	-
Cisplatin	91 ± 3.4 %	94.9 ± 2.5 %	94.2 ± 2.3 %	94.4 ± 2.3 %
Bosentan 100 µM	-	15.9 ± 0.5 %	-	16.6 ± 0.5 %
Fenoldopam 100 µM	8.6 ± 1.1 %	1.8 %	-	-

CHAPTER 7 (Yoda-1)

VWF release (N=4)	**1 hour**	**24 hours**
DMSO control	87.4 ± 2.8 %	93.0 ± 1.5 %
Yoda-1 1 µM	79.5 ± 6.0 %	63.9 ± 1.90 %
Minoxidil 100 µM	-	72.9 ± 2.2 %

EC junctional disruption (N=4)	**1 hour**	**24 hours**
DMSO control	1	1
Yoda-1 1 µM	0.45 ± 0.07	0.3 ± 0.04
Bosentan 100 µM	4.9 ± 2.8	21.0 ± 5.0
Fenoldopam 100 µM	7.7 ± 4.9	-
Minoxidil 100 µM	3.4 ± 2.0	-

EC death (N=5)	**-Yoda-1**	**+Yoda-1**
	24 hours	**24 hours**
DMSO control	-	-
Yoda-1 1 µM	-	-
Bosentan 100 µM	17.6 ± 2.4 %	37.1 ± 3.8 %
Fenoldopam 100 µM	24.1 ± 2.9 %	72.6 ± 4.9 %